Cell-specific impact of IER3 on inflammation and carcinogenesis in the colon

Dissertation

zur Erlangung des Doktorgrades

der Mathematisch-Naturwissenschaftlichen

Fakultät

der Christian-Albrechts-Universität zu Kiel

vorgelegt von

Florian Deisinger

Kiel, 2020

Erster Gutacher:	Prof. Dr. rer. nat. Heiner Schäfer
Zweiter Gutachter:	Prof. Dr. rer. nat. Thomas Roeder
Tag der mündlichen Prüfung:	16.07.2020

Zum Druck genehmigt.

Für Ilo

in Liebe

Yesterday I woke up sucking on a lemon

Radiohead

Contents

List of Tables

List of Figures

List of Abbreviations [1]

* (in statistics)	p-value ≤ 0.05 (statistical significant)
** (in statistics)	p-value ≤ 0.01 (statistical highly significant)
1400W	A specific inhibitor of the inducible nitric oxide synthase
Å	Ångström (unit)[2]
aa	Amino acid(s)
Ab	Antibody
AC	Affinity chromatography
AEC	3-Amino-9-ethylcarbazole
AF	AlexaFluor™ – Family of different fluorochromes
AG	Antigen
AKT	Protein kinase B
AMP	1. Adenosine monophosphate
	2. Antimicrobial peptide
	3. Ampicillin
AnU	Anson unit[3]
AOM	Azoxymethane
APC	1. Antigen presenting cell
	2. Adenomatous polyposis coli
APS	3. Ammonium peroxydisulfate
ARE	Antioxidant responsive element
ATCC	American type culture collection
ATP	Adenosine triphosphate
AU	Arbitrary unit

[1] SI-Units and their prefixes are not listed as well as IUPAC-conform one-letter symbols of nucleobases and three-letter symbols of amino acids. Fundamental constants and SI-derived units are only listed in exeption, if it seemed necessary to avoid a possibility of confusion.

[2] $1\,\text{Å} \hat{=} 1 \cdot 10^{-10}\,\text{m}$.

[3] A common dimension to describe enzyme activity. Definition: [21].

BALB/c	Laboratory mice inbreed strain
BLAST	Basic local alignment search tool – an algorithm used in bioinformatics
BMCs	Bone marrow cells
BMDCs	Bone marrow derived cells
BMI1	Polycomb complex protein BMI-1 – A proto-oncogene
bp	Base pair(s)
BSA	Bovine serum albumin
bw	Body weight
°C	Degree Celsius
C57BL/6	A laboratory mouse inbreed strain
CAC	Colitis associated cancer/carcinogenesis
β-Cat.	β-catenin
CD	1. Crohn's disease 2. Cluster of differentiation
cDNA	Complementary DNA
CFU	Colony forming unit
cGMP	Cyclic guanosine monophosphate
CJ	Cellular junction
CLDN	Claudin
cMyc	Cellular *Myc* – Member of the proto-oncogene *Myc* family
COX-2	Cyclooxygenase 2
cpm	Counts per minute
CRC	Colorectal cancer
Cre	Cre recombinase
Cx	Connexins
d	Diameter
Da	Dalton (unit)
DC	Dendritic cell

DMEM	Dulbecco's modified Eagle medium - semi-standardized cell culture medium formulation[4]
DMSO	Dimethyl sulfoxide
DNA	Deoxyribonucleic acid
DNase	Deoxyribonuclease
dNTPs	Deoxynucleotide triphosphates
ds	Double stranded
DSS	Dextran sodium sulfate
DTT	Dithiothreitol
E2	Ubiquitin-conjugating enzyme
E3	Ubiquitin ligase
E-Cdh.	E-cadherin
ECL	Enhanced chemiluminescence
EDTA	Ethylenediaminetetraacetic acid
EGF	Epidermal growth factor
Em	Emission
EMSA	Electrophoretic mobility shift assay
EMT	Epithelial–mesenchymal transition
EtBr	Ethidium bromide
Ex	Absorbance (excitation)
exc.	Except
F4/80	EGF-like module-containing mucin-like hormone receptor-like 1
F-12[5]	Standardized cell culture medium formulation
FACS[6]	Fluorescence-activated cell sorting
FCS	Fetal calf serum
FD	FITC conjugated dextran

[4] If not explicit mentioned, in this thesis the term DMEM always refers to a formulation with 4.5 g/l glucose, 3.7 g/l $NaHCO_3$ and w/o pyruvate (Biochrom ord.-no.: F0435).

[5] Also termed as Ham's F-12.

[6] This abbreviation is also often used to describe flow cytometry in general.

FD4	FITC conjugated dextran with an average molecular weight of 4000 g/mol
FD10	FITC conjugated dextran with an average molecular weight of 10000 g/mol
FEP	Fluorinated ethylene propylene
fig.	Figure
FITC	Fluorescein isothiocyanate
flox	Denotation for a DNA sequence flanked by a *loxP* sequence on its 5′ and 3′ site.
fwd	Forward
g	1. Gram 2. Standard acceleration of gravity[7]
G	Gauge (unit)
G6PD	Glucose-6-phosphate dehydrogenase
GALT	Gut-associated lymphoid tissue
GI	Gastrointestinal
GM-CSF	Granulocyte-macrophage colony-stimulating factor
GOI	Gene of interest
h	1. Hour(s) 2. Human
HAC	High affinity chromatography
HBSS	HANK's balanced salt solution – a standardized buffer formulation
HEPES	4-(2-hydroxyethyl)-1-piperazineethanesulfonic acid
HEK-293	Cell line derived from human embryonal kidney cells
HEK-293T	Cell line derived from HEK-293 cells, expressing a mutant version of the SV40 large T antigen
HK	Housekeeper

[7] $1\,g \mathrel{\widehat{=}} 9.80665\,m/s^2$ [43]

HO1	Heme oxygenase 1
HPRT	Hypoxanthine-guanine phosphoribosyltransferase 1
HSP90	Heat shock protein 90
HT-29	A human colon cancer cell line
IBD	Inflammatory bowel disease
IC	Isotype control
ICC	Immunocytochemistry
ICC-F	Fluorescence based immunocytochemistry
IEC	Intestinal epithelial cell(s)
IEC-6	Immortalized intestinal epithelial cell line of rat origin
IER3	Immediate early response gene 3 [8]
IFN	Interferon
IFT	Immunofluorescence test
IHC	Immunohistochemistry
IHC-F	Fluorescence based Immunohistochemistry
Ig*X* (H+L)	Heavy and light chain of the antibody from isotype *X*
IκB	Inhibitor of κB
IKK	Inhibitor of κB kinase
IL	Interleukin
INN	International non-proprietary name
iNOS	Inducible nitric oxide synthase, also denoted as NOS2
i.p.	Intraperitoneal
IP3	Inositol 1,4,5-trisphosphate
IU	International unit
IUPAC	International union of pure and applied chemistry
JAM	Junctional adhesion molecule

[8] Alternative abbreviations for this gene are listed in section 4.

JE	Murine homologue to the human monocyte chemotactic protein 1[9] (MCP-1) [219]
KLH	Keyhole limpet haemocyanin
ko	Knockout
$\lambda_{Em}(A/B)$	Emission wavelength / bandpass
$\lambda_{Ex}(A/B)$	Absorbance (excitation) wavelength / bandpass
L32	60 S ribosomal protein L32
loxP	Locus of X1-over P1, a term describing a distinct DNA-sequence in the genome of the bacteriophage P1[10]
LP	Lamina propria
LPS	Lipopolysaccharide
LSM	Laser scanning microscope
LysM	Lysozyme M
m	1. Milli (as SI unit prefix) 2. Murine / mouse
M.	(Culture) medium
M1-MΦ	Macrophage(s) of the M1 subpopulation[11]
M2-MΦ	Macrophage(s) of the M2 subpopulation[12]
M1 segment	2nd quartile of the murine colon (from proximal)
M2 segment	3rd quartile of the murine colon (from proximal)
mAb	Monoclonal antibody
MACS	Magnetic-activated cell sorting
max.	Maximum
M cells	Microfold cells – Subtype of intestinal cells
M-CSF	Macrophage colony-stimulating factor

[9] Also denoted to as chemokine C-C-motif ligand 2 (CCL2).
[10] Actually, this term describes the locus of the distinct DNA-sequence, but is also used in practice to describe the sequence itself.
[11] also referred to as classically activated, pro inflammatory MΦ (see sec. 2.2.1)
[12] also referred to as alternatively activated, anti-inflammatory MΦ (see sec. 2.2.1)

MHC II	Major histocompatibility complex II
MDP	Muramyl dipeptide
min	Minute(s)
min.	Minimum
MLN	Mesenteric lymph nodes
MLV	Murine leukemia virus
MΦ	Macrophage(s)
$M\Phi^{cult.}$-M.	MΦ cultivation medium
$M\Phi^{diff.}$-M.	MΦ differentiation medium
mRNA	Messenger RNA
MW	Molecular weight
n/a	1. Not available
	2. Not applicable
NADH	Reduced form of nicotinamide adenine dinucleotide
NADPH	Reduced form of nicotinamide adenine dinucleotide phosphate
Na_2-EDTA	Ethylenediaminetetraacetic acid di-sodium salt
NC	Negative control
NEAA	Not essential amino acids
NED	N-(1-Naphthyl)ethylenediamine di-hydrochloride
Neo	Neomycin
NF-κB	Nuclear factor kappa-light-chain-enhancer of activated B cells
no.	Number
NOD2	Nucleotide-binding oligomerization domain-containing protein 2
NOS2	see iNOS
NO_x	Nitric oxides
NQO1	NAD(P)H dehydrogenase quinone 1
NRF2	Nuclear factor erythroid 2-related factor 2
n.s.	Not significant
OCC	Occludin protein

Ocln	Occludin coding gene
oligo(dT)	Deoxythymidine oligomere
ord.-no.	Order number
Ⓟ-*X*	Phosphorylated form of protein *X*
p50	NF-κB p50 subunit
p53	Tumor protein p53 (also denoted as TP53)
p65	NF-κB p65 subunit
PAA	Polyacrylamide
pAb	Polyclonal antibody
PAGE	Polyacrylamide gel electrophoresis
PBS	Phosphate buffered saline
PCR	Polymerase chain reaction
PE	Phycoerythrin
PerCP	Peridinin chlorophyll
PEST sequence	a Pro-, Glu-, Ser- and Thr-rich peptide sequence associated with proteins of a short intracellular half-life time.
PET	Polyethylene terephthalate
PGK1	Phosphorglycerate kinase
p.i.	*Post infectionem*, after infection
PIC	Phosphatase inhibitor cocktail
PMSF	Phenylmethylsulfonyl fluoride
prim.	Primary
PS	Polystyrene
P/S	Penicillin / Streptomycin
PVDF	Polyvinylidene fluoride
PZN	*Pharmazentralnummer*, unique identification number for pharmaceuticals in Germany
qPCR	Quantitative real-time PCR
r	Radius

r_H	Hydrodynamic radius, also referred to as STOKES radius
Raji	Human BURKITT's lymphoma derived cell line - Suitable for transfection experiments
RAW264.7	A murine macrophage cell line established from a tumor induced by the ABELSON murine leukemia virus
rb	Rabbit
rec.	Recombinant
rev	Reverse
RIPA	Radioimmunoprecipitation assay
RNA	Ribonucleic acid
RNase	Ribonuclease
RNS	Reactive nitrogen species
ROS	Reactive oxygen species
RPL13a	Ribosomal protein L13a
rpm	Revolutions per minute
RPMI 1640	Roswell park memorial institute formulation 1640 – standardized cell culture medium formulation
rt	Rat
RT	1. Room temperature 2. Reverse transcription
RT-PCR	Reverse transcriptional PCR
S	Svedberg (unit)
SDS	Sodium dodecyl sulfate
SDS-PAGE	Sodium dodecyl sulfate polyacrylamide gel electrophoresis
sec.	Section
SI	1. Small intestine *2. Système international d'unités* – International System of Units
sic	*Sic erat scriptum* – thus it was written
SMP	Skim milk powder

SNAP	S-Nitroso-N-acetyl-DL-penicillamine – A nitric oxide donor
Soln.	Solution
ss	Single stranded
SV40 large T antigen	An oncoprotein derived from the polyomavirus SV40
Sv129	A laboratory mice inbreed strain
tab.	Table
Taq	*Thermus Aquatiqus*, a thermophilic, GRAM-negative bacterium
TBE	TRIS/borate/EDTA-buffer
TBS	TRIS buffered saline
TBS-T	TRIS buffered saline containing Tween-20
TC	Tissue culture
TE	TRIS/EDTA-buffer
TEMED	Tetramethylethylenediamine
temp.	Temperature
TEP	Trans epithelial permeability
TERT	Telomerase reverse transcriptase
TGF-β	transforming growth factor β
THP-1	Human monocytic cell line derived from an acute monocytic leukemia patient
TJ	Tight junction
TJP	Tight junction protein
TLR	Toll-like receptor
TNF	Tumor necrosis factor[13]
TNFR1/2	Tumor necrosis factor receptor 1/2
TRIS	Tris(hydroxymethyl)aminomethane
TSS	Target species specificity
U	Unit

[13]Formerly denoted as tumor necrosis factor alpha (TNF-α).

Ub	Ubiquitin
UC	Ulcerative colitis
UTR	Untranslated region
UV	Ultraviolet
v	Volume(s)
Vil	Villin
VP	Volume part
w	Weight
Wnt	Family of ligands binding to receptors of the Frizzled family
w/o	Without
w/o PR	Without phenol red
wt	Wild-type
YAMC	Young adult mouse colon – An immortalized murine colonic epithelial cell line
ZO1	Zonula occludens-1 protein (also denoted as TJP1)

Gene and protein nomenclature

Accordingly on the recommendation of ALBERTS et al. [20] for a simplified nomenclature of gene and protein abbreviations, in this thesis gene symbols are species-independent written in italic letters with the first letter in capital. Protein abbreviations are species-independent written in upright letters with the first or all letters in capitalization.

In case of different denotations for homologue genes and proteins between different species, only the human denotation is used in this thesis.

Abstract

Inflammatory bowel disease is a chronic inflammation disorder affecting mainly the colon and the small intestine. A common concomitant feature of this disease is the formation of colorectal cancer, causing worldwide about 38000 deaths per year. To date, the pathomechanisms underlying this disease are only partially known. Besides environmental factors and genetic alterations, an inadequate immune response to the host's microbiome significantly contributes to the onset as well to the progression of the disease. Furthermore, macrophages have been identified as a cell type, highly involved in the pathophysiology of inflammatory bowel disease and colorectal carcinogenesis. The immediate early response gene *Ier3*, whose expression is highly up-regulated in patients suffering from inflammatory bowel disease, plays an important role in the cellular response to stress stimuli. *Ier3* not only influences the regulation of apoptosis and proliferation but also affects several immunologic pathways, for instance by interacting with the NF-κB signaling cascade. In this project we analyzed the effects of a cell type specific depletion of *Ier3* on the outcome of colitis and colitis associated carcinogenesis using an AOM/DSS mouse model. We were able to show, that a macrophage specific depletion of *Ier3* significantly attenuates the severity of an AOM/DSS induced colitis as well as the formation of colorectal tumors. This protective effect was much less pronounced in an epithelial cell specific or genome wide depletion of *Ier3*. Furthermore, we observed a reduced responsiveness of *Ier3* deficient macrophages to immunogenic stimuli like bacterial LPS, which manifests in a significantly decreased expression of the inducible nitric oxide synthase and a diminished release of reactive nitrogen species. As a result, these macrophages affect the integrity of the intestinal epithelial cell barrier to a much lesser extent when compared to activated *Ier3* proficient macrophages. This relates to a differential effect on the transepithelial permeability caused by an altered expression and intracellular distribution of the cellular junction associated proteins E-cadherin and β-catenin as we could demonstrate *in vivo* and *in vitro*. In summary, our results reveal a novel mechanism how IER3 contributes to inflammatory bowel disease and colitis

associated carcinogenesis.

Zusammenfassung

Chronisch-entzündliche Darmerkrankungen und die daraus resultierende Entstehung kolorektaler Karzinome fordern weltweit etwa 38000 Tote pro Jahr. Die Pathomechanismen, die dieser Krankheit zugrunde liegen sind bisher nur zum Teil verstanden. Neben diversen genetischen- und Umweltfaktoren trägt vor allem eine inadäquate Immunreaktion gegenüber dem intestinalen Mikrobiom zur Initiation und Progression der Erkrankung bei. Des Weiteren konnten Makrophagen als ein Zelltyp identifiziert werden, welcher im hohen Maße an der Pathophysiologie chronisch-entzündlicher Darmerkrankungen und kolorektaler Karzinome beteiligt ist. Das *immediate early response* Gen *Ier3*, dessen Expression in dieser Patientengruppe deutlich hochreguliert ist, spielt eine wichtige Rolle in der zellulären Antwort auf eine Vielzahl von Stress-Stimuli. *Ier3* wirkt sich nicht nur auf die Regulation der Apoptose und Proliferation aus, sondern interagiert auch mit diversen immunologisch relevanten Signalwegen, wie zum Beispiel der NF-κB Kaskade. In dieser Arbeit wurden die Effekte einer Zelltyp-spezifischen Deletion von *Ier3* auf den Verlauf einer Kolitis und der damit einhergehenden kolorektalen Karzinogenese im AOM/DSS Mausmodell untersucht. Wir konnten zeigen, dass eine Makrophagen-spezifische *Ier3* Defizienz, die Schwere einer AOM/DSS-induzierten Kolitis signifikant abschwächt, sowie die Bildung kolorektaler Tumore signifikant reduziert. Dieser protektive Effekt war bei einer Epithel-spezifischen oder genomweiten Depletion von *Ier3* deutlich geringer ausgeprägt. Des Weiteren beobachteten wir eine reduzierte Responsivität *Ier3*-defizitärer Makrophagen gegenüber immunologischen Stimuli, wie zum Beispiel bakteriellem LPS, welche sich in einer verringerten iNOS-Expression sowie in einer verminderten Freisetzung reaktiver Stickstoffspezies manifestierte. Solche Makrophagen beeinflussten im Vergleich zu *Ier3*-profizienten Makrophagen die Integrität der intestinalen Epithelzellbarriere in signifikant geringerem Maße. Dies äußerte sich vor allem in einer unterschiedlichen transepithelialen Permeabilität, verursacht durch eine veränderte Expression sowie intrazellulären Distribution der Zellkontakt-assoziierten Proteine E-Cadherin und β-Catenin, welche sowohl *in vivo* wie auch *in vitro* nachgewiesen wurde.

Zusammengefasst zeigen diese Befunde einen neuen Mechanismus auf, wie IER3 zur Pathogenese chronisch-entzündlicher Darmerkrankungen und einer damit verbundenen kolorektalen Karzinogenese beiträgt.

Introduction

1 Anatomy and physiology of the gut

1.1 Anatomy

The gut (also intestine or bowel, fig. 1.1) is an organ mainly responsible for the digestion and resorption of nutrients and water as well as for discharging of indigestible food components [205]. With an surface area of 32 square meters[14] [89], it represents a major immunological barrier separating the human body from its luminal environment. It consists of two main segments, namely the small intestine and the large intestine (cecum and colon), which can be further subdivided in smaller anatomically segments. The small intestine (SI) is distinguished (from proximal to distal) into duodenum, jejunum and ileum. The colon, which is preceded by the cecum with its appendix, is divided into ascending colon[15], transverse colon[16], descending colon, sigmoid colon[17] and rectum. During the last decades, its role in the regulation of the immunological homeostasis has gained great attention in physiological and medical research [200, 89].

[14] Other sources report a surface area of 400 m^2 [159].
[15] The mouse equivalent to the ascending colon is termed proximal colon.
[16] The mouse equivalent to the transverse colon is denoted as middle colon (divided in M1 segment and M2 segment).
[17] The mouse equivalent to descending colon and sigmoid are denoted as distal colon.

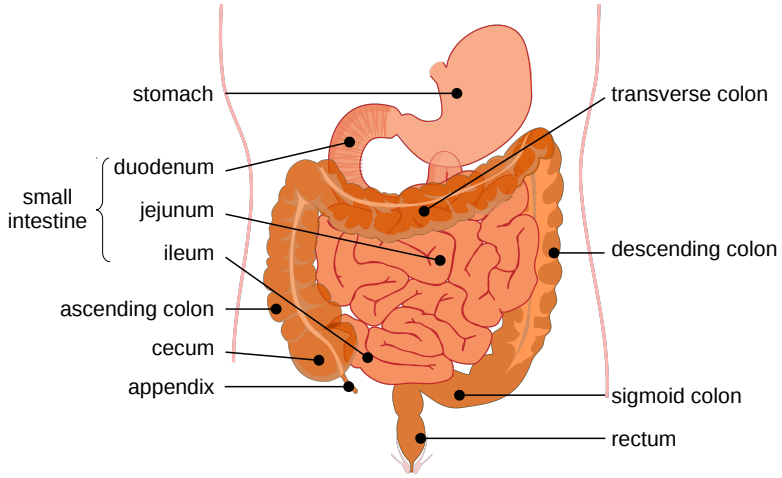

Figure 1.1: Illustration of the intestine and stomach. Modified after BLAUSEN [39].

In cross section, both, small and large intestine show the typical tissue layer structure of the gastrointestinal wall which consists of (from luminal to basal): mucosa, submucosa, muscularis and serosa. While this main structure is consistent over the whole gastrointestinal tract there are distinct differences in its manifestation between small intestine and colon.

The mucosa consists of a monolayer of polarized, columnar intestinal epithelial cells (IEC) of different types (sec. 1.3.1), sitting on a thin basal lamina. On its apical face, this epithelial layer is covered by a mucus layer (sec. 1.3.2). Underneath the basal lamina, the lamina propria is located, a layer of connective tissue containing blood capillaries and lymphatic vessels as well as lymphocytes and, to a lesser extend, myeloid cells. Lymphocytes are diffusely distributed trough the epithelial layer (interepithelial lymphocytes) and the lamina propria, whereas lymphocyte follicles only appear in the lamina propria. In the small intestine these follicles can appear in huge condensed clusters called PEYER's patch. As part of the gut-associated lymphatic tissue (GALT), these immune cells play a key role in the maintenance of the intestinal immunological homeostasis. The lamina muscularis mucosae, which is also a part of the mucosa, is a thin layer of muscle tissue, sitting underneath the lamina propria. The mucosa is the layer

with the greatest morphological variation within the gastrointestinal system, accounting for its specialization in distinct compartments. In the small intestine, the mucosa forms invaginations (crypts) and protrusions (villi) to increase its surface area, whereas the colon only contains crypts[18].

The submucosa is a layer of connective tissue underneath the mucosa, pervaded by a dense net of blood and lymph vessels to provide the transport of substances as well as immune cells from and to the mucosa. Lymphocytes and myeloid cells as well as lymphocyte follicles and PEYER's patches also appear in this layer. Furthermore, plexi (ganglia) of the enteric nerve system (MEISSNER plexi) are located in submucosa.

The muscularis consists of an inner circular and outer longitudinal muscle layer, responsible for the guts peristaltic. Plexi of the enteric nerve system (AUERBACH plexi) are found between these muscles layers. The longitudinal muscles are covered by the serosa, a thin connective tissue layer covered by squamous epithelial cells. Representing the outermost layer of the intestine, it reduces the friction to other organs during peristaltic movements.

1.2 Microbiota in the gut

In humans, the gut is colonized by estimated 10^{14}, mainly (99 %) anaerobic, bacteria, thus making up a complex microflora [211, 17]. Compared to the colon, which harbors the majority of the guts microbiome [82], the colonization of the small intestine is much lower, displaying a gradual increase towards its distal site (jejunum: 10^3-10^4 $CFU/_{ml}$ chyme, terminal ileum: 10^7-10^9 $CFU/_{ml}$ chyme) [163]. The gut's microflora is composed of estimated 100-500 different bacterial species [82, 179], whereby 30-40 different species comprise 99 % of all bacteria [33]. However, their composition varies over the different intestine segments and is modulated by other factors like dietary or the host's health condition [151, 82]. In healthy individuals, the bacteria populate the outer (luminal) layer

[18] In mice, the proximal colon additionally exhibits transversal folds, while the distal mouse colon has longitudinal folds.

of the mucus film (sec. 1.3.2), but do neither infiltrate the inner layer nor have direct contact to the epithelial surface [86]. Besides their appearance in the outer mucus layer, they make up 60 % of the dry mass of the feces (10^{10}-10^{12} CFU/ml fresh specimen) [193].

The gut microbiome establishes during the first two years after birth [188]. In parallel, the host develops an immunological tolerance to these bacteria, which exist in a commensal and mutualistic relationship [57, 211, 188]. While providing nutrients for the microbiota [211], the host benefits from them in several ways. Hence colonization and growth of pathogenic bacteria is prevented by the commensal microflora [218] and otherwise indigestible food components are converted into absorbable nutrients [41, 163, 69].

However, an exaggerated population with commensal or mutualistic bacteria can also lead to diseases [82, 164].

1.3 Intestinal epithelial cells

1.3.1 Types of intestinal epithelial cells

The epithelial cell layer of the mucosa consists of different subtypes of specialized cells, like enterocytes, goblet cells, enteroendocrine cells, PANETH cells and microfold cells (M cells) [205]. All those cells differentiate from omnipotent epithelial stem cells located at the bottom of the crypts. With an average lifetime of 4-5 days, they undergo a continues process of apoptosis and renewal [205]. They all show a high grade of polarization, giving rise of an apical side which faces the lumen, and a basal side which faces the lamina propria. Due to their functional specialization, the different types of intestinal epithelial cells (IEC) are variably distributed over the distinct segments of the intestinal system [205].

Enterocytes, which are the main type of intestinal cells are largely distributed over the whole small intestine and colon. Their main function is the absorption of water, electrolytes and (digested) nutrients like lipids, sugars and proteins from the gut lumen

as well as their transfer to the capillary system. For this purpose, they comprise a wide set of substance specific molecular transporters and ion channels, whereas small lipophilic molecules can be absorbed passively by diffusion through the cell membrane. Enterocytes form a vast number of cytoplasmic protrusions on their apical side to increase their surface area [139]. These protrusions are named microvilli. Because of its microscopic morphology, this microvilli forming epithelium is also named brush border epithelium. Besides their absorptive properties, enterocytes also secrete IgA, provided from mucosal B-cells, into the gut lumen [159].

Goblet cells are single cellular glands, producing and secreting a highly glycosylated mucus into the gut lumen. While found in the small intestine and in the colon, their number steadily increases from proximal to distal. Compared to enterocytes, their microvilli are shorter and smaller in number [102, 205].

As part of the endocrine system, enteroendocrine cells are spread over the whole intestine. They secrete a wide range of different hormones, mainly modulating the digestion and uptake of specific nutrients [77, 205].

Paneth cells are secretory cells sitting in the crypts of the small intestine. Their granule contain a range of defensins and other antimicrobial peptides as well as lysozyme, contributing to the immunological homeostasis [42, 205].

As part of the follicle associated tissue, M cells are found everywhere Peyer's patches appear. At their apical face, they are able to take up antigens from the gut lumen and deliver them to antigen presenting cells (APC) at their basal side [119, 205].

Tuft cells, named after their unique microvilli morphology, belong to the family of chemosensory cells. While their exact physiological function is not fully understood until now, it is assumed that they also play a role in modulating the gut immune system [68, 205].

1.3.2 The mucosa's mucus layer

As mentioned above, at its apical face, the mucosal epithelial cell layer is covered by a thin film of mucus continuously produced by goblet cells. The gel like mucus consists of water, glycans as well as different glycoproteins, so called mucins, and serves several purposes [101]. As lubricant, it reduces the friction during the transport of feces towards the anus. Furthermore, it acts as an additional immunological border between the gut microbiome and the epithelial cell surface [101]. The mucus film, can be divided in two distinct layers. An inner layer, which sits firmly on top of the epithelial cells, consists of a relative dense mucus and has a thickness of about 50 µm. Under physiological conditions this layer is free of bacteria. The outer layer (≈100 µm thickness) is organized more loosely and the habitat for the commensal and mutualistic microbiota [86, 101].

1.3.3 Intercellular junctions

The single IEC of the mucosa's cell composite are connected by several intercellular junctions [58] (fig. 1.2), impacting significantly its physical and biological properties [87, 200].

Tight junctions Tight junctions (TJ, fig. 1.2a) seal the intercellular space between IEC at their lateral side, thus preventing an unintended paracellular exchange of substances and cells between the apical lumen and lamina propria [87]. They appear as belt like structure completely surrounding single cells and connect them with adjacent cells [58]. From the lateral view, tight junctions can form several superimposed strands, to improve their sealing properties. While being composed of over 60 different proteins types [156], tight junctions, are divided into three main classes: Occludin based, claudin based and junction adhesion molecule (JAM) based tight junctions.

Occludin (OCC[19]) is a transmembrane protein of 60-82 kDa (in humans), encoded by the

[19] Alternative protein abbreviations for occludin are OCLN and OCLDN.

Ocln gene. Several isoforms of the OCC protein exist due to alternative splicing [142, 124]. Occludin consists of four transmembrane domains as well as of two extracellular and one intracellular loop. C- and N-termini are located intracellularly [87, 62]. The two extracellular loops form a bond with the extracellular loops from an OCC protein of an adjacent cell [81]. Near its C-terminus OCC binds to a variety of other junction related proteins like members of the zonula occludens family (mostly prominent ZO1), cadherins and cingulin, forming a huge protein complex [142, 124]. This complex again binds to cellular actin filaments, providing the tight junction's mechanical stability [64, 135].

The claudin (CLDN) protein family includes 24 known members of 20-27 kDa proteins [199, 63], which all share structural similarity to occludin [110]. Like OCC, the extracellular loops of claudins form bonds with their counterparts from adjacent cells [65, 110]. Near to their C-termini they also bind a variety of junction related proteins which then again interact with cellular actin filaments [140, 97, 128].

Junctional adhesion molecules (JAM) are proteins of about 40 kDa belonging the superfamily of immunoglobulins (Ig) [55, 31]. They consist of two Ig-like extracellular domains, a single-pass transmembrane domain and a cytoplasmic C-terminal domain [55, 31]. The extracellular domains of JAM can form homo- and heterophilic bonds, while the latter was only shown for endothelial JAM [32, 27]. At their C-terminus they have binding motifs for ZO1 and other junction related proteins, which can interact with cellular actin filaments [81].

Adherens junctions Adherens junctions (fig. 1.2b) belong to the group of anchoring junctions, improving the mechanical cohesion between the IEC in the mucosal layer [178, 87]. They indirectly connect the cytoskeletal actin filaments of two adjacent cells by linking them trough a intercellular bridge of E-cadherin[20] proteins [84]. In cellular junctions, the extracellular domains of an E-cadherin dimer form a homophilic bond with the extracellular E-cadherin domains of an adjacent cell [85]. The intracellular

[20] For more information on E-cadherin and its function in IBD and CAC see section 3.3.1.

domains bind to proteins of the catenin and vinculin family, which act as adapters facilitating the anchoring of actin filaments [157, 85]. While other forms are possible, in the mucosa's epithelial layer, adherens junctions appear as a belt like structure, named zonula adherens [58]. They are located directly underneath the tight junctions [200].

Desmosomes Like adherens junctions, desmosomes (fig. 1.2c) belong to the group of anchoring junctions. Desmosomes connect either two adjacent cells or, as hemidesmosomes, a single cell with the basal lamina [53, 208, 67]. They appear as ball shaped structures randomly distributed at the lateral or, in case of hemidesmosomes, at the basal side of the cells plasma membrane [58]. In contrast to adherens junctions, desmosomes connect the keratin filaments of adjacent cells [107]. While also linking two cells by cadherins, which protrude into the extracellular space, in desmosomes those cadherins are of the desmoglein or desmocollin type [150, 67]. At their intracellular end, those cadherins are anchored into a microscopical visible plaque consisting of desmoplakin, plakoglobin and proteins of the catenin family [53, 67]. This plaque serves as a linker to the intracellular keratin filaments [53, 67].

Gap junctions Gap junctions (fig. 1.2d) are clusters of intercellular transmembrane channels (pores), allowing a direct exchange of small molecules ($\approx\leq 500\,\mathrm{Da}$) between cells [71]. Each cell forms a hemichannel (connexon), consisting of a homo or hetero-hexamer of connexin (Cx) proteins, coupling to a connexon of an adjacent cell [173, 72]. Up to now, more than 20 different connexins are known [185, 186], accounting for the formation of a great number of different gap junction subtypes with a high substance specificity [90, 70]. Gap junctions connect cells chemically as well as electrically [132] and serve primarily the transduction of signals [173, 71]. Substance transport through gap junctions occurs passively by diffusion [132], but can be regulated by opening and closing the pores [173]. Typical substances exchanged trough gap junctions are second messengers like AMP, cGMP, IP3 as well as ions [113, 132].

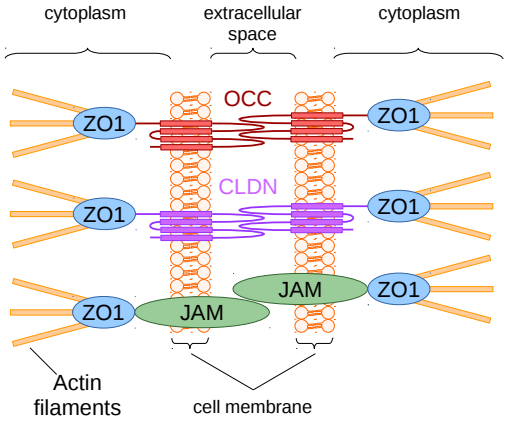

(a) Tight junctions. OCC: Occludin, CLDN: Claudins, ZO1: Zonula occludens 1, JAM: Junction adhesion molecules.

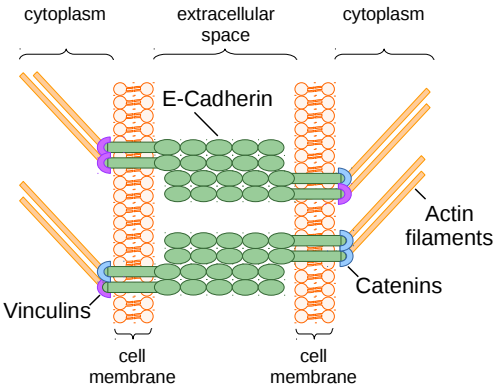

(b) Adherens junctions. Adherens junctions belong to the group of anchoring junctions, improving the mechanical cohesion between the IEC of the mucosal layer.

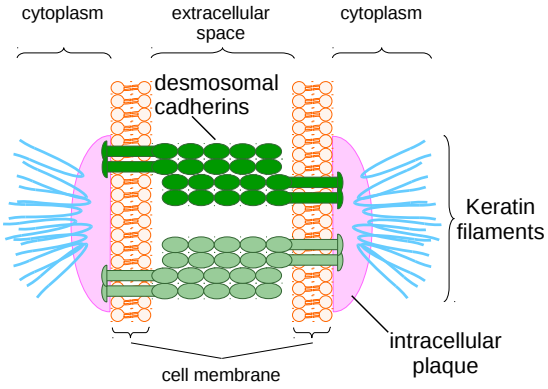

(c) Desmosome. Like adherens junctions, desmosomes belong to the group of anchoring junctions. The type of desmosomal cadherins which consist of desmogleins and desmocollins differ from type I cadherins like E-cadherin. The intracellular plaque consists of desmoplakin, plakoglobin and proteins of the catenin family.

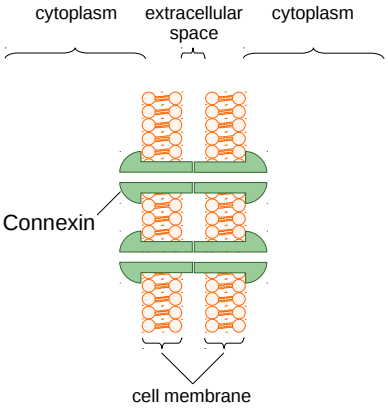

(d) Gap junction. Gap junctions are clusters of channels connecting the cytoplasm of two adjacent cells. Thus, they allow a direct exchange of small molecules ($\approx\leq 1$ kDa) between those cells. Each hemichannel (connexon) consist of 6 connexin proteins. At the site of gap junctions the intercellular gap has a wide of 2-4 nm.

Figure 1.2: Simplified illustrations of the four intercellular junction types in the gut's IEC layer. See the continuous text for a more detailed explanation.

However, during inflammatory processes cellular junctions allow the transmigration of immune cells like neutrophil granulocytes and macrophages from the lamina propria to the apical epithelial side due to their high plasticity [159].

2 The gut immune system

2.1 The mucosa as immunological barrier

The intestinal mucosa with its mucus and epithelial single cell layer equipped with tight junctions represents the border between the body and its luminal environment. On the one hand, it has to be ensured, that none of the myriad of bacteria can overcome this border. Due to their high number, even commensal or symbiotic bacteria comprise a high pathogenic risk if infiltrating the lamina propria [82]. On the other hand, an permanently exaggerated immune response would also negatively affect the host's health status [159]. So a well balanced equilibrium between immunologic tolerance and activity is pivotal for a proper function of the gut immune system.

2.2 Macrophages

2.2.1 General properties and functions

Macrophages (MΦ) are a subtype of leukocytes from the myeloid lineage, playing an important role in the innate as well in the adaptive immunity by killing pathogens and presenting microbial fragments on their surface. They appear as mononucleated cells of about 20 µm diameter and can be found in most tissue compartments of the human body. MΦ derive in multiple steps from hematopoietic stem cells of the bone marrow under the influence of the growth factor "macrophage colony stimulating factor" (M-CSF). Their direct precursor cells circulate as monocytes up to four days in the blood system before migrating into the tissue where they differentiate into mature MΦ . This differentiation is again mainly triggered by M-CSF, produced by cells of the respectively tissue compartment (e.g. by fibroblasts). During immunological events, monocytes get chemotactically attracted to those sites and activated, thus dramatically increasing the number of MΦ within a reasonable amount of time [143].

One of their main characteristics is the capability of phagocytosing particles, digest them and present the resulting fragments on their surface, where they can be recognized by other immune cells. Such particles can be bacterias and other pathogens, endogenous cells, cell debris as well as a variety of other exogenous or endogenous particles. After engulfing the particles in the phagosome, it fuses with the lysosome forming the phagolysosome. Besides its low pH value, the lysosome contains a broad variety of digestive enzymes as well as reactive oxygen and nitrogen species allowing an effective digestion respectively killing of the phagocytosed particles. The digested fragments are then coupled to major histocompatibility complex class II (MHC II) receptors and presented on the MΦ's surface where they can be recognized by T-cells. This ability, which they share with dendritic cells (DC), characterizes MΦ as professional antigen presenting cells (APC) [143].

MΦ can be activated by a variety of exogenous and endogenous stimuli like the bacterial antigens lipopolysaccharides (LPS) and muramyl dipeptide (MDP) or cytokines like IFN-γ, TNF, IL-1β and IL-6 produced by other immune cells. After activation, MΦ increase their phagocytotic activity, expression of the nitric oxides (NO_x) producing protein inducible nitric oxide synthase (iNOS) and the release of cytokines [143].

The ability to produce reactive nitrogen species (RNS), which can freely diffuse trough their cell membrane, allows MΦ to kill not only phagocytosed pathogens but also microorganisms in their direct neighborhood. On the other hand, this also bears the risk of damaging the surrounding tissue and endogenous cells [143].

On protein expression level, human MΦ are characterized by high amounts of CD11b and CD68 while CD11c expression is typically low [143]. Murine MΦ additionally express high levels of F4/80 [126]. There exist several attempts to identify additional subpopulations of MΦ, either by differences in the expression pattern of certain marker proteins or by an altered response to immunogenic stimuli as well as an altered cytokine release profile [74, 73]. There are two main classes of MΦ described in the literature:

Classically activated macrophages (M1 MΦ) exhibit a typical pro-inflammatory pro-

file [148, 134]. They show an elevated phagocytosis rate combined with high iNOS expression and an increased release of NO_x as well as pro-inflammatory cytokines like IFN-γ, TNF, IL-β and IL-6 [134, 143]. M1 polarized macrophages represent the typical MΦ prototype during the host defense against pathogens.

In contrast, alternatively activated macrophages (M2 MΦ) are characterized by their anti-inflammatory and immune suppressing properties [134, 143]. Compared to M1 MΦ, their iNOS expression is much lower or even absent, while they produce high levels of the anti inflammatory cytokines IL-10 and TGF-β.

While some authors divide the above mentioned two classes of MΦ in further subclasses [125, 170], the concept of M1/M2 macrophages itself is subject of an ongoing controversial debate. Some authors argue, that there only exists one type of MΦ, which underlies a certain plasticity regarding its pro- anti-inflammatory properties [144, 123, 83, 182, 117].

2.2.2 Intestinal macrophages

Though appearing in all segments of the gut, the highest number of MΦ is found in the colon [145, 54]. From all tissue layers, the lamina propria and the submucosa comprise the highest density of MΦ [94], while some MΦ are also found to a much lesser extent, in the muscle layers [133, 195]. One has to distinguish between resident and infiltrating mucosal MΦ. While the former resident in the mucosa permanently, the latter infiltrate the mucosa only in response to an immunological challenge. Resident MΦ comprise both, M1 and M2 features. As a result of their close localization to the guts microbiome they developed a high tolerance to bacterial antigens regarding their cytokine expression profile [28, 184, 88]. This could be explained by the continuous secretion of TGF-β and other anti-inflammatory cytokines from the adjacent stroma cells [29, 184, 88]. On the other hand, these MΦ comprise a high bactericidal activity

against infiltrating microbiota [184]. In contrast, infiltrating MΦ exhibit the typical M1 profile of classical activated macrophages [29].

3 Inflammatory bowel disease

Inflammatory bowel disease (IBD) describes a chronic inflammatory disorder affecting mainly the colon and small intestine, which results worldwide in about 38000 deaths per year [19]. It manifests in two major forms: Ulcerative colitis (UC) and Crohn's disease (CD) [15].

Crohn's disease was first noticed by the German surgeon Wilhelm Fabry in 1623 and later described by and named after the US physician Burril B. Crohn in 1932 [47, 2]. The onset of CD occurs mostly at an age of 14 and 30 years. First symptoms are abdominal pain, bloody diarrhea, fever and weight loss. Ileum and colon are the two sections of the gastrointestinal tract which are mostly affected by CD in a discontinuous pattern (fig. 3.1a) [161]. Extra-intestinal manifestations can also occur. Typical for CD is the transmural inflammation, affecting all layers of the gut, often accompanied by granulomas, strictures and fistulas [215].

Ulcerative colitis was first described by the British physician Sir Samuel Wilks in 1859 [210]. Its peek incidence is between the 15^{th} and 25^{th} year of age. Guiding symptoms are mucous bloody diarrhea accompanied by rectal tenesmus. Fever and weight loss are much more rare than in CD. The disease is marked by continuously inflammation pattern ascending from the rectum (figure 3.1b) [215]. On histological level, the inflammation is mostly confined to the mucosa. While granulomas, strictures and fistulas are rather untypical findings in UC, emerging of ulcers is an often observed characteristic [215].

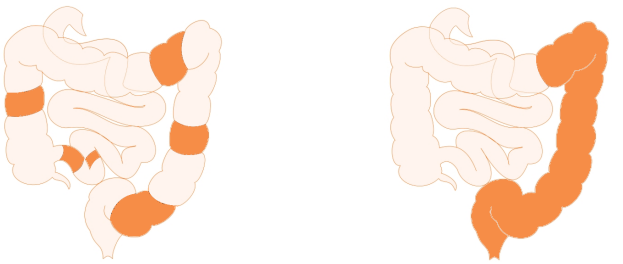

(a) Typical pattern of inflammation of Crohn's disease.

(b) Typical pattern of inflammation of ulcerative colitis.

Figure 3.1: Inflammatory bowel disease manifests in two major forms, Crohn's disease and ulcerative colitis. CROHN's disease (a) is characterized by a patchy inflammation pattern spreading over the whole colon and the terminal ileum. By contrast, ulcerative colitis (b) presents a continuously inflammation pattern ascending from the rectum.

The worldwide highest prevalence rates of IBD are seen in northern Europe (CD: 0.322 %, UC: 0.505 %) [138] and the United States of America (CD: 0.201 %, UC: 0.238 %) [103]. Lower rates are found in Asia, but with increasing incidence during the last decade [138]. The exact mechanisms leading to the pathophysiology of IBD are only partially elucidated until today [161]. However, several risk factors could be identified [15]. These are genetic predispositions and mutations as well as environmental factors like dietary and smoking status. Microbial-host interactions are getting more and more into the focus of science during the last years, emphasizing IBD as a disease caused by a disturbed barrier function along an inappropriate immune response. Besides mutations in *Nod2*, several other disease associated genes like e.g. *Ibd5* or *Atg16l1* have been identified, pointing out the importance of the innate immune system during diseases progression [30]. Luminal antigen recognition begins at the epithelial level. Epithelial expressed pattern recognition receptors (e.g. toll like receptors (TLR)) detect microbiome associated antigen motifs which trigger several intracellular signaling cascades culminating in the activation of the nuclear factor kappa-light-chain-enhancer of activated B cells (NF-κB, fig. 3.2) [30]. Under physiological conditions, there is a balanced equilibrium between active immune response and immunological tolerance. In patients suffering from IBD, an exceeded activation of NF-κB triggers an increased expression of pro-inflammatory cytokines. Amongst other effects, this causes a diminished barrier function of the epithelium by loosening

intercellular junctions. Thus, an increased number of antigens is detected by dendritic cells and macrophages, leading to their forced activation thereby to excessive secretion of pro-inflammatory chemo- and cytokines. The succeeded homing and activation of further immune-cells results in a pronounced inflammatory phenotype [15, 30].

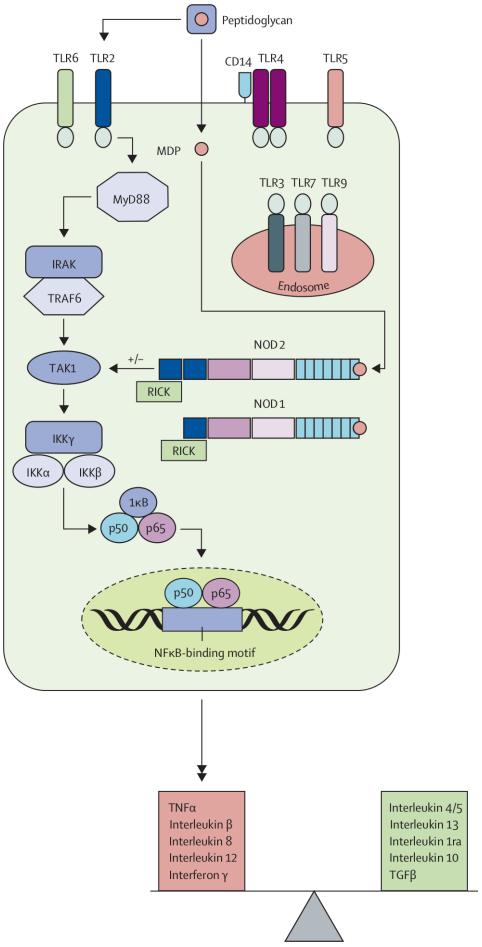

Figure 3.2: Signaling pathways of TLR and NOD proteins. All signaling cascades result in the activation of NF-κB. MDP=muramyl dipeptide, MyD=myeloid differentiation primary response protein, IRAK=IL-1-receptor associated kinase, TRAF=TNF-receptor-associated factor, TAK=TGF-β-activated kinase, IKK=inhibitor of NF-κB kinase, RICK= receptor-interacting ser/thr-kinase. For further abbreviations see the list at page XVII. Adapted from BAUMGART et al. [30].

In an experimental study it was shown, that some bacterial species of the luminal flora influence the intraepithelial expression of cyto- and chemokines [147]. Thus, their coexistence and interaction with the epithelial barrier and innate immune cells relies on a delicate balance governed by pattern recognition receptors (e. g. Toll like receptors (TLR))

expressed on epithelial and immune cells. These receptors detect antigens expressed by intestinal bacteria and upon their activation then induce several pro-inflammatory intracellular signaling cascades [30] that maintain the proper barrier function and keep the microbial-host interaction under tight control. As described above, an exceeding activation of this cascades is an initial event triggering the onset of IBD.

In all these complex interaction between genetic, luminal and environmental factors that normally warrant an appropriate mucosal immune response but are out of balance during IBD, the loss of integrity of the intestinal barrier has a pathologic key role [122].

Smoking is one environmental factor, diminishing the inflammatory phenotype of UC. Experimental studies suggest that the beneficial effect of nicotine, in respect to the inflammatory phenotype of IBD, is a result of an increased mucus production in the gut, strengthening the epithelial barrier function [45, 96].

3.1 IBD and colorectal cancer

Inflammatory bowel disease goes along with an increased risk for developing colitis-associated cancer (CAC). Such a colitis driven carcinogenesis is the main reason for mortality in patients suffering from IBD [60]. Although, the molecular mechanisms underlying CAC are not fully understood yet, it is assumed that they differ from the typical development pattern of sporadic colorectal carcinomas (CRC) (figure 3.3) [168, 59]. While *β-catenin* mutations are found in more than 90 % of all sporadic CRC, they occur rarely in CAC. The CRC-typical *Apc* mutations emerge in CAC at a much later time point than in sporadically developing neoplasms, whereas *p53* and *k-ras* mutations appear rather early. Reactive oxygen species (ROS) contribute to the development of CAC in a much more pronounced manner than they do during sporadic CRC. The continuous depletion of epithelial cells during IBD leads to an increased proliferation rate in the remaining tissue, while increased levels of NF-κB counteract apoptosis in epithelial

cells. Bacterial translocation across the epithelial barrier is also discussed being a factor promoting the development of CAC [168].

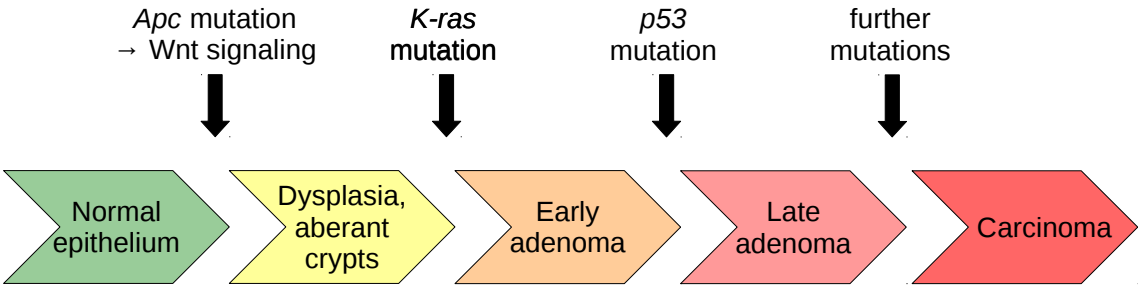

(a) Progression model sporadic colorectal cancer by VOGELSTEIN et al [59].

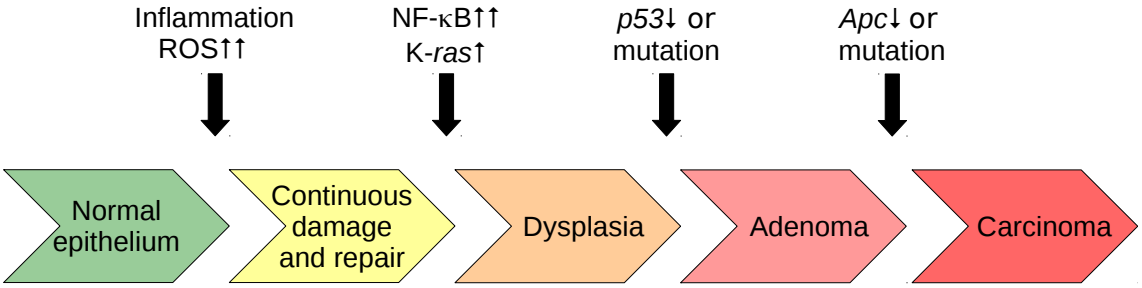

(b) Progression model of colitis-associated cancer by ROGLER et al [168].

Figure 3.3: Typical mutations occurring during sporadic and colitis-associated colorectal carcinogenesis. ↑ indicates a gain of function or increased levels, while ↓ indicates a loss of function.

3.2 M1 Macrophages in IBD in CAC

The infiltration of the LP with M1 MΦ is a critical step not only during the initial phase of acute and chronic colitis but also during the inflammation's progression. This pertains for human colitis and CAC as well as for murine DSS induced colitis (sec. 3.4) [192, 28]. These MΦ actively contribute to IBD by damaging the epithelial cell layer integrity and disrupting its barrier function [116]. While there was some controversy in the past, in which extend the expression of the iNOS and the release of RNS contributes to the pathogenesis of IBD in humans, newer studies clearly emphasize its importance for the onset as well for the progression of the disease [190, 56, 116].

Pro-inflammatory M1 polarized MΦ play an important role, especially during the onset phase of colitis associated carcinogenesis [171]. In later stages of colorectal cancer, tumor associated M2 polarized macrophages also contribute to the progression of the disease, mainly by suppressing the somatic antitumorigenic immune response.

3.3 The role of cellular E-cadherin and β-catenin in IBD and CAC

3.3.1 E-Cadherin

E-Cadherin, which belongs to the type I cadherins, is a single-pass transmembrane protein of 728 aa. It consists of five extracellular, one transmembrane and one intracellular domain, whereby the latter comprises its C-terminal end [197, 196]. In humans it is encoded by the *Cdh1* gene. Like all cadherins, E-cadherin is a calcium dependent protein, meaning it needs Ca^{2+} ions as cofactor to exert its functional properties. In its quaternary structure it appears as homodimer [197, 196]. Besides its function in intercellular junctions (sec. 1.3.3), E-cadherin is also involved in a variety of signal transduction processes [50, 105, 36, 37]. Several authors reported a dysregulation of E-cadherin in the intestinal mucosa during inflammatory processes and CAC [98, 130, 50, 36].

3.3.2 β-Catenin

β-Catenin is a protein of 85 kDa (781 aa) encoded by the *Ctnnb1* gene [109]. Besides its function in intercellular junctions (sec. 1.3.3) it plays an important role in signal transduction processes and as transcriptional cofactor [204]. Most notable is its involvement in the Wnt pathway, which plays an important role during embryonal development and carcinogenesis [120]. A number of studies reported an altered expression as well as an altered intracellular localization of β-catenin during IBD and CAC [130, 98, 36, 99].

3.4 The AOM/DSS-mouse-model

During the last decades several animal models were developed to study the pathogenesis of IBD and CAC. Although these models can not cover all aspects of the disease mechanisms in human IBD, they are valuable tools for investigating disease contributing factors [213, 212]. The application of dextran sodium sulfate (DSS) is a well-established model that has been used for over two decades to study mucosal inflammation [213]. However, the mechanisms underlying the effects of DSS have only been partially elucidated [51].

DSS is the sodium salt of the sulfated polysaccharide dextran (figure 3.4a). Usually, it is administered *ad libitum*, solved in drinking water in a concentration range from 0.5 g/l up to 50 g/l [158]. The main effect by which orally applied DSS induces a colitis, is its acute toxicity to the intestinal epithelium. Within 24 h, the epithelial expression of pro-inflammatory cytokines (e.g. TNF, IL-1β and IFN-γ) increases and the epithelial barrier starts to disintegrate as indicated by the growing loss of of proteins from the zonula occludens family [158]. First histological changes in the form of basal crypt loss and an increased mucosal infiltration by immune cells can be seen from day three [158]. These morphological changes are accompanied by an altered expression of tight junction proteins, such as occludin, claudin-1, -3, -4 and -5 as well as altered rates of proliferation and apoptosis in endothelial cells. DSS-induced tumorigenesis can be observed after about 30 weeks as consequence of sustaining inflammation [51].

Interestingly, germ free animals present only a very mild response to DSS, indicating a contribution of the commensal gut microbiome to diseases progression [93, 149].

DSS can be used to induce an acute or chronic inflammation, depending on its concentration and application intervals [158]. For instance, a DSS-administration over seven days at a high dose[21] causes an acute inflammation, while the administration of a low dose in three 7-day-cycles interrupted by recovery phases of seven days each, triggers a chronic inflammation. Whether the phenotype of a chronic inflammation corresponds more to

[21] Exactly concentrations depending among other factors on the used mouse-strain.

the clinical manifestation of CROHN's disease or ulcerative colitis, strongly depends on the molecular weight of the DSS used[22] [104, 91]. While DSS of 5 kDa triggers a CD-like phenotype, administration of DSS with a molecular weight of 40 kDa provokes a UC-like phenotype.

Besides concentration and application intervals, many other factors influence the outcome of a DSS-induced colitis and carcinogenesis [158]. Commercially available DSS is purchased in batches with a molecular weight between 5 kDa and 1 400 kDa. Most severe colitis in BALB/c mice was observed in animals treated with DSS of 40 kDa, while the application of 5 kDa DSS resulted in a less pronounced colitis [91, 104]. Animals treated with DSS of 500 kDa or more exhibited no lesions in the large intestine. Mice with different genetic background or gender show a distinct response to DSS. The same is true for different housing conditions and concomitant differences in the composition of the intestinal microbiome [121, 131].

One measure to increase the tumorigenicity of DSS is the additional administration of azoxymethane (AOM, figure 3.4b) [51]. AOM, which itself exhibits an own tumorigenic effect, is a metabolite of 1,2-dimethylydrazine, a precursor of biomolecules found in cycad flour [115]. After administration to the host, AOM requires further metabolic activation steps to induce DNA-reactive adducts. The main effect of AOM-derived metabolites is the methylation of guanine at its O6- or N7-position, resulting in the formation of promutagen lesions [52, 51]. Thus, the combined administration of AOM and DSS usually reduces latency time for tumor formation to 10 weeks compared to about 30 weeks in a pure DSS-model [51].

[22] The exact experimental conditions applied in this project are described in section 10.

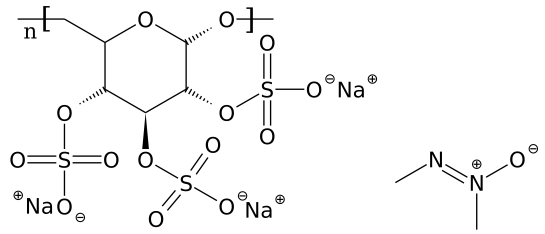

(a) DSS **(b)** AOM

Figure 3.4: Structural formulas of (a) DSS and (b) AOM.

Typically, AOM is applied as single or repeated dose by intra-peritoneal (i.p.) injection at a concentration of 20 $\mu g/g$ body weight prior to and/or during the DSS-administration [51].

Numerous different AOM/DSS-protocols have been described in the literature [169, 155, 38, 152, 35, 34, 198], accounting for the great variations of this model with respect to intrinsic or extrinsic factors which could influence the experimental outcome. Thus, it is necessary to develop an individual protocol adjusted to the specific experimental setup and questions posed.

4 IER3

In 1993 Charles et al. [40] identified a new growth factor-inducible immediate-early gene, encoding a short-living glycosylated protein in mice. Later it came up, that this gene was the murine orthologue of a human X-ray inducible immediate early gene cloned by Kontratyev et al. in 1996 [106]. The same year, Schaefer et al. cloned its rat orthologue [176]. While this gene initially named *Gly96*, *Iex-1*, *Prg2* or *Dif2*, it is since 2002 officially termed as *immediate early respone-3* (*Ier3*) [141].

Structurally, IER3 is highly conserved between different eutheria. Human IER3 comprises 156 amino acids (aa), while its murine and rat orthologues have a length of 153 and 160 aa, respectively. Interestingly, the sequence motif of *Ier3* shows no similarity with other

known vertebra genes [26]. Thus, it is not possible to identify putative cellular functions by comparing its tertiary structure to other proteins. However, several domains, like a putative transmembrane domain [106], a potential glycosylation site [106], a Ser/Thr phosphorylation site [66], a nuclear localization site as well a PEST like sequence [111] could be identified in all orthologues.

The human *Ier3*-gene consist of two exons interrupted by an 112 bp intron [26]. There is only one spliced mRNA variant expressed *in vivo* [174], while other reported expression variants [214] turned out as artifacts. A great number of binding motifs for regulated transcription factors could be identified in the promoter region of *ier3*, indicating its involvement in various cellular responses to quite distinct stimuli [26].

Ier3 expression is triggered in response to variety of different cellular stress related stimuli like radiation, increased levels of reactive oxygen species, immunogenic cytokines or apoptotic stimuli [26]. Several studies demonstrated the interdependency between IER3- and NF-κB expression [24, 25]. The *Ier3* promoter sequence not only contains a binding motif for NF-κB itself, but also binding motifs for other transcription factors under control of NF-κB [26]. In turn, IER3 acts as an NF-κB inhibitor as part of a tightly regulated negative feedback loop (figure 4.1a) [26]. Furthermore, a mutual modulation of IER3 and proteins involved in the regulation of proliferation and apoptosis like ERK, AKT, P53 or cMYC was reported [92, 95, 167]. However, there is some controversy in which way IER3 contributes to cellular proliferation and survival in different cell types. While Rocher et al. [167] demonstrated an IER3 mediated sustaining of ERK signaling in promegakaryoblasts in response to growth stimuli (fig. 4.1b), Osawa et al. [154] reported an negative interference between IER3 and AKT in hepatocytes.

IER3-triggered apoptosis in response to different apoptotic stimuli was shown for a wide range of cell types [22, 23, 25, 80, 177, 26]. Another study identified IER3 as part of P53 mediated apoptosis in response to DNA damage [175]. In contrast, anti-apoptotic effects of IER3 were shown in T-cells from transgenic mice [220] and in some laboratory cell-lines [181].

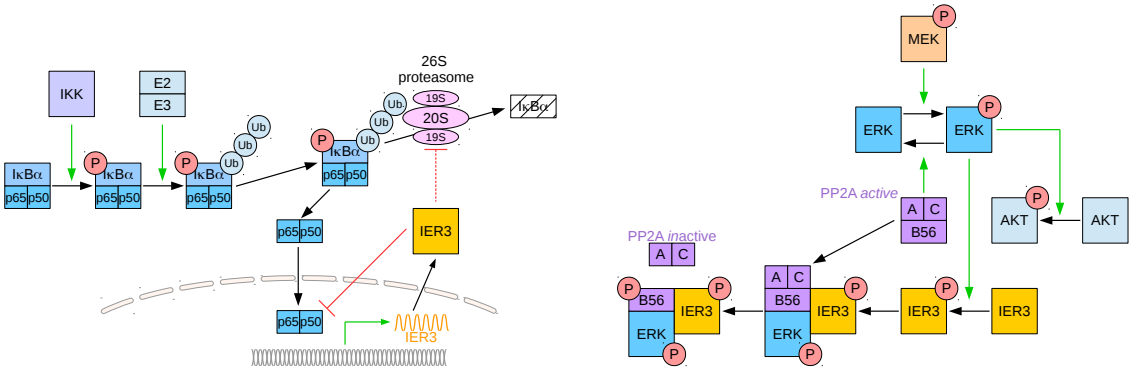

(a) Negative feedback loop regulation between NF-κB and IER3 described by ARLT et al. [24, 25]. While being a direct expression target of NF-κB mediated transcription, IER3 inhibits the activity of NF-κB (p65/p50) by two distinct mechanisms. First, nuclear IER3 interacts with the transactivation domain of p65, thereby suppressing the NF-κB mediated activation of certain gene promoters. Furthermore, IER3 indirectly attenuates the proteasomal activity by negatively interfering with the expression of proteasomal genes, resulting in a decreased IkBα degradation.

(b) IER3 mediated sustaining of ERK signaling in promegakaryoblasts described by Rocher et al. [167]. As a direct downstream target of P-ERK, P-IER3 interacts directly with PP2A and P-ERK, causing to a phosphorylation of the PP2A's B56 subunit leading to its inactivation. As conesquence the PP2A mediated P-ERK dephosphorylation is attenuated, resulting in an increased phosporylation of further P-ERK targets like AKT.

Figure 4.1: Exemplary illustration of the involvement of IER3 in different cellular signaling pathways. Adapted and modified after ARLT et SCHAEFER [26]. For abbreviations see list on page XVII.

Summarizing these results, IER3 seems to exhibit both, pro- as well as anti-apoptotic effects. The outcome of the actions of IER3 is influenced by several factors like the expression of other pro- or anti-apoptotic stimuli and the cellular context. Another important role have compartment specific effects of IER3, depending on the tissue type in which it is expressed [26].

4.1 IER3 in colitis and colitis associated cancer

A genome-wide microarray based mRNA-expression-analysis (figure 4.2) identified *ier3* as one of the most overexpressed genes in patients suffering from CD or UC, the both major manifestations of IBD [46]. The possible effect of this overexpression is a matter of some debate: One theory postulates, that the *Ier3*-overexpression is an initially or disease triggered event, actively contributing to the disease progression [18]. The other theory argues, that the *ier3*-overexpression is a physiological response to the exaggerated inflammation that finally manifests as a permanent but futile attempt

to reduce the inflammatory burden [183]. Both theories are supported by obviously contrary experimental results. A recent study conducted by Sina et al. [183] used a constitutive *Ier3*-knockout mouse-model. After exposing the animals to several cycles of dextran sodium sulfate (DSS) solved in drinking water, mice with ablated IER3 showed a pronounced disease phenotype compared to the wild-type cohort. This came up with severe erosions of the diseased colon epithelium, indicated by the loss of a regular crypt architecture and considerable infiltration of inflammatory cells such as macrophages. A striking feature along with the forced inflammatory response in IER3-deficient mice was the enhanced release of pro-inflammatory cytokines and greater activation of NF-κB. This was particularly shown for macrophages. Contrary, Ustyugova et al. [202] reported, that IER3-deficient mice are characterized by an ameliorated inflammatory response in a combined azoxymethane/DSS-model, along with a declined incidence of colorectal cancer.

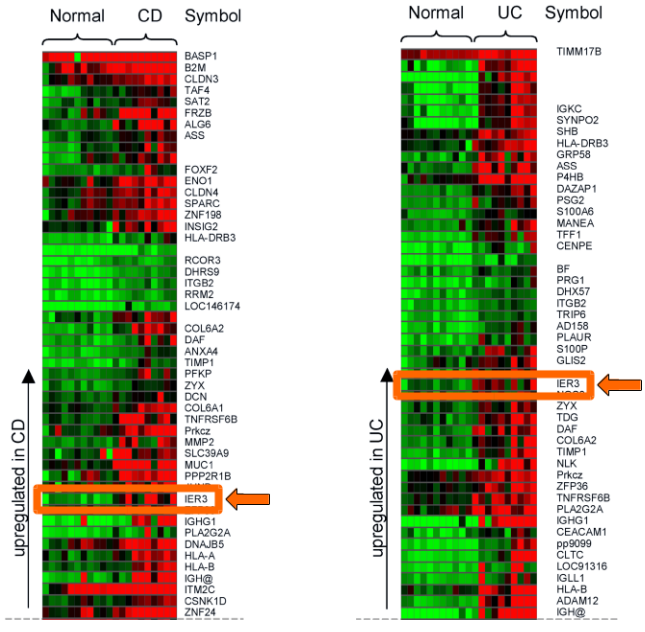

(a) *Ier3*-expression in CD. **(b)** *Ier3*-expression in UC.

Figure 4.2: Microarray based mRNA-expression-analysis in colon tissue from (a) CD- and (b) UC-patients. Green fields indicate a relative underexpression while red fields indicate an overexpression. Row of *ier3*-expression is marked by an orange box and arrow. Adapted from Costello et al. [46].

There are several possibilities which could explain the discrepancy between those findings,

e.g. mice-strains used for both experiments consisted of different genetic backgrounds and housing conditions. It was shown, that these both factors have a considerable impact on the progression of DSS-induced colitis and colitis associated carcinogenesis [158]. Furthermore, the mice used by Wu et al. comprised besides the IER3 deficiency also a depletion of the *rag*-gene. Thus, *Ier3* depletion in distinct cellular compartments seems to differently affect the outcome in DSS colitis and for this reason these two contrary studies are not comparable. Accordingly, an important conclusion from the discrepant results was that only a compartment specific depletion of IER3 can unveil its contribution to IBD and colitis associated colorectal cancer. For this purpose, our group generated a conditional *Ier3* knock-out mouse model based on the Cre/loxP-system[23] (see section 4.2) that allows a compartment specific deletion of this gene.

4.2 Specific depletion of IER3 in the myeloid or enterocyte compartment

As mentioned above, macrophages, which belong to the lineage of myeloid-derived cells [201, 129], are one cell-type contributing in a distinct manner to the progression of IBD and CAC. For this study, we used the Cre/loxP-system [165, 112] to investigate the impact of the specific knockout of *ier3* in these cells.

The enzyme Cre-recombinase (Cre) is a λ-integrase of 38 kDa encoded in the genome of the bacteriophage P1. It plays an important role in the life cycle of the bacteriophage by catalyzing DNA rearrangements between its own and the hosts genome in a topoisomerase-like manner [16, 146, 206]. Cre recognizes a specific DNA-sequence of 34 bp denoted as *loxP* (locus of X-over P1). In an arbitrary genomic DNA-sequence flanked by a *loxP*-sequence each at its 5'- and 3'-site[24], Cre causes a site specific recombination event, depending on the orientation of the *loxP*-sequences [194]. If both *loxP*-sites are orientated in the same direction, the intermediary DNA-sequence gets cut

[23] The generation was conducted in cooperation with Genoway.
[24] Such a site is commonly termed as "floxed".

out together with one of the *loxP*-sequences, while the other *loxP*-sequence remains in the genome (figure 4.3) [194].

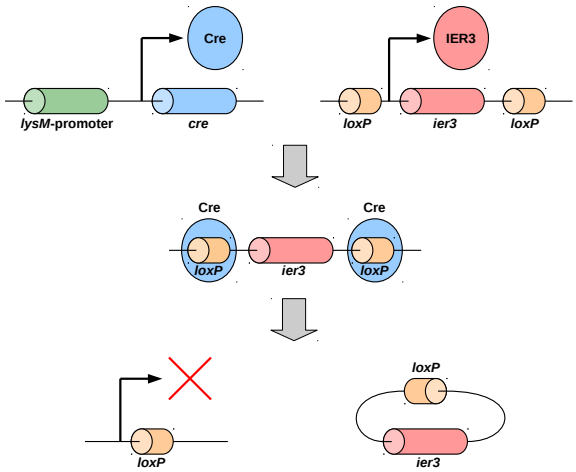

Figure 4.3: Exemplary illustration of the Cre/loxP-system using the example of a *lysM*-promoter-regulated Cre-expression and *ier3* as target-gene flanked by similar orientated *loxP*-sequences. For detailed information, see the continuous text.

In 1992 Orban et al. [153] reported of a mouse-model based up on the Cre/loxP-system to perform a tissue-specific gene-knockout, by putting the Cre-expression under the control of a tissue specific gene promoter.

Lysozyme M (LysM) is a murine derived hydrolase encoded by the *Lyz*-gene, exclusively expressed in cells of the myeloid lineage [48]. By crossing mice whose *Ier3*-gene is flanked on both sides by similar orientated *loxP*-sequences (*Ier3-flox*) with mice containing the *Cre*-gene under control of the *LysM*-promoter (*LysM-Cre*) we were able to generate mice with a specific depletion of IER3 in the myeloid compartment (*Ier3-flox*$^{+/+}$ *LysM-Cre*$^{+/+}$).

As one of the tissue compartments mostly affected by IBD and CAC, we also investigated the effects of an enterocyte specific IER3 depletion. For this purpose we used an *Ier3-flox/Cre* mouse model with the *Cre*-gene under control of the enterocyte specific villin promoter (*Vil-Cre*).

5 Aim

Aim of this project was to study the effects of myeloid *Ier3*-deficiency (thus in macrophages) on the onset and progression of colitis as well as on colitis associated carcinogenesis *in vivo*. These findings were compared to the effects of *Ier3* depletion in other tissue compartments.

Additionally, the molecular and cellular mechanisms underlying these effects were elucidated in detail by *in vivo* and *in vitro* experiments.

Materials and Methods

6 Devices

Table 6.1 lists the devices used in this project.

Table 6.1: List of used devices.

Device	Model	Company
Autoclave	5075 ELVC	Tuttnauer, (Breda, Netherlands)
Centrifuge I	Megafuge™ 1.0	Heraeus (Hanau, Germany)
Centrifuge II	5804R	Eppendorf (Hamburg, Germany)
Compartment dryer	B 6200	Heraeus (Hanau, Germany)
ECL imaging system	ChemiDocXRS™	BioRad (Munich, Germany)
Flow cytometer	FACS-Verse™	BD (Franklin Lakes, USA)
Fluorimeter	F200	Tecan (Maennedorf, Switzerland)
Grinding mill	MM400	Retsch (Haan, Germany)
Incubator	BBD 6220	Thermo (Waltham, USA)
Laboratory scale	PT1200	Sartorius (Goettingen, Germany)

Continuation on next page.

Continuation of table 6.1

Device	Model	Company
Laminar flow cabinet	Herasafe™	Heraeus (Hanau, Germany)
Magnetic stirrer	Ikamag RCT	IKA (Staufen, Germany)
Micro scale	CP1245-0CE	Sartorius (Goettingen, Germany)
Microscope 1 (transmission light)	Axiovert™ 25	Carl Zeiss (Jena, Germany)
Microscope 2 (transmission light + reflected light fluorescence)	Axioplan™ 2	Carl Zeiss (Jena, Germany)
Microscope 3 (LSM)	LSM800	Carl Zeiss (Jena, Germany)
Microscope 4 (scanning system)	BZ-II	Keyence (Osaka, Japan)
Microtome	HM 430	Micron (Boise, USA)
Microwave oven	M686	Miele (Guetersloh, Germany)
PCR cycler	2720	Thermo (former ABS, Waltham, USA)
PCR gradient cycler	T3000	Biometra (Goettingen, Germany)
Plate photometer	Opsys MR	Dynex (Denkendorf, Germany)
Power supply #1	P25	Biometra (Goettingen, Germany)

Continuation on next page.

Continuation of table 6.1

Device	Model	Company
Power supply #2	500	Desaga (Wiesloch, Germany)
pH-meter	pH537	WTW (Weilheim, Germany)
Realtime PCR device	CFX-Connect™	BioRad, (Hercules, USA)
Roller mixer	SRT6D	Bibby (former Stuart), Staffordshire, UK)
Spectrophotometer	Nanodrop™ ND-1000	Peqlab (Erlangen, Germany)
Thermomixer	5436	Eppendorf (Hamburg, Germany)
Thermostat	RM20	Lauda (Lauda-Koenigshofen, Germany)
Tumbling table	WT17	Biometra (Goettingen, Germany)
UV imaging system	Multiimage I	Alpha-Innotec (Kasendorf, Germany)
Vortex mixer	MS1	IKA (Staufen, Germany)
Water bath	U3	Julabo (Seelbach, Germany)
Water purification device	Labostar™	Siemens (Berlin, Germany)

7 Consumables

7.1 Cell culture vessels

Vessels used for cell culture are listed in table 7.1. They were either purchased from AFC (Courbevoie, France), Sarstedt (Nuembrecht, Germany) or VWR (Darmstadt, Germany).

Table 7.1: Cell culture vessels.

Label	Company	Order no.
T75 culture flask for adherent cells exc. MΦ	Sarstedt	83.3910.002
T75 culture flask for sensitive adherent cells	Sarstedt	83.3911.302
T75 culture flask for RAW264.7 and suspension cells	Sarstedt	83.3911.502
VueLife^{TM} FEP bags (C series)	AFC	2PF-0032-C
Petri dish ⌀=92 mm (untreated PS)	Sarstedt	82.1473.001
6-well culture dish for adherent cells exc. MΦ	Sarstedt	83.3920
6-well culture dish for sensitive adherent cells	Sarstedt	83.3920.300
6-well culture dish for RAW264.7 and suspension cells	Sarstedt	83.3920.500
6-well culture dish for MΦ (untreated PS)	VWR	734-2777
6-well Transwell TC inserts, pore size: 0.4 µm	Sarstedt	83.3930.041
12-well culture dish for adherent cells exc. MΦ	Sarstedt	83.3921
12-well culture dish for MΦ (untreated PS)	VWR	734-2778
12-well Transwell TC inserts, pore size: 0.4 µm	Sarstedt	83.3931.041
24-well culture dish for adherent cells exc. MΦ	Sarstedt	83.3922
24-well culture dish for sensitive adherent cells	Sarstedt	83.3922.300
24-well Transwell TC inserts, pore size: 0.4 µm	Sarstedt	83.3932.041
96-well culture dish for adherent cells exc. MΦ	Sarstedt	83.3924.300

7.2 Kits

A list of the kits used for this project is given in table 7.2.

Table 7.2: List of used kits.

Application	Product name	Company	Order no.
Flow cytometry staining	Fixation / Permeabilization kit™ for flow cytometry	BD (Franklin Lakes, USA)	554714
Protein quantification assay	DC™ protein assay	BioRad (Hercules, USA)	500-0116
ECL substrate/reaction kit I for wb	ECL clarity™ kit	BioRad (Hercules, USA)	170-5061
ECL substrate/reaction kit II for wb	ECL super signal™ kit	Thermo (Waltham, USA)	34096
Occult blood detection kit	Haemoccult™ kit	Beckman (Brea, USA)	PZN: 01933716
PCR	PeqGold™ Taq-DNA-Polymerase kit	VWR (Darmstadt, Germany)	PEQL 01-1020
RNA extraction and purification kit	RNeasy™ kit	Qiagen (Hilden, USA)	74106
RT-PCR	RevertAid™ Reverse Transcriptase kit	Thermo (Waltham, USA)	EP0442

7.3 Further consumables

PVDF membranes for western blot were purchased from Roth (Karlsruhe, Germany; order no. T830.1). Further consumable materials were purchased from B. Braun (Melsungen, Germany), Eppendorf (Hamburg, Germany), Roth (Karlsruhe, Germany), Sarstedt (Nuembrecht, Germany), Thermo (Waltham, USA) and VWR (Darmstadt, Germany).

8 Reagents

8.1 Water

8.1.1 Ultrapure water

Ultrapure water was generated by using a laboratory own purification device (Siemens Labostar^{TM}) based on ion exchange, reverse osmosis and ultrafiltration.

8.1.2 Sterile and nuclease free water

Sterile, RNase as well DNase free ultra pure water (Merck order no.: L0015) was used for DNA and RNA treatment as well as for sterile applications.

8.1.3 Drinking water for experimental mice

Autoclaved taped water served as drinking water for the experimental mice. This water was also used to prepare the DSS drinking solutions.

8.2 Commercially available reagents, solutions, buffers and cell culture media

Reagents, solutions, buffers and cell culture media were purchased from Biochrom (Berlin, Germany), Biomol (Hamburg, Germany), Biozym (Hamburg, Germany), Corning (New York, USA), Dako (Jena, Germany), Fermentas (Waltham, USA), Gibco (Carlsbad, USA), Invitrogen (Carlsbad, USA), Menarini (Florence, Italy), Merck (Darmstadt, Germany), MP Biomedicals (Eschwege, Germany), Peprotech (Hamburg, Germany), Ratiopharm (Ulm, Germany), R&D Systems (Minneapolis, USA), Roth (Karlsruhe, Germnay), Sigma-Aldrich (St. Louis, USA), Thermo (Waltham, USA) and Tocris (Bristol, UK).

8.2.1 Growth factors, cytokines and stimulants

Growth factors, cytokines and stimulants used in cell culture are listed in table 8.1. Table 8.2 lists the stock solutions of the exogenous nitric oxide donor S-nitroso-N-acetylpenicillamin (SNAP) as well as the iNOS inhibitor 1400W used for *in vitro* cell culture experiments. Their structural formulas are given in figure 8.1.

Table 8.1: Growth factors and stimulants for cell culture.

Label	Company	Order no.	Stock solution
Rec. mouse EGF	Gibco	PMG8044	100 µg/ml in PBS containing 1 g/l BSA; sterile; aliquots á 50 µl, stored at -80 °C.
Rec. mouse GM-CSF	Peprotech	SRP3201	20 µg/ml in aqueous sucrose solution 50 g/l; sterile, aliquots á 50 µl; stored at -80 °C.
Rec. mouse IFN-γ	R&D Systems	485-MI-100	100 µg/ml[25] in PBS containing 1 g/l BSA; sterile; aliquots á 50 µl; stored at -80 °C.
LPS	Sigma-Aldrich	L7895	1 mg/ml in water; sterile; aliquots á 50 µl; stored at -20 °C.
Rec. mouse M-CSF	Peprotech	SRP3221	20 µg/ml in aqueous sucrose solution 50 g/l; sterile; aliquots á 50 µl; stored at -80 °C.
Rec. mouse Noggin	Peprotech	250-38	100 µg/ml in PBS containing 1 g/l BSA; sterile; aliquots á 50 µl; stored at -80 °C.
Rec. human normal insulin	Menarini	PZN: -07221224[26]	100 IU/ml ready to use formulation; sterile; stored at 4 °C.
Rec. mouse R-Spondin-1	Peprotech	315-32	100 µg/ml in PBS containing 1 g/l BSA; sterile; aliquots á 50 µl; stored at -80 °C.
Rec. mouse Wnt-3a	Peprotech	315-20	50 µg/ml in PBS containing 1 g/l BSA; sterile; aliquots á 50 µl, stored at -80 °C.
Y-27632·2 HCl	Tocris	1254	10 mmol/l in PBS; sterile; aliquots á 50 µl, stored at -20 °C.

[25] ≙ $843 \cdot 10^3$ IU/ml.

[26] This formulation is free of preservatives.

Table 8.2: Nitric oxide donor and iNOS inhibitor.

Name	Company	Order no.	Stock solution
SNAP	Sigma-Aldrich	N3398	100 mmol/l in dried DMSO, sterile, light protected, aliquots á 50 µl, stored at -80 °C, not re-frozen/ re-thawed.
1400W	Sigma-Aldrich	W4262	4 mmol/l in dried DMSO, sterile, aliquots á 20 µl, stored at -80 °C.

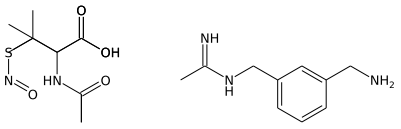

(a) SNAP **(b)** 1400W

Figure 8.1: Structural formulas of the nitric oxide donor SNAP and the iNOS inhibitor 1400W.

8.2.2 Animal experiment reagents

Reagents used for animal experiments are listed in table 8.3.

Table 8.3: Reagents used for animal experiments.

Label	Company	Order no.
AOM	Sigma-Aldrich	A5486
DSS (M=36 kDa-50 kDa)	MP Biomedicals	216011090

8.2.3 FITC conjugated dextrans

FITC-conjugated dextrans (fig. 8.2) used for permeability experiments are listed in table 8.4.

Table 8.4: FITC conjugated dextrans used for permeability experiments.

Label	Approx. MW	Approx. Stokes radius	Company	Order no.
FD4	4000 g/mol	14 Å	Sigma-Aldrich	FD-4
FD10	10000 g/mol	23 Å	Sigma-Aldrich	FD-10S

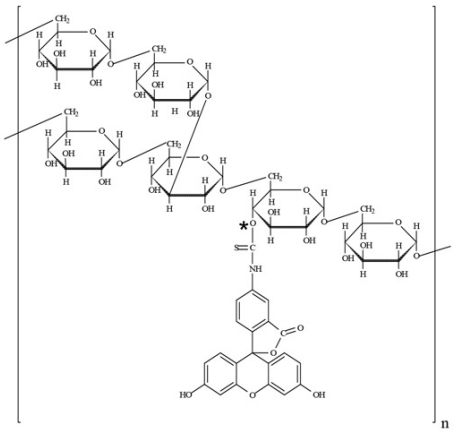

Figure 8.2: Structural formula of FITC dextran. *: The site of attachment of FITC is randomly associated with any free hydroxyl group. Adapted from [11].

8.2.4 Further commercially available reagents, solutions, buffers and cell culture media

Table 8.5 lists further commercially available reagents, solutions, buffers and cell culture media. Additional chemicals and reagents, which are not listed here, were purchased from the companies listed above. Their degree of purity conformed at least as *pro analysis* or equal.

Table 8.5: List of commercially available reagents, solutions and cell culture media.

Label	Company	Order no.
General reagents, solutions and buffers:		
BSA	Biomol	01400
FCS	Biochrom	S0115
HBSS	Biochrom	L2045
PBS (DULBECCO), sterile	Biochrom	L1842
Cell culture:		
Accutase™	Merck	SCR005
CellStripper™ solution	Corning	25-056-CI

Continuation on next page.

Continuation of table 8.5.

Label	Company	Order no.
DMEM[27]	Biochrom	F0435
DMEM$^{w/o\ PR}$	Biochrom	F0475
DMEM/F-12 (1:1)	Biochrom	F4815
Gentamycine solution	Ratiopharm	PZN: 3942435
Glutamine solution	Biochrom	K0283
HEPES solution	Gibco	15630-056
Na-pyruvate solution	Biochrom	L0473
P/S soulution	Biochrom	A2213
RPMI 1640	Biochrom	F1640
Trypsin/EDTA solution	Biochrom	L2143
DNA-PAGE, SDS-PAGE and western blot:		
100 bp DNA ladder	Invitrogen	15628-019
Acrylamide solution (Rothiphorese^{TM}) 40 %	Roth	T802.1
Antibody stripping solution	Merck	2504
Aprotinin solution	Sigma-Aldrich	A6279
APS	Merck	1.01201
Ethidium bromide stock solution	Roth	161-0433
PageRuler^{TM} protein ladder	Thermo	26619
Phosphatase inhibitor cocktail #2	Sigma-Aldrich	P5726
Phosphatase inhibitor cocktail #3	Sigma-Aldrich	P0044
Skim milk powder	Roth	T145.3
TEMED	Roth	2367.3
Genotyping, PCR, RT-PCR and qPCR:		
10x RXN buffer	Invitrogen	Y02028
Biozym Blue S'Green qPCR mix	Biozym	331416
dNTP's 10 mmol/l	Fermentas	R0192
Magnesium chloride solution	Invitrogen	Y02016
Oligo(dT)$_{18}$ primer	Thermo	S0132
Quick Extract DNA solution 1.0	Biozym	QE0905
RiboLock^{TM} RNase inhibitor	Thermo	EO0381
Taq DNA polymerase	Invitrogen	18038-042

Continuation on next page.

[27] This DMEM formulation contains 4.5 g/l glucose, 3.7 g/l $NaHCO_3$ and no pyruvate. Without the addition of further buffers, it requires a atmospheric CO_2concentration of 10 % (v/v) to acquire a pH-value of 7.4.

Continuation of table 8.5.

Label	Company	Order no.
ICC and IHC:		
AEC substrate chromogen	Dako	K3464
Buffered formaline, ≥37 %, stabilized, acid free	Merck	1.039993
EnVision+^{TM} anti mouse polymer (HRP-conjugated)	Dako	K4000
EnVision+^{TM} anti rabbit polymer (HRP-conjugated)	Dako	K4002
Eosin Y solution	Merck	1.09844
FluorSave^{TM} mounting medium	Merck	345789
Hoechst bisbenzimide H33258	Calibochem	382061
Immersion oil for microscopy	Roth	X899.1
KAISER's glycerol gelatine	Merck	109242
MAYER's haematoxylin	Merck	1.09249
Proteinase K solution (600 $^{mAnU}/_{ml}$)	Merck	1.07393

8.3 Self prepared solutions, buffers and cell culture media

Self prepared solutions, buffers and cell culture media are listed in table 8.6. If not mentioned else, cell culture media were stable for approximate 14 days when stored at 4 °C. All other solutions were stored at RT if not mentioned else.

Table 8.6: List of self prepared solutions, buffers and cell culture media.

Label	Composition			
General buffers:				
Glycine buffer stock soln. 1	0.5	$^{mol}/_{l}$	Glycine in water	
Glycine buffer stock soln. 2	0.5	$^{mol}/_{l}$	Na-Glycinate in water	
Glycine buffer 0.5 $^{mol}/_{l}$, pH 9.6	≈1.0	VP	Stock soln. 1	PH adjusted by mixing stock soln. in correct ratio.
	≈1.0	VP	Stock soln. 2	

Continuation on next page.

Continuation of tab. 8.6.

Label	Composition			
MACS buffer	5.0	g/l	BSA	Always prepared fresh.
	2.0	mmol/l	Na_2-EDTA	
			in PBS, pH 7.4	
PBS pH 7.4[28]	8.1	g/l	NaCl	
	0.2	g/l	KCl	
	1.44	g/l	Na_2HPO_4	
	0.25	g/l	KH_2PO_4	
			in water	
			adjusted to pH 7.4 with HCl/NaOH soln.	
10x TRIS / borate / EDTA-buffer (10x TBE)	0.45	mol/l	TRIS base	
	0.45	mol/l	H_3BO_4	
	5.0	mmol/l	EDTA	
			in water	
TRIS buffered saline (TBS)	2.0		TRIS base	
	14.0	mmol/l	NaCl	
			in water	
			adjusted with HCl-soln. to pH 7.6	
Cell culture media:				
CaCo-2 medium	20.0	% (v/v)	FCS	
	2.0	mmol/l	L-Glutamine	
	1.0	mmol/l	Na-Pyruvat	
	5.0	mmol/l	HEPES	
			in DMEM	
HT-29 medium	10.0	% (v/v)	FCS	
	2.0	mmol/l	L-Glutamine	
			in Mc Coy's 5A modified medium	
IEC-6 medium	5.0	% (v/v)	FCS heat inactivated[29]	
	2.0	mmol/l	L-Glutamine	
	1.0	mmol/l	Na-Pyruvat	
	0.1	IU/ml	Rec. human normal insulin	
			in DMEM / F-12	

Continuation on next page.

[28] For sterile or nuclease / proteinase sensitive applications a commercial ready-to-use solution was used.

[29] 56 °C for 30 min.

Continuation of tab. 8.6.

Label	Composition				
Macrophage basal medium (MΦ-M.)	2.5	% (v/v)	FCS		
	2.0	mmol/l	L-Glutamine		
	1.0	mmol/l	Na-Pyruvat		
	100.0	IU/ml	Penicillin		
	0.1	g/l	Streptomycin		
	40.0	mg/l	Gentamycin		
			in DMEM / F-12		
Macrophage differentiation medium($M\Phi^{diff.}$-M.)	50.0	ng/ml	mM-CSF		Added just before application.
	50.0	IU/ml	mIFN-γ		
			in macrophage basal medium		
Macrophage cultivation medium ($M\Phi^{cult.}$-M.)	20.0	ng/ml	mM-CSF		Added just before application.
	50.0	IU/ml	mIFN-γ		
			in macrophage basal medium		
Neutralization medium	10.0	% (v/v)	FCS		
			in DMEM		
Raji medium	10.0	% (v/v)	FCS		
	2.0	mmol/l	L-Glutamine		
			in RPMI 1640		
RAW264.7 medium	10.0	% (v/v)	FCS		
	4.0	mmol/l	L-Glutamine		
	5.0	mmol/l	HEPES		
			in DMEM		
YAMC basal medium	5.0	% (v/v)	FCS		Stable for 5 days at 4 °C.
	2.0	mmol/l	L-Glutamine		
	0.5	IU/ml	Rec. human normal insulin		
	5.5	mg/l	Transferrin		
	6.7	µg/l	Na_2SeO_3		
	10.0	µmol/l	1-Thioglycerol		
	1.0	µmol/l	Hydrocortisone		
	100.0	IU/ml	Penicillin		
	0.1	g/l	Streptomycin		
			in RPMI 1640		
YAMC culture medium	5.0	IU/ml	mIFN-γ		Added just before application.
			in YAMC basal medium		

Continuation on next page.

Continuation of tab. 8.6.

Label	Composition			
Protein extracts:				
RIPA stock solution	150.0	mmol/l	NaCl	Storage in aliquots at -20 °C. Thawing on ice. No re-freezing/thawing.
	50.0	mmol/l	TRIS/TRIS-HCl, pH 7.8	
	1.0	g/l	SDS	
	5.0	g/l	Na-Deoxycholat	
	1.0	% (v/v)	Triton X-100	
	5.0	mmol/l	Na_2-EDTA	
	1.0	mmol/l	EGTA	
	1.0	tbl./10 ml	Protease inhibitor	
			in water	
RIPA working solution	1.0	mmol/l	PMSF	Stock solutions stored at -20 °C. Addition just before application.
	1.0	mmol/l	DTT	
	1.0	mmol/l	Na_3VO_4	
optional	1.0	% (v/v)	PIC No2	Addition just before application.
optional	1.0	% (v/v)	PIC No3	
			in RIPA stock solution	
SDS-PAGE and western blot:				
4x Laemmli loading dye[30]	250.0	mmol/l	TRIS/TRIS·HCl pH 6,8	Storage at -20 °C.
	80.0	g/l	SDS	
	20.0	% (v/v)	2-Mercaptoethanol	
	30.0	% (v/v)	Glycerol	
	200.0	mg/l	Bromophenol blue	
			in water	
WB separating gel buffer, pH 8.8	1.5	mol/l	TRIS base	
	4.0	g/l	SDS	
			in water	
			adjusted with HCl-soln. to pH 8.8	
WB stacking gel buffer, pH 6.8	1.5	mol/l	TRIS base	
	4.0	g/l	SDS	
			in water	
			adjusted with HCl-soln. to pH 8.8	

Continuation on next page.

[30] This solution differs in composition distinctly from Laemmli's original formulation.

Continuation of tab. 8.6.

Label	Composition				
1x SDS-PAGE electrophoresis running buffer	25.0	mmol/l	TRIS base		
	192.0	mmol/l	glycine		
	1.0	g/l	SDS		
			in water		
WB blotting buffer A	300.0	mmol/l	TRIS base		
	20.0	% (v/v)	Methanol		
			in water		
WB blotting buffer B	25.0	mmol/l	TRIS base		
	20.0	% (v/v)	Methanol		
			in water		
WB blotting buffer C	25.0	mmol/l	TRIS base		
	20.0	% (v/v)	Methanol		
	5.0	g/l	Amino caproic acid		
			in water		
TBS-T for WB	0.05	% (v/v)	Tween-20		
			in TBS		
Skim milk powder based blocking and incubation solution for wb	50.0	g/l	Skim milk powder in TBS-T	☐	Always prepared fresh.
BSA based incubation solution for wb	50.0	g/l	BSA in TBS-T	☐	Always prepared fresh.
PCR and DNA-PAGE[31]					
Sucrose solution	300.0	g/l	Sucrose in water	☐	Storage at -20 °C.

Continuation on next page.

[31] PCR master mix and PAGE gel compositions are given in section 23.3 together with the respectively primer sequences and PCR-conditions.

Continuation of tab. 8.6.

Label	Composition				
SucRed solution	1.5	g/l	Cresol red		Storage at -20 °C.
	0.10	% (v/v)	TRIS/TRIS·HCl buffer, c=1.0 mol/l, pH 9.0		
	300.0	g/l	Sucrose in water		
Ethidium bromide staining buffer	1.0	mg/l	Ethidium bromide in 1x TBE		Stable for 1 week at RT.
ICC & IHC:					
Carnoy's fixative modified after Putchler	6.0	% (v/v)	Dried methanol		
	3.0	% (v/v)	Trichloromethane		
	1.0	% (v/v)	Dried acetic acid		
Lillie's formol	3.6	% (m/m)	Neutral formaline in PBS		Always prepared fresh.
Citrate antigen retrieval stock soln. A	0.01	mol/l	Citric acid in water		Storage at 4 °C.
Citrate antigen retrieval stock soln. B	0.01	mol/l	Na_3-Citrate in water		Storage at 4 °C.
Citrate antigen retrieval solution for histology, pH 6.0	≈9.0	% (v/v)	Stock solution A		Storage at 4 °C. Pre-warm to RT before use. PH adjusted by mixing stock soln. in correct ratio.
	≈41.0	% (v/v)	Stock solution B		
TRIS/EDTA antigen retrieval solution for histology, pH 9.0	10.0	mmol/l	TRIS/TRIS·HCl, pH 9.0		
	1.0	mmol/l	Na_2-EDTA in water		
TBS-T for histology	0.10	% (v/v)	Tween-20 in TBS		
Permeabilization solution for IHC	0.20	% (v/v)	Triton X-100 in TBS		
Blocking solution for ICC	20.0	g/l	BSA in TBS-T		Always prepared fresh.

Continuation on next page.

Continuation of tab. 8.6.

Label	Composition				
Blocking solution for IHC	40.0	g/l	BSA in TBS-T		Always prepared fresh.
Ab diluent for ICC and IHC	10.0	g/l	BSA in TBS-T		Always prepared fresh.
Acidic alum solution	1.74 6.48	g/l g/l	K_2SO_4 $Al_2(SO_4)_3 \cdot 17H_2O$ in water		Storage at 4 °C. Pre-warmed to RT before use.
Scott's solution	10.0 20.0	g/l g/l	$NaHCO_3$ $MgCl_2$ in water		
Griess test					
Griess reagent I Griess reagent II	30.0 3.0	g/l g/l	Sulfanilamide in 5 % (m/m) H_3PO_4 NED in 5 % (m/m) H_3PO_4		Usable as long as solutions stay colorless.

9 Animals

9.1 Housing and breeding

All animals were housed and bred under S1 conditions in the central animal housing facility of the Christian Albrechts University Kiel (Building U39, UKSH Campus Kiel) pursuant to the German animal welfare regulations.

9.1.1 Constitutive *Ier3* ko-mice

Ier3$^{-/-}$-mice genetically based on a Sv129 background [189] were used at backcross generation >10 [183]. Heterozygous parental animals were intercrossed to yield *Ier3*$^{+/+}$ and *Ier3*$^{-/-}$ offspring. Those mice served as constitutive *Ier3* wt- and *Ier3* ko-mice.

9.1.2 Conditional *Ier3* ko-mice

Ier3-flox -/+ and *LysM-Cre* -/+ mice genetically based on a C57BL/6 background (Genoway, Lyon, France) were mated to generate *Ier3-flox*$^{+/+}$ *LysM-Cre*$^{-/-}$ and *Ier3-flox*$^{+/+}$ *LysM-Cre*$^{+/+}$ mice at later generations.

Ier3-flox -/+ and *Vil-Cre* -/+ mice genetically based on a C57BL/6 background (Genoway, Lyon, France) were mated to generate *Ier3-flox*$^{+/+}$ *Vil-Cre*$^{-/-}$ and *Ier3-flox*$^{+/+}$ *Vil-Cre*$^{+/+}$ mice at later generations.

9.2 Genotyping of constitutive and conditional *ier3*-knockout mice

During breeding, all mice were routinely genotyped regarding their *Ier3* status by PCR and subsequently DNA-PAGE. Additionally, all mice used for experiments were tested again after termination of the experiments for validation.

Constitutive *Ier3* wt/ko-mice were tested for the genomic *Ier3*-sequence. The PCR amplification led to a product size of 1160 bp (wt-allele) or 960 bp (ko-allele).

Conditional *Ier3* wt/ko-mice were genotyped for the *lysM-cre* or *vil-cre* sequence as well as for the ***Ier3*-containing *loxP* cassette** (*Ier3-flox*). The amplification product of the *Ier3*-flox cassette had a size of 542 bp while the *Ier3* wt-allele led to a product size of 413 bp.

The existence of the ***LysM-Cre*** allele was performed by two different PCRs. In presence of the *LysM-Cre* allele, one PCR amplified a product of approximate 700 bp (=positive), while the allels's absence led to no PCR-product. The ohter PCR provided a product of approximate 350 bp in the absence of the *LysM-Cre* sequence (=negative) while it's presence generated no amplicon.

The ***Vil-Cre*** allele generated an amplicon of 1000 bp (=positive), while its absence led to no PCR product.

9.2.1 DNA extraction from source tissue

Genomic DNA was extracted from tail tips, harvested during weaning. Additionally, a tail tip from each experimental animal was harvested directly after sacrifice. Until DNA extraction they were stored at -20 °C.

DNA extraction was performed using *Quick Extract DNA solution 1.0*™ (QEDS, BioRad) with an adjusted protocol. After thawing QEDS aliquots on ice, 25 µl were added to each tail clip containing micro reaction tube. After vigorous vortexing for 15 s, the tubes were spun down shortly and incubated in a prewarmed thermomixer for 30 min at 65 °C and 750 rpm. Following the incubation, the tubes were vortexed again for 15 s. After spinning down the liquid, the tubes were incubated in a prewarmed thermomixer for 5 min at 98 °C (without shaking) and cooled on ice subsequently. The DNA containing solution was aspirated and applied directly for PCR or alternatively stored at -20 °C still containing the tail tip remains.

9.2.2 PCR

Primer for mouse genotyping Primer for mouse genotyping were purchased from Eurofins Genomics (Ebersberg, Germany). After receiving, they were solved in nuclease free water to a concentration of 100 $^{pmol}/_{µl}$ and stored at -20 °C. Primer sequences are listed in table 9.1.

PCR conditions PCR was performed using the PeqGOLD™ Taq DNA polymerase kit (Peqlab) with an adjusted buffer system. For the reaction (total volume per batch 23 µl), 3 µL DNA solution were added to 20 µL PCR-mastermix into a PCR micro tube. PCR reaction was performed straight afterwards using an ABS 2720 thermal cyler. The master mix composition is given in table 9.2, while the composition of self prepared master mix ingredients is listed in table 8.6. The respective PCR conditions are given in Table 9.3.

Table 9.1: Mouse genotyping primer sequences.

Label	Sequence
Constitutive *Ier3* allele:	
gly96 fwd:	5′- G C A G T T T T G T G T C C G T G T G C T C -3′
gly96 rev:	5′- T T C T T C G G A C T G T G A C C C A T C G -3′
Neo rev:	5′- G G G C T G A C C G C T T C C T C G T G C T T T -3′
Ier3-flox allele:	
45flp fwd:	5′- G G A A A G C G G T C T C T C A A G C A T T A C G -3′
46flp rev:	5′- G T G A A G T C C A G C A A G A T C A A G G G A C C -3′
LysM-Cre allele:	
398 fwd:	5′- C C C A G A A A T G C C A G A T T A C G -3′
399 rev:	5′- C T T G G G C T G C C A G A A T T T C T C -3′
400 rev:	5′- T T A C A G T C G G C C A G G C T G A C -3′
Vil-Cre allele:	
vil-cre78 fwd:	5′- G T G T G G G A C A G A G A A C A A A C C -3′
vil-cre79 rev:	5′- A C A T C T T C A G G T T C T G C G G G -3′

Table 9.2: PCR mastermix for mouse genotyping.

Volume		Component	included in kit
2.353	µl	Buffer “S” 10x	yes
2.353	µl	Sucrose soln 300 g/l	no
2.353	µl	SucRed soln	no
0.471	µl	dNTP mix 10 mmol/l, each	no
0.882	µl	each Primer 10 µmol/l	no
0.147	µl	PeqGOLD^{TM} Taq DNA polymerase	yes
	ad	H_2O 20 µl	no

Table 9.3: PCR conditions for mouse genotyping.

Amplicon	Primer label	PCR conditions			Product size	
		temperature	time	cycles		
ier3-	gly96 fwd	95 °C	300 s		wt:	1160 bp
allele	gly96 rev (wt)	95 °C	60 s	↻ 45×	ko:	960 bp
(constitutive)	Neo rev (ko)	58 °C	60 s			
		72 °C	120 s			
		72 °C	600 s			
ier3-flox-	45flp	95 °C	300 s		neg:	413 bp
allele	46flp	95 °C	45 s	↻ 38×	pos:	542 bp
		63 °C	45 s			
		72 °C	60 s			
		72 °C	600 s			
lysM-cre-	398	94 °C	300 s		pos:	≈700 bp
allele	399	94 °C	30 s	↻ 45×		
positive		56 °C	45 s			
		72 °C	60 s			
		72 °C	600 s			
lysM-cre-	399	95 °C	300 s		neg:	≈350 bp
allele	400	95 °C	60 s	↻ 3×		
negative		65 °C	40 s			
		72 °C	40 s			
				↓		
		95 °C	60 s	↻ 3×		
		64 °C	40 s			
		72 °C	40 s			
				↓		
		95 °C	60 s	↻ 3×		
		63 °C	40 s			
		72 °C	40 s			
				↓		
		95 °C	60 s	↻ 36×		
		62 °C	30 s			
		72 °C	40 s			
		72 °C	600 s			
vil-cre-	vil-cre78	94 °C	300 s		pos:	≈1000 bp
allele	vil-cre79	94 °C	30 s	↻ 45×		
positive		62 °C	45 s			
		72 °C	75 s			
		72 °C	600 s			

Detection of PCR products PCR products were separated by polyacrylamide gel electrophoresis, subsequently stained with ethidium bromide and detected under UV-light:

10 µl PCR product were directly loaded onto a 8 % ($^{m}/_{m}$) PAA gel[32] (tab. 9.4). Additionally, one lane was loaded with 2.5 µL 100 bp DNA ladder (Fermentas). Electrophoresis was performed in 1x TBE at 200 V for 90 minutes.

Afterwards, the gel was incubated in 1x TBE containing 1 $^{\mu g}/_{ml}$ ethidium bromide for 5 minutes. Detection of bands was conducted under UV-light (365 nm) using the Multiimage I^{TM} imaging system (Alpha-Innotec).

Table 9.4: Composition of PAA gels for DNA-PAGE.

Label	Composition		
Separating gel 8 %	20.0	% ($^{v}/_{v}$)	Rotiphorese^{TM} solution 40 %
	10.0	% ($^{v}/_{v}$)	TBE buffer 10x
	0.1	% ($^{v}/_{v}$)	TEMED
	1.0	$^{g}/_{l}$	APS
			solved in water

10 DSS and AOM/DSS animal experiments

Several dextran sodium sulphate (DSS) or azoxymethane (AOM)/DSS animal experiments were conducted to study putative effects of IER3 in different tissue compartments in the context of acute and chronic colitis as well as colitis associated carcinogenesis (CAC). This experimental design closely mimics the pathogenic processes appearing in the colons of patients suffering from IBD [166].

All experiments were conducted in accordance with the European and German animal welfare regulations and were approved by the admission authorities of the Federal State of Schleswig-Holstein (File no. 155-11/13).

[32] Due to the PCR mastermix composition, no additional loading buffer was necessary.

The experiments were conducted in the campus' central animal housing facility. Only male mice were used for the experiments to avoid possible perturbations caused by the hormone system of female mice.

10.1 Induction of acute colitis

To explore effects of IER3 in different tissue compartments during acute colitis, mice with and average age of 9-10 weeks were supplied with 30 g/l DSS in drinking water *ad libitum* over a period of 9-10 days.

10.2 Induction of chronic colitis

The putative effects of constitutive as well as of epithelial expressed IER3 on the progress of a chronic colitis were studied in several interval DSS experiments. Animals with an average age of 9 weeks received three 5-day and one 4-day cycles of 15 g/l DSS in drinking water *ad libitum*. Each DSS cycle was followed by a 5 day treatment free interval.

10.3 Induction of chronic colitis and colitis associated carcinogenesis

The effects of myeloid IER3 on the progress of chronic colitis and its subsequent colorectal tumor formation were studied in a long term AOM/DSS experiment (fig. 10.1). Animals with an average age of $13^1/_2$ weeks were injected intraperitoneal (i.p.) with 10 µg/g body weight (bw) AOM at day -7 to induce an inflammation triggered carcinogenesis at a later time-point. To induce a chronic inflammation, the animals were treated with 10 g/l DSS in the drinking water *ad libitum* in three cycles (interrupted by three treatment free recovery phases) beginning at day 0. The first DSS cycle endured for seven days, followed by a 14 day lasting treatment free interval. The second cycle was shortened to three days (day 21-24) to avoid a premature termination of the experiment due to the animals health condition (see sec. 10.6 for abort criteria). This cycle was followed by an 11 days treatment

free interval. The last DSS cycle endured again for seven days from day 35-42. The experiment was terminated at day 85.

Figure 10.1: Experimental design to induce a chronic inflammation and subsequent tumor formation in *Ier3-flox*$^{+/+}$ *LysM-Cre*$^{-/-}$ and *Ier3-flox*$^{+/+}$ *LysM-Cre*$^{+/+}$ mice. Animals were injected i.p. with AOM 10 µg/g bw at day -7. 10 g/l DSS in drinking water was administered *ad libitum* from day 0-7, day 21-24 and day 35-42. The experiment was terminated at day 85.

An additional experiment was conducted to closer evaluate the processes during the initiation phase of a chronic AOM/DSS induced colitis in *Ier3-flox*$^{+/+}$ *LysM-Cre*$^{-/-}$ and *Ier3-flox*$^{+/+}$ *LysM-Cre*$^{+/+}$ mice. Accordingly to the long term AOM/DSS experiment, these animals were injected intraperitoneal (i.p.) with 10 µg/g body weight (bw) AOM at day -7. DSS was administered in a concentration of 10 g/l in the drinking water *ad libitum* from day 0-7. The experiment was aborted at day 13.

10.4 Parameters gathered during the experiments[33]

During the experiments the following parameters were gathered on a regular basis[34]:

- vitality score[35]
- body weight
- rectal bleeding score
- occult blood in stool
- stool consistency

[33]Not all parameters were gathered in all experiments.
[34]The intervals of measuring were adjusted to the current condition of the experimental animals.
[35]For definition of the vitality score see section 10.6.

Rectal bleeding and blood in feces Rectal bleeding was assessed optical. Occult blood in feces was detected using the *Haemoccult*^{TM}-kit (Beckman). The principle of this kit bases on the guaiac method modified by GREEGOR [76]. Scores had a range from 0 (no detection of occlult blood) up to 4 (rectal bleeding).

Stool consistency Stool consistency was rated by a simplified *Bristol stool scale* in a range from 0 (normal consistency) up to 4 (practical liquid).

10.5 Parameters and samples gathered after termination

After killing the following parameters were gathered:

- liver weight
- spleen weight
- cecum weight
- colon length
- number and localization of tumors in the colon
- tumor size
- anatomical abnormalities

The following organs and samples were achieved:

- blood / serum[36]
- colon (formalin or CARNOY fixation as well as cryo conservation (-80 °C))

[36] Blood was achieved directly before killing by heart puncture. The blood was collected into EDTA containing tubes and centrifuged at 1000 g for 5 minutes. The supernatant (blood serum) was transferred into a micro reaction tube and stored at -80 °C until its further use.

- ileum (cryo conservation (-80 °C))
- cecum(formalin fixation and cryo conservation (-80 °C))
- spleen (formalin fixation and cryo conservation (-80 °C))
- liver (formalin fixation and cryo conservation (-80 °C))
- 3 tumors if available (cryo conservation (-80 °C))
- mesenterial lymph nodes (cryo conservation (-80 °C))
- tail tips[37]

The colon of each animal was cut longitudinal in two halves. One half was rolled to a "swiss-roll" and fixated in Lillie's formaline or modified Carnoy's solution for histological analysis. The other half was divided in 4 segments (proximal, M1, M2 and distal) and cryo-preserved. A scheme of the segmentation is given in figure 10.2.

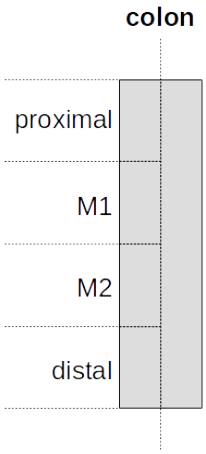

Figure 10.2: Segmentation of the colon from experimental animals after killing for further analysis.

[37]Mice were re-genotyped post mortem for reasons of redundancy.

10.6 Abort criteria

Mice were prematurely excluded from the experiments if matching at least on abortion criterion:

- Body weight < 75 % compared to body weight at day 0.
- Signs of severe pain.
- A low vitality score.

Severe signs of pain and/or a low vitality score were assessed by at least one of the following behavioral patterns:

- No elopement after touching the animal with a finger.
- Sitting in a corner of the cage without movement (except shivering).
- Narrowing one's eyes to slits with or without shivering.

For KAPLAN-MEIER survival-curve analysis, matching an exclusion criterion was rated to be equivalent to a treatment caused death of the animal.

11 *In vivo* permeability to FITC-Dextrans

The guts permeability of 8-12 week old[38] *Ier3-flox*$^{+/+}$ *LysM-Cre*$^{-/-}$ and *Ier3-flox*$^{+/+}$ *LysM-Cre*$^{+/+}$ animals to FITC conjugated dextrans (FD) of different molecular weights was determined in several *in vivo* experiments to identify putative differences in the intestinal barrier function between the genotypes. Experiments were conducted with DSS pretreated as well as with unchallenged, healthy animals.

Four hours after oral administration of a body weight adjusted dose (tab. 11.1), the FD blood serum concentration was determined photometrically. Two sorts of FD with different molecular weights (see tab. 8.4) were applied for the experiments.

[38] Animals were age matched for the particular experiments.

11.1 Pretreatment with DSS

If applied, animals were pretreated with 10 g/l DSS in drinking water *ad libitum* for 24 h before the FD administration.

11.2 Admimistration of FITC dextrans

The FD solutions (tab. 11.1) were always prepared freshly at each experimental day and stored protected from light. A body weight adjusted amount (tab. 11.1) was administrated directly to the pylorus trough a bulb-headed stomach probe[39].

Table 11.1: FITC dextran solutions for oral administration.

Solution	Conc.	Solvent	Administrated amount (referred to FD dry mass)
FD4	100 mg/ml	water	0.5 mg/g bw
FD10	100 mg/ml	water	1.0 mg/g bw

11.3 Blood sampling and measurement

3:40 h after the FD administration, the animals were narcotized i.p. injection (tab. 11.2). After pain reflex falsification, blood samples were taken by heart puncture exactly 4:00 h after the FD administration[40]. The fresh samples were transfered into a polymer based serum tube (BD Microtainer^{TM} SST, ord.-no. 365968) and processed pursuant manufacturers declaration[41].

[39] Before administration, the probe was coated in sugared water for reasons of compliance.
[40] Animals were killed by cervical dislocation directly after blood sampling.
[41] The centrifugal forces were limited to 6000 g, to avoid FD precipitation.

Table 11.2: Narcotization compound for intraperitoneal injection.

Component	Dosage	
Fentanyl	0.075	$^{mg}/_{kg}$ bw
Medetomidine	0.75	$^{mg}/_{kg}$ bw
Midazolam	7.5	$^{mg}/_{kg}$ bw

The processed blood serum was diluted 1:100 in 0.5 $^{mol}/_{l}$ glycine buffer, pH 9.6 and pipetted in triplicates into a 96-well microtiter plate (150 $^{µl}/_{well}$). Fluorescence intensity was measured in a plate fluorimeter at λ_{Ex}=485/20 nm and λ_{Em}=535/25 nm.

12 Histology

12.1 Specimen preparation

After fixating the the achieved specimen in either Lillie's formaline for 72 h or modified Carnoy's solution for 24 h they were completely dehydrated and embedded into paraffin blocks. The blocks were cut into slices of 3 µm thickness using a sledge microtome (Micron) and mounted onto silanized microscopic slides (Labsolute). The slides were stored upright and incubated for 24 h at 40 °C before further use.

12.2 Deparaffinization and rehydration

The slides were deparffinated and rehydrated in an xylene-alcohole-water sequence accordingly to table 12.1.

Table 12.1: Deparaffination and rehydration of thin layer paraffin sections.

Step	Solution	Incubation time
1	Xylene I	10 min
2	Xylene II	10 min
3	Ethanol absolute I	10 min
4	Ethanol absolute II	10 min
5	Ethanol 95 % (v/v)	5 min
6	Ethanol 70 % (v/v)	2 min
7	Ethanol 50 % (v/v)	2 min
8	Water I	2 min
9	Water II	5 min

12.3 Staining

12.3.1 Haematoxylin / Eosin staining

Specimen were deparaffinated and rehydrated as described in section 12.2. Next, the specimen were submersed in a 1:2 dilution of Meyer's Haematoxylin solution[42] (Merck) in water for 5 min to stain the nuclei. The slides were subsequently rinsed in water and incubated 2 times for 60 s each in acidic potassium aluminium sulfate solution ($c(KAl(SO_4)_2) = 20\,mmol/l$) to reduce unspecific cytoplasmic staining. After shortly rinsing the slides in water, bluing was conducted by incubating them in Scott's solution for 3x 10 min, each.

Cytoplasmatic counterstaining was performed by submersing the specimen in a solution of 1 g/l Eosion Y (Merck) in water for 4 min. Afterwards, the specimen were differentiated in water and embedded subsequently using Kaiser's glycerol gelantine.

12.3.2 Conventional Immuno-Staining

Specimen were deparaffinated and rehydrated as described in section 12.2. Unspecific peroxidase activity was blocked by incubating the slides for 10 min 2 % (m/m) H_2O_2-

[42] The Haematoxylin dilution was filtered trough a 595 1/2 pleated filter directly before use.

solution at RT. Afterwards, the slides were shortly rinsed 3x in water. Antigen retrieval was performed by transferring the slides into a plastic cuvette filled with an antibody (Ab) depending retrieval solution (tab. 12.4). The cuvette was heated in a microwave oven at 300 W for 6x 5 min, each. Evaporated retrieval solution was replaced between the heating steps. After cooling down for 15 min, the specimen were encircled using a grease pencil. Depending on the antigen, the specimen were incubated in approx. 100 µl permeabilization buffer for 7 min, if necessary[43]. Afterwards the slides were rinsed two times in washing buffer and unspecific bonds were blocked by incubating the specimen in approximately 100 µl blocking solution for 90 min at RT in a humidified chamber. After the slides were shortly rinsed in washing buffer, the specimen were covered with 60 µl of the diluted primary antibody or a respectively isotype control. Incubation took place overnight at 4 °C in a humidified chamber.

The next day, the slides were washed 3 times in wahsing buffer for 5 min, each. Subsequently, the specimen were incubated for 60 min at RT with 1-2 drops of a HRP-conjugated polymer based reagent (Dako), directed against the host species of the primary antibody. Afterwards, the slides were washed 3 times in washing buffer for 5 min, each. Developing of the specimen was performed using an 3-Aminocr-9-ethylcarbazole (AEC) based substrate (Dako). For this, 1-2 drops of the substrate solution were dripped onto the specimen and incubated for 10-45 min at RT until the reaction reached its optimal chromogenic intensity. The reaction was stopped by immersing the slides in water for 10 min.

Counterstaining of the cell nulclei was performed by immersing the slides in a 1:2 dilution of Meyer's Haematoxylin solution[44] (Merck) in water for 5 min. The slides were subsequently rinsed in water and incubated 2 times for 60 s, each in acidic potassium aluminium sulfate solution ($c(KAl(SO_4)_2) = 20\,^{mmol}/_{l}$) to reduce unspecific cytoplasmic staining. After shortly rinsing the slides in water, bluing was conducted by incubating

[43] Despite the addition of Tween-20 to the blocking and washing buffer, the usage of a designated triton X-100 based permeabilization solution has proven for the staining of some intracellular epitops.

[44] The Haematoxylin dilution was filtered trough a 595½ pleated filter directly before use.

them in SCOTT's solution for for 3x 10 min, each. Afterwards, the slides were shortly rinsed in water and specimen were embedded subsequently using KAISER's glycerol gelatine.

12.3.3 Fluorescence immunohistochemistry (IHC-F)

Specimen were deparaffinized and re-hydrated as described in section 12.2. If fixated in formalin, specimen were incubated for 10 min in freshly prepared sodium borohydride solution (10 g/l $NaBH_4$in PBS, pH 7.4) to reduce background fluorescence (*Cave*: Explosion hazard due to hydrogen gas formation). Afterwards, the slides were shortly washed 3x in water. Antigen retrieval was performed by transferring the slides into a plastic cuvette filled with an antibody depending retrieval soulution (tab. 12.4 on page 66). The cuvette was heated in a microwave oven at 300 W for 6x 5 min, each. Evaporated retrieval solution was replaced between the heating steps. After cooling down for 15 min, the specimen were encircled using a grease pencil. Depending on the antigen, the specimen were incubated in approximately 100 µl permeabilization buffer for 5-10 min, if necessary[45]. Afterwards the slides were rinsed two times in washing buffer and unspecific bonds were blocked by incubating the specimen in approximately 100 µl blocking solution for 90 min at RT in a humidified chamber. After the slides were shortly rinsed in washing buffer, the specimen were covered with 60 µl of the diluted primary antibody or a respectively isotype control. Incubation took place overnight at 4 °C in a humidified chamber.

The next day, the slides were washed 3 times in washing buffer for 5 min, each. The specimen were covered with 60 µl of the diluted, fluorochrome conjugated secondary antibodies together with 665 ng/ml Hoechst bisbenzimide H33258 for nucleic counter staining. After incubation for 40 min in the dark at RT, the slides were washed 3 times in washing buffer for 5 min, each. Following, the slides were rinsed shortly in water and subsequently mounted with cover slips using FluorSave™ (Merck) mounting medium.

[45] Despite the addition of Tween-20 to the blocking and washing buffer, the usage of a designated triton X-100 based permeabilization solution has proven for the staining of some intracellular epitops.

24 h after the mounting, the specimen were sealed with nail polish and stored 4 °C until analysis.

Table 12.2: Isotype control antibodies for conventional and fluorescence based immunohistochemistry and immunocytochemistry.

Host	Clonality/ Isotype	Stock conc.	Company/ order-no.	
m	mAb IgG	0.5 mg/ml	R&D	MAB002
rb	pAb IgG	1.0 mg/ml	CST	2729

Legend:
Manufacturer: CST: Cell Signaling Tech., R&D: R&D Systems.
For further abbreviations see the list on page XVII.

Table 12.3: Secondary antibodies for ICC-F and IHC-F.

Target		Host-species	Conjugated fluoro-chrome	TSS purification	Stock conc.	Dilution ICC-F & IHC-F	Company/ order-no.	
Species	Ab Isotype							
m	IgG (H+L)	donkey	AF-488	EAC	2 mg/ml	1: 1000	Thermo	A-21202
rb	IgG (H+L)	goat	AF-555	AC	2 mg/ml	1: 750	Thermo	A-21428

Legend:
TSS: Target species specificity.
AC: Cross adsorption chromatography; EAC: Enhanced cross adsorption chromatography.
For further abbreviations see the list on page XVII.

Table 12.4: List of primary antibodies for IHC.

Antigen	Species-reactivity	Host	Clonality/ Isotype	Stock conc.	Dilution IHC/ IHC-F		AG retrieval	Extra permeabilization step	Company/ order-no.	
β-Catenin	h, m, rt	rb	pAb IgG	*50 µg/ml	IHC-F	1:200	Citrate	yes	CST	9562
E-Cadherin	h, m, rt	m	mAb IgG2a	250 µg/ml	IHC-F	1:100	Citrate	yes	BD	610182
F4/80	m	rb	mAb IgG	*433 µg/ml	IHC	1:600	Citrate	no	CST	70076
					IHC-F	1:433	Citrate	no		
F4/80	m	rt	mAb IgG2b	1 mg/ml	IHC	1:100	Citrate	no	BioRad	MCA497
OCC	h, m, rt	rb	pAb IgG	250 µg/ml	IHC-F	1:250	Citrate	yes	Thermo	40-4700
ZO1	h, m, rt	rb	pAb IgG	400 µg/ml	IHC-F	1:200	EDTA	yes	GTX	GTX108613

Legend:

Species reactivity: letters: manufacturer recommendation, underlined: successfully applied.

*: Concentration Lot depending.

Manufacturer abbreviations: BD: Becton Dickinson, CST: Cell Signaling Technologies, GTX: GeneTex

For further abbreviations see the list on page XVII.

13 Cell culture

Cell lines were either purchased from ATCC or provided by other research groups[46]. Table 13.1 lists the name of the cell line specific culture media, while their exact formulation is given in table 43.

The differentiation, cultivation and detachment of primary BMC derived MΦ differs in parts from the methods described here. See section. 13.1 for further informations.

Table 13.1: List of culture media used for the different cell lines.

Cell line	Culture medium
3T3	RAW-M.
CaCo-2	CaCo-M.
HEK-293T	RAW-M.
HT29	HT29-M.
IEC-6	IEC-6-M.
Med. for *in vitro differentiation* of primary MΦ from murine BMC	$M\Phi^{diff.}$-M.
Med. for *cultivation* of *in vitro* differentiated primary MΦ from murine BMC	$M\Phi^{cult.}$-M.
MODE-K	RAW-M
Primary murine IEC	*
Raji	Raji-M.
RAW 264.7	RAW-M.
THP-1	RAW-M.
YAMC	YAMC-M.

*: For the cultivation as well as for the immortalization of primary IEC, a variety of different culture media formulations was tested.
See the list on page XVII for abbreviations.

13.1 Seeding an cultivation of cells

If not mentioned else, cells were seeded in a concentration of $1 \cdot 10^5$ $^{cells}/_{ml}$. Table 13.2 gives the volumes of cell suspension/culture medium used for the regarding culture vessels.

[46]Cell lines were kindly provided by the groups of Prof. Frey, Prof. Reiss, Dr. Tiwari and Prof. Zeissig.

Table 13.2: Volumes of cell suspension / culture medium for different culture vessels.

Vessel	Volume	
24-well plate	0.5 ml	per well
12-well plate	1.0 ml	per well
Transwell insert for 12-well plate	0.5 ml	per insert
6-well plate	2.0 ml	per well
Culture dish ⌀=80 mm	8.0 ml	per dish
T75 culture flask	14.0 ml	per flask
FEP bag 32-AC	30.0 ml	per bag

BMCs for MΦ differentiation were seeded and cultivated on untreated PS surfaces not suitable for adherent cells. MΦ were seeded and cultivated either in untreated PS or FEP surfaces. RAW264.7 and undifferentiated THP-1 cells (monocyte stadium) were seeded and cultivated in PS vessels with a hydrophobic surface treatment (Sarstedt color code green). Primary cells were cultured on PS surfaces with an enhanced hydrophilic treatment for sensitive adherent cells (Sarstedt color code yellow). These surfaces were additionally coated with a combination of collagen and fibronectin before use. All other cell lines were cultured in PS vessels with a hydrophilic surface treatment, suitable for cell adherence (Sarstedt color code red).

For ICC experiments, cells were cultivated on coverslips, optionally precoated with collagen and fibronectin if necessary.

Coating of surfaces with collagen and fibronectin As mentioned above, for some experiments it was necessary to pre-coat the surfaces of the culture vessels or cover slips with a combination of collagen and fibronectin for optimal cell adherence.

Surfaces were coated with 10 $\mu g/cm^2$ collagen and 2 $\mu g/cm^2$ fibronectin. The necessary amount of the stock solution was solved in an appropriate volume water. The volume of water was chosen pursuant, the solution had a coating thickness of approximate 1-2 mm when covering the surface of the culture vessel.

The surfaces were allowed to dry overnight under a running[47] lamina flow cabinet. The next day, the surfaces were carefully rinsed with PBS[48] before seeding the cells.

13.2 Culture conditions

13.2.1 General culture conditions

Except from YAMC, which require a temperature of 33 °C for proliferation[49], all cell lines as well as primary murine BMC/MΦ were cultured in an incubator at 37 °C in an atmosphere of 85 % (v/v) relative humidity and 5 % (v/v) CO_2[50] (in this thesis these conditions are designated as *standard conditions*).

13.2.2 Generation of IEC monolayers

To establish dense IEC monolayers, the cells were cultivated over a period of 10-20 days without passaging. During this period, the culture medium was exchanged every second day.

13.3 Passaging & harvesting of cultivated cells

If not mentioned else, cells were passaged 2-3 times a week, according to their proliferation rate and confluence.

After aspirating the supernatant, the cells were rinsed shortly with prewarmed PBS containing 2 mmol/l Na_2-EDTA. Next, the cells were covered with Trypsin/EDTA solution[51]

[47] The constant vibrations ensured an equal wetting during the drying process.

[48] This step was necessary to remove putative HCl residues from the collagen stock solution as well as to rehydrate the collagen fibers.

[49] The differentiation of YAMC into cells with a putative epithelial like phenotype appears at 37 °C.

[50] Even cells cultivated in pure DMEM normally require a CO_2 concentration of 10 % (v/v) for an optimal pH-value of the culture medium, they could be cultivated at 5 % (v/v) CO_2 due to the addition of HEPES and/or FCS to the culture medium.

[51] For some applications, which required the integrity of trypsin sensitive surface antigens, alternative detachment solutions were utilized.

(Biochrom) and incubated at 37 °C for 3-15 minutes depending on their specific adherence. The cells were intermittently resuspended with a serological pipette to facilitate their detachment. After all cells were detached, the suspension was transfered into a reaction tube and mixed with an equal volume neutralization medium.

The cell suspension was centrifuged at 350 g for 10 min. Afterwards, the supernatant was aspirated and discarded. For passaging, the remaining pellet was resuspended in an appropriate volume of the culture medium or in an appropriate volume buffer if meant to be used for other experiments. After determining the cell concentration, they were re-seeded into a new culture vessel in the desired concentration or utilized for other applications.

14 Primary Macrophages from bone marrow cells

Primary murine macrophages (MΦ) were generated from bone marrow cells (BMC) of 8-14 weeks old[52] *Ier3-flox*$^{+/+}$ *LysM-Cre*$^{-/-}$ and *Ier3-flox*$^{+/+}$ *LysM-Cre*$^{+/+}$ animals.

14.1 Harvesting of BMC

BMC were harvested from the animal's femurs and tibias. After killing the mice by cervical dislocation, they were disinfected by wetting them with 70 % v/v ethanol. Next, the animals were skinned. The musculus quadriceps as well as it's attached tendons and ligaments were intersected completely. The femur head was luxated by simultaneous dislocating and pulling the femur against its socket. Femur and tibia were removed by cutting trough the intra-articular space. The bones were stored in sterile, ice cold PBS until further use.

[52] Animals for each particular experiment were age matched.

The bones were pruned of all tissue remains using a scalpel and cleaning tissues. After shortly immerse them in 70 %$_{v}/_{v}$ ethanol, the bones were stored in sterile, ice cold PBS until further use.

All following steps were conducted under a laminar flow cabinet. Femur and tibia were cut trough in the middle. The bone fragments were threaded onto a hypodermic needle (27 G·$^{3}/_{4}$) attached to a syringe filled with sterile, ice cold PBS. Subsequently, the bone marrow cells were flushed out into a petri dish. The suspension was transfered into a 50 ml tube and remaining cell aggregates were dislodged by repeated resuspending of the suspension using a serological 10 ml pipette. After centrifugation for 10 min at 350 g and 4 °C, the supernatant was discarded. The remaining pellet was resuspended in an adequate volume $M\Phi^{diff.}$-M. and stored on ice until further use.

14.2 Differentiation of BMC into MΦ

After counting the cells, they were adjusted to a concentration of $1 \cdot 10^{6}$ $^{cells}/_{ml}$ using $M\Phi^{diff.}$-M.. They were seeded in PET cell culture vessels with an untreated surface[53], only and cultured under standard conditions at 37 °C. At day 3 after seeding, the supernatant was discarded and the cells were gently washed twice using prewarmed PBS to remove not adherent cells and debris. The culture medium was exchanged against fresh $M\Phi^{diff.}$-M.. At day 7, the cells were completely differentiated into MΦ.

Further experiments were were conducted using mGM-CSF and/or mIFN-γ in different concentrations to differentiate BMCs into MΦ (Results not shown).

[53] Standard culture vessels for adherent cells showed up to be inappropriate.

14.3 Culture of differentiated BMC derived MΦ

14.3.1 Culture medium

For the long-term culture of fully differentiated macrophages, the supplementation of the macrophage basal medium (MΦ-M.) with 20 $^{ng}/_{ml}$ mM-CSF and 50 $^{IU}/_{ml}$ mIFN-γ ($M\Phi^{cult.}$-M.) has proven successful. The culture medium was exchanged every 3rd day. Fully differentiated MΦ were conducted for experiments from day 7 to day 10 after BMC harvesting. Although not applied for experiments anymore at this time point, MΦ survived up to 20 days without morphological changes under these conditions.

14.3.2 FEP culture bags

Additional to the culture in PET vessels with an untreated surface, for some applications fully differentiated MΦ were also cultivated in specialized FEP culture bags (VueLife^{TM}, AFC) with reduced adhesion potential. However, the approach of differentiating BMC into MΦ directly in these bags led to a relatively low yield.

14.4 Detachment and harvesting of MΦ

14.4.1 Detaching MΦ from PET vessels

Due to their strong surface adherence, harvesting of BMC derived MΦ differed from the standard protocol for harvesting adherent cells. First, the culture medium was discarded and the cells were washed 3 times using prewarmed PBS containing 2 $^{mmol}/_{l}$ Na_2-EDTA. Afterwards, the cells were covered with Accutase^{TM} solution and incubated for 30 min at 37 °C. Subsequent to the incubation, $^{1}/_{2}$ volume freshly Accutase^{TM} solution was added and the cells were incubated for additional 10 min on a plate shaker at 200 rpm and RT. After all cells were detached (microscopic control), the suspension was mixed with an

equal volume DMEM containing 10 %$_{v/v}$ FCS. After centrifugation for 10 min at 350 g and 4 °C, the supernatant was discarded and the cell pellet could be used for further experiments.

14.4.2 Detaching MΦ from FEP bags

To detach MΦ from FEP bags, the bags were immersed into an ice/water bath for 30 min. Next, the bag was scrubbed multiple times over a round edge with a low radius. Afterwards, the now detached cells could be transfered into a reaction tube. Remaining cells were collected by flushing the bag with ice cold PBS. After centrifugation for 10 min at 350 g and 4 °C, the supernatant was discarded and the cell pellet could be used for further experiments.

15 RNA expression profile of IER3 proficient and deficient MΦ

Putative differences in the RNA expression profile of immunologically relevant genes in fully differentiated primary MΦ derived from the bone marrow of *Ier3-flox*$^{+/+}$ *LysM-Cre*$^{-/-}$ and *Ier3-flox*$^{+/+}$ *LysM-Cre*$^{+/+}$ mice (sec. 14) were analyzed by qPCR. The MΦ were optionally stimulated with different concentrations of LPS (0.5 $^{ng}/_{ml}$ or 1.0 $^{ng}/_{ml}$) as immunological activator, simulating the contact with gram negative bacterias. Cells were harvested 6 h after LPS stimulation and RNA extraction was performed as described in section 23. The RNAs of the ribosomal protein L13a (RPL13a) as well as of the hypoxanthine-guanine phosphoribosyltransferase (HPRT) coding genes proved as rather constantly expressed during these experiments and served as housekeepers for normalization of the qPCR results.

16 Protein expression profile of IER3 proficient and deficient MΦ

Putative differences in the Protein expression profile of immunological relevant genes in fully differentiated primary MΦ derived from the bone marrow of *Ier3-flox*$^{+/+}$ *LysM-Cre*$^{-/-}$ and *Ier3-flox*$^{+/+}$ *LysM-Cre*$^{+/+}$ mice (sec. 14) were analyzed by western blot (sec. 22). The MΦ were optionally stimulated with different concentrations of LPS (2.0 $^{ng}/_{ml}$ or 4.0 $^{ng}/_{ml}$) as immunological activator, simulating the contact with gram negative bacterias. Cells were harvested 6 h after LPS stimulation and RIPA lysates were generated subsequently as described in section 22.1.

17 Griess test

17.1 Background

The production and release of reactive nitrogen species (RNS) of MΦ derived from the bone marrow of *Ier3-flox*$^{+/+}$ *LysM-Cre*$^{-/-}$ and *Ier3-flox*$^{+/+}$ *LysM-Cre*$^{+/+}$ mice (sec. 14) was quantified indirectly in a photometrically assay based on a specific azo coupling reaction firstly described by Griess [79]. A stoichiometric fraction of the iNOS produced nitric oxide radicals ($NO^{\cdot}$) as well as their nitrogen dioxide radical intermediates ($NO_2^{\cdot}$) can freely diffuse trough the cellular membrane [136]. Under *in vitro* conditions, these radicals immediately react with components of the culture medium to form nitric anions (NO_2^{-}). During the Griess reaction, the nitric anions react with the reagents to form a photometrically detectable azo dye.

17.2 Stimulation

BMC derived MΦ from IER3 proficient and deficient mice were cultured in 12-well culture plates as described above in a concentration of $1 \cdot 10^6$ $^{cells}/_{ml}$. The cells were

optionally stimulated for 6 h with different concentrations of LPS (0.5 ng/ml or 1.0 ng/ml) as immunological activator. After the LPS incubation, the culture medium was exchanged against LPS free $M\Phi^{cult.}$-M. and the cells were incubated for further 18 h.

17.3 Griess Test

At the end of the incubation, the medium was aspirated[54] and centrifuged for 20 min at 400 g and 4 °C. The supernatant was transfered into new micro reaction tubes and stored on ice. The Griess test was performed subsequently in a 96-well microtiter plate. All samples as well as a sodium nitrite standard series were measured as triplicates. 250 µl sample solution was pipetted into each well. Next, 25 µl Griess reagent I (sulfanilamide) were added to each well and the plate was incubated protected from light for 8 min at RT on a plate shaker at 500 rpm. Afterwards, 25 µl Griess reagent II (NED) were added added to each well and the plate was incubated for 15 min at RT on a plate shaker at 500 rpm. During 15 min after the incubation has ended, the optical absorbance was measured on a plate photometer (Dynex) at λ_{Ex}=550 nm. The composition of the reagents is listed in table 8.6.

17.4 Normalization

The determined concentrations of nitrite were normalized against the MΦ number. The cell number was determined fluorimetrically by staining the nuclei with Hoechst bisbenzimide H33258 and determining the overall fluorescence intensity per well. In brief, the MΦ in the culture plates were fixated with 4 % (m/m) phosphate buffered formaline for 20 min. After a permeabilization step with 0.2 % (v/v) Triton X-100 in PBS for 5 min, cells were washed 3 times with PBS. For nuclei staining, the cells were incubated protected from light in 2 µg/ml Hoechst H33258 in PBS for 15 min. After washing washing the cells 5 times with PBS, each cell layer was covered with 0.5 ml PBS to prevent

[54] The cells were covered in PBS directly after the aspiration.

desiccation. Fluorescence intensity was measured subsequently on a plate fluorimeter (Tecan) at λ_{Ex}=340/10 nm and λ_{Em}=460/35 nm with 144 data points per well.

18 Immunocytochemistry

For fluorescence based immunocytochemistry (ICC-F), cells were cultivated on coverslips as described in section 13.1. For the staining procedure, the supernatant was aspirated and the cells were shortly rinsed with PBS. Next, the PBS was aspirated most thoroughly. For fixation, the cells were covered with dried, pre-cooled (-20 °) methanol and incubated at -20 °C for 15 min. After the fixation, the methanol was aspirated and the cells were rinsed shortly with PBS. After aspirating the PBS, cells were covered with blocking solution and incubated at RT for 60 min.

During the incubation, a glass plate was covered with parafilm and placed in a humidified chamber. Per specimen, 50 µl of primary antibodies (tab. 18.1) or respectively isotype controls (tab. 12.2) diluted in incubation solution were pipetted onto the parafilm. After blocking unspecific binding sites, the coverslips were shortly dripped off and placed on top the antibody dilution. Incubation took place in a humidified chamber overnight at 4 °C.

The next day coverslips were washed 3 times for 5 min, each with PBS (RT). A parafilm covered glass plate was prepared as described above. Per specimen, appropriate, fluorochrome conjugated secondary antibodies (tab. 12.3) were diluted in 50 µl incubation solution together with 665 $^{ng}/_{ml}$ Hoechst bisbenzimide H33258 and pipetted onto the parafilm. After shortly dripping off the coverslips, they were placed on top the antibody dilution and incubated in the dark for 40 min at RT.

Next, the coverslips were washed 3 times for 5 min, each with PBS (RT). After rinsing the specimen two times shortly with water, they were dripped off and subsequently mounted onto a microscope slide using FluorSave mounting medium (Merck).

24 h after the mounting, the specimen were sealed with nail polish and stored 4 °C until analysis.

Table 18.1: List of primary antibodies for fluorescence based Immunocytochemistry.

Antigen	Species-reactivity	Host	Clonality / Isotype	Stock conc.	Dillution	Company / order-no.	
β-Catenin	h, m, rt	rb		*50 µg/ml	1:200	CST	9562
E-Cadherin	h, m, rt	m	mAb IgG2a	250 µg/ml	1:150	BD	610182
OCC	h, m, rt	rb	pAb IgG	250 µg/ml	1:100	Thermo	40-4700
ZO1	h, m, rt	rb	pAb IgG	400 µg/ml	1:250	GTX	GTX108613

Legend:
Species reactivity: letters: manufacturer recommendation, underlined: successfully applied.
*: Concentration Lot depending.
Manufacturer abbreviations: BD: Becton Dickinson, CST: Cell Signaling Technologies, GTX: GeneTex
For further abbreviations see the list on page XVII.

19 Protein and mRNA expression of IEC monolayers during direct co-culture with primary MΦ

Putative effects of *in vitro* generated primary MΦ derived from BMCs of *Ier3-flox*$^{+/+}$ *LysM-Cre*$^{-/-}$ and *Ier3-flox*$^{+/+}$ *LysM-Cre*$^{-/-}$ animals to the protein and mRNA-expression in IEC monolayers were investigated in direct co-culture experiments.

Monolayers of intestinal epithelial cell lines were generated in 6-well culture plates over a period of 14 days as described in section 8.6. In parallel, BMCs from *Ier3-flox*$^{+/+}$ *LysM-Cre*$^{-/-}$ and *Ier3-flox*$^{+/+}$ *LysM-Cre*$^{+/+}$ animals were harvested and differentiated *in vitro* into MΦ as described in section 14.

After harvesting the fully differentiated MΦ (sec. 14.1), they were adjusted to a concentration of $5 \cdot 10^5$ cells/ml using MΦ$^{cult.}$-M. The supernatant of the IEC monolayers was aspirated and exchanged against the MΦ containing cell suspension. Subsequently the co-culture was optionally stimulated with 5 ng/ml LPS. NC experiments were conducted

with MΦ free $M\Phi^{cult.}$-M.±LPS. Macrophages and IEC monolayers were co-cultured for 24 h or 48 h. Following the incubation, protein or RNA extracts were generated as described in sections 22.1 and 23.1.

20 Protein and mRNA expression of IEC monolayers in response to exogenous nitric oxide

To investigate putative effects of nitric oxide on the protein and mRNA-expression in IEC monolayers, they were cultured in presence of the NO-donor S-nitroso-N-acetylpenicillamine (SNAP).

IECs were either seeded in 6-well plates (for western blot and qPCR analysis) or on coverslips in 12-well plates (for ICC-F) as describe in section 13.1. The IECs were cultivated over a period of 14 days, during which they formed a dense monolayer. At day 14, the culture medium was exchanged against freshly prepared medium containing either 2.5 $^{mmol}/_{l}$ or 5.0 $^{mmol}/_{l}$ SNAP or an equal amount of DMSO in the negative control. The monolayers were incubated under standard conditions for 24 h or 48 h.

Afterwards, either RIPA protein lysates for wb (sec. 22.1) or mRNA lysates for qPCR (sec. 23.1) were generated. Alternatively, the IEC monolayers were processed for ICC-F staining of cellular junction related proteins as described in section 18.

21 *In vitro* permeability of epithelial cell monolayers to FITC-dextran

21.1 Permeability in co-culture with primary MΦ

Putative IER3 depending effects of activated primary MΦ from *Ier3-flox*$^{+/+}$ *LysM-Cre*$^{-/-}$ and *Ier3-flox*$^{+/+}$ *LysM-Cre*$^{+/+}$ animals on the permeability of IEC monolayers to small molecules

were investigated in these experiments.

Intestinal epithelial cells were seeded on transwell inserts and monolayers were established over a period of 14 days as described in sections 13.1 and 13.2. In parallel, BMC from *Ier3-flox*$^{+/+}$ *LysM-Cre*$^{-/-}$ and *Ier3-flox*$^{+/+}$ *LysM-Cre*$^{+/+}$ animals were harvested and differentiated *in vitro* into MΦ as described in section 14.

24 h before the start of the experiment, the respectively culture medium in the IEC culture was exchanged against a culture medium of identical formulation, except the containing of phenol red (M.$^{w/o\,PR}$).

For the experiment, the fully differentiated MΦ were harvested as described in section 14.4 and washed 1x with the respective IEC-M.$^{w/o\,PR}$. Next, the MΦ were adjusted to a concentration of $5 \cdot 10^5$ cells/ml suspended in the respective IEC-M.$^{w/o\,PR}$ supplemented with 5 mg/ml FD4 and 5 ng/ml LPS.

The culture medium in the lower and upper compartments of the IEC culture were aspirated and discarded. The medium in the lower compartment was replaced with fresh IEC-M.$^{w/o\,PR}$, while the medium in the upper compartment was exchanged against the FD4 and LPS containing MΦ suspension.

The co-culture was incubated for 24 h or 48 h at 37 °C under standard conditions before determining the trans epithelial permeability.

21.1.1 Analysis

Fluorescence intensity After the incubation, the medium from the upper and lower compartments were transfered into a micro reaction tube and centrifuged for 10 min at 350 g to precipitate potential debris. The supernatant was transfered into fresh micro reaction tubes. Next, the samples from the upper compartment were diluted 1:10000 while the samples from the lower compartment were diluted 1:10 in 0.5 mol/l glycine

buffer pH 9.6. 150 µl aliquots of the diluted sample solution were pipetted in triplicates into the wells of 96-well microtiter plate.

The fluorescence intensity of the diluted samples was measured in a plate fluorimeter (Tecan) at λ_{Ex}=485/20 nm and λ_{Em}=535/25 nm.

Calculation of trans epithelial permeability The experimental design sufficiently fulfills the following conditions:

1. $c_{upper} \gg c_{lower}$

2. $c_{upper}(t_0) \approx c_{upper}(t_1)$

$c_{upper}(t_0)$: FITC-dextran concentration in the upper compartment at the begin of the experiment.

$c_{lower}(t_0)$: FITC-dextran concentration in the lower compartment at the begin of the experiment.

$c_{upper}(t_1)$: FITC-dextran concentration in the upper compartment at the time point of analysis.

$c_{lower}(t_1)$: FITC-dextran concentration in the lower compartment at the time point of analysis.

Hence, differences in transepithelial permeability μ between different experimental setups can be approximated by the following equation:

$$\bar{\mu}(t) = \frac{c_{lower}(t_1)}{c_{upper}(t_1)}$$

$\bar{\mu}(t)$: Average time depending transepithelial permeability of the monolayer to FITC-dextran between begin of the experiment and the time point of analysis.

21.2 Nitric oxide induced permeability

In these experiments putative effects of nitric oxide on the permeability of IEC monolayers to small molecules were investigated. For this, confluent IEC monolayers were cultured in presence of the nitric oxide donor S-Nitroso-N-acetyl-DL-penicillamine (SNAP).

21.2.1 Experimental design

Intestinal epithelial cells were seeded on transwell inserts and monolayers were established over a period of 14 days as described in section 13.2.2. 24 h before the start of the experiment, the respectively culture medium was exchanged against a culture medium of identical formulation, except the containing of phenol red (M.$^{w/o\,PR}$).

For the experiment, the medium in lower compartment was exchanged against freshly prepared medium$^{w/o\,PR}$ containing 2.5 $^{mmol}/_{l}$, 5.0 $^{mmol}/_{l}$ SNAP or an equal amount DMSO in the NC. The culture medium in the upper compartment was also exchanged against freshly prepared medium$^{w/o\,PR}$ with an SNAP/DMSO concentration identical to the one in the lower compartment but with the addition of 5 $^{mg}/_{ml}$ FD4[55]. Afterwards the cells were incubated under standard conditions for 24 h or 48 h.

After the incubation, the transepithelial permeability was determined as described in sec 21.1.1.

22 SDS-PAGE and western blot

22.1 RIPA protein extracts

For the generation of RIPA protein extracts, only protease free materials and reagents were used. The cell culture medium was aspirated and cells were washed twice using PBS (RT). All following procedures were conducted on ice. Remaining traces of PBS were aspirated thoroughly. Subsequently, an appropriate volume[56] freshly prepared, ice cold RIPA buffer was added. The cells were scraped off and the suspension was transfered into an pre-coold micro reaction tube. Afterwards, the tubes were vortexed for 40 min at

[55] An additional medium$^{w/o\,PR}$/SNAP batch w/o FD4 served as blank value during the analysis.
[56] E. g. 250 µl for a confluent grown well of a 6-well culture plate.

1400 rpm and 4 °C. Following this, the suspension was centrifuged for 20 min at 13000 g[57] and 4 °C. Subsequently, the protein containing supernatant was transfered into a fresh pre-cooled micro reaction tube and directly used for experiments or stored at -20 °C.

22.2 Measurement of total protein concentration in cell extracts

Total protein concentration in whole cell lysates was measured colorimetric using the DC™ [58] protein assay kit (BioRad) based on the Lowry method [118] according to the manufacturer's manual. A five-point calibration curve was generated using a BSA standard in a concentration range from 0.1 mg/ml up to 1.0 mg/ml, diluted in RIPA buffer. Detection was performed at 630 nm using a Opsys MR™ plate photometer (Dynex). While standards were measured in triplicates, samples were measured in duplicates to reduce random errors.

22.3 SDS-PAGE

Three volumes protein solution adjusted[59] exactly to a total protein concentration of approximate 0.5-1.5 µg/µl[60] were mixed with 1 volume 4x Laemmli loading buffer and incubated at 95 °C for 7 minutes. Afterwards, the samples were spun down shortly and cooled on ice.

The samples were loaded onto a SDS-PAGE stacking gel (10 µl/lane). The PAA concentration of the separating gel was 10 %, 12.5 % or 15 % PAA, depending on the molecular weight of the target proteins. The composition of the gels is given in table 22.1. One lane of each gel was loaded with 2 µL PageRuler plus ™ protein ladder (Fermentas) for

[57] Optimal conditions for centrifugation have to be determined in reference to the used cell line and proteins of interest.
[58] DC: Detergent compatible.
[59] Protein concentration adjustment was performed using RIPA buffer.
[60] All samples of a particular experiment were adjusted to equal concentrations.

molecular weight verification of the detected proteins. The PAGE was performed in SDS running buffer at 35 mA per gel.

Table 22.1: Composition of PAA gels for SDS-PAGE.

Label	Composition		
Separating gel	25.0	% (v/v)	WB separating gel buffer pH 8.8
10 %/12.5 %/15 % PAA	25.0/31.3/37.5	% (v/v)	Rotiphorese™ solution 40 %
	0.075	% (v/v)	TEMED
	0.35	g/l	APS
			solved in water
Stacking gel 4 %	25.0	% (v/v)	WB stacking gel buffer pH 6.8
	10.0	% (v/v)	Rotiphorese™ solution 40 %
	0.1	% (v/v)	TEMED
	0.5	g/l	APS
			solved in water

22.4 Western blot

22.4.1 Electro blot

Western blot was performed using the semi-dry technique. The proteins from a SDS-PAGE gel were blotted onto a PVDF membrane (Roth). Lamination of the single layers of the blotting system is given in figure 22.1. Buffer composition is listed in table 8.6. Electro blots were performed at 1.5 $^{mA}/_{cm^2}$ for 50 minutes.

22.4.2 Detection of blotted proteins

After finishing the electro blot, the membrane was washed in in TBS-T for 5 minutes. Subsequently, it was blocked in wb blocking solution for 2 h at room temperature. Then the membrane was transferred into a 50 ml reaction tube containing 5 ml of a primary antibody diluted in its appropriate diluent[61]. A comprehensive list of the applied

[61] If the diluent of the primary Ab was BSA based, the blot was washed 3x for 5 min, each prior incubation.

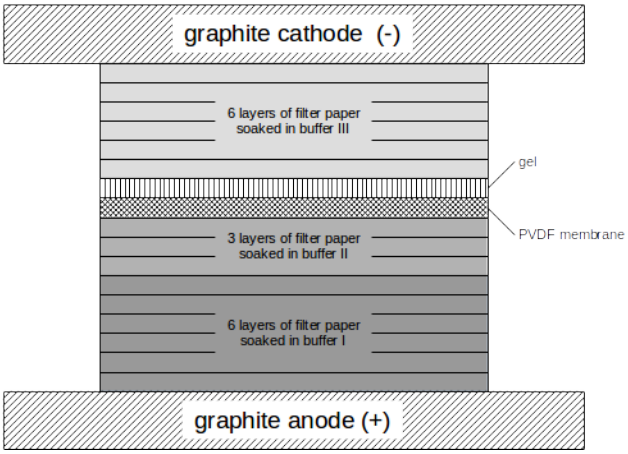

Figure 22.1: Design layout of the semi-dry electro-blotting system. Buffer compositions are listed in table 8.6.

antibodies including their characteristics and incubation parameters (species reactivity, dilutions, etc.) is given in table 22.2. Incubation was performed on a roller mixer overnight at 4 °C. Following the incubation, 3 washing cycles in TBS-T for 10 minutes each at room temperature were performed. Afterwards, the membrane was incubated with a corresponding, HRP-conjugated secondary antibody (sec. 22.4.3) diluted in 5 ml skim milk powder (smp) based blocking solution for 2 h at room temperature on a roller mixer. Next, the membrane was washed 3 times with TBS-T for 10 minutes each at room temperature. Afterwards the membrane was incubated in ECL developing solution (BioRad) for 5 minutes at room temperature. The chemoluminescence reaction was detected using the ChemiDocXRS^{TM} scanning system (BioRad).

To allow staining of several epitopes on a membrane, the membrane was washed 3 times in TBS-T after each detection. Then the staining with another primary antibody was performed like described above. Between different stainings, an antibody stripping was performed if necessary. For this, the membrane was incubated in 5 ml 1x Re-Blot Plus^{TM} antibody stripping solution (Millipore) on a shaker at room temperature for 20 minutes followed by a repeated 2 h incubation in wb blocking solution.

22.4.3 Western blot antibodies

Table 22.2 lists the primary antibodies used for detection of blotted proteins. The HRP conjungated secondary antibodies (anti-mouse IgG: CST ord.-no.: 7076, anti-rabbit: ord.-no.: 7074) were diluted 1:3000 in 5 ml SMP-based blocking solution (50 g/l SMP in TBS-T).

Table 22.2: Primary antibodies used for western blot.

Antigen	Species-reactivity	Host	Clonality/ Isotype	Stock conc.	Dillution		Diluent	Company/ order-no.	
Actin	h, m, rt	rb	pAb IgG	200 µg/ml		1:100	SMP	SC	sc-1616R
P-AKT (Ser473)	h, m	rb	mAb IgG	n/a*		1:2000	BSA	CST	4060
β-Catenin	h, m, rt, f	rb	pAb IgG	n/a*		1:1000	BSA	CST	9562
E-Cadherin	h, m, rt, f	m	mAb IgG2	250 µg/ml		1:3000	SMP	BD	610182
HMOX 1	h, m	m	mAb IgG2	200 µg/ml		1:500	SMP	SC	sc-390991
HSP90 α/β	h, m, rt	m	pAb IgG	200 µg/ml	h:	1:2000	SMP	SC	sc-7947
					m/rt:	1:200	SMP		
IkB*a*	h, m, rt, f	m	mAB IgG2a	n/a*		1:1000	SMP	CST	9247
P-IkB*a* (Ser32)	h, m, rt, f	rb	pAb IgG	n/a*		1:1000	BSA	CST	9241
iNOS	m	m	mAb IgG2a	250 µg/ml		1:2000	SMP	BD	610328
NF-κB	h, m, f	rb	pAb IgG	200 µg/ml		1:1000	SMP	SC	sc-109
NQO1	h, m, rt	m	mAb IgG2b	200 µg/ml		1:200	SMP	SC	sc-376023
NRF2	h, m, rt	rb	pAb IgG	200 µg/ml		1:500	SMP	SC	sc-13032
Occludin	h, m, rt, f	m	mAb IgG	250 µg/ml		1:500	SMP	BD	611090
a-Tubulin	h, m, rt, f	m	mAb IgG1	23.6 µg/ml*	h:	1:10000	SMP	SA	T5168
					m/rt:	1:2500	SMP		
Vimentin	h, m, rt	m	mAb IgG1	200 µg/ml		1:250	SMP	SC	sc-32322
Villin-1	h, m, rt	rb	pAb IgG	n/a*		1:1000	SMP	CST	2369
ZO1	h, m, rt	rb	pAb IgG	400 µg/ml		1:1000	SMP	GTX	GTX108613

Legend:

Species reactivity: letters: manufacturer recommendation, underlined: successfully applied.

*: Concentration Lot depending.

Company abbreviations: BD: Becton Dickinson, CST: Cell Signaling Tech., GTX: GeneTex, SA: Sigma-Aldrich, SC: Santa Cruz Bio.

For further abbreviations see the list on page XVII.

23 RNA extraction and quantitative real time PCR

23.1 RNA extraction and purification

Cell harvesting with subsequent RNA extraction and purification was performed using the column based RNeasy^{TM} mini RNA extraction Kit (Qiagen) in combination with QiaShredder^{TM} columns accordingly manufacturers instructions. An additional DNAse digestion was conducted during the purification process. The processed samples were stored at -80 °C until further use.

Purity and RNA concentration of generated samples was verified photometrically using the Nanodrop^{TM} ND1000 photometer (Peqlab).

23.2 Reverse transcription of RNA into complementary DNA

An 0.5 – 1.5 µg total RNA containing volume RNA-solution was adjusted with water to a total volume of 11.5 µl. After addition of 1 µL oligo dT primers (Fermentas, 100 µmol/l) the solution was incubated at 65 °C for 5 minutes. After cooling down on ice, 7.5 µl mastermix were added. The composition of the mastermix is listed in table 23.1. The reverse transcription was performed by incubating the reaction mix at 42 °C for 60 minutes. Afterwards, the reaction mix was heated up to 70 °C for 5 minutes to deactivate the reverse transcriptase. The processed samples were diluted 1:5 in water. Purity and complementary DNA (cDNA) concentration of the generated samples was verified photometrically using the Nanodrop^{TM} ND1000 photometer (Peqlab). The samples were stored at -20 °C until further use.

Table 23.1: Master mix composition for RT-PCR.

Volume	Component
4.0 µl	5x RT reaction buffer
2.0 µl	dNTP solution (c=10 $^{mmol}/_{l}$, each)
0.5 µl	RiboLock^{TM} RNase inhibitor (c=40 $^{U}/_{µl}$)
1.0 µl	RevertAid^{TM} mMLV reverse transcriptase (c=200 $^{U}/_{µl}$)

23.3 Quantitative real time PCR

23.3.1 General

Quantitative real-time PCR (qPCR) was performed using the Blue S'Green^{TM} qPCR mix kit (Biozym) in combination with a CFX^{TM} 96-well qPCR cycler (BioRad). 2 µl cDNA containing sample were transfered as duplicates or triplicates into a well of a 96-well reaction plate. Next, 10 µl freshly prepared mastermix (composition is listed in table 23.2) were added. The plate was sealed, shaken and the samples were spun down shortly. Subsequently, the qPCR reaction was performed. The qPCR conditions are listed in table 23.3. Primer sequences for the respectively target genes as well as their optimal annealing temperatures are listed in table 23.4.

Table 23.2: Master mix composition for qPCR.

Volume	Component
6.000 µl	5x Blue S'Green^{TM} reaction buffer
0.048 µl	Fwd primer (100 $^{µmol}/_{l}$)
0.048 µl	Rev primer (100 $^{µmol}/_{l}$)
3.904 µl	water

23.3.2 qPCR primer sequences and corresponding annealing temperatures

Primer sequences for qPCR (tab. 23.4) were designed using the NCBI PrimerBlast^{TM} software. All primers were purchased from Eurofins and adjusted with water to a stock concentration of 100 $^{µmol}/_{l}$. They were stored at -20 °C. Optimal annealing temperatures were established experimentally.

23.3.3 qPCR quality control

The following measures were implemented to ensure the quality of the generated qPCR data:

- All samples were measured as duplicates or triplicates.
- Melting curves of all qPCR products were achieved.
- For all applied Primer/cDNA combinations, a gel electrophoresis of the qPCR product was performed at least once to verify the molecular size and purity of the product.
- For each cDNA sample at least two different housekeeping genes were used for normalization.

Table 23.3: qPCR conditions.

Step	PCR conditions		
	temperature	time	cycles
Initial melting step	95 °C	120 s	
Melting	95 °C	5 s	↻ 40×
Annealing	* °C	10 s	
Elongation	65 °C	20 s	
Melting curve	65-95 °C		

*: The optimal annealing temperature for each sample/primer combination was determined theoretical as well as experimental. The distinct temperatures are listed in table 23.4 together with the primer sequences.

Table 23.4: qPCR primer sequences and their corresponding annealing temperatures.

Gene	Primer sequence	Annealing temp.
m*Hprt*		
fwd:	5′- G C T G A C C T G C T G G A T T A C A T -3′	64 °C
rev:	5′- T T G G G G C T G T A C T G C T T A A C -3′	
m*Ier3*		
fwd:	5′- G A T A T G C C T C C C C T G C T G T A A -3′	62 °C
rev:	5′- A A G G G T C T T C C A A A G C C T T A -3′	
m*Il-1β*		
fwd:	5′- C C C A A C T G G T A C A T C C A G C A C -3′	62 °C
rev:	5′- T C T G C T C A T T C A C G A A A A G G -3′	
m*Il-6*		
fwd:	5′- T A G T C C T T C C T A C C C C A A T T T C C -3′	65 °C
rev:	5′- T T G G T C C T T A G C C A C T C C T T C -3′	
m*Il-10*		
fwd:	5′- G G C G C T G T C A T C G A T T T C T C -3′	64 °C
rev:	5′- A T G G C C T T G T A G A C A C C T T G G -3′	
m*Nos2 (iNos)*		
fwd:	5′- T C C C T T C C T T G C A T G T G C C C -3′	62 °C
rev:	5′- T G A C C A T C T C G G G T G C G G T A -3′	
m*Rpl13a*		
fwd:	5′- A T G A C A A G A A A A A G C G G A T G -3′	64 °C
rev:	5′- C T T T T C T G C C T G T T T C C G T A -3′	
m*Tgf-β*		
fwd:	5′- A G C T G C G C T T G C A G A G A T T A -3′	62 °C
rev:	5′- A G C C C T G T A T T C C G T C T C C T -3′	
m*Tnf*		
fwd:	5′- C C C A C T C T G A C C C C T T T A C T -3′	62 °C
rev:	5′- T T T G A G T C C T T G A T G G T G G T -3′	

24 Flow cytometry

24.1 Cell detachment and harversting

Adherent cells were detached and harvested by the respectively standard protocol (see sections 13.3 and 14.1). For the staining of some extracellular antigens, the detachment process had to be adjusted, due to the enzymatic shedding activity of the actual detachment reagent.

24.2 Staining

- All antigen staining were performed using fluorophor conjugated REA^{TM}antibodies (Miltenyi) exclusively, according to manufacturer's recommendations. A list of the applied antibodies is given in table 24.1. Table 24.2 lists the respective isotype controls.

- Due to the specific design of REA^{TM}antibodies (Miltenyi), it was not necessary to perform an F_C-receptor block before staining[62].

- Following staining batch combinations were performed for each experiment:

  - Unstained (for optimal PMT-Voltage adjustment).

  - Single staining of each antigen (for channel compensation).

  - Combined staining of with all isotype control antibodies (for negative/positive gating)

  - Combined staining of all antigens in one batch (actually sample).

[62] Nevertheless, for each new experiment an F_C-receptor block was performed once for validation.

Table 24.1: Fluorochrome conjugated REA* antibodies applied for flow cytometry analysis.

Antigen	Species-reactivity	Host	clonality/ Isotype	Fluoro-chrome conjugate	Stock conc.	Dilution	Order-no.***
CD11b	m	Rec. (h)	mAb IgG1 (REA*)	APC	150 µg/ml	1:50	130-113-802
CD11c	m	Rec. (h)	mAb IgG1 (REA*)	PE	150 µg/ml	1:50	130-110-701
CD68	m	Rec. (h)	mAb IgG1 (REA*)	VioBlue**	150 µg/ml	1:50	130-112-861
CD200R	m	Rec. (h)	mAb IgG1 (REA*)	APC	150 µg/ml	1:50	130-112-531
F4/80	m	Rec. (h)	mAb IgG1 (REA*)	FITC	30 µg/ml	1:10	130-102-988
MHC II	m	Rec. (h)	mAb IgG1 (REA*)	PE	150 µg/ml	1:50	130-104-625

Legend:
*: REA is a trademark of recombinant antibodies from Miltenyi.
**: VioBlue is a fluorochome distributed by Miltenyi, with a em/ex-spectrum comparable to AF-405.
***: All antibodies were purchased from Miltenyi.
For further abbreviations see the list at page XVII.

Table 24.2: Fluorochrome conjugated REA isotype control antibodies applied for flow cytometry analysis.

Host	Clonality/ isotype	Fluorochrmome conjugate	Stock conc.	Order no.***
Rec. (h)	mAb IgG1 (REA*)	APC	30 µg/ml	130-104-630
Rec. (h)	mAb IgG1 (REA*)	FITC	30 µg/ml	130-104-626
Rec. (h)	mAb IgG1 (REA*)	PE	30 µg/ml	130-104-628
Rec. (h)	mAb IgG1 (REA*)	VioBlue**	30 µg/ml	130-104-625

Legend:
*: REA is a trademark of recombinant antibodies from Miltenyi.
**: VioBlue is a fluorochome distributed by Miltenyi, with a em/ex-spectrum comparable to AF-405.
***: All antibodies were purchased from Miltenyi.
For further abbreviations see the list at page XVII.

24.3 Gating strategy

First, the optimal FSC and SSC PMT-voltages were adjusted to detect the majority of all events. After excluding all debris from the parental population by inverse gating, the optimal PMT-voltage for each single channel was adjusted in a live color/SSC dot plot

diagram as well in a histogram using unstained (*sic*!) cells[63]. Next, a channel bleeding compensation was performed using single stained samples. Gates to discriminate between negative and positive events were set in reference to the fluorescence intensity of the isotype controls.

25 Statistics

The statistical significance of the results was calculated either by an adjusted two-sided Wilcoxon-Mann-Whitney test or by two-sided Student's *t*-test, depending on the experimental design. A p-value ≤ 0.05 was considered as statistical significant (*), while a p-value ≤ 0.01 was considered as statistical highly significant (**). Calculations were performed using the *Gnumeric* software application [203] in version 1.12.28.

[63] The goal of this approach is to to set the mean fluorescence intensity for each channel to zero without overcompensating the respectively channel. This ensures a optimal channel sensitivity while avoiding the risk of detecting false positive events despite correct gating.

Results

26 Phenotype comparison between *Ier3-flox$^{+/+}$ LysM-Cre$^{-/-}$* and *Ier3-flox$^{+/+}$ LysM-Cre$^{+/+}$* mice

Before starting experimental colitis experiments with mice exhibiting *Ier3* proficiency and deficiency in the myeloid compartment, their basal status was analyzed.

26.1 Body weight and organs

Body weight and parameters of immunological relevant organs of from male *Ier3-flox$^{+/+}$ LysM-Cre$^{-/-}$* and *Ier3-flox$^{+/+}$ LysM-Cre$^{+/+}$* mice ($n_{\text{each GT}} \geq 5$) with an average age of 14 weeks (±6 days) were compared (fig. 26.1). With a median body weight of 34.0 g, *Ier3-flox$^{+/+}$ LysM-Cre$^{+/+}$* animals were on average 23 % heavier than *Ier3-flox$^{+/+}$ LysM-Cre$^{-/-}$* mice (27.6 g; fig. 26.1a; p=0.050). Both genotypes showed no significant differences in their median colon length (fig. 26.1b), liver weight (fig. 26.1d) and spleen weight (fig. 26.1e), while their medial cecum weight differed significant (p=0.014) from 16.72 $^{\text{mg}}/_{\text{g body weight}}$ in the *Ier3-flox$^{+/+}$ LysM-Cre$^{-/-}$* cohort to 14.81 $^{\text{mg}}/_{\text{g body weight}}$ (fig. 26.1c).

26.2 Histology

Histologically, there were no morphological differences observable between both genotypes (fig. 26.2). Furthermore, tissue and cell morphology did not deviate from the one of healthy non-transgenic wild-type mice, including the presence of a moderate number of F4/80-positive MΦ.

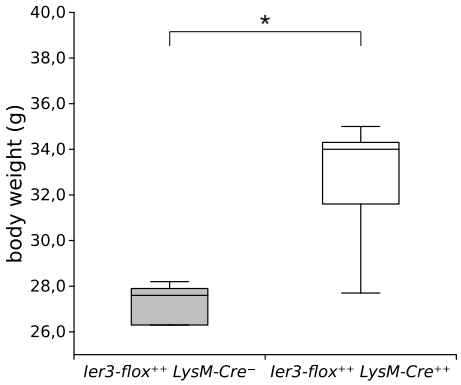

(a) Absolute, median **body weight**.

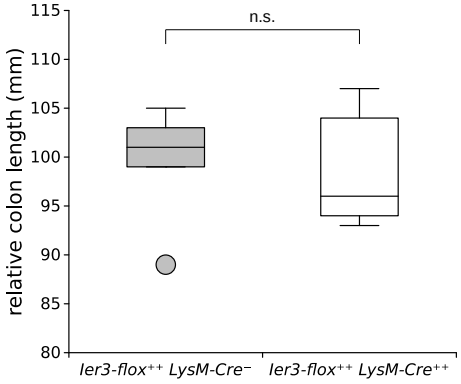

(b) Absolute, median **colon length**.

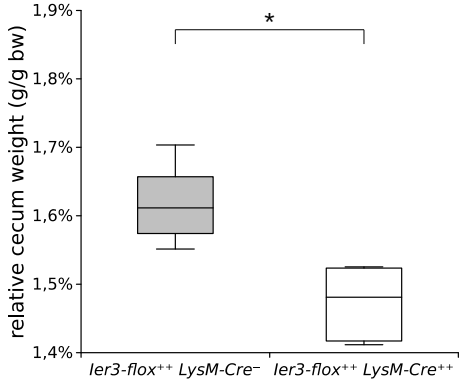

(c) Relative, median **cecum weight**, normalized to body weight.

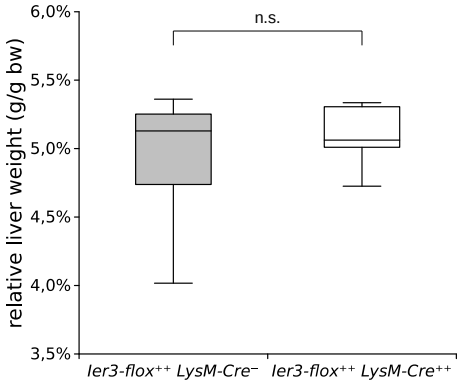

(d) Relative, median **liver weight**, normalized to body weight.

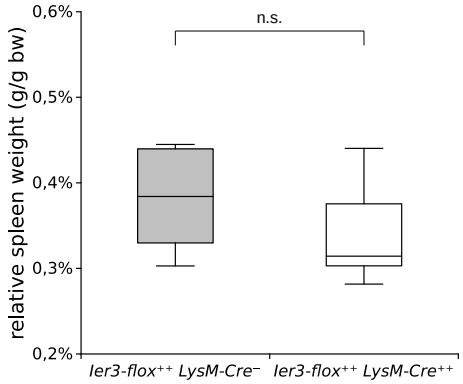

(e) Relative, median **spleen weight**, normalized to body weight.

Figure 26.1: Comparison of body weight and immunological relevant organs from *Ier3-flox$^{+/+}$ LysM-Cre$^{-/-}$* and *Ier3-flox$^{+/+}$ LysM-Cre$^{+/+}$* mice. Animals had an age of 14 weeks (± 6 days) on the day they were sacrificed ($n_{\text{each GT}} \geq 5$). Shown are median values of the analyzed parameters (crossbar within the box). Boxes cover the 25 % and 75 % quantiles. Whisker length corresponds to values with a maximal medial deviation of the 1.5-folds interquartile range, while extreme values are indicated as bullets. Statistical significance in the difference between the two cohorts was determined by adjusted WILCOXON-MANN-WHITNEY-test. A p-value ≤ 0.05 is considered as statistically significant (*).

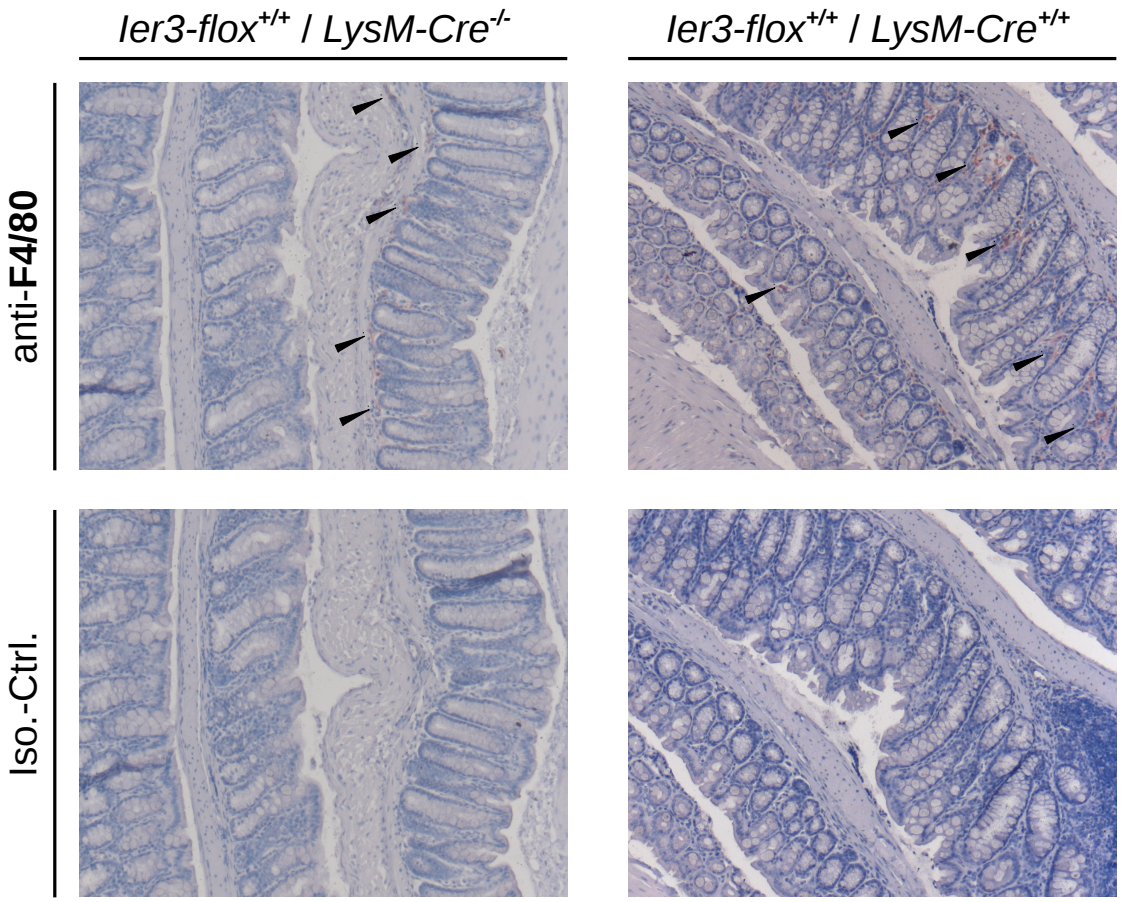

Figure 26.2: IHC staining of MΦ in the colons of healthy *Ier3-flox$^{+/+}$ LysM-Cre$^{-/-}$* and *Ier3-flox$^{+/+}$ LysM-Cre$^{+/+}$* mice with an average age of 14 weeks ($\pm$6 days). Colons were removed immediately after killing the animals and the specimen were processed subsequently as described in sec. 12.1. Conventional immunostaining was performed as described in sec. 12.3.2. MΦ were stained using an anti *F4/80* antibody (CST) or an respectively isotype control Ab. Detection was performed by chromogenic AEC reaction (*red*) using a HRP-conjugated secondary antibody. Areas of increased MΦ accumulation are additionally indicated by black arrow heads. Cell nuclei were counterstained using MEYER'S haematoxylin (*blue*). Shown are representative pictures.

27 *In vivo* effects of myeloid IER3-deficiency in response to DSS and AOM

Several dextran sodium sulphate (DSS) or azoxymethane (AOM)/DSS animal experiments were conducted to study putative effects of myeloid IER3 in the context of acute as well chronic colitis and colitis associated carcinogenesis (CAC) *in vivo*.

27.1 Myeloid *Ier3* knockout mitigates acute DSS colitis

27.1.1 Weight loss and survival

The role of myeloid IER3 in acute colitis was investigated in two independent animal experiments by applying high DSS (30 g/l) in drinking water *ad libitum* over a period of 9-10 days. Animals of both genotypes started to loose body weight from day 4-5 after having started the DSS treatment (fig. 27.1). Until day 6, weight loss in the *Ier3-flox*$^{+/+}$ *LysM-Cre*$^{+/+}$ cohort was slightly greater compared to the *Ier3-flox*$^{+/+}$ *LysM-Cre*$^{-/-}$ group (exp. #1: -9 % vs. -8 %; exp. #2: -7 % vs. -5 %). This trend started to reverse between day 6 and 7. While weight loss in both genotypes continued until the end of the experiments, it was markedly more pronounced in *Ier3-flox*$^{+/+}$ *LysM-Cre*$^{-/-}$ animals. Moreover, the weight difference between both genotypes increased during time. At the endpoint, *Ier3-flox*$^{+/+}$ *LysM-Cre*$^{-/-}$ animals in exp. #1 on average had lost 23 % body weight (exp. #2: 17 %), while *Ier3-flox*$^{+/+}$ *LysM-Cre*$^{+/+}$ animals in exp. #1 lost 17 % (exp. #2: 9 %). Even though both experiments similarly show differential weight loss patterns, differences within each experiment were statistically not significant. Weight loss in both genotypes was accompanied by diarrhea and the appearance of occult blood in the feces, though without distinct differences between both genotypes.

In both experiments, all *Ier3-flox*$^{+/+}$ *LysM-Cre*$^{+/+}$ mice survived until the scheduled endpoint (fig. 27.2), whereas one animal from the *Ier3-flox*$^{+/+}$ *LysM-Cre*$^{-/-}$ cohorts had to

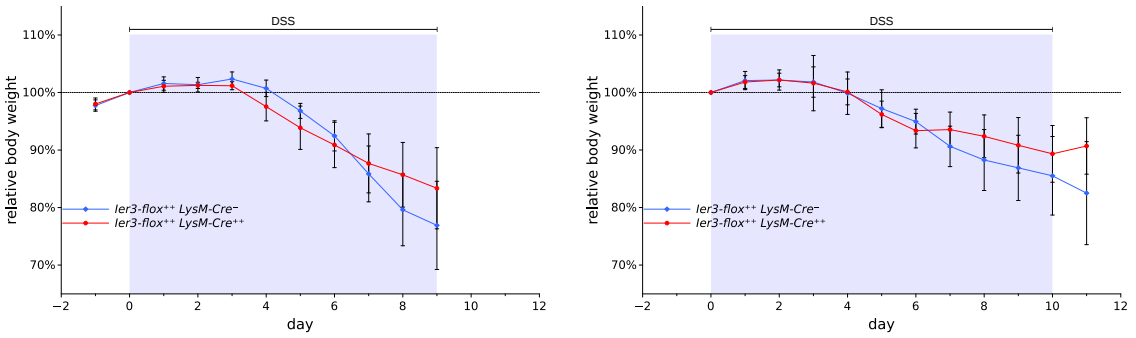

(a) Experiment *#1*. $n_{\text{each GT}} = 8$.

(b) Experiment *#2*. $n_{\text{LysM-Cre}^{-/-}} = 8$. $n_{\text{LysM-Cre}^{+/+}} = 9$.

Figure 27.1: Comparison of *body-weight* loss between *Ier3-flox*$^{+/+}$ *LysM-Cre*$^{-/-}$ and *Ier3-flox*$^{+/+}$ *LysM-Cre*$^{+/+}$ animals during *acute* DSS colitis. 9 week (±3 days) old *Ier3-flox*$^{+/+}$ *LysM-Cre*$^{-/-}$ and *Ier3-flox*$^{+/+}$ *LysM-Cre*$^{+/+}$ mice received 30 g/l DSS in drinking water *ad libitum* over a period of 9 days (exp. #1) or 10 days (exp. #2). Mice were prematurely excluded from the experiment if matching at least one abort criterion. Shown is the mean relative body-weight of each cohort in relation to the absolute body-weight at day 0. Error bars represent relative standard deviation.

be excluded prematurely (exp. #1: day seven, fig. 27.2a; exp. #2: day nine, fig. 27.2b) due to its poor health condition.

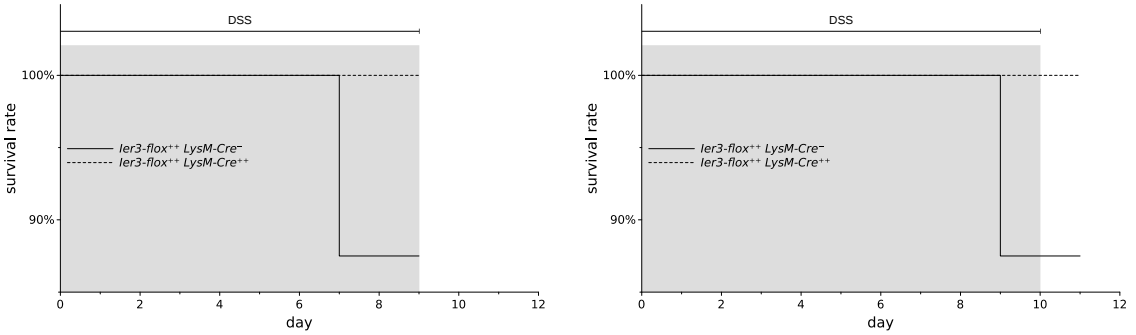

(a) Experiment *#1*. $n_{\text{each GT}} = 8$.

(b) Experiment *#2*. $n_{\text{LysM-Cre}^{-/-}} = 8$. $n_{\text{LysM-Cre}^{+/+}} = 9$.

Figure 27.2: Kaplan Meyer *survival curve* of *Ier3-flox*$^{+/+}$ *LysM-Cre*$^{-/-}$ and *Ier3-flox*$^{+/+}$ *LysM-Cre*$^{+/+}$ animals during the onset of acute DSS colitis. Experimental design as described in figure 27.1.

27.1.2 Post mortem analysis of immunological relevant organs

At the end point of the experiments, there were no differences in colon length (fig. 27.3a) as well in the cecum weight (fig. 27.3b) between both genotypes. Interestingly, in experiment #1, *Ier3-flox*$^{+/+}$ *LysM-Cre*$^{+/+}$ animals showed a significant higher liver weight compared to *Ier3-flox*$^{+/+}$ *LysM-Cre*$^{-/-}$ animals (p=0.049, fig. 27.3c). In addition, the spleen

weights were significantly lower in *Ier3-flox*$^{+/+}$ *LysM-Cre*$^{+/+}$ mice than in *Ier3-flox*$^{+/+}$ *LysM-Cre*$^{-/-}$ mice ($p \leq 0.002$, fig. 27.3d). However, those differences were not observed in experiment #2 (fig. 27.3a-27.3d).

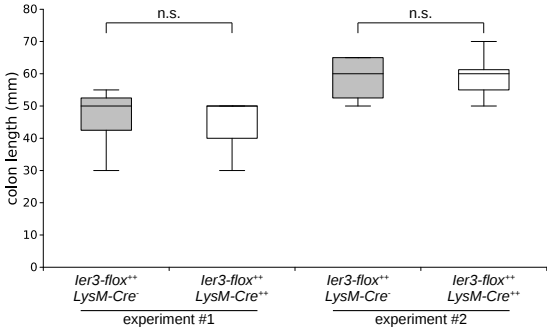

(a) Absolute, median **colon length**.

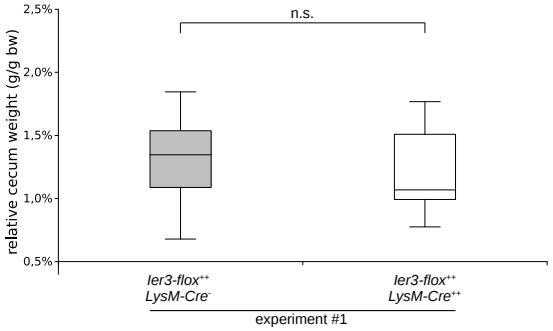

(b) Relative, median **cecum weight**, normalized to body weight.

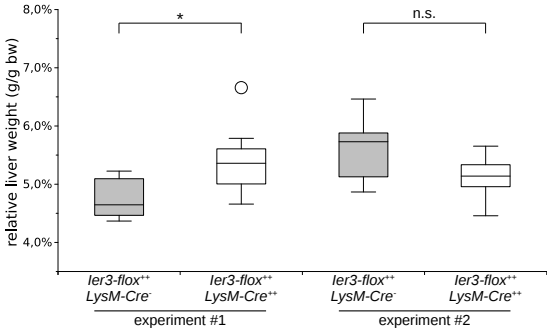

(c) Relative, median **liver weight**, normalized to body weight.

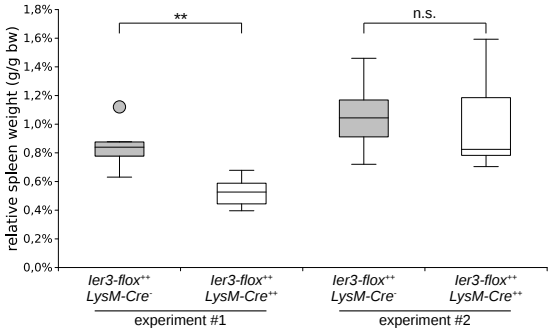

(d) Relative, median **spleen weight**, normalized to body weight.

Figure 27.3: Comparison of immunological relevant organs from *Ier3-flox*$^{+/+}$ *LysM-Cre*$^{-/-}$ and *Ier3-flox*$^{+/+}$ *LysM-Cre*$^{+/+}$ mice after induction of *acute* AOM/DSS colitis. Animals had an age of 14 weeks (± 6 days) on the day they were sacrificed ($n_{\text{each GT}} \geq 5$). Experimental design as described in figure 27.1. Shown are median values of the analyzed parameters (crossbar within the box) from seven *Ier3-flox*$^{+/+}$ *LysM-Cre*$^{-/-}$ and nine *Ier3-flox*$^{+/+}$ *LysM-Cre*$^{+/+}$ animals (experiment #1), respectively seven *Ier3-flox*$^{+/+}$ *LysM-Cre*$^{-/-}$ and eight *Ier3-flox*$^{+/+}$ *LysM-Cre*$^{+/+}$ animals (experiment #2) after experimental termination. Boxes cover the 25 % and 75 % quantiles. Whisker length corresponds to values with a maximal medial deviation of the 1.5-folds interquartile range, while extreme values are indicated as bullets. Statistical significance in the difference between the two cohorts was determined by adjusted WILCOXON-MANN-WHITNEY-test. A p-value ≤ 0.05 is considered as statistically significant (*), while a p-value ≤ 0.01 is considered as statistically highly significant (**).

27.2 Myeloid IER3-deficiency protects during initiation phase of chronic DSS colitis

27.2.1 Weight loss and survival

Mice were injected intraperitoneally (i.p.) with 10 µg/g bw AOM at day -7. DSS was applied at at a concentration of 10 g/l in drinking water *ad libitum* from day 0 until day seven to induce a colitis. *Ier3-flox*$^{+/+}$ *LysM-Cre*$^{-/-}$ animals started to loose weight up from day 6 (fig. 27.4a). Weight loss in *Ier3-flox*$^{+/+}$ *LysM-Cre*$^{-/-}$ animals continued until day ten, where it reached its maximum of -16 % (*Ier3-flox*$^{+/+}$ *LysM-Cre*$^{+/+}$: ±0 %). *Ier3-flox*$^{+/+}$ *LysM-Cre*$^{-/-}$ mice started to recover their body weight from day 11 until they fully gained their initial weight at day 13. However, this is due the fact, that some *Ier3-flox*$^{+/+}$ *LysM-Cre*$^{-/-}$ animals had to be excluded already earlier from the experiment due to their poor health condition (fig. 27.4b). In contrast, all *Ier3-flox*$^{+/+}$ *LysM-Cre*$^{+/+}$ animals showed no significant weight loss during the whole experiment. Strikingly, the individual weight distribution within the *Ier3-flox*$^{+/+}$ *LysM-Cre*$^{-/-}$ cohort was much higher compared to the *Ier3-flox*$^{+/+}$ *LysM-Cre*$^{+/+}$ cohort.

As mentioned above, some animals of the *Ier3-flox*$^{+/+}$ *LysM-Cre*$^{-/-}$ cohort matched at least one abortion criterion during the experiment. One animal was excluded on day 11, while two further animals had to be excluded at day 12 (fig. 27.4b). This led to an overall 13 days survival rate of 50 % in the *Ier3-flox*$^{+/+}$ *LysM-Cre*$^{-/-}$ group compared 100 % in the *Ier3-flox*$^{+/+}$ *LysM-Cre*$^{+/+}$ cohort.

27.2.2 Post mortem analysis of organs

At the time point of termination, none of the animals from both genotypes showed any signs of neoplasms. There were no significant differences in the colon length between both cohorts (fig. 27.5a). The same was seen for cecum weights (fig. 27.5b). Interestingly,

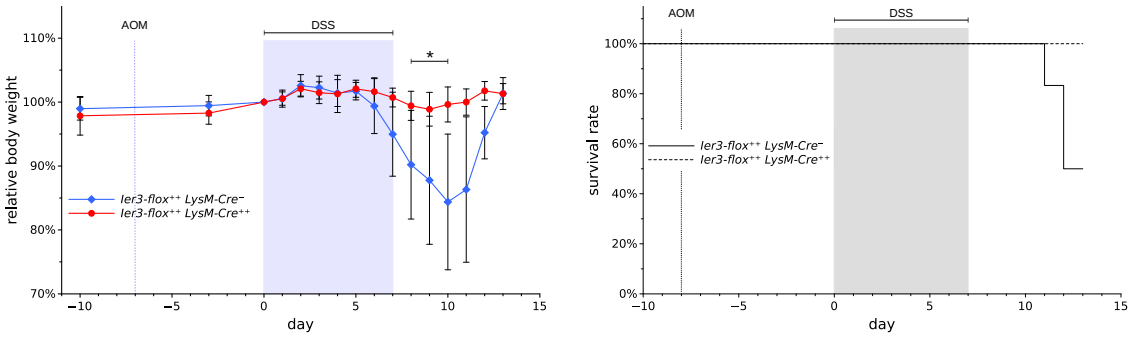

(a) *Body-weight* alterations between *Ier3-flox*$^{+/+}$ *LysM-Cre*$^{-/-}$ and *Ier3-flox*$^{+/+}$ *LysM-Cre*$^{+/+}$ animals in response to AOM/DSS. Shown is the mean relative body-weight of each cohort in relation to the absolute body-weight at day 0. Error bars represent relative standard deviation. Significance of body-weight differences between both cohorts was determined by two-sided Student's t-test. A p-value ≤ 0.05 is considered as statistically significant (*).

(b) Kaplan Meyer *survival curve* of *Ier3-flox*$^{+/+}$ *LysM-Cre*$^{-/-}$ and *Ier3-flox*$^{+/+}$ *LysM-Cre*$^{+/+}$ animals in response to AOM/DSS.

Figure 27.4: Onset of *chronic* AOM/DSS colitis. Six *Ier3-flox*$^{+/+}$ *LysM-Cre*$^{-/-}$ and five *Ier3-flox*$^{+/+}$ *LysM-Cre*$^{+/+}$ mice with an average age of $10\,1/2$ weeks (± 10 days) were injected i.p. with AOM ($10\ \mu g/g$ body weight) at day -7. Animals received 10 g/l DSS in drinking water *ad libitum* from day 0-7. The experiment was terminated at day 13. Mice were excluded earlier from the experiment if matching at least one abortion criterion.

the livers ($p = 0.034$, fig. 27.5c) and spleens ($p = 0.025$, fig. 27.5d) of *Ier3-flox*$^{+/+}$ *LysM-Cre*$^{-/-}$ mice were significant greater compared to *Ier3-flox*$^{+/+}$ *LysM-Cre*$^{+/+}$ animals.

27.2.3 Tissue damage and pathology

Pictures of the whole colon stained with HE from each animal were generated (fig. 27.6) to estimate tissue damage and the extend of inflammatory infiltrates. It can be appreciated, that colons from both genotypes similarly contained both, unobtrusive areas with the typical tissue morphology of healthy animals, as well as areas with tissue damages characteristic for DSS colitis. This includes surface epithelium erosions and an increased mucosal infiltration with cells, *presumptive (!)* of the leukocyte lineage.

However, morphological tissue damages in *Ier3-flox*$^{+/+}$ *LysM-Cre*$^{-/-}$ animals were slightly increased in both, number and severity, when compared to *Ier3-flox*$^{+/+}$ *LysM-Cre*$^{+/+}$ mice.

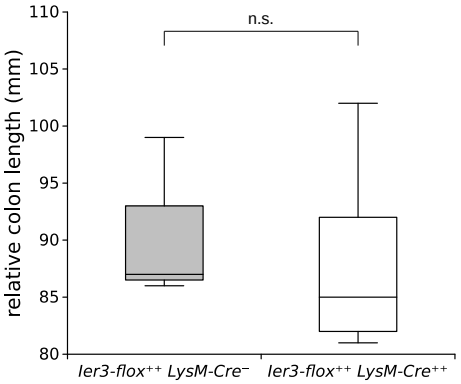

(a) Absolute, median **colon length**.

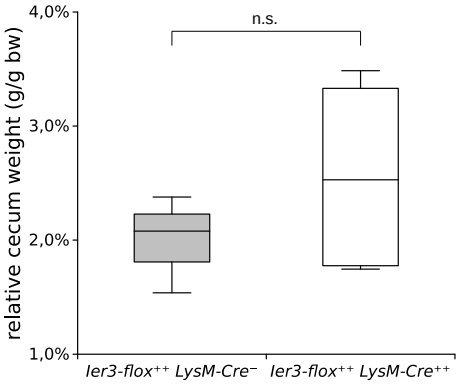

(b) Relative, median **cecum weight**, normalized to body weight.

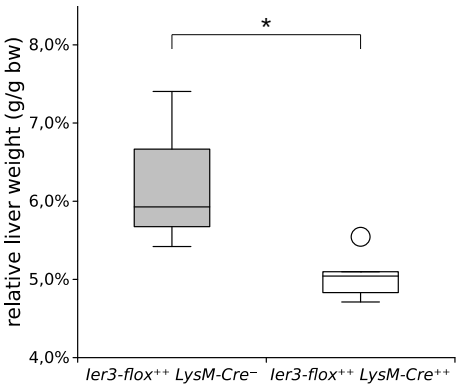

(c) Relative, median **liver weight**, normalized to body weight.

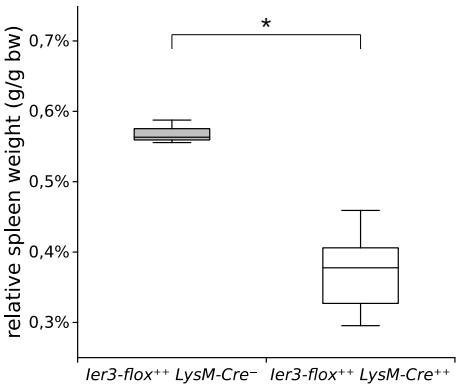

(d) Relative, median **spleen weight**, normalized to body weight.

Figure 27.5: Comparison of immunological relevant organs from *Ier3-flox$^{+/+}$ LysM-Cre$^{-/-}$* and *Ier3-flox$^{+/+}$ LysM-Cre$^{+/+}$* mice after induction of chronically AOM/DSS colitis. Experimental design as described in figure 27.4. Shown are median values of the analyzed parameters (crossbar within the box) from three *Ier3-flox$^{+/+}$ LysM-Cre$^{-/-}$* and five *Ier3-flox$^{+/+}$ LysM-Cre$^{+/+}$* animals after experiment termination at day 13. Boxes cover the 25 % and 75 % quantiles. Whisker length corresponds to values with a maximal medial deviation of the 1.5-folds interquartile range, while extreme values are indicated as bullets. Statistical significance in the difference between the two cohorts was determined by adjusted WILCOXON-MANN-WHITNEY-test. A p-value ≤ 0.05 is considered as statistically significant (*).

27.2.4 Macrophage infiltration

Macrophage infiltration into the mucosa was determined histologically by conventional AEC based immunostaining against F4/80 (fig 27.7). The specificity of the staining was verified by an appropriate isotype control. Specimen from both genotypes exhibited a massive infiltration of MΦ into all layers of the mucosa. There was no difference

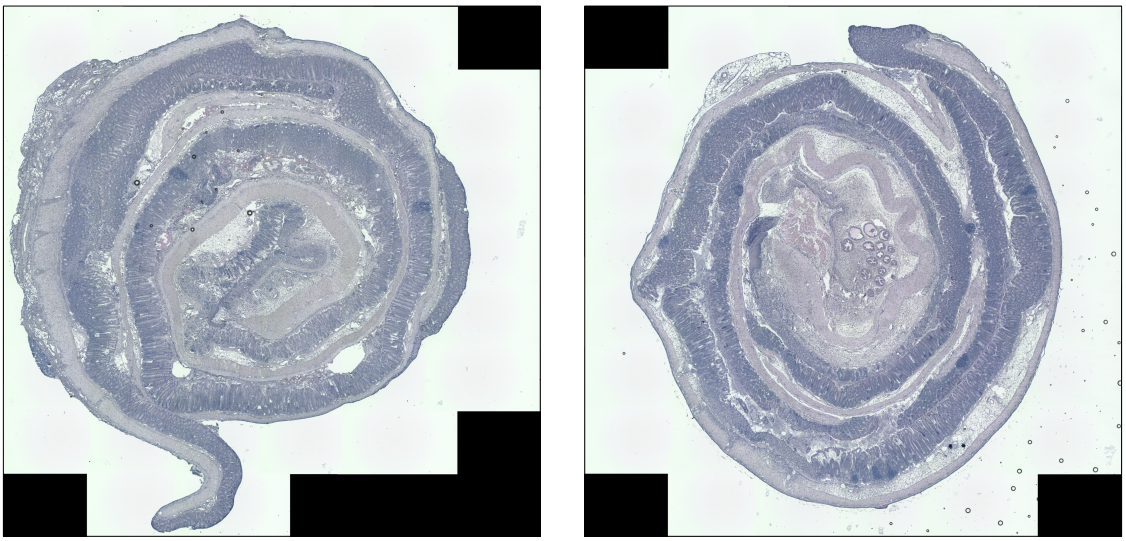

(a) *Ier3-flox*$^{+/+}$ *LysM-Cre*$^{-/-}$ **(b)** *Ier3-flox*$^{+/+}$ *LysM-Cre*$^{+/+}$

Figure 27.6: Exemplary HE staining of colons from *Ier3-flox*$^{+/+}$ *LysM-Cre*$^{-/-}$ and *Ier3-flox*$^{+/+}$ *LysM-Cre*$^{-/-}$ animals treated with AOM/DSS. Experimental design as described in figure 27.4. After termination, colons were dissected, rinsed with PBS and cut open longitudinally. Histological specimen were processed as described in sec. 12.1. HE staining was performed as described in sec. 12.3.1.

seen in the grade of infiltration between *Ier3-flox*$^{+/+}$ *LysM-Cre*$^{-/-}$ and *Ier3-flox*$^{+/+}$ *LysM-Cre*$^{+/+}$ animals.

27.2.5 Expression of cellular junction related proteins

As the disintegrity of cellular junctions (CJ) is an critical aspect during the pathogenesis of IBD and CAC in humans (sec. 3.3), respectively during AOM/DSS colitis in mice, we analyzed the *in vivo* expression of several CJ related proteins.

The expression of the CJ related proteins E-cadherin and β-catenin in the colonic mucosa was determined by fluorescence based immunostaining (fig. 27.8). The specificity of the staining was verified by an appropriate isotype control (not shown).

In both genotypes, there were high fluctuations in the expressional intensity of the two proteins within a single colon. Nevertheless, the overall expression of E-cadherin as well as of β-catenin was much higher in *Ier3-flox*$^{+/+}$ *LysM-Cre*$^{+/+}$ animals when compared to *Ier3-flox*$^{+/+}$ *LysM-Cre*$^{-/-}$ mice.

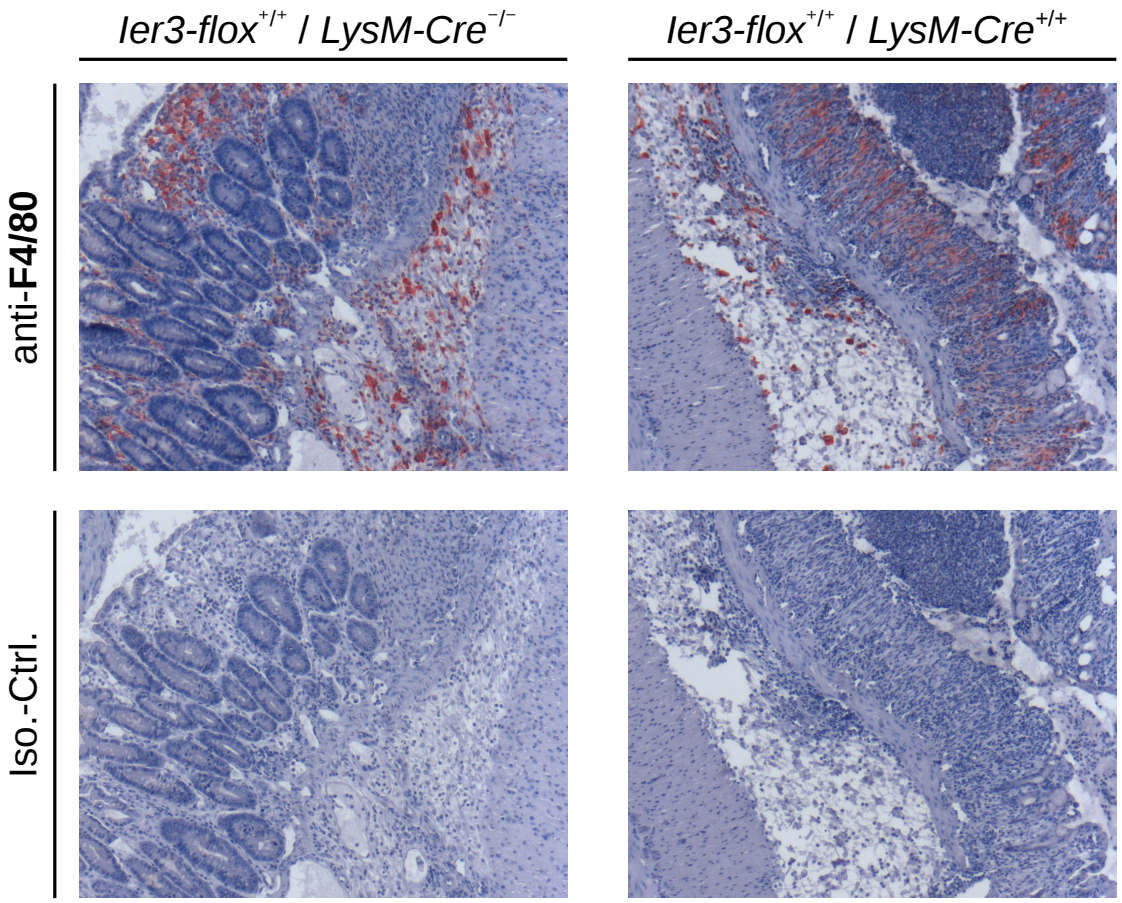

Figure 27.7: MΦ infiltration in the colonic mucosa of *Ier3-flox$^{+/+}$ LysM-Cre$^{-/-}$* and *Ier3-flox$^{+/+}$ LysM-Cre$^{+/+}$* animals after AOM/DSS-treatment. Experimental design as described in figure 27.4. After termination, colons were dissected, rinsed with PBS and cut open longitudinally. Histological specimen were processed as described in sec. 12.1. Conventional immunostaining was performed as described in sec. 12.3.2. MΦ were stained using an anti *F4/80* antibody (CST) or an respectively isotype control Ab. Detection was performed by chromogenic AEC reaction (*red*) using a HRP-conjugated secondary antibody. Cell nuclei were counterstained using MEYER'S Haematoxylin (*blue*). Shown are representative pictures of colons from *Ier3-flox$^{+/+}$ LysM-Cre$^{-/-}$* and *Ier3-flox$^{+/+}$ LysM-Cre$^{+/+}$* mice at day 13.

Furthermore, there was a decreasing gradient in the expressional intensity of both proteins from the lumen facing site towards the crypts. In some colon segments of *Ier3-flox$^{+/+}$ LysM-Cre$^{-/-}$* mice this resulted in a distinctly weakened protein expression in the apical surface, whereas β-catenin and especially E-cadherin, were barely detectable in the crypts of these segments.

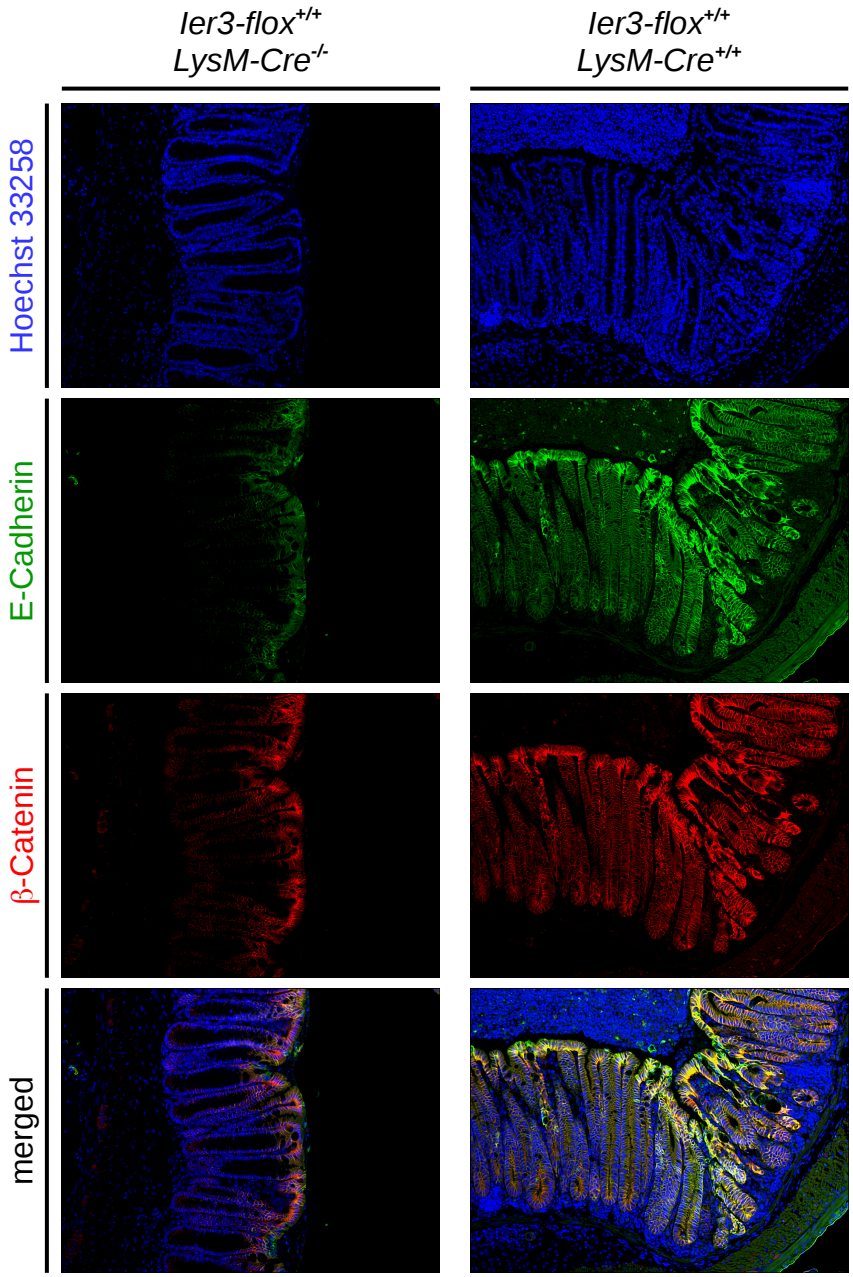

Figure 27.8: Expression of E-cadherin and β-catenin – IHC-F. Experimental design as described in figure 27.4. After termination, colons were dissected, rinsed with PBS and cut open longitudinally. Histological specimen were processed as described in sec. 12.1. IHC-F staining was performed as described in sec. 12.3.3. E-Cadherin appears *green*, while β-catenin appears *red*. Appropriate isotype controls were performed for all specimen (not shown). Cell nuclei were counterstained with Hoechst bisbenzimide H33258 (*blue*). Shown are representative pictures from colons of *Ier3-flox*$^{+/+}$ *LysM-Cre*$^{-/-}$ and *Ier3-flox*$^{+/+}$ *LysM-Cre*$^{+/+}$ mice.

27.3 Myeloid depletion of IER3 protects mice from colitis associated carcinogenesis

The pathogenesis of UC and subsequent carcinogenesis was explored by employing long term AOM/DSS treatment.

27.3.1 Weight loss

Figure 27.9 illustrates the body weight course of both cohorts during the experiment. *Ier3-flox*$^{+/+}$ *LysM-Cre*$^{-/-}$ animals started to loose weight at the beginning of the first DSS cycle. Until day four, they lost on average 11 % body weight before sustaining on this level. In contrast, *Ier3-flox*$^{+/+}$ *LysM-Cre*$^{+/+}$ mice showed no weight loss during or after the first DSS cycle. The difference in body weight between both cohorts was highly significant from day two until day 11. *Ier3-flox*$^{+/+}$ *LysM-Cre*$^{-/-}$ animals started to regain weight up from day 11 until they reached their initial weight at day 21. The second DSS cycle was shortened to 3 days to prevent premature discontinuation of the experiment[64]. However, this cycle had no impact on the body weight of neither the cohorts. Animals from both genotypes started again to loose body weight from day 42, which was the seventh day of the third DSS cycle. Weight loss continued until day 44 in the *Ier3-flox*$^{+/+}$ *LysM-Cre*$^{-/-}$ group (-13 %) and day 45 in the *Ier3-flox*$^{+/+}$ *LysM-Cre*$^{+/+}$ group (-17 %) respectively. After the third DSS cycle, *Ier3-flox*$^{+/+}$ *LysM-Cre*$^{-/-}$ animals recovered faster compared to *Ier3-flox*$^{+/+}$ *LysM-Cre*$^{+/+}$ mice, so that there was a significant difference in the body weight between both cohorts from day 48 until day 57. *Ier3-flox*$^{+/+}$ *LysM-Cre*$^{-/-}$ animals fully regained their initial weight until day 48 (99 %), while for *Ier3-flox*$^{+/+}$ *LysM-Cre*$^{+/+}$ animals this was not before day 63 (100 %). Animals in both cohorts slightly continued to gain body weight until the scheduled end of the experiment at day 85.

[64] Compare to abortion criteria listed in section 10.6.

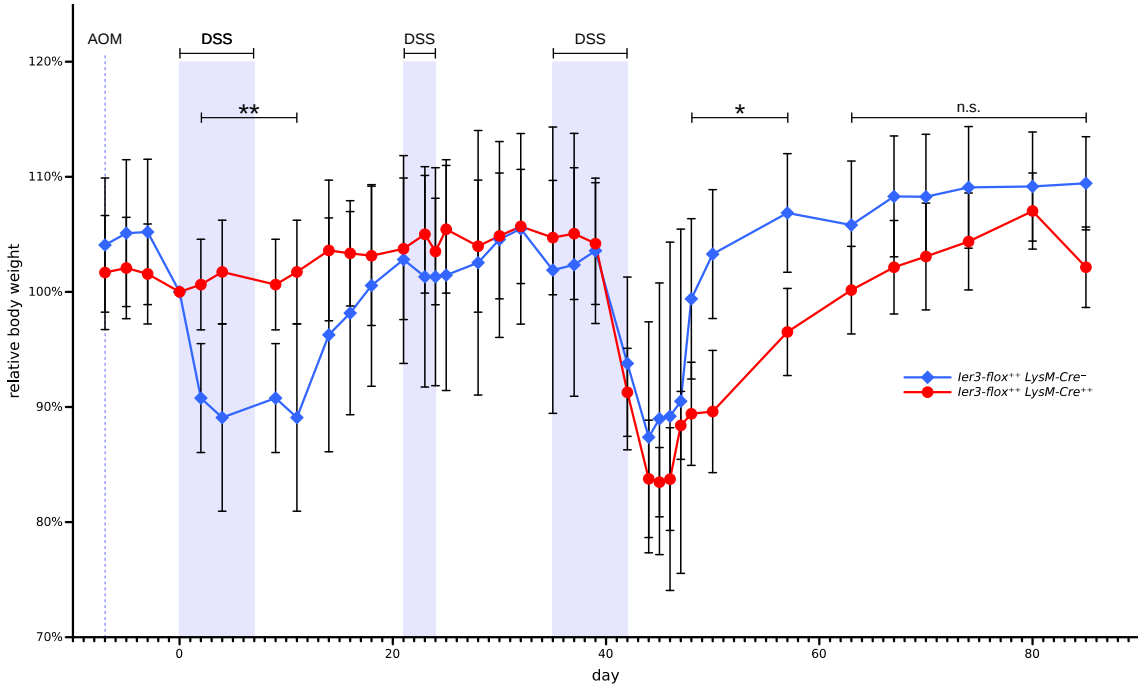

Figure 27.9: Long term comparison of body-weight alterations between *Ier3-flox$^{+/+}$ LysM-Cre$^{-/-}$* and *Ier3-flox$^{+/+}$ LysM-Cre$^{+/+}$* animals in response to AOM/DSS. Ten *Ier3-flox$^{+/+}$ LysM-Cre$^{-/-}$* and nine *Ier3-flox$^{+/+}$ LysM-Cre$^{+/+}$* mice with an average age of $13\,1/2$ weeks were injected i.p. with AOM (10 µg/g body weight) at day -7. DSS (10 g/l in drinking water *ad libitum*) was applied from day 0-7, day 21-24 and day 35-42. The experiment was terminated at day 85. Mice were prematurely excluded from the experiment if matching at least one abort criterion. Shown is the mean relative body-weight of each cohort in relation to the absolute body-weight at day 0. Error bars represent relative standard deviation. Significance of body-weight differences between both cohorts was determined by two-sided Student's t-test. A p-value ≤ 0.05 is considered as statistically significant (*), while a p-value ≤ 0.01 is considered as statistically highly significant (**).

27.3.2 Stool consistency and rectal bleeding

Stool consistency was rated by a simplified *Bristol stool scale* in a range from 0 (normal consistency) up to 4 (practical liquid). Furthermore, the appearance of occult or fresh blood in the feces as well as rectal bleeding was rated in a scale from 0 (no detection of occult blood) up to 4 (rectal bleeding). At experimental day 16, animals from both cohorts suffered from diarrhea. However, symptoms were more pronounced in the *Ier3-flox$^{+/+}$ LysM-Cre$^{-/-}$* group. While symptoms in both groups alleviated between the second and the third DSS cycle (day 30), they impaired shortly after the begin of the third DSS cycle at day 35. Again, they were more pronounced in the *Ier3-flox$^{+/+}$ LysM-Cre$^{-/-}$* group. When having reached the half period of the third DSS cycle at day 39, none of animals

from the *Ier3-flox*$^{+/+}$ *LysM-Cre*$^{+/+}$ group had an score higher than 1, while all mice in the *Ier3-flox*$^{+/+}$ *LysM-Cre*$^{-/-}$ group were rated with a score of 2 or 3. The severity of diarrhea in both cohorts further increased, even after the end of the third DSS cycle at day 42. At days 44 and 45, *Ier3-flox*$^{+/+}$ *LysM-Cre*$^{+/+}$ animals had a score between 2 and 4, while the majority of the *Ier3-flox*$^{+/+}$ *LysM-Cre*$^{-/-}$ mice were rated with a score of 3. Stool consistency in both cohorts improved between day 45 and 63, so that on the latter only one *Ier3-flox*$^{+/+}$ *LysM-Cre*$^{-/-}$ animal was rated with a score of 2, while all other animals were rated with a score of 1. Interestingly, during the last two weeks of the experiment stool consistency in both genotypes partially aggravated without being challenged by DSS.

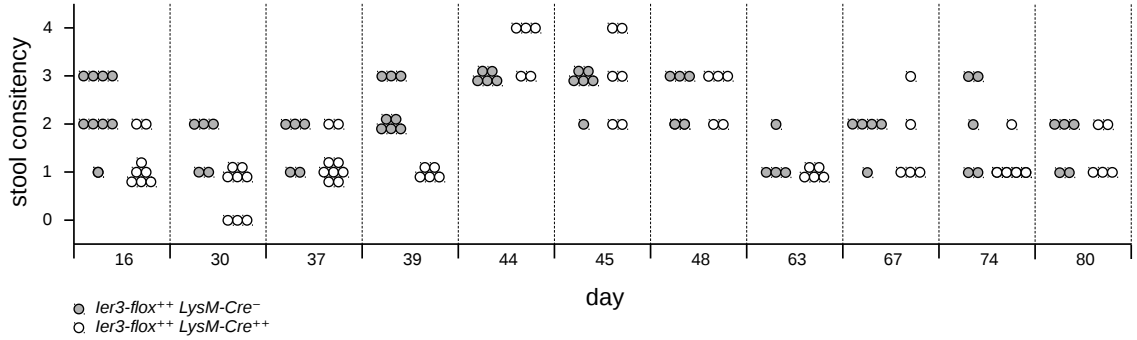

Figure 27.10: Stool consistency of *Ier3-flox*$^{+/+}$ *LysM-Cre*$^{-/-}$ and *Ier3-flox*$^{+/+}$ *LysM-Cre*$^{+/+}$ mice during AOM/DSS colitis. Experimental design as described in figure 27.9. Stool consistency was analyzed at selected days and rated by a simplified *bristol stool scale*. Scores ranged from 0 (normal consistency) up to 4 (practical liquid). Variations in sample sizes between days are explained by the fact, that it was not always possible to obtain samples from all animals at each probing day.

At experimental day 16, occult blood was detectable only in the feces from four *Ier3-flox*$^{+/+}$ *LysM-Cre*$^{-/-}$ animals but not in any of the *Ier3-flox*$^{+/+}$ *LysM-Cre*$^{+/+}$ mice (fig. 27.11). Likewise, creneg mice likewise were more affected by the second DSS cycle, resulting in increased bleeding scores in over the half of the evaluable *Ier3-flox*$^{+/+}$ *LysM-Cre*$^{-/-}$ animals at day 30. In contrast, only one out of seven *Ier3-flox*$^{+/+}$ *LysM-Cre*$^{+/+}$ animals had an increased bleeding score. While bleeding scores increased in both genotypes during the third DSS cycle (day 35-42), they rose faster in the *Ier3-flox*$^{+/+}$ *LysM-Cre*$^{-/-}$ cohort. However, at day 39 all evaluable animals suffered from severe rectal bleeding. crepos animals recovered mostly until day 48. In contrast, the majority of *Ier3-flox*$^{+/+}$ *LysM-Cre*$^{-/-}$ mice

kept suffering from rectal bleeding or bloody feces until the end of the experiment. Notably, bleeding scores in both cohorts raised during the last 14 days of the experiment without being challenged with DSS again.

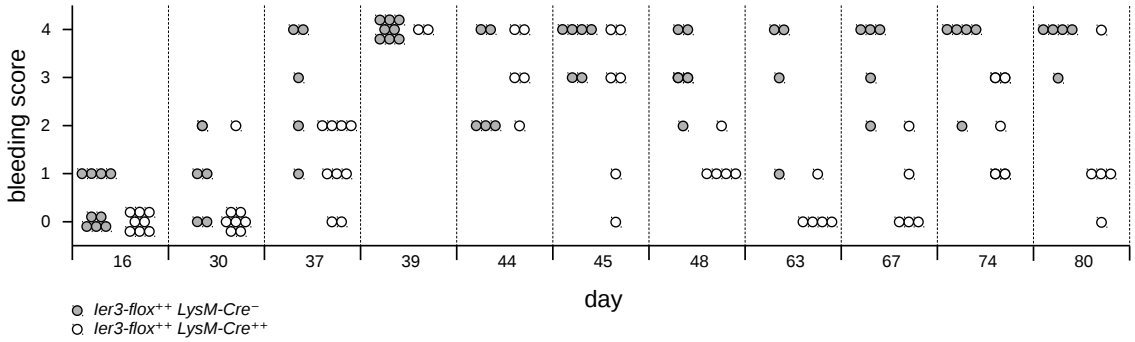

Figure 27.11: Occult blood and rectal bleeding in *Ier3-flox$^{+/+}$ LysM-Cre$^{-/-}$* and *Ier3-flox$^{+/+}$ LysM-Cre$^{+/+}$* mice during AOM/DSS colitis. Experimental design as described in figure 27.9. Appearance of occult or fresh blood in feces as well as rectal bleeding was analyzed at selected days. Traces of blood in feces were detected using a commercial guaiac based test kit. Scoring ranged from 0 points (no detection of occult blood) up to 4 points (rectal bleeding). Variations in sample sizes between days are explained by the fact, that it was not always possible to obtain samples from all animals at each probing day.

27.3.3 survival

Even tough animals in both cohorts suffered from diarrhea and rectal bleeding none of them died or had to be excluded during the first five weeks of the experiment (fig. 27.12). At day 38, which was the third day of the third DSS cycle, two *Ier3-flox$^{+/+}$ LysM-Cre$^{-/-}$* mice died, respectively had to be excluded due to their poor health conditions. At day 44 another two and at day 47 one of the *Ier3-flox$^{+/+}$ LysM-Cre$^{-/-}$* animals had to be excluded, too. From the *Ier3-flox$^{+/+}$ LysM-Cre$^{+/+}$* animals, only two mice had to be excluded at day 45 and 46.

The remaining animals survived until the scheduled termination at day 85, resulting in an overall 85-day survival rate of 50 % and 71 %[65] in the *Ier3-flox$^{+/+}$ LysM-Cre$^{-/-}$* and *Ier3-flox$^{+/+}$ LysM-Cre$^{+/+}$* cohort respectively.

[65] Two moderately affected animals from the *Ier3-flox$^{+/+}$ LysM-Cre$^{+/+}$* cohort, which did not match any abortion criteria, were also excluded at day 38 for histological comparison.

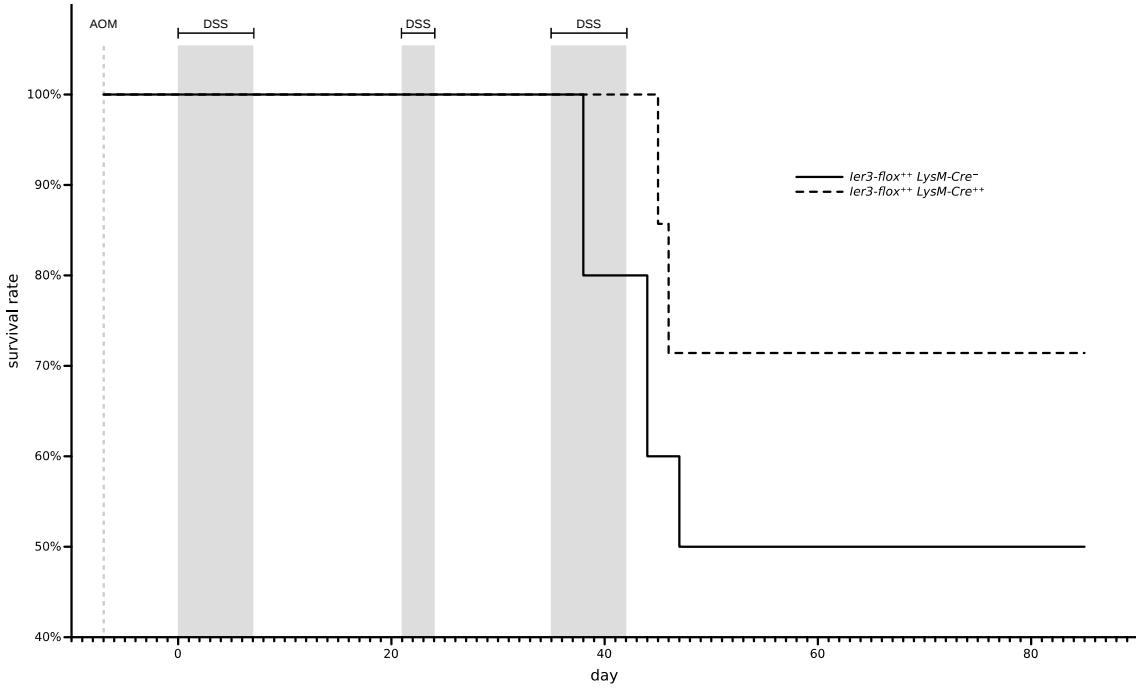

Figure 27.12: Kaplan Meyer *survival curve* of *Ier3-flox*$^{+/+}$ *LysM-Cre*$^{-/-}$ and *Ier3-flox*$^{+/+}$ *LysM-Cre*$^{+/+}$ animals during chronic AOM/DSS colitis. Experimental design as described in figure 27.9.

27.3.4 Post mortem analysis of organs

Compared to *Ier3-flox*$^{+/+}$ *LysM-Cre*$^{+/+}$ animals, colons of *Ier3-flox*$^{+/+}$ *LysM-Cre*$^{-/-}$ animals were shorter by trend (fig. 27.13a), although not significantly (p=0.05004). The median cecum weights (fig. 27.13b) in *Ier3-flox*$^{+/+}$ *LysM-Cre*$^{-/-}$ mice were slightly higher than in *Ier3-flox*$^{+/+}$ *LysM-Cre*$^{+/+}$ animals (p=0.084), while their livers weighted significant more (p = 0.021, fig. 27.13c), thus indicating a higher inflammation score. In contrast, their spleen weights (fig. 27.13d) were significantly lower (p = 0.014) compared to *Ier3-flox*$^{+/+}$ *LysM-Cre*$^{+/+}$ animals.

27.3.5 Colorectal Carcinogenesis

At the endpoint of the experiment, colons of all animals were examined for neoplasm formation (fig. 27.14). Colons from *Ier3-flox*$^{+/+}$ *LysM-Cre*$^{-/-}$ mice showed on median eight local neoplasms per animal (fig. 27.15a), while *Ier3-flox*$^{+/+}$ *LysM-Cre*$^{+/+}$ mice suffered from

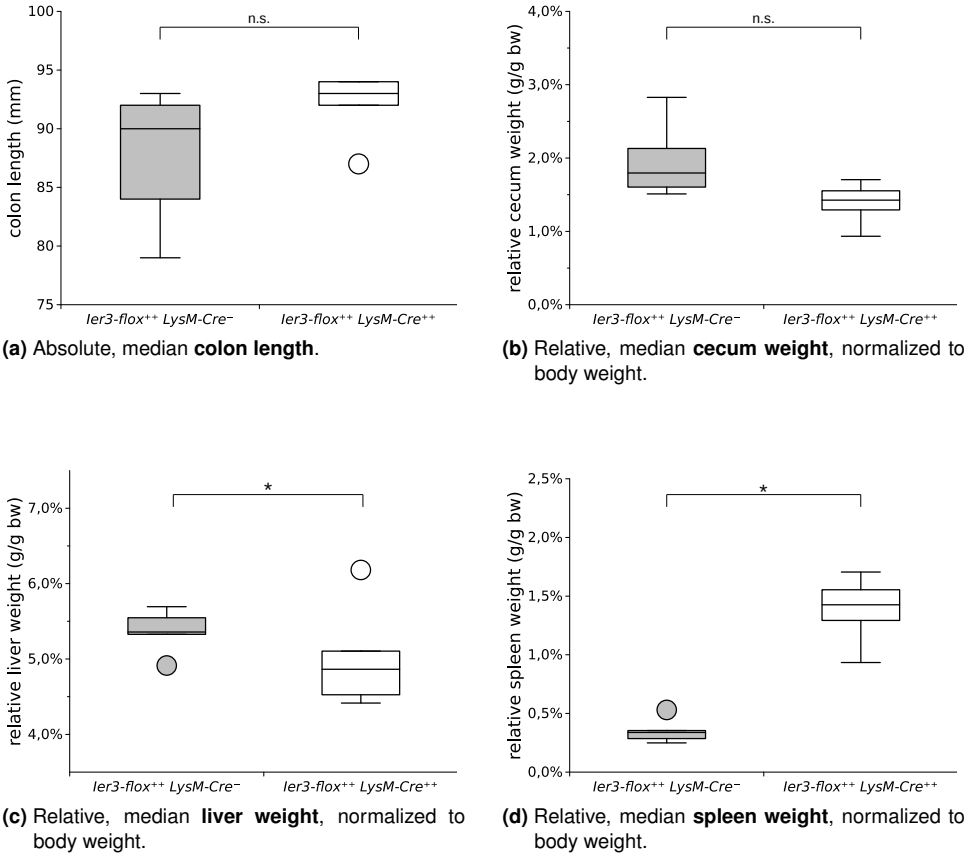

(a) Absolute, median **colon length**.

(b) Relative, median **cecum weight**, normalized to body weight.

(c) Relative, median **liver weight**, normalized to body weight.

(d) Relative, median **spleen weight**, normalized to body weight.

Figure 27.13: Comparison of immunological relevant organs from *Ier3-flox$^{+/+}$ LysM-Cre$^{-/-}$* and *Ier3-flox$^{+/+}$ LysM-Cre$^{+/+}$* mice after chronically AOM/DSS colitis. Experimental design as described in figure 27.9. Shown are median values of the analyzed parameters (crossbar within the box) from five *Ier3-flox$^{+/+}$ LysM-Cre$^{-/-}$* and five *Ier3-flox$^{+/+}$ LysM-Cre$^{+/+}$* animals after experimental termination at day 85. Boxes cover the 25 % and 75 % quantiles. Whisker length corresponds to values with a maximal medial deviation of the 1.5-folds interquartile range, while extreme values are indicated as bullets. Statistical significance in the difference between the two cohorts was determined by adjusted WILCOXON-MANN-WHITNEY-test. A p-value ≤ 0.05 is considered as statistically significant (*).

three neoplasms (p = 0.009). In both cohorts, tumors were mostly located in the distal and M2 segments of the colon. Occasionally, tumors were detected in the M1 quartile but not in further proximal regions. The neoplasms itself were mostly free of MΦ but surrounded by high numbers of them (fig. 27.16). Interestingly, with an median tumor diameter of 3 mm, the median tumor size between both cohorts did not differ (p = 0.328, fig. 27.15b).

(a) Colons from *Ier3-flox*$^{+/+}$ *LysM-Cre*$^{-/-}$ animals. **(b)** Colons from *Ier3-flox*$^{+/+}$ *LysM-Cre*$^{+/+}$ animals.

Figure 27.14: Colorectal neoplasms in *Ier3-flox*$^{+/+}$ *LysM-Cre*$^{-/-}$ and *Ier3-flox*$^{+/+}$ *LysM-Cre*$^{+/+}$ animals after AOM/DSS-treatment. Experimental design as described in figure 27.9. After termination, colons were dissected, rinsed with PBS and cut open longitudinally. Shown are representative pictures from colons of *Ier3-flox*$^{+/+}$ *LysM-Cre*$^{-/-}$ and *Ier3-flox*$^{+/+}$ *LysM-Cre*$^{+/+}$ mice at day 85. Red arrows indicate neoplasms.

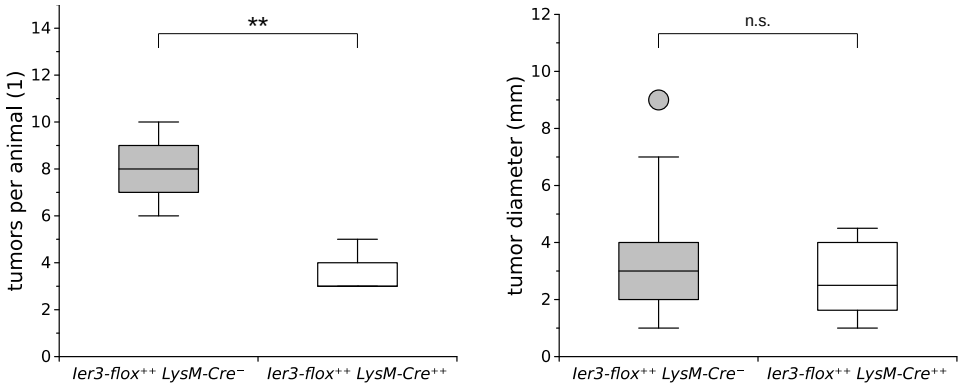

(a) Tumor *number* per animal. **(b) Average Tumor *diameter***.

Figure 27.15: Tumor number and size after AOM/DSS induced carcinogenesis in *Ier3-flox*$^{+/+}$ *LysM-Cre*$^{-/-}$ and *Ier3-flox*$^{+/+}$ *LysM-Cre*$^{+/+}$ animals. Experimental design as described in figure 27.9. Shown are median values of the analyzed parameters (crossbar within the box) from five *Ier3-flox*$^{+/+}$ *LysM-Cre*$^{-/-}$ and five *Ier3-flox*$^{+/+}$ *LysM-Cre*$^{+/+}$ animals after experimental termination at day 85. Boxes cover the 25 % and 75 % quantiles. Whisker length corresponds to values with a maximal medial deviation of the 1.5-folds interquartile range, while extreme values are indicated as bullets. Statistical significance in the difference between the two cohorts was determined by adjusted WILCOXON-MANN-WHITNEY-test. A p-value ≤ 0.01 is considered as statistically highly significant (**).

27.3.6 Macrophage Infiltration

The mucosa of both *Ier3-flox*$^{+/+}$ *LysM-Cre*$^{-/-}$ as well *Ier3-flox*$^{+/+}$ *LysM-Cre*$^{+/+}$ animal was highly infiltrated by macrophages (fig. 27.16). There could be no differences determined in the overall number of infiltrating MΦ between both genotypes. However, MΦ were not consistently distributed over all colon segments in both genotypes. As described above, neoplasms (Tu) themselves were mostly free of MΦ but surrounded by high numbers of them.

27.3.7 Expression of E-cadherin and β-catenin

The expression and distribution of the CJ related proteins E-cadherin andβ-catenin as well as their colocalization with MΦ infiltrates in the colons of AOM/DSS treated *Ier3-flox*$^{+/+}$ *LysM-Cre*$^{-/-}$ and *Ier3-flox*$^{+/+}$ *LysM-Cre*$^{+/+}$ animals was analyzed by IHC-F (fig. 27.17). There were considerable differences in the expression intensity of E-cadherin and β-catenin in different colon segments, independently of the animals genotype. In most cases, the expression of both proteins, correlated inversely with the morphological grade of tissue damage. Interestingly, in *Ier3-flox*$^{+/+}$ *LysM-Cre*$^{-/-}$ animals, an inverse correlation between the number of infiltrating MΦ and the expression of E-cadherin and β-catenin was observed, whereas no such correlation was seen in *Ier3-flox*$^{+/+}$ *LysM-Cre*$^{+/+}$ animals.

Hence, in colon segments with comparable grades of tissue integrity and MΦ infiltration, the expression of E-cadherin and β-catenin were significantly down-regulated in *Ier3-flox*$^{+/+}$ *LysM-Cre*$^{-/-}$ animals compared to *Ier3-flox*$^{+/+}$ *LysM-Cre*$^{+/+}$ animals, as shown in figure 27.17. Interestingly, the detection of both proteins was not limited to sites of intercellular contacts but they were also found in cytoplasmic regions, independently of the animals genotype.

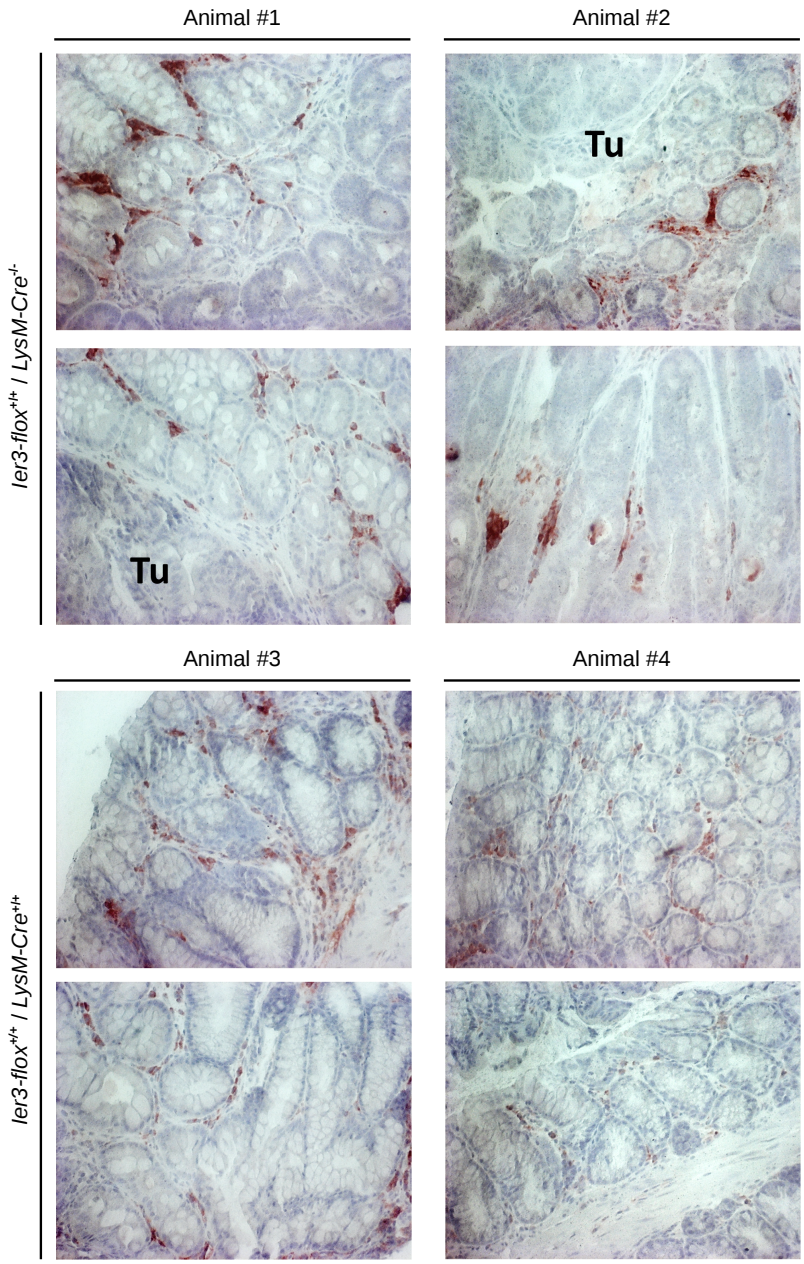

Figure 27.16: Macrophage infiltration into the mucosa of *Ier3-flox$^{+/+}$ LysM-Cre$^{-/-}$* and *Ier3-flox$^{+/+}$ LysM-Cre$^{+/+}$* animals after AOM/DSS-treatment. Experimental design as described in figure 27.9. After termination, colons were dissected, rinsed with PBS and cut open longitudinally. Histological specimen were generated as described in sec. 12.1. Conventional immunostaining was performed as described in sec. 12.3.2. MΦ were stained using an anti *F4/80* antibody (CST). or an respectively isotype control Ab. Detection was performed by chromogenic AEC reaction (*red*) using a HRP-conjugated secondary antibody. Cell nuclei were counterstained using MEYER'S Haematoxylin (*blue*). Neoplastic tissue is indicated by "*Tu*". Shown are representative pictures of colons *Ier3-flox$^{+/+}$ LysM-Cre$^{-/-}$* and *Ier3-flox$^{+/+}$ LysM-Cre$^{+/+}$* mice at day 85.

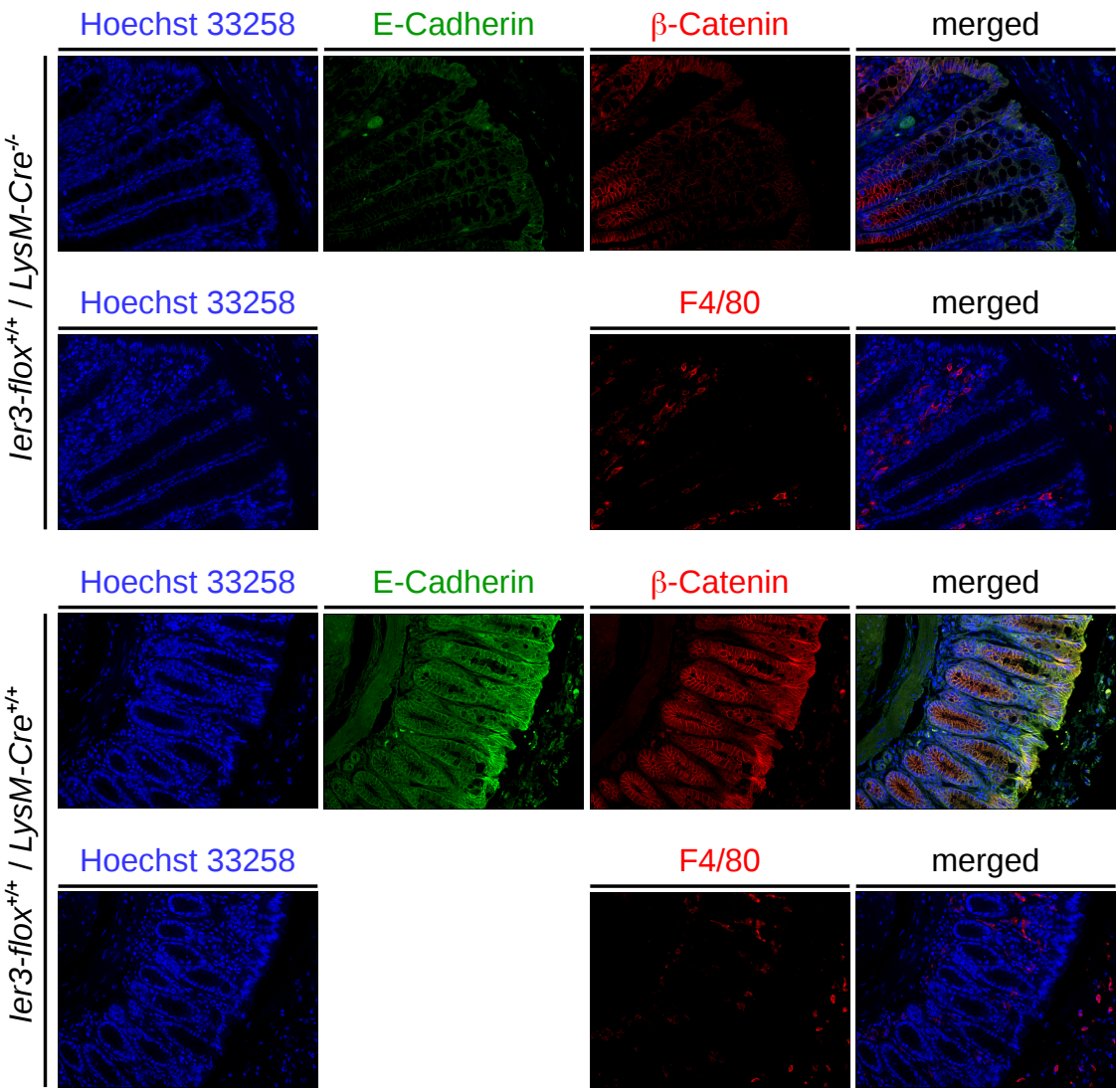

Figure 27.17: Expression of cellular junction related proteins in *Ier3-flox$^{+/+}$ LysM-Cre$^{-/-}$* and *Ier3-flox$^{+/+}$ LysM-Cre$^{+/+}$* animals after AOM/DSS-treatment. Experimental design as described in figure 27.9. After termination, colons were dissected, rinsed with PBS and cut open longitudinally. Histological specimen were generated as described in sec. 12.1. IHC-F staining was performed as described in sec. 12.3.3. MΦ (*red*) were stained using an anti *F4/80* antibody. E-Cadherin appears *green*, while β-catenin is also stained *red*. Appropriate isotype controls were performed for all specimen (not shown). or an respectively isotype control Ab. Cell nuclei were counter-stained with Hoechst bisbenzimide H33258 (*blue*). Shown are representative pictures from colons of *Ier3-flox$^{+/+}$ LysM-Cre$^{-/-}$* and *Ier3-flox$^{+/+}$ LysM-Cre$^{+/+}$* mice at day 85.

27.4 *Ier3-flox*$^{+/+}$ *LysM-Cre*$^{+/+}$ mice exhibit reduced intestinal permeability to FITC-dextran after DSS challenge

Based on the previous findings, it could be assumed that *Ier3* status of macrophages could affect the intestinal barrier integrity *in vivo*. To test this assumption, the intestinal permeability to fluorescein isothiocyanate (FITC) labeled dextrans (FD) of different molecular weights (FD4: 4000 g/mol, FD10: 10 000 g/mol) was measured by determining their serum concentrations after oral application.

In healthy animals, there was no significant difference in serum concentrations of FD4 between both genotypes (p=0.40). If challenged with DSS (10 g/l in drinking water *ad libitum*) for 24 h before application, *Ier3-flox*$^{+/+}$ *LysM-Cre*$^{-/-}$ animals showed an 2.37-fold increased permeability to FD4 compared to *Ier3-flox*$^{+/+}$ *LysM-Cre*$^{+/+}$ mice (p=0.004). Interestingly, this difference diminished mainly when using FD with an average molecular weight of 10000 g/mol (p=0.08), whose intestinal permeability was in general much lesser in both genotypes compared to FD4.

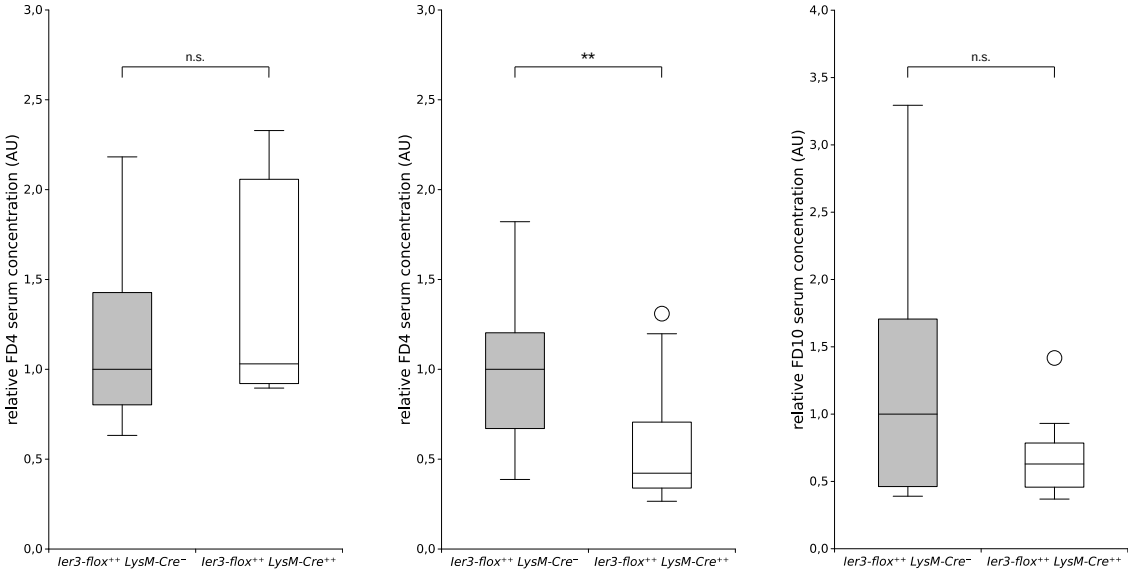

(a) Relative **FD4** serum concentrations in mice **not pretreated**. $n_{\text{each GT}} = 9$.

(b) Relative **FD4** serum concentrations in mice **pretreated with DSS**. $n_{\textit{Ier3-flox}^{+/+}\textit{ LysM-Cre}^{-/-}} = 18$, $n_{\textit{Ier3-flox}^{+/+}\textit{ LysM-Cre}^{+/+}} = 17$.

(c) Relative **FD10** serum concentrations in mice **pretreated with DSS**. $n_{\textit{Ier3-flox}^{+/+}\textit{ LysM-Cre}^{-/-}} = 14$, $n_{\textit{Ier3-flox}^{+/+}\textit{ LysM-Cre}^{+/+}} = 13$.

Figure 27.18: Intestinal permeability of *Ier3-flox$^{+/+}$ LysM-Cre$^{-/-}$* and *Ier3-flox$^{+/+}$ LysM-Cre$^{+/+}$* mice to FITC-dextran. 12 ± 3 week old *Ier3-flox$^{+/+}$ LysM-Cre$^{-/-}$* and *Ier3-flox$^{+/+}$ LysM-Cre$^{+/+}$* mice were optional pretreated with 10 g/l DSS in drinking water *ad libitum* for 24 h. FITC-dextrans of different molecular weights (FD4 or FD10) were directly applied into the pylorus using a buttoned hypodermic needle (FD4: 0.5 mg/g bw, FD10: 0.2 mg/g bw). Blood samples were taken 4 h after administration and FD serum concentrations were determined using a fluorescence based assay. Shown are normalized median serum concentrations (crossbar within the box). Relative serum concentrations in *Ier3-flox$^{+/+}$ LysM-Cre$^{-/-}$* mice were set to 1. Boxes cover the 25 % and 75 % quantiles. Whisker length corresponds to values with a maximal medial deviation of the 1.5-folds interquartile range, while extreme values are indicated as bullets. Statistical significance in the difference between the two cohorts was determined by adjusted WILCOXON-MANN-WHITNEY-test. A p-value ≤ 0.01 is considered as statistically highly significant (**).

28 Effects of IER3-deficiency in other compartments in response to DSS

In order to extend the insight into the role of IER3 deficiency in the pathogenesis of DSS colitis, it was further explored whether the deletion of the *Ier3* gene in other tissue compartments has also an effect.

28.1 Epithelial IER3 status has impact on acute but not on chronic DSS colitis

After identifying the myeloid *Ier3* status affecting the integrity of the intestinal barrier in response to DSS, we also wanted to address the question if an epithelial specific *Ier3* depletion has an impact on the inflammatory phenotype during DSS colitis. For this purpose, two DSS experiments were conducted using an *Ier3-flox/Villin-Cre* (*Vil-Cre*) mouse model based on a C57/BL6 background.

28.1.1 Body weight differences between healthy *Ier3-flox$^{+/+}$ Vil-Cre$^{-/-}$* and *Ier3-flox$^{+/+}$ Vil-Cre$^{+/+}$* mice

There were no significant differences in the body weight between healthy *Ier3-flox$^{+/+}$ Vil-Cre$^{-/-}$* and *Ier3-flox$^{+/+}$ Vil-Cre$^{+/+}$* mice, as shown in figure 28.1.

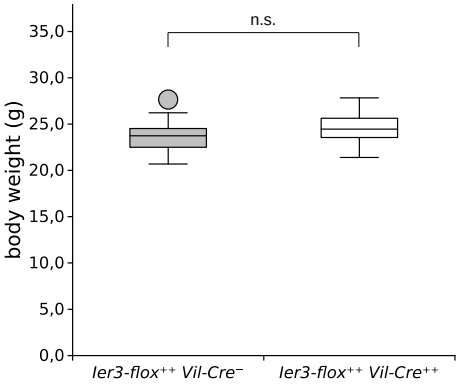

Figure 28.1: Body weight differences between healthy *Ier3-flox$^{+/+}$ Vil-Cre$^{-/-}$* and *Ier3-flox$^{+/+}$ Vil-Cre$^{+/+}$* mice. Shown are median body weights (crossbar within the box) of 9 *Ier3-flox$^{+/+}$ Vil-Cre$^{-/-}$* and 7 *Ier3-flox$^{+/+}$ Vil-Cre$^{+/+}$* animals with an average age of 9 ± 1 weeks. Boxes cover the 25 % and 75 % quantiles. Whisker length corresponds to values with a maximal medial deviation of the 1.5-folds interquartile range, while extreme values are indicated as bullets. Statistical significance in the difference between the two cohorts was determined by adjusted WILCOXON-MANN-WHITNEY-test. A p-value ≤ 0.05 is considered as statistically significant (*).

28.1.2 Acute DSS colitis in *Ier3-flox/Vil-Cre* mice

Nine *Ier3-flox$^{+/+}$ Vil-Cre$^{-/-}$* and seven *Ier3-flox$^{+/+}$ Vil-Cre$^{+/+}$* mice with an average age of 9 weeks ($\pm$1 week) were challenged with *30 g/l DSS* in drinking water *ad libitum* for nine

days to induce an acute colitis (fig. 28.2). Animals in both cohorts started to loose weight up from day 4 (fig. 28.2a). While weight loss proceeded until the end of the experiment at day 9 in both genotypes, this decline was more pronounced in the *Ier3-flox*$^{+/+}$ *Vil-Cre*$^{-/-}$ cohort ($p\,(\Delta\text{bw}) \leq 0.05$ from day 5-8). Maximal weight differences between both genotypes were observed at day 8, with an average weight loss of $-21 \pm 7\,\%$ in the *Ier3-flox*$^{+/+}$ *Vil-Cre*$^{-/-}$ group vs. $-10 \pm 4\,\%$ in the *Ier3-flox*$^{+/+}$ *Vil-Cre*$^{+/+}$ cohort.

Differences would have been even more distinct, if not 4 animals of the *Ier3-flox*$^{+/+}$ *Vil-Cre*$^{+/+}$ group had to be excluded prematurely from the experiment due to a poor general health condition (fig. 28.2b). This led to an overall 9 day survival rate of 44.4 % in the *Ier3-flox*$^{+/+}$ *Vil-Cre*$^{-/-}$ group vs. 100 % in the *Ier3-flox*$^{+/+}$ *Vil-Cre*$^{+/+}$ group (p=0.029).

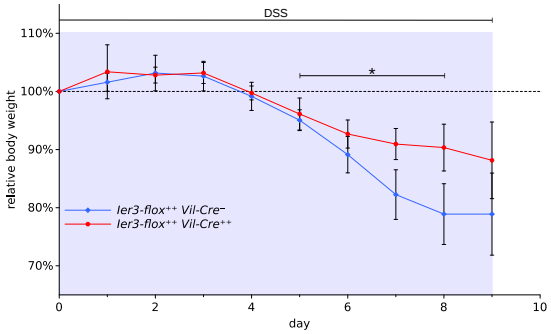

(a) *Body-weight* loss in *Ier3-flox*$^{+/+}$ *Vil-Cre*$^{-/-}$ and *Ier3-flox*$^{+/+}$ *Vil-Cre*$^{+/+}$ mice during *acute* DSS colitis. Shown is the mean relative body-weight of each cohort in relation to the absolute body-weight at day 0. Error bars represent relative standard deviation. Significance in of body weight differences between both cohorts was determined by two-sided Student's t-test. a p-value ≤ 0.05 is considered as statistically significant (*).

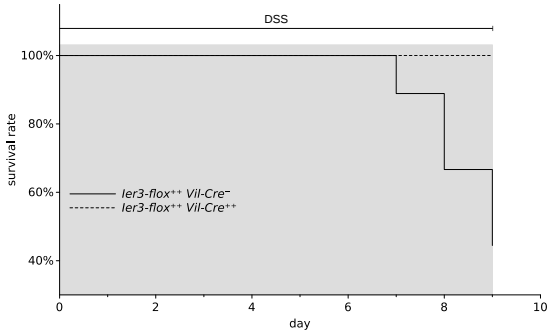

(b) Kaplan Meyer *survival* curve of *Ier3-flox*$^{+/+}$ *Vil-Cre*$^{-/-}$ and *Ier3-flox*$^{+/+}$ *Vil-Cre*$^{+/+}$ mice during acute DSS colitis.

Figure 28.2: *Acute* DSS colitis in *Ier3-flox*$^{+/+}$ *Vil-Cre*$^{-/-}$ and *Ier3-flox*$^{+/+}$ *Vil-Cre*$^{+/+}$ mice. Nine *Ier3-flox*$^{+/+}$ *Vil-Cre*$^{-/-}$ and seven *Ier3-flox*$^{+/+}$ *Vil-Cre*$^{+/+}$ mice with an average age of 9 weeks (±1 week) received *30* g/l *DSS* in drinking water *ad libitum* to induce an acute colitis. Mice were prematurely excluded from the experiment if matching at least one abort criterion.

28.1.3 Chronic DSS colitis in *Ier3-flox/Vil-Cre* mice

Eight *Ier3-flox*$^{+/+}$ *Vil-Cre*$^{-/-}$ and seven *Ier3-flox*$^{+/+}$ *Vil-Cre*$^{+/+}$ mice with an average age of 9 weeks were challenged with three 5 day cycles and one 4 day cycle of *15* g/l *DSS* in drinking water *ad libitum* to induce a chronic colitis. Each cycle was interrupted by

a 5 day treatment free interval (fig. 28.3). Mice from both genotypes began to loose weight up from the last day of the first DSS cycle (fig. 28.3a). Weight loss in both groups continued until day 8 where it reached its maximum (*Ier3-flox*$^{+/+}$ *Vil-Cre*$^{-/-}$: $-12 \pm 6\,\%$ vs. *Ier3-flox*$^{+/+}$ *Vil-Cre*$^{+/+}$: $-18 \pm 12\,\%$). Though, *Ier3-flox*$^{+/+}$ *Vil-Cre*$^{+/+}$ animals had lost slightly more weight at this time point, there were no significant weight differences between both genotypes observed during the whole experiment.

Animals regained weight until the end of the second DSS cycle at day 15 (*Ier3-flox*$^{+/+}$ *Vil-Cre*$^{-/-}$: $99 \pm 4\,\%$ vs. *Ier3-flox*$^{+/+}$ *Vil-Cre*$^{+/+}$: $98 \pm 8\,\%$). A reoccurring weight drop after the second cycle came off weaker compared to the first cycle. The weight drop after the second cycle was again followed by a recovery phase until the begin of the third cycle. This pattern occurred again during and after the third DSS cycle. Animals kept their weight during the last DSS cycle until the end of the experiment at day 35 (*Ier3-flox*$^{+/+}$ *Vil-Cre*$^{-/-}$: $100 \pm 5\,\%$ vs. *Ier3-flox*$^{+/+}$ *Vil-Cre*$^{+/+}$: $97 \pm 3\,\%$).

Respectively one animal from each genotype had to be prematurely excluded from the experiment at day 10 due to a poor general health condition (fig. 28.3b). This led to an overall 35 day survival rate of 87.5 % in the *Ier3-flox*$^{+/+}$ *Vil-Cre*$^{-/-}$ group vs. 85.7 % in the *Ier3-flox*$^{+/+}$ *Vil-Cre*$^{+/+}$ group ($p > 0.9$).

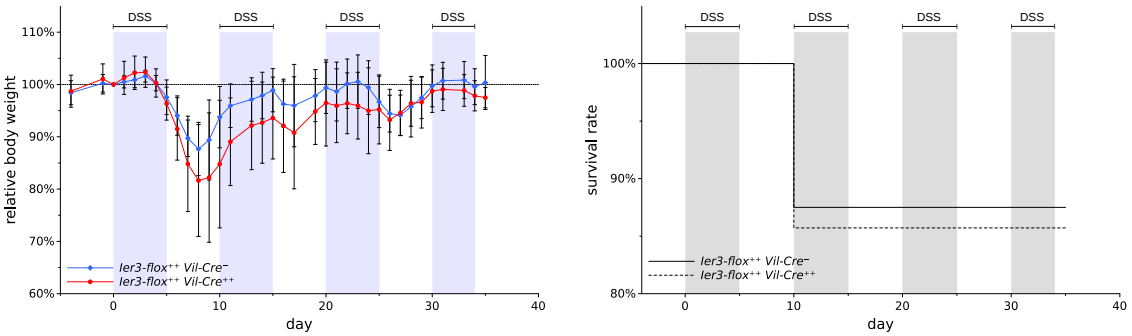

(a) *Body-weight* loss in *Ier3-flox*$^{+/+}$ *Vil-Cre*$^{-/-}$ and *Ier3-flox*$^{+/+}$ *Vil-Cre*$^{+/+}$ mice during chronic DSS colitis.

(b) Kaplan Meyer *survival* curve of *Ier3-flox*$^{+/+}$ *Vil-Cre*$^{-/-}$ and *Ier3-flox*$^{+/+}$ *Vil-Cre*$^{+/+}$ mice during chronic DSS colitis.

Figure 28.3: *Chronic* DSS colitis in *Ier3-flox*$^{+/+}$ *Vil-Cre*$^{-/-}$ and *Ier3-flox*$^{+/+}$ *Vil-Cre*$^{+/+}$ mice. Eight *Ier3-flox*$^{+/+}$ *Vil-Cre*$^{-/-}$ and seven *Ier3-flox*$^{+/+}$ *Vil-Cre*$^{+/+}$ mice with an average age of 9 weeks (±10 days) received three 5-day and one 4-day cycles of *15* g/l *DSS* in drinking water *ad libitum*. Each DSS cycle was followed by a 5 day treatment free interval. Mice were prematurely excluded from the experiment if matching at least one abortion criterion.

Parameters of immunological relevant organs were exploited after the end of the experiment at day 34. Median Colon length did not differ significantly between both genotypes (p=0.144, fig. 28.4a). Also, there were no significant differences in the relative cecum (p=0.732, fig. 28.4b), liver (p=0.131, fig. 28.4c) or spleen weight (p=0.291, fig. 28.4d) between *Ier3-flox*$^{+/+}$ *Vil-Cre*$^{-/-}$ and *Ier3-flox*$^{+/+}$ *Vil-Cre*$^{+/+}$ animals detectable.

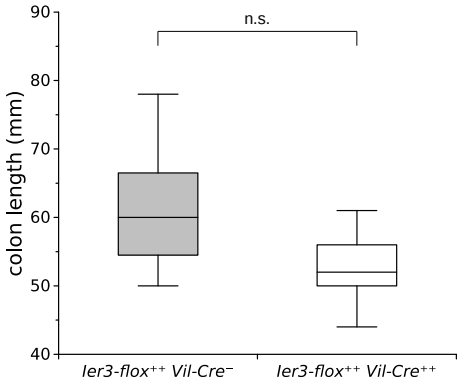

(a) Absolute, median **colon length**.

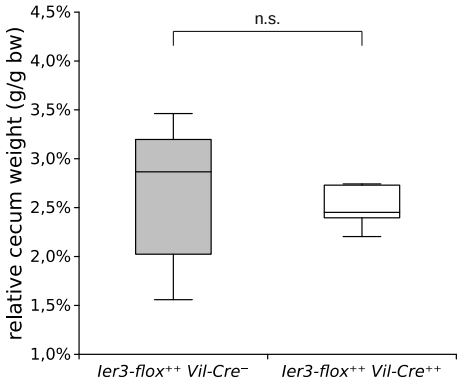

(b) Relative, median **cecum weight**, normalized to body weight.

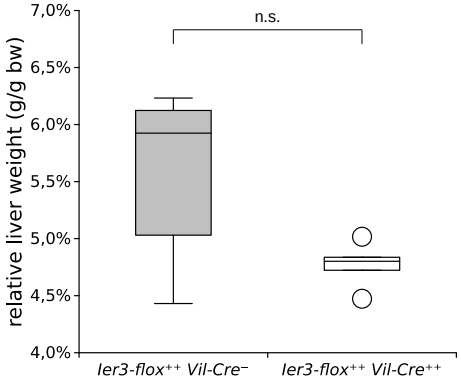

(c) Relative, median **liver weight**, normalized to body weight.

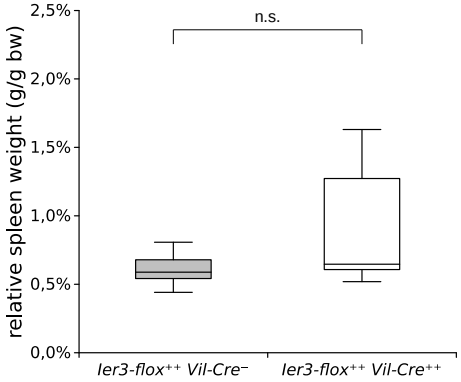

(d) Relative, median **spleen weight**, normalized to body weight.

Figure 28.4: Comparison of immunological relevant organs from *Ier3-flox*$^{+/+}$ *Vil-Cre*$^{-/-}$ and *Ier3-flox*$^{+/+}$ *Vil-Cre*$^{+/+}$ mice after chronically DSS colitis. Experimental design as described in figure 28.3. Shown are median values of the analyzed parameters (crossbar within the box) from seven *Ier3-flox*$^{+/+}$ *Vil-Cre*$^{-/-}$ and five *Ier3-flox*$^{+/+}$ *Vil-Cre*$^{+/+}$ animals after experimental termination at day 34. Boxes cover the 25 % and 75 % quantiles. Whisker length corresponds to values with a maximal medial deviation of the 1.5-folds interquartile range, while extreme values are indicated as bullets. Statistical significance in the difference between the two cohorts was determined by adjusted WILCOXON-MANN-WHITNEY-test. A p-value ≤ 0.05 is considered as statistically significant (*).

28.2 Constitutive *Ier3* knockout

Two experiments were conducted using a mouse strain with an constitutive *Ier3* knockout based on an Sv129 background.

28.2.1 Body weight comparison between healthy *Ier3* wt and *Ier3* ko mice

There were no significant differences in the body weight between healthy *Ier3* wt and *Ier3* ko mice, as shown in figure 28.5.

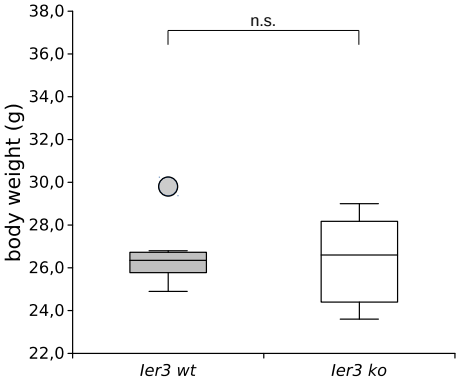

Figure 28.5: Body weight differences between healthy *Ier3* wt and *Ier3* ko mice. Shown are median body weights (crossbar within the box) of 8 *Ier3* wt and 8 *Ier3* ko animals with an average age of 9 weeks ($\pm$10 days). Boxes cover the 25 % and 75 % quantiles. Whisker length corresponds to values with a maximal medial deviation of the 1.5-folds interquartile range, while extreme values are indicated as bullets. Statistical significance in the difference between the two cohorts was determined by adjusted WILCOXON-MANN-WHITNEY-test. A p-value ≤ 0.05 is considered as statistically significant (*).

28.2.2 Acute DSS colitis in constitutive *Ier3* wt and ko mice

Five *Ier3* wt and six constitutive *Ier3* ko mice with an average age of 10 weeks were challenged with *30* g/l *DSS* in drinking water *ad libitum* for nine days to induce an acute colitis. Animals in both cohorts started to loose weight up from day 4 (fig. 28.6a). Weight loss continued until the scheduled endpoint at day 9, where animals in both cohorts had lost on average 14 % of their initial body weight at day 0. No significant body weight differences between both genotypes were observed during the whole experiment. One

animal of the *Ier3* wt group had be prematurely excluded at day 8 due to its poor general health condition (fig. 28.6b).

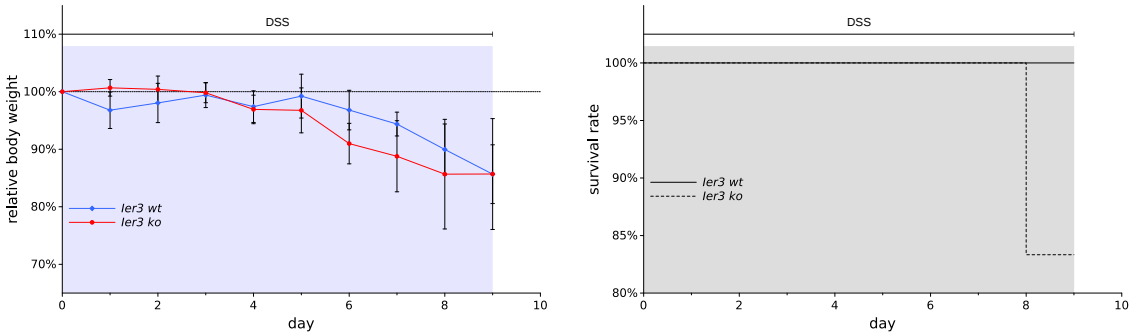

(a) *Body-weight* loss during acute DSS colitis. Shown is the mean relative body-weight of each cohort in relation to the absolute body-weight at day 0. Error bars represent relative standard deviation.

(b) Kaplan Meyer *survival* curve of ier wt and ko animals during acute DSS colitis.

Figure 28.6: *Acute* DSS colitis in *Ier3* wt and *Ier3* ko mice. Five *Ier3* wt and six *Ier3* ko mice with an average age of 10 weeks (±4 days) received *30* g/l *DSS* in drinking water ad libitum for nine days to induce an acute colitis. Mice were prematurely excluded from the experiment if matching at least one abort criterion.

28.2.3 Chronic DSS colitis in constitutive *Ier3* wt and ko mice

Eight *Ier3* wt and eight *Ier3* ko mice with an average age of 9 weeks were challenged with three 5 day cycles and one 4 day cycle of *15* g/l *DSS* in drinking water *ad libitum* to induce a chronic colitis. Each cycle was interrupted by a 5 day treatment free interval. Animals in both cohorts started to loose weight up from the fourth day of the first DSS cycle (fig. 28.7a). In terms of weight loss, *Ier3* wt mice responded much more to the first DSS cycle (-25 % at day nine) compared to *Ier3* ko animals (-13 % at day nine), even if statistical not significant due to their high intra-cohortal variation. While *Ier3* ko animals did not loose further weight during the second DSS cycle (88 % bw at day 16), *Ier3* wt mice could even gain some weight (85 % bw at day 16). Tough, this is in parts own to the fact, that respectively two animals from the *Ier3* wt group had be excluded at day 11 and day 16 due to their poor general health condition (fig. 28.7b). Animals from both genotypes continued to gain weight up to the middle of the third DSS cycle (day 23: wt: 93 % bw, ko: 98 % bw), before loosing weight again. At day 26, animals

in both groups had on average 90 % of their initial body weight at day 0. After this point, animals in both cohorts gained weight until the beginning of the third DSS cycle, with only minimal differences between genotypes. Weight levels in both groups stayed approximately constant until the end of the experiment at day 34 (bw_{wt}=bw_{ko}=96 %).

As mentioned above, respectively two animals from the *Ier3* wt group had be excluded prematurely at day 11 and day 16 due to their poor general health condition (fig 28.7b). This led to an overall 34 day survival rate of 50 % in the *Ier3* wt cohort, compared to 75 % in the *Ier3* ko group due to two prematurely exclusions at day 17 and 19.

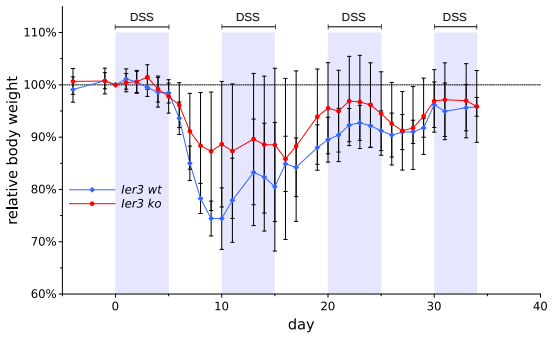

(a) *Body-weight* loss during chronic colitis. Shown is the mean relative body-weight of each cohort in relation to the absolute body-weight at day 0. Error bars represent relative standard deviation.

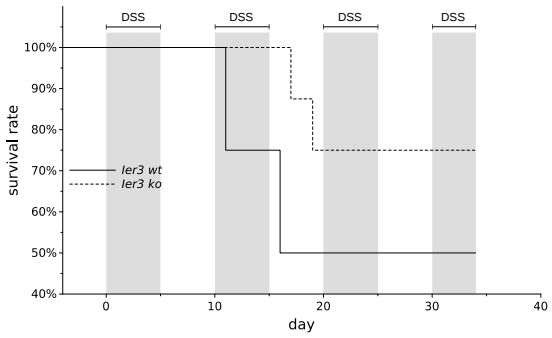

(b) Kaplan Meyer *survival curve* of *Ier3* wt and ko animals during chronic colitis.

Figure 28.7: *Chronic* DSS colitis in *Ier3 wt* and constitutive *Ier3 ko* mice. Eight *Ier3* wt and eight *Ier3* ko mice with an average age of 9 weeks (±10 days) received three 5-day and one 4-day cycles of *15* g/l *DSS* in drinking water *ad libitum*. Each DSS cycle was followed by a 5 day treatment free interval.

After the end of the experiment at day 34, parameters of immunological relevant organs were harvested (fig. 28.8). With a median length of 53 mm, colons from *Ier3* wt animals were significant shorter (p=0.033, fig. 28.8a) compared to *Ier3* ko animals (61 mm), indicating an increased inflammation. The increased median cecum weight in ko animals (3.5 % bw vs. 2.1 % bw, p=0.014, fig. 28.8b) also refers to a higher inflammation score. Whereas, liver and spleen weights did not differ significant between both genotypes (fig. 28.8c and 28.8d).

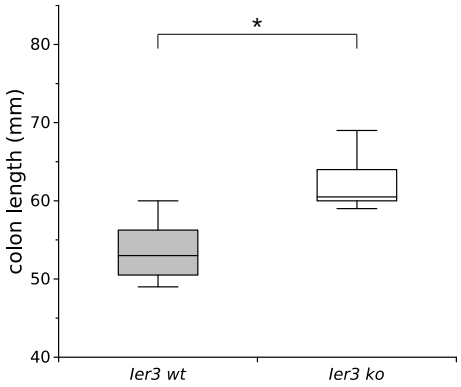

(a) Absolute, median **colon length**.

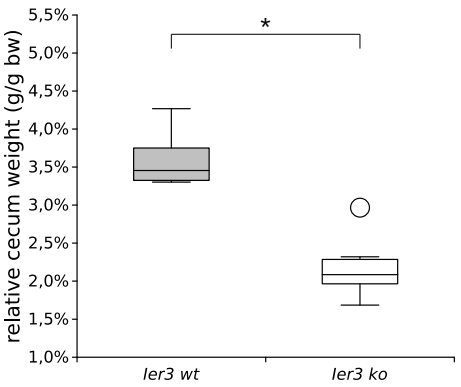

(b) Relative, median **cecum weight**, normalized to body weight.

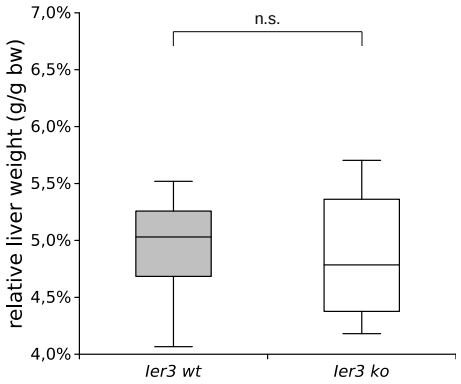

(c) Relative, median **liver weight**, normalized to body weight.

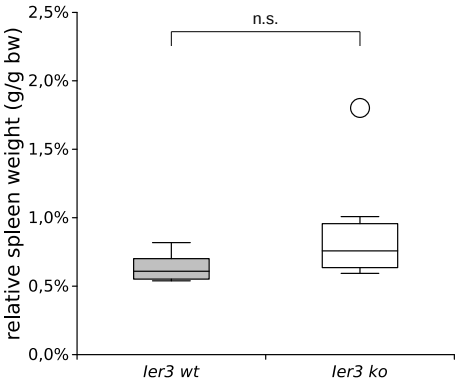

(d) Relative, median **spleen weight**, normalized to body weight.

Figure 28.8: Comparison of immunological relevant organs from *Ier3* wt and constitutive *Ier3* ko mice after chronically DSS colitis. Experimental design as described in figure 28.7. Shown are median values of the analyzed parameters (crossbar within the box) from four *Ier3* wt and six *Ier3* ko animals after experimental termination at day 34. Boxes cover the 25 % and 75 % quantiles. Whisker length corresponds to values with a maximal medial deviation of the 1.5-folds interquartile range, while extreme values are indicated as bullets. Statistical significance in the difference between the two cohorts was determined by adjusted WILCOXON-MANN-WHITNEY-test. A p-value ≤ 0.05 is considered as statistically significant (*).

29 In-vitro differentiation of murine bone-marrow-cells into MΦ

We generated primary macrophages (MΦ) by ex vivo differentiation of bone marrow cells (BMC) from *Ier3-flox*$^{+/+}$ *LysM-Cre*$^{-/-}$ and *Ier3-flox*$^{+/+}$ *LysM-Cre*$^{+/+}$ animals to further investigate the effects of myeloid IER3 *in vitro*.

The differentiated cells (fig. 29.1) were analyzed by flow cytometry for the murine

macrophage antigens CD11b and F4/80 by (fig. 29.2). Gates to identify CD11b and F4/80 positive cells were set in reference to corresponding isotype controls (fig. 29.2c and 29.2d). The majority of cells from both genotypes were double positive for CD11b and F4/80 (*Ier3-flox*$^{+/+}$ *LysM-Cre*$^{-/-}$: 64.9 %, *Ier3-flox*$^{+/+}$ *LysM-Cre*$^{+/+}$: 62.9 %). In contrast, 7.5 % of *Ier3-flox*$^{+/+}$ *LysM-Cre*$^{-/-}$ and 8.7 % of the *Ier3-flox*$^{+/+}$ *LysM-Cre*$^{+/+}$ cells were negative for CD11b as well as for F4/80. Interestingly, in both genotypes a population which was positive for F4/80 but negative for CD11b was identified (*Ier3-flox*$^{+/+}$ *LysM-Cre*$^{-/-}$: 11.6 %, *Ier3-flox*$^{+/+}$ *LysM-Cre*$^{+/+}$: 14.7 %). In the *Ier3-flox*$^{+/+}$ *LysM-Cre*$^{-/-}$ group 15.9 % of all cells were CD11b^{+} F4/80^{-}, while in the *Ier3-flox*$^{+/+}$ *LysM-Cre*$^{+/+}$ group 13.7 % of all cells were CD11b^{+} F4/80^{-}.

Overall, 92.1 % of all *Ier3-flox*$^{+/+}$ *LysM-Cre*$^{-/-}$ cells (fig. 29.2a) and 91.3 % of all *Ier3-flox*$^{+/+}$ *LysM-Cre*$^{+/+}$ cells (fig. 29.2b) were positive for at least one of the analyzed antigens.

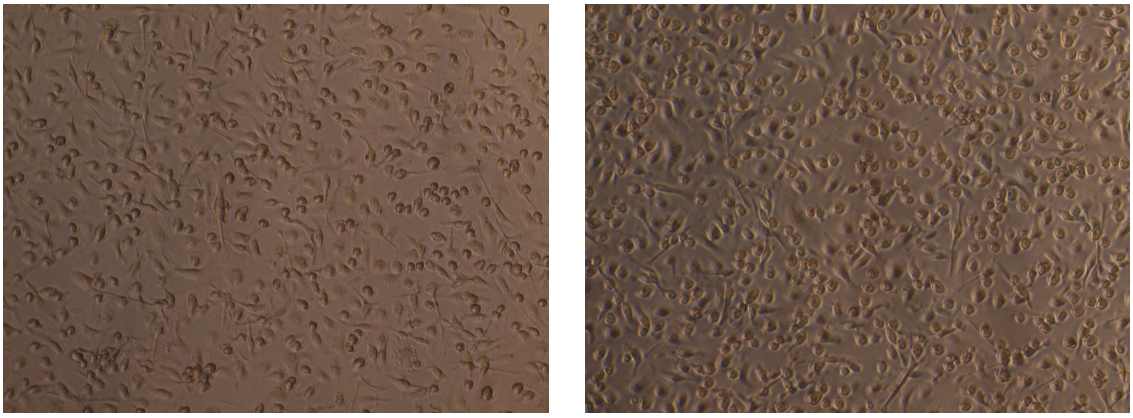

(a) MΦ from ***Ier3-flox*$^{+/+}$ *LysM-Cre*$^{-/-}$** animals at day 7.

(b) MΦ from ***Ier3-flox*$^{+/+}$ *LysM-Cre*$^{+/+}$** animals at day 7.

Figure 29.1: *In vitro* differentiation of MΦ from murine BMC. After dissection of femur and tibia, BMCs were rinsed out under sterile conditions using a syringe containing ice cold PBS. The cell suspension was centrifuged at 400 g and 4 °C for 10 minutes. The pellet was resuspended in MΦ differentiation medium containing 50 $^{ng}/_{ml}$ mM-CSF and 50 $^{IU}/_{ml}$ mIFN-γ (M$\Phi^{diff.}$-M.) and adjusted to a concentration of $5 \cdot 10^5$ $^{cells}/_{ml}$. Cells were seeded in uncoated PS culture vessels. At day three, cultures were gently washed twice using PBS to remove non attached cells and the medium was exchanged against fresh M$\Phi^{diff.}$-M.. At day 7 cells were fully differentiated into MΦ.

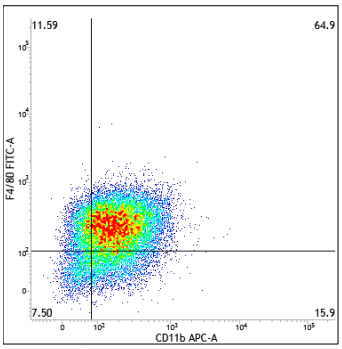

(a) CD11b and **F4/80** staining of cells from ***Ier3-flox$^{+/+}$ LysM-Cre$^{-/-}$*** animals.

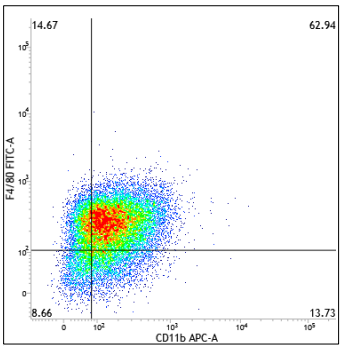

(b) CD11b and **F4/80** staining of cells from ***Ier3-flox$^{+/+}$ LysM-Cre$^{+/+}$*** animals.

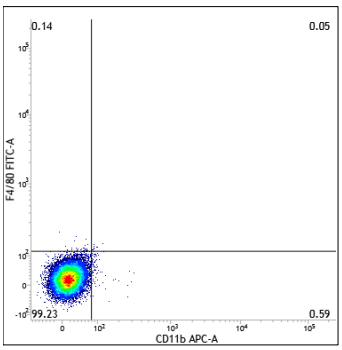

(c) CD11b and F4/80 **isotype control** of cells from ***Ier3-flox$^{+/+}$ LysM-Cre$^{-/-}$*** animals.

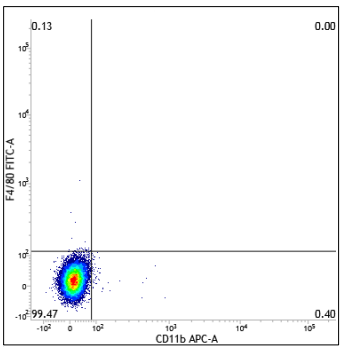

(d) CD11b and F4/80 **isotype control** of cells from ***Ier3-flox$^{+/+}$ LysM-Cre$^{+/+}$*** animals.

Figure 29.2: Flow cytometric analysis of *in vitro* differentiated MΦ from murine BMC. BMC were harvested and differentiated into MΦ as described in sec. 14. At day 7 of cultivation, the MΦ were detached using EDTA and Accutase™. Cell staining was performed as described in sec. 24.2. In short, $5 \cdot 10^5$ cells each were resuspended in 100 µl cold MACS buffer containing 3 µg/ml FITC conjugated anti-F4/80 REA™ IgG and/or APC conjugated anti-CD11b REA™ IgG, respectively equal amounts of appropriate REA™ isotype controls. After incubation for 10 min at 4 °C, cells were washed twice using cold MACS buffer. The cells were resuspended in 1 ml MACS buffer and analyzed subsequently. Signal thresholds to identify CD11b and F4/80-positive cells were set in reference to corresponding isotype controls.

30 mRNA expression in *in vitro* derived *Ier3-flox$^{+/+}$* MΦ

30.1 *Ier3* mRNA expression is up-regulated by LPS

Ier3 mRNA expression of *in vitro* differentiated MΦ from *Ier3-flox$^{+/+}$ LysM-Cre$^{-/-}$* and *Ier3-flox$^{+/+}$ LysM-Cre$^{+/+}$* mice in response to LPS was determined by qPCR (fig. 30.1). Figure 30.1a shows the results plotted against a linear ordinate, while in figure 30.1b

the ordinate has a logarithmic scale. In *Ier3-flox*$^{+/+}$ *LysM-Cre*$^{-/-}$ MΦ *Ier3* expression is triggered by LPS in a dose dependent manner. The activation with 0.5 $^{ng}/_{ml}$ LPS increases the *Ier3* expression seven-fold, while an activation with 1.0 $^{ng}/_{ml}$ increases the expression by factor 12.5 compared to unstimulated MΦ. In *Ier3-flox*$^{+/+}$ *LysM-Cre*$^{-/-}$ MΦ, the basal *Ier3*-expression is about 170 times higher compared to *Ier3-flox*$^{+/+}$ *LysM-Cre*$^{+/+}$ MΦ. This difference between the genotypes increases after the stimulation with LPS (factor 423 at 0.5 $^{ng}/_{ml}$LPS, respectively factor 251 at 1.0 $^{ng}/_{ml}$ LPS).

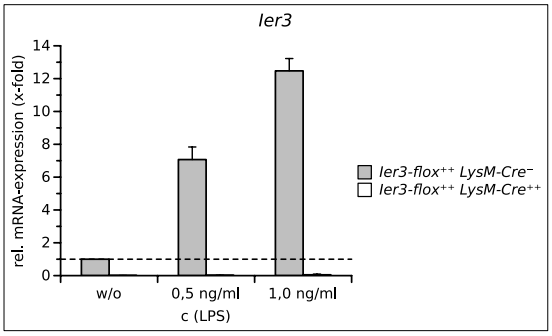

(a) Relative ***Ier3* mRNA expression** of *Ier3-flox*$^{+/+}$ *LysM-Cre*$^{-/-}$ and *Ier3-flox*$^{+/+}$ *LysM-Cre*$^{+/+}$ MΦ in response to LPS (***linear* ordinate**)

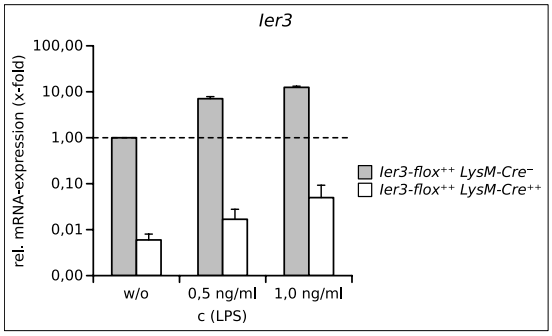

(b) Relative ***Ier3* mRNA expression** of *Ier3-flox*$^{+/+}$ *LysM-Cre*$^{-/-}$ and *Ier3-flox*$^{+/+}$ *LysM-Cre*$^{+/+}$ MΦ in response to LPS (***logarithmic* ordinate**)

Figure 30.1: Basal and LPS induced *Ier3* mRNA expression of *Ier3-flox*$^{+/+}$ MΦ. MΦ were generated as described in fig. 29.1. At day seven, they were stimulated with with different concentrations of LPS for 6 h. Cells were subsequently harvested and RNA isolation was performed using QiaShredder™ and RNeasy™ kits (both Qiagen) accordingly to manufacturers instructions. RT-PCR was performed as described in section 23.2 using 1.0 µg total RNA per sample. Per batch, 50 ng cDNA template were mixed with 6 µl S'green blue™ qPCR reaction mix (Biozym), primers in an end-concentration of 400 $^{nmol}/_{l}$, each and adjusted with water to a total volume of 12 µl. QPCR was conducted using a BioRad CFX-Connect™ cycler. All samples were measured as triplicates. At least two different housekeeping genes were used for normalization. Shown are normalized average permeabilities from a least 3 independent experiments. Bars represent absolute standard deviation.

30.2 mRNA expression of cytokines

Furthermore, the mRNA expression for several anti- and proinflammatory proteins in *Ier3-flox*$^{+/+}$ *LysM-Cre*$^{-/-}$ and *Ier3-flox*$^{+/+}$ *LysM-Cre*$^{+/+}$ MΦ was determined (fig. 30.2).

At basal levels, there was no difference in the the expression of *Tnf* mRNA between both genotypes (fig. 30.2a). After stimulation with 0.5 $^{ng}/_{ml}$ LPS, in the *Ier3-flox*$^{+/+}$ *LysM-Cre*$^{-/-}$ group *Tnf* mRNA levels increased by factor 24, while in the *Ier3-flox*$^{+/+}$ *LysM-*

Cre$^{+/+}$ group they increased by factor 46. Due to their standard deviation, these differences where not significant. In the presence of 1.0 ng/ml LPS, *Tnf* mRNA expression in both genotypes increased by factor 65 compared to unstimulated cells.

In the *Ier3-flox*$^{+/+}$ *LysM-Cre*$^{+/+}$ MΦ, basal expression levels of *Il-1β* mRNA where 1.8 times higher compared to *Ier3-flox*$^{+/+}$ *LysM-Cre*$^{-/-}$ cells (fig 30.2b). LPS mediated activation increased the *Il-1β* expression in both genotypes to factor 1300 at 0.5 ng/ml LPS, respectively up to factor 3300 at 1.0 ng/ml LPS, compared to the basal expression of *Ier3-flox*$^{+/+}$ *LysM-Cre*$^{-/-}$ cells.

Even tough basal *Il-6* mRNA levels in *Ier3-flox*$^{+/+}$ *LysM-Cre*$^{+/+}$ cells were 1.7 times higher compared to *Ier3-flox*$^{+/+}$ *LysM-Cre*$^{-/-}$ cells, the differences were not significant (fig. 30.2c). In *Ier3-flox*$^{+/+}$ *LysM-Cre*$^{-/-}$ MΦ, LPS augmented the *Il-6* expression by factor 1000 (0.5 ng/ml LPS), respectively by factor 3300 (1.0 ng/ml LPS).

In parallel, *Ier3-flox*$^{+/+}$ *LysM-Cre*$^{+/+}$ MΦ expressed 1 150-fold higher *Il-6* levels at 0.5 ng/ml LPS and 3000-fold higher levels at 0.5 ng/ml LPS, compared to unstimulated *Ier3-flox*$^{+/+}$ *LysM-Cre*$^{-/-}$ cells.

Il-10 expression in both genotypes was triggered by LPS in a dose dependent manner (fig. 30.2d). However, there were no significant expression differences between *Ier3-flox*$^{+/+}$ *LysM-Cre*$^{-/-}$ and *Ier3-flox*$^{+/+}$ *LysM-Cre*$^{+/+}$ MΦ detectable.

There was no difference in the basal expression of *Tgf-β* between both genotypes (fig. 30.2e). Furthermore, the treatment with 0.5 ng/ml or 1.0 ng/ml LPS did not affect the *Tgf-β* expression in *Ier3-flox*$^{+/+}$ *LysM-Cre*$^{-/-}$ as well as in *Ier3-flox*$^{+/+}$ *LysM-Cre*$^{+/+}$ MΦ.

Although the results revealed a high responsiveness of the generated MΦ even to small amounts of LPS, it was not possible to evaluate potential differences in cytokine expression on mRNA level between both genotypes due to the high standard deviation of the samples. Since the usage of several housekeeping genes as well as a meticulous design and quality control of the primers and PCR products (see section 23.3.3) did not reveal

any improvement, the high standard deviation could be ascribed to the heterogeneity and purity of the specimen.

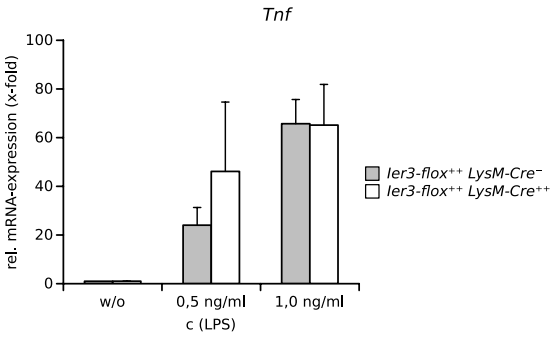

(a) *Tnf* mRNA expression.

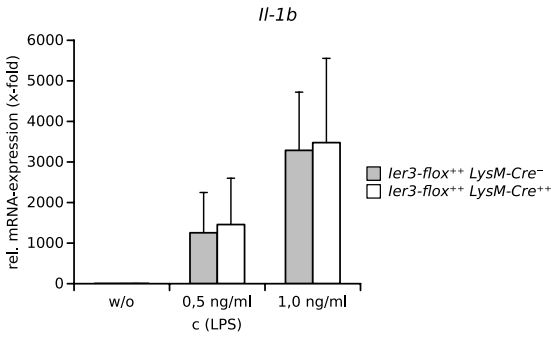

(b) *Il-1*βmRNA expression.

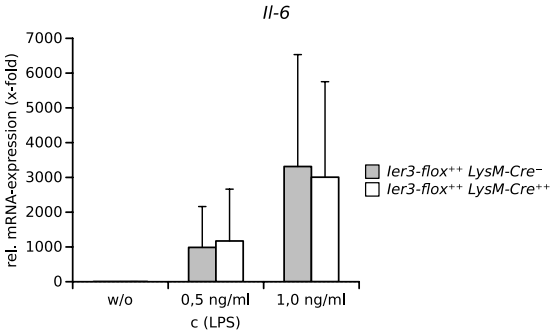

(c) *Il-6* mRNA expression.

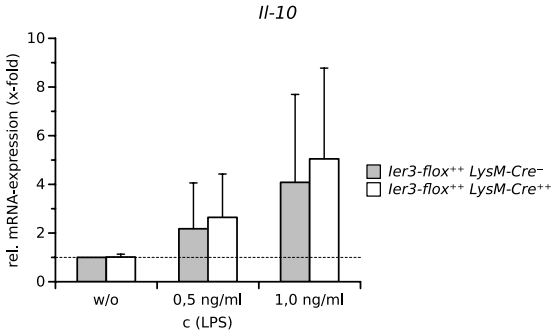

(d) *IL-10* mRNA expression.

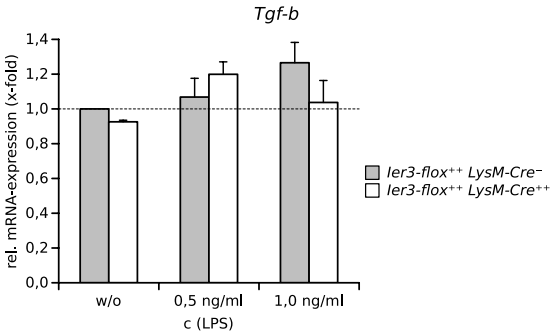

(e) *Tgf-*β mRNA expression.

Figure 30.2: Basal and LPS-induced mRNA expression of several pro- and anti-inflammatory cytokines in *Ier3-flox$^{+/+}$ LysM-Cre$^{-/-}$* and *Ier3-flox$^{+/+}$ LysM-Cre$^{+/+}$* MΦ. MΦwere generated as described in section 14. At day seven, they were stimulated with with different concentrations of LPS for 6 h and subsequently harvested. RNA isolation and processing was performed as described in sections23.2 23.1 and . QPCR was conducted using a BioRad CFX-Connect™ cycler as described in section 23.3. Shown are normalized average expressions from a least 3 independent experiments. All samples were measured as triplicates. Two different housekeeping genes were used for normalization. Bars represent absolute standard deviation.

31 Nitric oxide production and iNOS expression in *Ier3-flox$^{+/+}$ LysM-Cre$^{-/-}$* and *Ier3-flox$^{+/+}$ LysM-Cre$^{+/+}$* MΦ

Representing one of the key features of activated MΦ, the expression of inducible nitric oxide synthase (iNOS) as well as nitric oxide (NO_x) production in LPS stimulated *Ier3-flox$^{+/+}$ LysM-Cre$^{-/-}$* and *Ier3-flox$^{+/+}$ LysM-Cre$^{+/+}$* MΦ was analyzed.

31.1 *Ier3-flox$^{+/+}$ LysM-Cre$^{+/+}$* MΦ produce less nitric oxide

Nitric oxide (NO_x) production of *in vitro* differentiated macrophages from *Ier3-flox$^{+/+}$ LysM-Cre$^{-/-}$* and *Ier3-flox$^{+/+}$ LysM-Cre$^{+/+}$* animals was measured indirectly (as NO_2^-) in the cell culture supernatant using an assay based on the Griess-reaction [78]. NO_x production in unstimulated MΦ was below the limit of quantification in both genotypes. After stimulation with 5 $^{ng}/_{ml}$ LPS, the NO_x concentration in the supernatant of *Ier3-flox$^{+/+}$ LysM-Cre$^{+/+}$* MΦ was 40 % below the level in the supernatant of *Ier3-flox$^{+/+}$ LysM-Cre$^{+/+}$* MΦ ($p < 0.002$, fig. 31.1a). Interestingly, this difference diminishes at much higher LPS concentrations (100 $^{ng}/_{ml}$) (fig 31.1b). A simultaneous treatment with the iNOS inhibitor 1400W (10 $^{nmol}/_{ml}$) reduced the LPS induced NO_x-production by 94 % (fig 31.1b).

31.2 LPS induced iNOS expression is attenuated in *Ier3-flox$^{+/+}$ LysM-Cre$^{+/+}$* MΦ

INOS expression of *in vitro* differentiated macrophages from *Ier3-flox$^{+/+}$ LysM-Cre$^{-/-}$* and *Ier3-flox$^{+/+}$ LysM-Cre$^{+/+}$* animals was determined by western blot (fig. 31.2). Without stimulus, iNOS-expression in both genotypes was close to the quantification limit. However, iNOS-expression in *Ier3-flox$^{+/+}$ LysM-Cre$^{-/-}$* MΦ was 1.75 times higher compared to *Ier3-flox$^{+/+}$ LysM-Cre$^{+/+}$* MΦ(fig. 31.2b). LPS induced the iNOS-expression in both

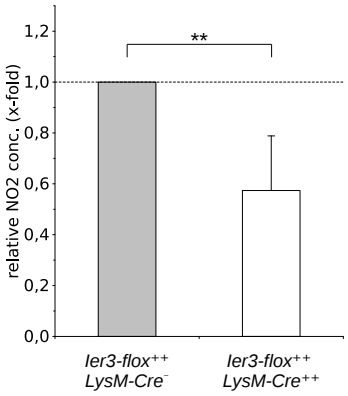

(a) Relative NO_x production of *Ier3-flox*$^{+/+}$ *LysM-Cre*$^{-/-}$ and *Ier3-flox*$^{+/+}$ *LysM-Cre*$^{+/+}$ MΦ after stimulation with **5 ng/ml LPS**. NO_x production in *Ier3-flox*$^{+/+}$ *LysM-Cre*$^{-/-}$ MΦ was set to 1.

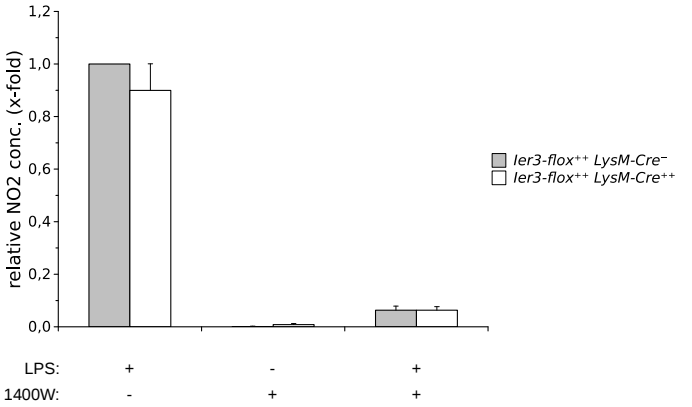

(b) Relative NO_x production (as NO_2) in *Ier3-flox*$^{+/+}$ *LysM-Cre*$^{-/-}$ and *Ier3-flox*$^{+/+}$ *LysM-Cre*$^{+/+}$ MΦ after stimulation with **100 ng/ml LPS and/or 10 nmol/ml 1400W**. NO_x production in LPS stimulated *Ier3-flox*$^{+/+}$ *LysM-Cre*$^{-/-}$ MΦ without 1400W was set to 1.

Figure 31.1: NO_x production of *Ier3-flox*$^{+/+}$ *LysM-Cre*$^{-/-}$ and *Ier3-flox*$^{+/+}$ *LysM-Cre*$^{+/+}$ MΦ in response to LPS. Primary MΦ were differentiated from BMC as described in fig. 29.1. At day 7, the MΦ were treated with different concentrations of LPS and/or 1400W for 6 h. Afterwards, the culture medium was exchanged against normal MΦM$^{M\text{-}CSF}$ and the cells were further incubated for 18 h. Nitric oxide production was measured indirectly by determining the NO_2^- concentration in the cultures supernatant using a photometric assay based on the GRIESS reaction. Values were normalized to the cell number using a Hoechst 33258 based fluorimetric assay. Shown are normalized average NO_2^- concentrations from a least 3 independent experiments. Error bars represent absolute standard deviation. Statistical significance was calculated by adjusted WILCOXON-MANN-WHITNEY-test. A p-value ≤ 0.01 is considered as statistically highly significant (**).

genotypes in a dose dependent manner. At 2 ng/ml LPS, iNOS levels in*Ier3-flox*$^{+/+}$ *LysM-Cre*$^{-/-}$ MΦ raised by factor 33, while 4 ng/ml LPS increased the iNOS-expression 45-fold compared to the basal level.

Ier3-flox$^{+/+}$ *LysM-Cre*$^{+/+}$ MΦ showed a 13-fold increase of iNOS level in presence of 2 ng/ml LPS, while iNOS levels in *Ier3-flox*$^{+/+}$ *LysM-Cre*$^{-/-}$ MΦ were 33 times higher compared to unstimulated cells.

In a direct comparison between both genotypes, *Ier3-flox*$^{+/+}$ *LysM-Cre*$^{-/-}$ MΦ showed a much higher response to LPS than *Ier3-flox*$^{+/+}$ *LysM-Cre*$^{+/+}$ MΦ. After stimulation with 2 ng/ml LPS, iNOS expression in *Ier3-flox*$^{+/+}$ *LysM-Cre*$^{-/-}$ MΦ was 2.5 times as high as in *Ier3-flox*$^{+/+}$ *LysM-Cre*$^{+/+}$ MΦ, while after stimulation with 4 ng/ml LPS the expression levels differed by factor 1.7.

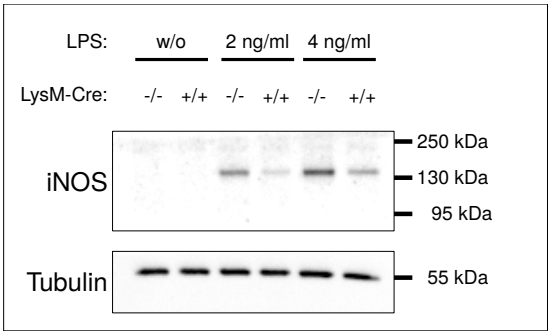

(a) Western blot.

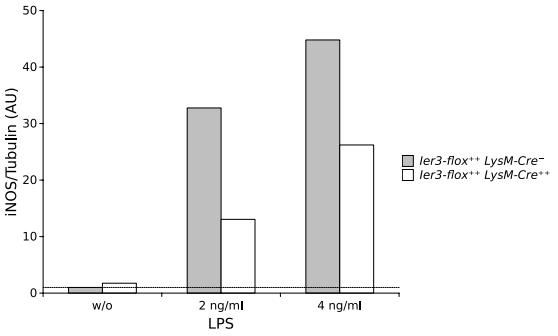

(b) Densitometric analysis. Relative iNOS expression normalized to tubulin. INOS expression in unstimulated *ler3-flox$^{+/+}$ LysM-Cre$^{-/-}$* MΦ is set to 1.

Figure 31.2: INOS protein expression in *ler3-flox$^{+/+}$ LysM-Cre$^{-/-}$* and *ler3-flox$^{+/+}$ LysM-Cre$^{+/+}$* MΦ in response to LPS. Primary MΦ were differentiated from BMC as described in fig. 29.1. At day 7, the MΦ were treated with different concentrations of LPS for 6 h. Subsequently, RIPA lysates of the cells were generated as described in section 22.1. After adjusting all samples to equal protein concentrations, SDS-PAGE and western blot were performed as described in section 22. Tubulin staining served as loading control.

32 Testing enterocyte model system for studying barrier function

To explore the impact of MΦon the barrier function of enterocytes it was necessary to establish an appropriate enterocyte model system. For this purpose, we first tried to immortalize freshly prepared murine IECs by employing a combined mTERT/BMI-1 transduction. After having selected immortalized IEC clones it turned out that these cells have largely lost their epithelial properties. This includes a significant loss of E-cadherin and villin expression, whereas the expression of vimentin as a mesenchymal marker was increased. Either, the transduced cell clones were derived from fibroblast contaminations or the transduction itself resulted in a marked EMT.

Next, two commercially available murine enterocyte cell lines – MODE-K [207] and YAMC [209] – were tested for their suitability as enterocyte model system. However, both cell lines also exhibited a considerable loss of epithelial properties, as indicated again by the loss of E-cadherin and villin expression and a gain of vimentin.

Thus, immortalized murine IECs were not suitable fort he planned experiments that require a largely maintained epithelial phenotype. Therefore, other cell systems were

chosen. Fortunately, the rat enterocyte cell line IEC-6 [162] and the well differentiated human colon cancer cell line Caco2 [61] had been proven suitable as bot cell lines not only express the epithelial marker at high level but also form intact monolayers in culture which is a prerequisite for conducting experiments on barrier functions.

33 *In vitro* permeability of CaCo-2 monolayers to FITC-dextran

Owing to their suitability as model system and their capability to form perfect monolayers, Caco2 cells were first used for the determination of *in vitro* permeability in the transwell setting with MΦ.

33.1 The Ier3 status of MΦ affects the permeability of CaCo-2 monolayers during direct co-culture

Monolayers of CaCo-2 cells showed on average an 38 % increased permeability ($p \leq 0.021$) to FD4 when directly co-cultivated with LPS (5 $^{ng}/_{ml}$) activated MΦ for 24 h (fig. 33.1a), independently of the macrophage's IER3 status ($p=0.248$). After 48 h of co-cultivation with *Ier3-flox*$^{+/+}$ *LysM-Cre*$^{-/-}$ MΦ , the FD4 permeability was 3.7 times higher compared to mono-cultured CaCo-2 monolayers, whereas *Ier3-flox*$^{+/+}$ *LysM-Cre*$^{+/+}$ mac increased the permeability only by factor 2.0. ($p \leq 0.034$). The FD4 permeability induced by *Ier3-flox*$^{+/+}$ *LysM-Cre*$^{-/-}$ MΦ was 1.8 times higher compared to *Ier3-flox*$^{+/+}$ *LysM-Cre*$^{+/+}$ MΦ ($p=0.034$).

33.2 Nitric oxide increases the permeability of CaCo-2 monolayers in a dose dependent manner

The CaCo-2 monolayers revealed an 6-fold increased permeability to FD4 when incubated in the presence of 5.0 $^{mmol}/_{l}$ of the nitric oxide donor S-Nitroso-N-acetylpenicillamine

(SNAP) (p=0.003), while a concentration of 2.5 $^{mmol}/_{l}$ SNAP had no effect on their FD4-permeability (fig 33.1b). Noteworthy, monolayers of the rat intestinal epithelial cell line IEC-6 partially detached from the transwell insert in the presence of SNAP. Thus, it was not possible to determine their permeability to FD4 with these cells here.

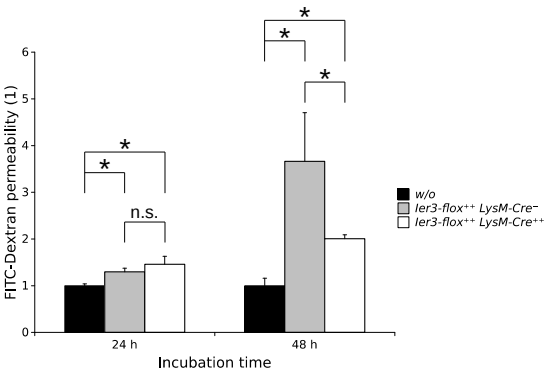

(a) MΦ induced permeability of CaCo-2 monolayers to FD4. At day 14 of cultivation, the culture medium was exchanged against CaCo-2-M.$^{w/o\ PR}$ medium containing $5 \cdot 10^5$ MΦ (*Ier3-flox*$^{+/+}$ *LysM-Cre*$^{-/-}$ or *Ier3-flox*$^{+/+}$ *LysM-Cre*$^{+/+}$, generated as described in fig. (29.1), 5 $^{ng}/_{ml}$ LPS and 5 $^{mg}/_{ml}$ FD4 in the apical compartment or phenol red free CaCo-2 medium without supplements in the basal compartment. FD4 concentrations in the basal and apical compartments were determined after 24 h and 48 h using a fluorimetric assay.

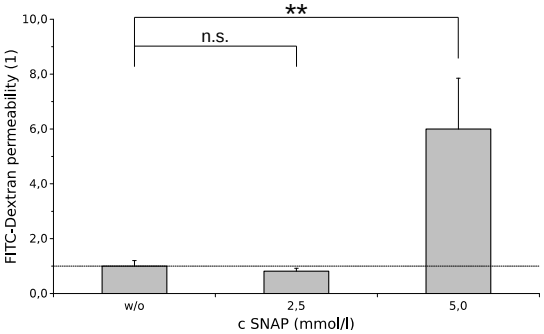

(b) SNAP induced permeability of CaCo-2 monolayers to FD4. At day 14 of cultivation, the culture medium was exchanged against CaCo-2-M.$^{w/o\ PR}$ containing SNAP (basal compartment) or SNAP and 5 $^{mg}/_{ml}$ FD4 (apical compartment). After 24 h FD4 concentrations in the basal and apical compartments were determined using a fluorimetric assay.

Figure 33.1: Permeability of CaCo-2 monolayers to FD4. $5 \cdot 10^5$ CaCo-2 cells were seeded on Transwell TC-inserts with a pore size of 0.4 µm (Sarstedt). Cells were cultivated for 14 days until a uniform cell monolayer had established. Medium was exchanged three times a week. At day 13 of cultivation, the culture medium was exchanged against CaCo-2-M.$^{w/o\ PR}$. Permeability experiments were conducted at day 14 after seeding. Shown are normalized average permeabilities from a least 3 independent experiments. Error bars represent absolute standard deviation. Statistical significance was calculated by adjusted WILCOXON-MANN-WHITNEY-test. A p-value ≤ 0.05 is considered as statistically significant (*), while a p-value ≤ 0.01 is considered as statistically highly significant (**).

34 Expression of tight junction related proteins in IEC-6 and CaCo-2 monolayers during direct co-culture with activated macrophages

After having shown that activated macrophages increase the permeability of CaCo-2 monolayers to small molecules, it was next investigated whether and how the expression

of cell junction related proteins in the enterocyte monolayers were affected during direct MΦ co-culture.

34.1 IEC-6

In IEC-6, the macrophages IER3-status had a huge impact on the expression of β-catenin and tubulin during direct co-culture (fig. 34.1a). While *Ier3*-knockout MΦ did hardly affect β-catenin expression (97 %, fig. 34.1d), *Ier3*-sufficient MΦ diminished its expression by 32 %. The expression of tubulin (fig. 34.1e) is even more affected by the macrophages *Ier3* genotype. *Ier3* wt MΦ reduce its expression by 64 %, whereas its expression is even slightly increased (103 %) during cocultivation with *Ier3* ko MΦ. E-Cadherin expression (fig. 34.1c) was indeed attenuated by MΦ of both genotypes, however the reduction was more pronounced during co-culture with wt MΦ (-21 % vs. -16 %). In contrast, ZO1 expression (fig. 34.1b) was not altered during co-culture with wt MΦ (102 %), but in the presence of *Ier3* ko MΦ (91 %). Occludin was not detectable in IEC-6 by the used antibody (fig 34.1a).

34.2 CaCo-2

In CaCo-2 cells, the effects of macrophages on the expression of cell junction related proteins were much weaker (fig. 34.2a). Furthermore, there were no distinct differences between *Ier3* wt and ko macrophages observable. E-Cadherin expression (fig. 34.2c) was reduced by 16 % during cocultivation with *Ier3* wt MΦ and by 21 % during cocultivation with *Ier3* ko MΦ. The expression of ZO1 (wt: 96 %, ko: 94 %, fig. 34.2b), β-catenin (wt: 99 %, ko: 96 %, fig. 34.2d) and occludin (wt: 100 %, ko: 97 %, fig. 34.2e) was not affected by the cocultivation of macrophages. In contrast, the cultivation with *Ier3* ko MΦ increased the tubulin expression (fig. 34.2f) by 11 % compared to normal cultivated CaCo-2 cells, whereas *Ier3* wt MΦ had no effect (101 %).

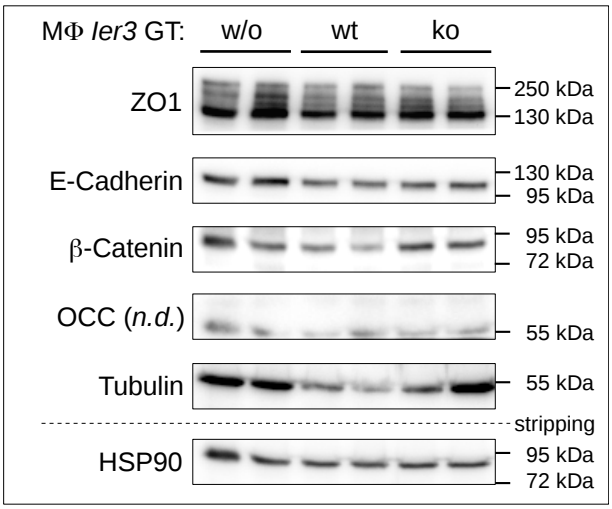

(a) Western blot.

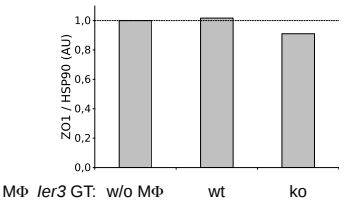

(b) Relative **ZO1** expression normalized to HSP90.

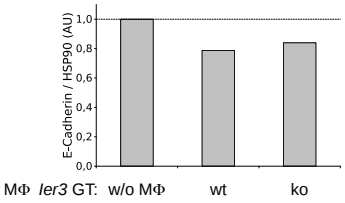

(c) Relative **E-cadherin** expression normalized to HSP90..

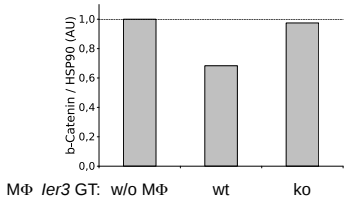

(d) Relative**β-catenin** expression normalized to HSP90..

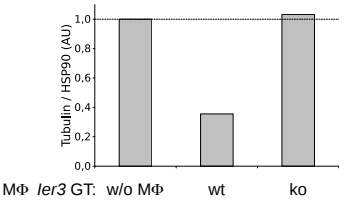

(e) Relative **Tubulin** expression normalized to HSP90..

Figure 34.1: Expression of tight junction related proteins in IEC-6 cells after direct co-culture with LPS activated *Ier3-flox*$^{+/+}$ *LysM-Cre*$^{-/-}$ and *Ier3-flox*$^{+/+}$ *LysM-Cre*$^{+/+}$ MΦ. IEC-6 cells were cultivated in 6-well-plates over a period of 14 days. Primary MΦ were differentiated from BMC as described in section 14. At day 7 of differentiation, the MΦ were harvested and counted. They were seeded on top the IEC-6 monolayer in a concentration of $5 \cdot 10^5$ cells/ml in MΦ-M. containing 5 ng/ml LPS ($1 \cdot 10^6$ MΦ in total, NC: only LPS). After 48 h of cocultivation, cells were harvested and RIPA lysates were generated as described in section 22.1. After adjusting all samples to equal protein concentrations, SDS-PAGE and western blot were performed as described in section 22. HSP90 staining served as loading control. Relative protein expression normalized to HSP90 was determined densitometrically. Expression in the negative control was set to 1. Shown is a representative blot from at least two experiments.

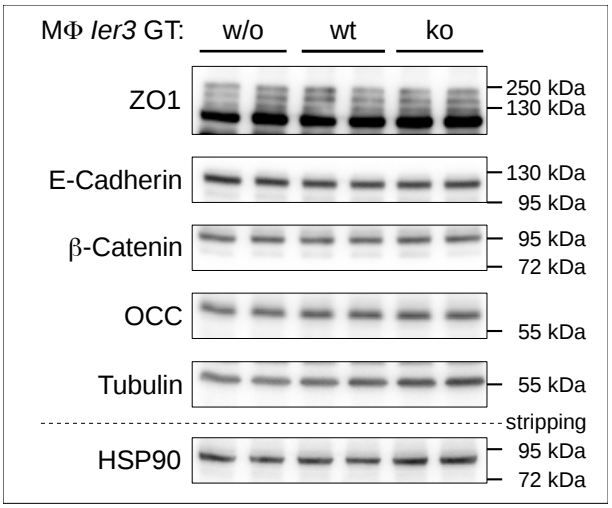

(a) Western blot.

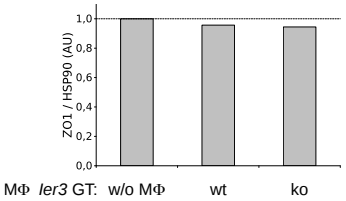

(b) Relative **ZO1** expression normalized to HSP90.

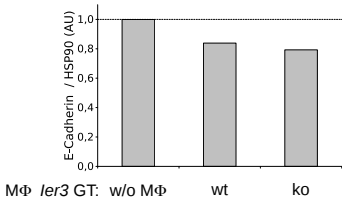

(c) Relative **E-cadherin** expression normalized to HSP90.

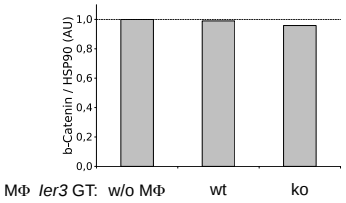

(d) Relative β**-catenin** expression normalized to HSP90.

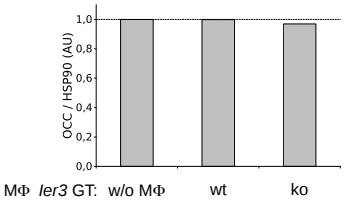

(e) Relative **occludin** expression normalized to HSP90.

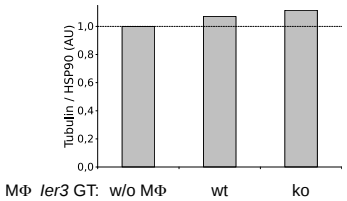

(f) Relative **Tubulin** expression normalized to HSP90.

Figure 34.2: Expression of tight junction related proteins in CaCo-2 cells after direct co-culture with LPS activated *Ier3-flox*$^{+/+}$ *LysM-Cre*$^{-/-}$ and *Ier3-flox*$^{+/+}$ *LysM-Cre*$^{+/+}$ MΦ. CaCo-2 cells were cultivated in 6-well-plates over a period of 14 days. Primary MΦ were differentiated from BMC as described in section 14. At day 7 of differentiation, the MΦ were harvested and counted. They were seeded on top the CaCo-2 monolayer in a concentration of $5 \cdot 10^5$ cells/ml in MΦ-M. containing 5 ng/ml LPS ($1 \cdot 10^6$ MΦ in total, NC: only LPS). After 48 h of cocultivation, cells were harvested and RIPA lysates were generated as described in section 22.1. After adjusting all samples to equal protein concentrations, SDS-PAGE and western blot were performed as described in section 22. HSP90 staining served as loading control. Relative protein expression normalized to HSP90 was determined densitometrically. Expression in the negative control (w/o) was set to 1. Shown is a representative blot from at least two experiments.

35 Expression of tight junction related proteins in CaCo-2 and IEC-6 monolayers in response to Nitric oxide

To verify, that the effects of MΦ on the expression of cell junction related proteins, as described in section 34, are caused by nitric oxide, we cultivated IEC-6 and CaCo-2 monolayers in presence of the NO-donor SNAP.

35.1 IEC-6

In IEC-6, the expression of E-cadherin, β-catenin as well as tubulin was highly attenuated by SNAP in a dose dependent manner (fig. 35.1a). A concentration of 2.5 $^{mmol}/_{l}$ SNAP reduced the E-cadherin expression by 24 % (fig. 35.1b), whereas 5.0 $^{mmol}/_{l}$ diminished its expression by 54 %. The effect of SNAP on expression of tubulin (fig. 35.1d) was similar, with -20 % at 2.5 $^{mmol}/_{l}$and -49 % at 5.0 $^{mmol}/_{l}$. β-catenin expression (fig. 35.1c) was attenuated by 32 % in the presence of 2.5 $^{mmol}/_{l}$ SNAP and by 55 % in the presence of 5.0 $^{mmol}/_{l}$.

35.2 CaCo-2

In CaCo-2 cells, the expression of β-catenin was also highly affected by SNAP, while E-cadherin and tubulin showed only a marginal and no response, respectively (fig. 35.2a). In the presence of 2.5 $^{mmol}/_{l}$ SNAP β-catenin expression (fig. 35.2c) was reduced by 31 %, whereas a concentration of 5.0 $^{mmol}/_{l}$ SNAP reduced its expression by 51 %. E–Cadherin expression (fig. 35.2b) was diminished by 5 % and 10 % at 2.5 $^{mmol}/_{l}$ and 5.0 $^{mmol}/_{l}$ SNAP, respectively. In contrast, tubulin expression (fig. 35.2d) was not affected at all by the SNAP treatment.

The results of the western blot most closely correspond to the observations from the immunohistochemically analysis (fig. 35.3). In response to NO, the overall expression

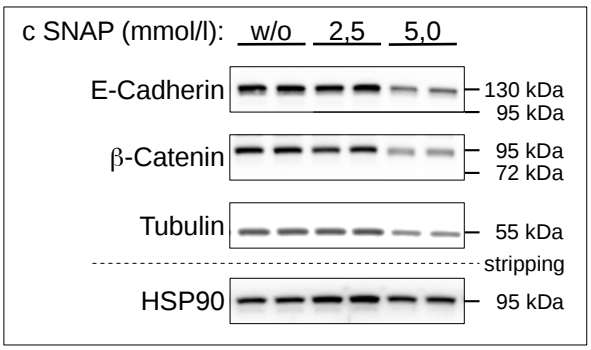

(a) Western blot.

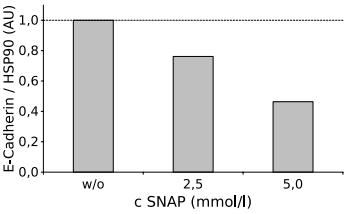

(b) Relative **E-cadherin** expression normalized to HSP90.

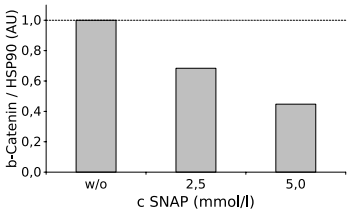

(c) Relative β**-catenin** expression normalized to HSP90.

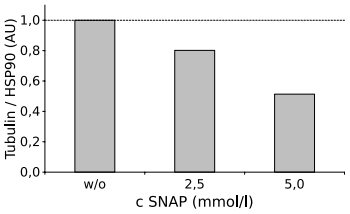

(d) Relative **Tubulin** expression normalized to HSP90.Tubulin

Figure 35.1: Effects of Nitric oxide on the expression of tight junction related proteins in IEC-6 cells. IEC-6 cells were cultivated in 6-well-plates over a period of 14 days. At day 14, culture medium was exchanged against freshly prepared medium containing either 2.5 or 5.0 mmol/l of the NO-donor SNAP or an equivalent amount DMSO in the negative control. After incubated for 24 h, cells were harvested and RIPA lysates were generated as described in section 22.1. After adjusting all samples to equal protein concentrations, SDS-PAGE and western blot were performed as described in section 22. HSP90 staining served as loading control. Relative protein expression normalized to HSP90 was determined densitometrically. Expression in the negative control was set to 1. Shown is a representative blot from at least two experiments.

of E-cadherin and β-catenin is not only down-regulated in general, but the continuous cell encompassing ring of both proteins exhibits several gaps. Furthermore, a significant fraction of both proteins is not longer only discretely located at the membraneous sites of cell-cell contacts, but is also detected diffusely distributed in the cytoplasm.

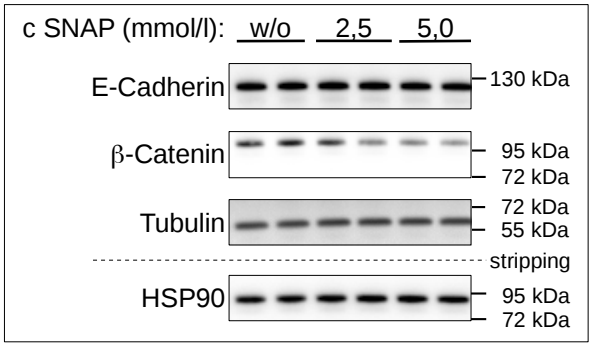

(a) Western blot.

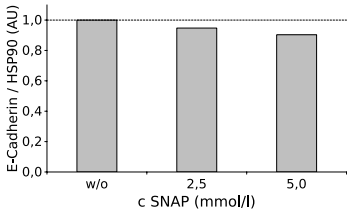

(b) Relative **E-cadherin** expression normalized to HSP90.

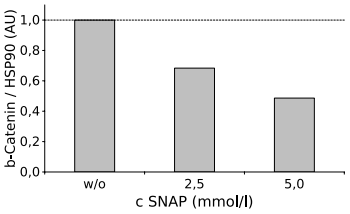

(c) Relative **β-catenin** expression normalized to HSP90.

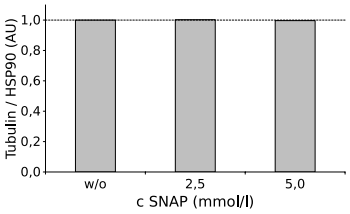

(d) Relative **Tubulin** expression normalized to HSP90.

Figure 35.2: Effects of Nitric oxide on the expression of tight junction related proteins in CaCo-2 cells – Western blot. CaCo-2 cells were cultivated in 6-well-plates over a period of 14 days. At day 14, the culture medium was exchanged against freshly prepared medium containing either 2.5 or 5.0 $^{\text{mmol}}/_{\text{l}}$ of the NO-donor SNAP or an equivalent amount DMSO in the negative control. After incubated for 24 h, cells were harvested and RIPA lysates were generated as described in section 22.1. After adjusting all samples to equal protein concentrations, SDS-PAGE and western blot were performed as described in section 22. HSP90 staining served as loading control. Relative protein expression normalized to HSP90 was determined densitometrically. Expression in the negative control was set to 1. Shown is a representative blot from at least two experiments.

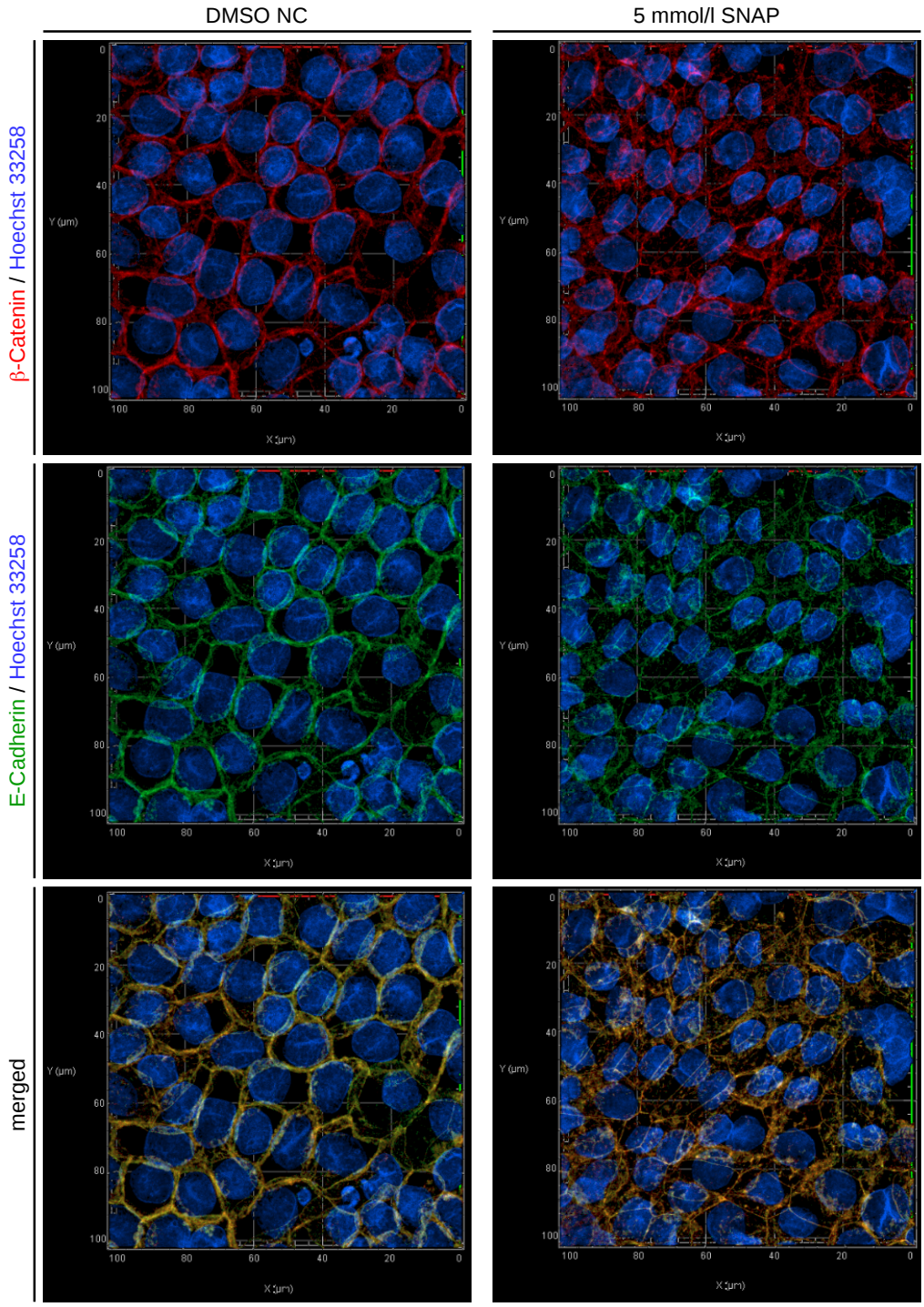

Figure 35.3: Effects of Nitric oxide on the expression of E-cadherin and β-catenin in CaCo-2 cells – ICC-F. CaCo-2 cells were seeded on coverslips and cultivated in 12-well-plates over a period of 14 days. Culture medium was exchanged with freshly prepared medium containing 5.0 $^{mmol}/_{l}$ of the NO-donor SNAP or an equivalent amount DMSO in the negative control. After incubated for 24 h, the cells were fixated and an ICC-F staining against E-cadherin (*green*) and β-catenin (*red*) was performed as described in sec. 18. Cell nuclei were counterstained with Hoechst bisbenzimide H33258 (*blue*). Shown are representative pictures from multiple experiments.

Discussion

Its ubiquitous expression not only in nearly all tissue compartments of the human body [14] but also in the majority of all eukaryotes up to *drosophila* and *C. elegans* [100], emphasizes the crucial role of IER3 in the regulation of cellular processes. For the first time we address the myeloid specific effects of IER3 expression in the context of AOM/DSS colitis and carcinogenesis in mice.

The infiltration of the lamina propria with M1 polarized MΦ is a critical step not only during the initial phase of acute and chronic colitis but also during the progression of inflammation. Thereby, macrophages have an essential role in the course of both IBD in humans and DSS induced colitis in mice [192].

36 Phenotype differences and similarities between *Ier3-flox$^{+/+}$ LysM-Cre$^{-/-}$* and *Ier3-flox$^{+/+}$ LysM-Cre$^{+/+}$* mice

In our experiments we did not observe any genotype specific difference in the number of resident colonic MΦ between genotypes in *Ier3-flox$^{+/+}$ LysM-Cre$^{-/-}$* and *Ier3-flox$^{+/+}$ LysM-Cre$^{+/+}$* animals or between constitutive *Ier3* wt and ko mice. Furthermore, the number of MΦ infiltrating the mucosa and submucosa during DSS respectively AOM/DSS colitis did not differ between the respectively genotypes. Hence, two important conclusions can be drawn from these observations:

First, the macrophage's IER3 status has no impact on the recruitment of MΦ to the colonic mucosa under both, physiological and inflammatory conditions. Second, the differential severity of the DSS as well as AOM/DSS induced colitis seen in *Ier3-flox$^{+/+}$ LysM-Cre$^{-/-}$* and *Ier3-flox$^{+/+}$ LysM-Cre$^{+/+}$* animals is not caused by a different number of infiltrating MΦ but is, instead, the result of their distinct behavior depending on their respective IER3 status.

Furthermore, our experiments revealed no differences in the integrity of the intestinal barrier between healthy *Ier3-flox*$^{+/+}$ *LysM-Cre*$^{-/-}$ and *Ier3-flox*$^{+/+}$ *LysM-Cre*$^{+/+}$ animals. There were not only no differences in their intestinal permeability to orally administered FITC conjugated dextrans, but we could also not observe any difference in the expression and localization of the tight junction related proteins E-cadherin and β-catenin in the colon tissue of both genotypes (results not shown). This leads to the assumption, that under physiological conditions, the IER3 expression in residual colonic macrophages does not affect the expression of cellular junction related proteins in adjacent intestinal epithelial cells. These findings correspond with the results of our *in vitro* experiments, where we did not observe any differences in the permeability of CaCo-2 and IEC-6 monolayers to FITC dextran when co-cultivated with unstimulated primary MΦ derived from BMCs of *Ier3-flox*$^{+/+}$ *LysM-Cre*$^{-/-}$ or *Ier3-flox*$^{+/+}$ *LysM-Cre*$^{+/+}$ origin.

In contrast to the colon, where the macrophage's IER3 status had no observable effect on adjacent cells under physiological conditions, in other tissue compartments it had. As described in the results, age matched *Ier3-flox*$^{+/+}$ *LysM-Cre*$^{+/+}$ animals showed on average an 23 % increased body weight compared to their *Ier3-flox*$^{+/+}$ *LysM-Cre*$^{-/-}$ littermates. While many studies addressing the interplay of MΦ and mature adipocytes in fat tissue, little is known about the role of MΦ in the physiological processes during adipogenesis and adipocyte differentiation. However, there is a huge consensus, that the paracrine secretion of several pro- and anti-inflammatory factors of tissue MΦ not only affects the mitochondrial energy metabolism of mature adipocytes but also plays an important role during the differentiation of their progenitors. Cheng et al. [221] demonstrated, that the secretion of a typical M1 MΦ associated chemokine profile suppresses adipogenesis while a more M2 like shifted profile promotes the differentiation into mature adipocytes. The fat tissue itself secretes a variety of different hormones and cytokines, affecting the phenotype of adjacent cells in a paracrine manner. It is conceivable that IER3 proficient and deficient MΦ react differently to these stimuli. Hence, the body-weight differences between healthy *Ier3-flox*$^{+/+}$ *LysM-Cre*$^{-/-}$ and *Ier3-flox*$^{+/+}$ *LysM-Cre*$^{+/+}$ mice, could be an indicator of a differential cytokine expression profile of the fat tissue associated MΦ in

these two mouse genotypes. However, it remains unclear whether these differences are also true for the lamina propria populating MΦ Furthermore, we could not observe any difference in the expression of typical M1 and M2 markers between genotypes in our *in vitro* generated BMC derived MΦ (Results not shown). SHADID et al. [180] reported an involvement of IER3 in the fat metabolism of mice. However, their results referred to a genome wide Ier3 depletion in combination with a high-fat diet. Therefore, it seems reasonable to further characterize the fat tissue as well as the LP populating MΦ *in vivo* in prospective experiments.

Interestingly, there were no differences in the body weight between healthy constitutive *Ier3* wt and ko mice.

From all examined organs, only the ceca differed in their relative weight between genotypes, while the absolute ceca weights were similar. This can be explained by the fact, that the cecum size is independent of the body fat content, whereas the absolute liver weight and, to a lesser degree, the spleen weight are.

Keeping in mind the body weight differences between the two mouse genotypes, the dosages of all agents used in our *in vivo* experiments were body-weight adjusted to exclude biases of the results due to body-weight related variations.

37 Myeloid IER3 deficiency protects mice during the initiation of chronic DSS and AOM/DSS colitis

Mice with a myeloid IER3 depletion showed only very mild signs of inflammation during the initial phase of both, chronic DSS and combined AOM/DSS colitis. This obvious protective effect by *Ier3* deficiency in MΦ became evident in all analyzed disease parameters. Most importantly, in all conducted experiments *Ier3-flox*$^{+/+}$ *LysM-Cre*$^{+/+}$ animals did not show significant loss of body weight during the initial phase, whereas *Ier3-flox*$^{+/+}$ *LysM-Cre*$^{-/-}$ lost on average 16 % in the DSS only experiment and

11 % in the AOM/DSS experiment. The relative standard deviation of body weight within the *Ier3-flox*$^{+/+}$ *LysM-Cre*$^{-/-}$ cohort was remarkably high in contrast to the group of *Ier3-flox*$^{+/+}$ *LysM-Cre*$^{+/+}$ mice, an observation that explains the fast recovery of body weight in the *Ier3-flox*$^{+/+}$ *LysM-Cre*$^{-/-}$ cohort until day 6 after termination of the DSS treatment. Moreover, the most severely affected *Ier3-flox*$^{+/+}$ *LysM-Cre*$^{-/-}$ animals had to be excluded earlier from the experiment due to their poor health condition, so that only the less affected animals account for the body weight curve during the last third of the experiment. This also explains the reduced standard deviation in body weight curve of *Ier3-flox*$^{+/+}$ *LysM-Cre*$^{-/-}$ mice during this period.

The generally higher DSS responsiveness of *Ier3-flox*$^{+/+}$ *LysM-Cre*$^{-/-}$ animals during the DSS experiment also manifested in their already mentioned poorer overall survival rate of 50 % compared to 100 % in the *Ier3-flox*$^{+/+}$ *LysM-Cre*$^{+/+}$ cohort. Interestingly, during the AOM/DSS experiment non of the animals from both cohorts had to be excluded at this time point, whereas a lower bleeding score and stool consistency herein clearly revealed the protective effect of the myeloid IER3 deficiency.

Additionally, relative liver and spleen weights of the animals in the *Ier3-flox*$^{+/+}$ *LysM-Cre*$^{-/-}$ group were significantly increased compared to *Ier3-flox*$^{+/+}$ *LysM-Cre*$^{+/+}$ animals. Both parameters are indicators of intense inflammation and/or a systematic infection.

A potential cause of the divergent DSS responsiveness between the individuals of the *Ier3-flox*$^{+/+}$ *LysM-Cre*$^{-/-}$ cohort would be a variation of their gut microbiome or other housing related conditions. However, the responsiveness also varied between animals in the same cage and deriving from the same mother. Thus, the mice had experienced an identical vertical transmission (from the mother) of the microbiome, thus excluding housing or microbiome dependent differences.

On the histological level, all animals in the DSS only experiment exhibited moderate morphological tissue damages in some colon segments. As mentioned in the results, an exact grading of the lesions in each colon has proven very difficult. However, colons

in mice of both genotypes displayed a massive infiltration with MΦ, not only into segments with visible tissue damage. As MΦ infiltrations take place already in quite early stages of inflammation and before considerable tissue lesions develop, it is likely, that the *Ier3* deficient MΦ in *Ier3-flox*$^{+/+}$ *LysM-Cre*$^{+/+}$ animals are more supportive of maintaining tissue integrity, whereas the *Ier3* proficient (wild-type) M1-MΦ enhance the inflammatory processes in *Ier3-flox*$^{+/+}$ *LysM-Cre*$^{-/-}$ mice and contribute to the DSS induced tissue damage in a positive feedback loop.

In support of the hypothesis above, *in vivo* permeability experiments revealed a 2.4-fold higher intestinal permeability for FD4 ($r_H \approx 14$ Å) in *Ier3-flox*$^{+/+}$ *LysM-Cre*$^{-/-}$ mice after 24 h treatment with DSS as compared with *Ier3-flox*$^{+/+}$ *LysM-Cre*$^{+/+}$ animals, whereas both cohorts revealed only a marginal and statistically not relevant intestinal permeability to FD10 ($r_H \approx 23$ Å).

While an effective lesion size of less than 23 Å is to small for whole bacterias to transmigrate into the mucosa, it allows the diffusion of soluble factors like LPS fragments from disintegrated bacteria and other immunogenic antigens.

These findings could also be reproduced *in vitro*, where a co-cultivation with activated primary MΦ derived from BMC of *Ier3-flox*$^{+/+}$ *LysM-Cre*$^{-/-}$ animals for 48 h increased the permeability of CaCo-2 cell monolayers to FD4 by factor 3.7, whereas the co-cultivation with *Ier3-flox*$^{+/+}$ *LysM-Cre*$^{+/+}$ MΦ increased the permeability only by factor 2.0 (p=0.034).

38 Myeloid IER3 deficiency affects the expression of cellular junction associated proteins in mucosal epithelial cells

Several authors reported altered expression profiles of the tight junction associated proteins E-cadherin and β-catenin in the epithelial cell layer of the colonic mucosa during both IBD in humans and DSS colitis in mice [130, 81, 44, 114, 156, 200]. We demonstrated,

that the expression as well as the intracellular localization of these proteins is strongly affected by the myeloid cells's IER3 status during AOM/DSS colitis.

As described in the results, the expression level of both proteins was highly variable per se, even within the colon of each mouse. However, in colon segments with a comparable MΦ infiltration, the overall expression of E-cadherin as well as of β-catenin was much higher in the *Ier3-flox*$^{+/+}$ *LysM-Cre*$^{+/+}$ cohort when compared to *Ier3-flox*$^{+/+}$ *LysM-Cre*$^{-/-}$ animals. These observations are particularly in line with the results from our *in vitro* co-culture experiments of activated primary BMC derived IER3$^{pos/neg}$ MΦ and intestinal epithelial cell monolayers of rat origin (IEC-6). Surprisingly, these IER3 related differences in the expression of E-cadherin and β-catenin were not observable when the co-cultivating the MΦ with intestinal epithelial cell monolayers of human adenocarcinomal origin (CaCo-2). This leads to the assumption, that at least one species dependent factor expressed by the MΦ, which is compatible with rat but not with human cells, is responsible for the altered expression of E-cadherin and β-catenin in the these cells. Martini et al. [127] and Turner [200] point out the negative effects of increased TNF, IFN-γ and IL-6 levels on the integrity on cellular junction proteins in IEC during IBD. While we could not observe differences in the expression of these cytokines between *in vitro* generated *Ier3* proficient and deficient MΦ, these cytokines do not necessary arise from them, but are also produced by IEC themselves in response to stimulation by immune cells [127]. Another explanation could be, that CaCo-2 cells are generally not affected in their expression of E-cadherin and β-catenin regarding this factor, due to their transformed genotype as adenocarcinomal cell line.

Not only the intensity but also the intracellular localization of E-cadherin and β-catenin differed between AOM/DSS challenged *Ier3-flox*$^{+/+}$ *LysM-Cre*$^{-/-}$ and *Ier3-flox*$^{+/+}$ *LysM-Cre*$^{+/+}$ mice. In segments with a moderate to high E-cadherin and β-catenin expression, *Ier3-flox*$^{+/+}$ *LysM-Cre*$^{-/-}$ mice revealed a higher grade of cytoplasmic internalization compared to *Ier3-flox*$^{+/+}$ *LysM-Cre*$^{+/+}$ animals.

This severely altered expression/localization pattern of E-cadherin and β-catenin in

Ier3-flox$^{+/+}$ *LysM-Cre*$^{-/-}$ animals is presumably an essential cause for a disturbed tight junction integrity as described by other authors [130, 114, 127].

The postulated maintenance of the junctional integrity in *Ier3-flox*$^{+/+}$ *LysM-Cre*$^{+/+}$ animals reflects the results of our in-vivo and ex-vivo trans epithelial permeability (TEP) experiments discussed above. Remarkably, the ex-vivo TEP experiments were not affected by the species dependent differences between the MΦ and the CaCo-2 monolayers which leads to two possible assumptions:

Either the increased permeability of the CaCo-2 monolayers caused by IER3 proficient MΦ can be attributed exclusively to their increased release of RNS, which act across species borders. The other possibility would be, that activated IER3 proficient and deficient MΦ additionally differ in their expression profile of cellular junction integrity affecting cytokines. The latter assumption is contradicted by the fact, that the number of murine cytokines capable of binding to human receptors is limited and that we did not find any expressional differences between *Ier3* proficient and deficient MΦ of the gene candidate analyzed by us.

However, further evidence could be provided by co-cultivating murine MΦ and human IEC monolayers in presence of the iNOS inhibitor 1400W.

39 Myeloid IER3 deficiency protects mice from colitis associated AOM/DSS carcinogenesis

As described in the results, at the end of the experiment all animals suffered from the formation of colonic neoplasms, which were mostly located in the M2 and distal quartile. However, with an average number of 3 neoplasms per animal, the number of tumors in the *Ier3-flox*$^{+/+}$ *LysM-Cre*$^{+/+}$ cohort was significantly lower compared to the *Ier3-flox*$^{+/+}$ *LysM-Cre*$^{-/-}$ cohort (8 neoplasms per animal, p=0.009).

These results clearly prove that the myeloid depletion of IER3 has a protective effect on the formation of colitis associated neoplasms in the AOM/DSS mouse model. Still, the underlying mechanisms are not fully clear and further investigations are needed to elucidate whether the reduced tumor formation in *Ier3-flox*$^{+/+}$ *LysM-Cre*$^{+/+}$ animals is a direct result of the attenuated inflammation or whether other mechanisms are involved.

Interestingly, in both cohorts the average size of the tumors did not differ (3 mm, p=0.328) thus allowing two assumptions. On the one hand, it is possible that the neoplasms in both genotypes arise at the same time point yielding in equal sizes when explored at the end of experiment. On the other hand, the tumor formation in *Ier3-flox*$^{+/+}$ *LysM-Cre*$^{-/-}$ animals commences at an earlier time-point but their growth rate is lower than in *Ier3-flox*$^{+/+}$ *LysM-Cre*$^{+/+}$ animals.

While the tumors themselves are mostly free of MΦ infiltrates, they are surrounded by a huge number of them. It still needs to be investigated, if these surrounding MΦ are of the same phenotype as the colitis associated M1 polarized MΦ or if they bear the phenotype of typical M2 polarized tumor associated MΦ . If the tumor surrounding MΦ should mainly posses the characteristics of the colitis associated MΦ, it could be envisioned that the same effects which mitigate the inflammatory processes and the onset of CAC in *Ier3-flox*$^{+/+}$ *LysM-Cre*$^{+/+}$ animals rather promote the growth of an already existing neoplasm.

Our results are in accordance with the findings of Ustyugova et al. [202] who also proposed an CAC protecting effect of IER3 deficiency in an AOM/DSS mouse model. However, their experimental design differed in several aspects from ours, especially by using a mouse model with a constitutive *Ier3* knockout.

When analyzing the body weight recovery of the *Ier3-flox*$^{+/+}$ *LysM-Cre*$^{-/-}$ animals after the first DSS cycle, it could be appreciated that both cohorts exhibited similar responses regarding their body weight during the following DSS cycles. The obviously faster body weight recovery rate of the *Ier3-flox*$^{+/+}$ *LysM-Cre*$^{-/-}$ cohort after the third DSS cycle, is

due to the fact, that several *Ier3-flox*$^{+/+}$ *LysM-Cre*$^{-/-}$ animals were at a poor general health condition during this period and had to be excluded from the experiment.

Despite the reduced inflammatory activity of IER3 deficient MΦ, the initially unaffected colonic tissue in *Ier3-flox*$^{+/+}$ *LysM-Cre*$^{+/+}$ animals became more vulnerable of acute toxicity by the DSS treatment during the third cycle giving rise of some tissue damage at this later stage. However, except the similar weight loss in both cohorts after the third DSS cycle, other colitis associated parameters like bleeding scores and stool consistency were less pronounced in the *Ier3-flox*$^{+/+}$ *LysM-Cre*$^{+/+}$ cohort. This also reflects in the higher overall survival rate of 70 % compared to 50 % in the *Ier3-flox*$^{+/+}$ *LysM-Cre*$^{-/-}$ group.

Unexpectedly, the relative spleen weights in the *Ier3-flox*$^{+/+}$ *LysM-Cre*$^{-/-}$ cohort were significantly lower compared to those in the *Ier3-flox*$^{+/+}$ *LysM-Cre*$^{+/+}$ group. This observation could be explained by the fact that the majority of the *Ier3-flox*$^{+/+}$ *LysM-Cre*$^{-/-}$ animals had to be excluded earlier from the experiment due to their poor health condition, before a systemic infection could manifest.

40 The tissue protective effect of myeloid IER3 deficiency is less pronounced in acute high DSS colitis

The body weight loss of *Ier3-flox*$^{+/+}$ *LysM-Cre*$^{+/+}$ animals after the administration of high DSS (30 g/l) over a period of 9 days to induce an acute colitis was indeed less pronounced compared to *Ier3-flox*$^{+/+}$ *LysM-Cre*$^{-/-}$ animals. We assume, that in these experiment the putative colitis protecting effects of a myeloid IER3-deficiency were mostly prevailed by the massive disruption of the mucosal epithelial cell barrier caused by the acute toxicity of high dose DSS. However, in one experiment, the animals of the *Ier3-flox*$^{+/+}$ *LysM-Cre*$^{-/-}$ cohort exhibited a significantly higher relative spleen weight, indicating a systemic bacterial infection.

41 Comparison with effects of *Ier3* depletion in other tissue compartments

Even if statistically significant, the putative protective effects of an epithelial IER3 deficiency during the onset of an acute DSS colitis should not be overestimated, since they could not be observed during the initial phase of chronic DSS colitis in a second experiment. Hence, further DSS experiments are necessary to conclusively assess the impact of epithelial IER3 expression on the outcome of DSS colitis.

In mice with a constitutive IER3 deficiency, differences in the clinical outcome of both, acute as well chronic DSS colitis are much less pronounced between genotypes compared to *Ier3-flox*$^{+/+}$ *LysM-Cre*$^{-/-}$ and *Ier3-flox*$^{+/+}$ *LysM-Cre*$^{+/+}$ animals. This is a strong indicator, that an IER3 depletion in other tissue compartments than the myeloid exhibits rather inflammation promoting properties contrasting the protective effects of IER3 deficient MΦ. This is in line with previous observations of our group, that IER3 in general attenuates the expression of pro-inflammatory cytokines under control of NF-κB. Sina et al. even proposed a putative protective effect of a genome wide IER3 expression during DSS colitis in mice [183]. However, such deviations can be explained not only by genomic differences between diverse mouse strains but also by different housing conditions and hereby alterations in the mice's microbiome, which both have a considerable impact on the outcome of a DSS experiment.

42 Similarities and differences between IER3 proficient and deficient *in vitro* generated BMC derived primary MΦ

42.1 *Ier3* mRNA expression

Besides the prove of the specific depletion of the *Ier3* gene in the *Ier3-flox*$^{+/+}$ *LysM-Cre*$^{+/+}$ mice used in the experiments, we demonstrated a successfully suppression

of *Ier3* on the mRNA level in primary MΦ derived from BMC of *Ier3-flox*$^{+/+}$ *LysM-Cre*$^{+/+}$ mice. Furthermore we could show, that the *Ier3* mRNA expression in primary MΦ from *Ier3-flox*$^{+/+}$ *LysM-Cre*$^{-/-}$ mice is triggered by LPS in a dose dependent manner. These results are in accordance with former findings of our and other groups, describing a general upregulation of IER3 in response to immunogenic stimuli [183, 160].

42.2 Polarization

As described in the introduction, M1 polarized MΦ are the main subpopulation of MΦ mostly contributing to inflammatory processes as well as to the induction of inflammatory associated neoplasm in the gut[66]. Therefore it was our goal to generate MΦ with typical M1 characteristics for our ex vivo experiments. Due to the high number of different protocols described in the literature, we tested several approaches and characterized the generated cells by flow cytometry (results not shown). Eventually, we decided to use M-CSF instead of GM-CSF as main cytokine for MΦ differentiation, because the latter one leads not only to the generation of MΦ but also to a variety of other cell populations, mainly dendritic cells and granulocytes. The addition of IFN-γ in combination with M-CSF directed the differentiation of the MΦ towards a M1-like phenotype. We could observe no differences in the expression of typical M1 markers like CD80 and MHC II between M-CSF/IFN-γ and GM-CSF differentiated F4/80-positive cells derived from BMC (results not shown). The same is true for the absence of the M2 marker CD200R. Interestingly, the GM-CSF differentiated bone marrow cells exhibited greater morphological differences between the genotypes (results not shown), which were not manifested in M-CSF differentiated MΦ.

An expansion of the M-CSF differentiation period longer than seven days had no effect on the yield of F4/80-positive cells of ≥ 75 %. A possible explanation is, that a fraction of the BMC was already in an early differentiated state towards other cell types, which

[66] In later stages the mostly M2 polarized tumor associated MΦ contribute significantly to the progression of tumor.

could not be altered anymore by M-CSF/IFN-γ. This assumption is supported by the fact, M-CSF triggers not only the differentiation of MΦ but is also involved in the differentiation of a variety of other cell types.

However, there were no significant differences in the yield of F4/80$^+$/CD11b$^+$, F4/80$^+$/CD11b$^-$ and F4/80$^-$/CD11b$^+$ cells between both genotypes. This is even more remarkably, as Pietzsch et al. [160] assume the involvement of IER3 in differentiation process from monocytes to MΦ. It remains to be investigated if our findings from these ex vivo experiments can be transfered to MΦ under *in vivo* conditions.

42.3 Cytokine expression

Surprisingly, we did not observe significant differences in the mRNA-expression profile of inflammation related cytokines between *in vitro* generated BMC-derived MΦ from both genotypes on basal level as well as after stimulation with LPS. This, in combination with the relative high standard deviation, could be an additional indicator for a putative contamination of the MΦ population with other cell types, masking the effects of a MΦ specific *Ier3* depletion.

Considering the much higher LPS induced mRNA-expression of the pro-inflammatory cytokines TNF (up to 65-fold), IL-1β (up to 3300-fold), and IL-6 (up to 3000-fold) compared to the much lower LPS induced expression of the anti-inflammatory cytokines IL-10 (up to factor 5) and TGF-β (up to factor 1.5) is a further indicator for the M1 polarization of the *in vitro* generated MΦ.

42.4 IER3 deficient MMΦ produce less RNS in response to immunogenic stimuli

We demonstrate for the first time, that IER3 has a direct impact on the expression of the iNOS as well as on the release of RNS in MΦ in response to immunogenic stimuli.

While previous studies of our group clearly showed an attenuation of the NF-κB cascade by IER3 in a variety of different cell lines, these mechanism seem to be superimposed in MΦ from *Ier3-flox*$^{+/+}$ *LysM-Cre*$^{+/+}$ animals by other effects, leading to a decreased iNOS expression and a diminished production of RNS. Although the exact mechanisms underlying these effects are not yet elucidated, we could identify some starting points for further investigations. The macrophage cell lines RAW264.7 and THP-1 express higher levels of heme oxygenase in response to LPS when *Ier3* is depleted [75]. Furthermore, it is conceivable that *Ier3* deficient MΦexpress lower levels of immunogenic receptors, which would make them less responsive to certain stimuli. For instance, Akilov et al. [18] reported a correlation between the expression levels TNF receptor 1 (TNFR1) and IER3 in patients suffering from the Sézary syndrome.

43 Increased levels of NO_x induce *in vitro* a damage pattern similar to the one caused by activated wt MΦ

When administered exogenously, the damages nitric oxide causes to CaCo-2 and IEC-6 monolayers resembles the effects of LPS activated *Ier3-flox*$^{+/+}$ *LysM-Cre*$^{-/-}$ BMC derived MΦ. NO_x inhibits the expression of E-cadherin as well as of β-catenin in these cells in a dose dependent manner. Additionally, we demonstrated for CaCo-2 monolayers that NO_x not only inhibits the expression of these proteins but also but also elicits their translocation from the cell-cell contact sites towards the cytoplasm.

Furthermore, we demonstrated that these effects result in an increased transepithelial permeability of CaCo-2 monolayers to FD4, similar to the one caused by *Ier3-flox*$^{+/+}$ *LysM-Cre*$^{-/-}$ BMC derived MΦ.

44 Conclusion

When summarizing the results from our in-vivo and in-vitro experiments, one can conclude that the reduced severity of an AOM/DSS colitis in *Ier3-flox*$^{+/+}$ *LysM-Cre*$^{+/+}$ animals is mainly due to the decreased release of reactive nitrogen species from their intestinal macrophages in response to immunogenic stimuli. The lower concentration of RNS in their periphery allows intestinal epithelial cells to maintain their physiological expression and localization of E-cadherin and β-catenin, thereby preventing the disintegration of the cellular junction complex (fig. 44.1). Our experiments clearly demonstrate the similarity between the damage pattern caused by NO_x *in vitro* on the one hand and by infiltrating proinflammatory MΦ on the other hand. All these effects are distinctly attenuated in *Ier3-flox*$^{+/+}$ *LysM-Cre*$^{+/+}$ MΦ which distinguish from *Ier3-flox*$^{+/+}$ *LysM-Cre*$^{-/-}$ MΦ mainly in their release of RNS in response to LPS.

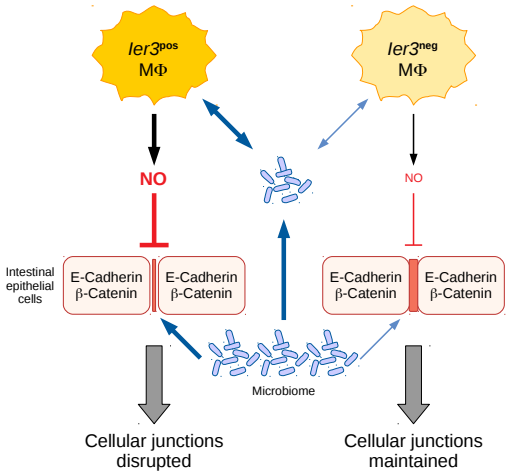

Figure 44.1: Proposed effects of myeloid IER3 on the interplay between the colonic microbiome, macrophages and the integrity of cellular junctions in the mucosa's epithelial cell layer.

As an important mechanisms of the attenuated NO_x release in *Ier3* deficient MΦ it could be shown that in the absence of IER3 the activity of the antioxidant transcription factor NRF2 increased - due to its elevated AKT mediated derepression - as we already demonstrated *in vitro* and *in vivo* [191, 75]. Under the control of NRF2, its target gene heme oxygenase 1 (HO1) could interfere with iNOS expression and activation, thus

resulting in the dampened NO_x formation seen in *Ier3* deficient MΦ (fig. 44.2).

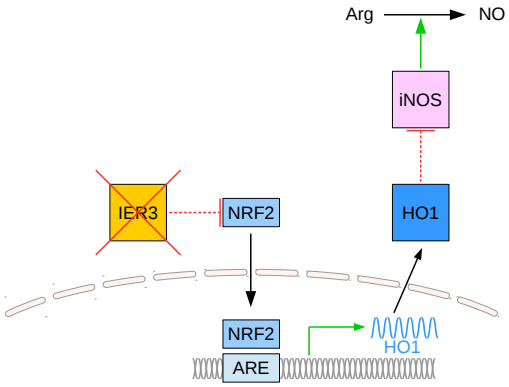

Figure 44.2: Hypothesis for the attenuated NO_x release of *Ier3* deficient MΦ. After data from STACHEL et al. [191] and GRAEBER [75]. ARE: Antioxidant responsive element; HO1: heme oxygenase 1; NRF2: Nuclear factor erythroid 2-related factor 2. Dotted line: Indirect impact.

References

[1] Gnome Chemistry Utils - official webpage. https://www.nongnu.org/gchemutils/.

[2] WILHELM FABRY (1560-1624)–THE OTHER FABRICIUS. *JAMA*, 190:933, dec 1964.

[3] AlphaInnotec. https://www.alpha-innotec.de, February 2020.

[4] BD. https://www.bd.com, February 2020.

[5] BioRad. https://www.bio-rad.com, February 2020.

[6] Carl Zeiss AG. https://www.zeiss.com, February 2020.

[7] Dynex. https://www.dynextechnologies.com, February 2020.

[8] Keyence. https://www.keyence.com, February 2020.

[9] LibreOffice. https://www.libreoffice.org/, February 2020.

[10] Motifolio. https://www.motifolio.com, February 2020.

[11] Sigma-Aldrich. https://www.sigmaaldrich.com, February 2020.

[12] Tecan. https://www.tecan.com, February 2020.

[13] ThermoFisher. https://www.thermofisher.com, February 2020.

[14] Tissue expression of IER3 - Summary - The Human Protein Atlas. https://www.proteinatlas.org/ENSG00000137331-IER3/tissue, 2020.

[15] Clara Abraham and Judy H Cho. Inflammatory bowel disease. *The New England journal of medicine*, 361(21):2066–78, nov 2009.

[16] K Abremski and R Hoess. Bacteriophage P1 site-specific recombination. Purification and properties of the Cre recombinase protein. *The Journal of biological chemistry*, 259(3):1509–14, feb 1984.

[17] M. R. Adams and M. O. Moss. *Food microbiology, 1995*. 1995.

[18] Oleg E Akilov, Mei X Wu, Irina V Ustyugova, Louis D Falo, and Larisa J Geskin. Resistance of Sézary cells to TNF-α-induced apoptosis is mediated in part by a loss of TNFR1 and a high level of the IER3 expression. *Experimental dermatology*, 21(4):287–92, apr 2012.

[19] Sudabeh Alatab, Sadaf G Sepanlou, Kevin Ikuta, Homayoon Vahedi, Catherine Bisignano, Saeid Safiri, Anahita Sadeghi, Molly R Nixon, Amir Abdoli, Hassan Abolhassani, Vahid Alipour, Majid A H Almadi, Amir Almasi-Hashiani, Amir Anushiravani, Jalal Arabloo, Suleman Atique, Ashish Awasthi, Alaa Badawi, Atif A A Baig, Neeraj Bhala, Ali Bijani, Antonio Biondi, Antonio M Borzì, Kristin E Burke, Félix Carvalho, Ahmad Daryani, Manisha Dubey, Aziz Eftekhari, Eduarda Fernandes, João C Fernandes, Florian Fischer, Arvin Haj-Mirzaian, Arya Haj-Mirzaian, Amir Hasanzadeh, Maryam Hashemian, Simon I Hay, Chi L Hoang, Mowafa Househ, Olayinka S Ilesanmi, Nader Jafari Balalami, Spencer L James, Andre P Kengne, Masoud M Malekzadeh, Shahin Merat, Tuomo J Meretoja, Tomislav Mestrovic, Erkin M Mirrakhimov, Hamid Mirzaei, Karzan A Mohammad, Ali H Mokdad, Lorenzo Monasta, Ionut Negoi, Trang H Nguyen, Cuong T Nguyen, Akram Pourshams, Hossein Poustchi, Mohammad Rabiee, Navid Rabiee, Kiana Ramezanzadeh, David L Rawaf, Salman Rawaf, Nima Rezaei, Stephen R Robinson, Luca Ronfani, Sonia Saxena, Masood Sepehrimanesh, Masood A Shaikh, Zeinab Sharafi, Mehdi Sharif, Soraya Siabani, Ali Reza Sima, Jasvinder A Singh, Amin Soheili, Rasoul Sotoudehmanesh, Hafiz Ansar Rasul Suleria, Berhe E Tesfay, Bach Tran, Derrick Tsoi, Marco Vacante, Adam B Wondmieneh, Afshin Zarghi, Zhi-Jiang Zhang, Mae Dirac, Reza Malekzadeh, and Mohsen Naghavi. The global, regional, and national burden of inflammatory bowel disease in 195 countries and territories, 1990–2017: A systematic analysis for the Global Burden of Disease Study 2017. *The Lancet Gastroenterology & Hepatology*, 5(1):17–30, January 2020.

[20] Alberts. *Molecular Biology of the Cell*. Garland, 5th edition, 2007.

[21] M L Anson. THE ESTIMATION OF PEPSIN, TRYPSIN, PAPAIN, AND CATHEPSIN WITH HEMOGLOBIN. *The Journal of general physiology*, 22(1):79–89, sep 1938.

[22] A Arlt, O Grobe, A Sieke, M L Kruse, U R Fölsch, W E Schmidt, and H Schäfer. Expression of the NF-kappa B target gene IEX-1 (p22/PRG1) does not prevent cell death but instead triggers apoptosis in Hela cells. *Oncogene*, 20(1):69–76, jan 2001.

[23] Alexander Arlt, Marie-Luise Kruse, Maike Breitenbroich, Andre Gehrz, Bülent Koc, Jörg Minkenberg, Ulrich R Fölsch, and Heiner Schäfer. The early response gene IEX-1 attenuates NF-kappaB activation in 293 cells, a possible counter-regulatory process leading to enhanced cell death. *Oncogene*, 22(21):3343–51, may 2003.

[24] Alexander Arlt, Jörg Minkenberg, Marie-Luise Kruse, Frauke Grohmann, Ulrich R Fölsch, and Heiner Schäfer. Immediate early gene-X1 interferes with 26 S proteasome activity by attenuating expression of the 19 S proteasomal components S5a/Rpn10 and S1/Rpn2. *The Biochemical journal*, 402(2):367–375, 2007.

[25] Alexander Arlt, Philip Rosenstiel, Marie-Luise Kruse, Frauke Grohmann, Jörg Minkenberg, Neil D Perkins, Ulrich R Fölsch, Stefan Schreiber, and Heiner Schäfer. IEX-1 directly interferes with RelA/p65 dependent transactivation and regulation of apoptosis. *Biochimica et biophysica acta*, 1783(5):941–52, may 2008.

[26] Alexander Arlt and Heiner Schäfer. Role of the immediate early response 3 (IER3) gene in cellular stress response, inflammation and tumorigenesis. *European journal of cell biology*, 90(6-7):545–52, 2011.

[27] Anna Babinska, Mamdouh H. Kedees, Humra Athar, Tomasz Sobocki, Malgorzata B. Sobocka, Tahir Ahmed, Yigal H. Ehrlich, M. Mahmood Hussain, and Elizabeth Kornecki. Two regions of the human platelet F11-receptor (F11R) are critical for platelet aggregation, potentiation and adhesion. *Thrombosis and Haemostasis*, 2002.

[28] C. C. Bain, C. L. Scott, H. Uronen-Hansson, S. Gudjonsson, O. Jansson, O. Grip, M. Guilliams, B. Malissen, W. W. Agace, and A. Mc I. Mowat. Resident and pro-inflammatory macrophages in the colon represent alternative context-dependent fates of the same Ly6C hi monocyte precursors. *Mucosal Immunology*, 2013.

[29] Calum C. Bain and Allan Mci Mowat. Macrophages in intestinal homeostasis and inflammation, 2014.

[30] Daniel C Baumgart and Simon R Carding. Series Gastroenterology 1 Infl ammatory bowel disease: cause and immunobiology. 369:1627–1640, 2007.

[31] Gianfranco Bazzoni. The JAM family of junctional adhesion molecules, 2003.

[32] Gianfranco Bazzoni, Ofelia Maria Martìnez-Estrada, Francis Mueller, Peter Nelboeck, Georg Schmid, Tamas Bartfai, Elisabetta Dejana, and Manfred Brockhaus. Homophilic interaction of junctional adhesion molecule. *Journal of Biological Chemistry*, 2000.

[33] Laurent Beaugerie and Jean Claude Petit. Antibiotic-associated diarrhoea, 2004.

[34] C. Becker, M. C. Fantini, S. Wirtz, A. Nikolaev, R. Kiesslich, H. A. Lehr, P. R. Galle, and M. F. Neurath. In vivo imaging of colitis and colon cancer development in mice using high resolution chromoendoscopy. *Gut*, 54(7):950–954, July 2005.

[35] Christoph Becker, Massimo C. Fantini, Christoph Schramm, Hans A. Lehr, Stefan Wirtz, Alexei Nikolaev, Jürgen Burg, Susanne Strand, Ralf Kiesslich, Samuel Huber, Hiroaki Ito, Norihiro Nishimoto, Kazuyuki Yoshizaki, Tadamitsu Kishimoto, Peter R. Galle, Manfred Blessing, Stefan Rose-John, and Markus F. Neurath. TGF-beta suppresses tumor progression in colon cancer by inhibition of IL-6 trans-signaling. *Immunity*, 21(4):491–501, October 2004.

[36] J. Behrens. Cadherins and catenins: Role in signal transduction and tumor progression. *Cancer Metastasis Reviews*, 18(1):15–30, 1999.

[37] Tanay Bhatt, Abrar Rizvi, Surya Prakash Rao Batta, Sunny Kataria, and Colin Jamora. Signaling and Mechanical Roles of E-cadherin. *Cell Communication & Adhesion*, 20(6):189–199, December 2013.

[38] Anika Bissahoyo, R. Scott Pearsall, Kathleen Hanlon, Vicky Amann, Donna Hicks, Virginia L. Godfrey, and David W. Threadgill. Azoxymethane is a genetic background-dependent colorectal tumor initiator and promoter in mice: Effects of dose, route, and diet. *Toxicological Sciences: An Official Journal of the Society of Toxicology*, 88(2):340–345, December 2005.

[39] Blausen.com staff and Blausen com staff. Medical gallery of Blausen Medical 2014. *WikiJournal of Medicine*, 1(2):10, 2014.

[40] C H Charles, J K Yoon, J S Simske, and L F Lau. Genomic structure, cDNA sequence, and expression of gly96, a growth factor-inducible immediate-early gene encoding a short-lived glycosylated protein. *Oncogene*, 8(3):797–801, mar 1993.

[41] Gerard Clarke, Roman M. Stilling, Paul J. Kennedy, Catherine Stanton, John F. Cryan, and Timothy G. Dinan. Minireview: Gut microbiota: The neglected endocrine organ, 2014.

[42] Hans C. Clevers and Charles L. Bevins. Paneth Cells: Maestros of the Small Intestinal Crypts. *Annual Review of Physiology*, 2013.

[43] E R Cohen. The 1986 CODATA Recommended Values Of the Fundamental Physical Constants. *Journal of Research of the National Bureau of Standards*, 92:85–95, 1986.

[44] Mehmet Coskun. Intestinal epithelium in inflammatory bowel disease. *Frontiers in medicine*, 1(August):24, 2014.

[45] Jacques Cosnes. Tobacco and IBD: relevance in the understanding of disease mechanisms and clinical practice. *Best practice & research. Clinical gastroenterology*, 18(3):481–96, jun 2004.

[46] Christine M Costello, Nancy Mah, Robert Häsler, Philip Rosenstiel, Georg H Waetzig, Andreas Hahn, Tim Lu, Yesim Gurbuz, Susanna Nikolaus, Mario Albrecht, Jochen Hampe, Ralph Lucius, Günther Klöppel, Holger Eickhoff, Hans Lehrach, Thomas Lengauer, and Stefan Schreiber. Dissection of the inflammatory bowel disease transcriptome using genome-wide cDNA microarrays. *PLoS medicine*, 2(8):e199, aug 2005.

[47] B B Crohn, L Ginzburg, and G D Oppenheimer. Landmark article Oct 15, 1932. Regional ileitis. A pathological and clinical entity. By Burril B. Crohn, Leon Ginzburg, and Gordon D. Oppenheimer. *JAMA*, 251(1):73–9, jan 1984.

[48] M Cross and R Renkawitz. Repetitive sequence involvement in the duplication and divergence of mouse lysozyme genes. *The EMBO journal*, 9(4):1283–1288, apr 1990.

[49] Fatima Cvrčková. From Data to Illustrations: Common (Free) Tools for Proper Image Data Handling and Processing. *Methods in Molecular Biology (Clifton, N.J.)*, 1992:121–133, 2019.

[50] Amanda C. Daulagala, Mary Catherine Bridges, and Antonis Kourtidis. E-cadherin Beyond Structure: A Signaling Hub in Colon Homeostasis and Disease. *International Journal of Molecular Sciences*, 20(11), June 2019.

[51] Mariangela De Robertis, Emanuela Massi, Maria Luana Poeta, Simone Carotti, Sergio Morini, Loredana Cecchetelli, Emanuela Signori, and Vito Michele Fazio. The AOM/DSS murine model for the study of colon carcinogenesis: From pathways to diagnosis and therapy studies. *Journal of carcinogenesis*, 10(1):9, jan 2011.

[52] D A Delker, S J McKnight, and D W Rosenberg. The role of alcohol dehydrogenase in the metabolism of the colon carcinogen methylazoxymethanol. *Toxicological sciences : an official journal of the Society of Toxicology*, 45(1):66–71, sep 1998.

[53] Emmanuella Delva, Dana K. Tucker, and Andrew P. Kowalczyk. The desmosome., 2009.

[54] Timothy L. Denning, Brian A. Norris, Oscar Medina-Contreras, Santhakumar Manicassamy, Duke Geem, Rajat Madan, Christopher L. Karp, and Bali Pulendran. Functional Specializations of Intestinal Dendritic Cell and Macrophage Subsets That Control Th17 and Regulatory T Cell Responses Are Dependent on the T Cell/APC Ratio, Source of Mouse Strain, and Regional Localization. *The Journal of Immunology*, 2011.

[55] Klaus Ebnet, Atsushi Suzuki, Shigeo Ohno, and Dietmar Vestweber. Junctional adhesion molecules (JAMs): More molecules with dual functions? *Journal of Cell Science*, 2004.

[56] Timothy R Elliott, Neil B Rayment, Barry N Hudspith, Rebecca E Hands, Kirstin Taylor, Gareth C Parkes, Natalie J Prescott, Liljana Petrovska, John Hermon-Taylor, Jonathan Brostoff, Alex Boussioutas, Christopher G Mathew, Stephen A Bustin, and Jeremy D Sanderson. Lamina propria macrophage phenotypes in relation to Escherichia coli in Crohn's disease. *BMC gastroenterology*, 15(1):75, 2015.

[57] Martin Faderl, Mario Noti, Nadia Corazza, and Christoph Mueller. Keeping bugs in check: The mucus layer as a critical component in maintaining intestinal homeostasis, 2015.

[58] M. G. Farquhar and G. E. Palade. Junctional complexes in various epithelia. *The Journal of cell biology*, 1963.

[59] Eric R. Fearon and Bert Vogelstein. A genetic model for colorectal tumorigenesis, 1990.

[60] Sebastian Foersch, Maximilian J Waldner, and Markus F Neurath. Colitis and colorectal cancer. *Digestive diseases (Basel, Switzerland)*, 30(5):469–76, jan 2012.

[61] Jorgen Fogh, editor. *Human Tumor Cells in Vitro*. Springer US, 1975.

[62] Carola Förster. Tight junctions and the modulation of barrier function in disease, 2008.

[63] Mikio Furuse, Kohji Fujita, Takashi Hiiragi, Kazushi Fujimoto, and Shoichiro Tsukita. Claudin-1 and -2: Novel integral membrane proteins localizing at tight junctions with no sequence similarity to occludin. *Journal of Cell Biology*, 1998.

[64] Mikio Furuse, Masahiko Itoh, Tetsuaki Hirase, Akira Nagaftichi, Shigenobu Yonemura, Sachiko Tsukita, and Shoichiro Tsukita. Direct association of occludin with ZO-1 and its possible involvement in the localization of occludin at tight junctions. *Journal of Cell Biology*, 1994.

[65] Mikio Furuse, Hiroyuki Sasaki, and Shoichiro Tsukita. Manner of interaction of heterogeneous claudin species within and between tight junction strands. *Journal of Cell Biology*, 1999.

[66] Josefina Garcia, Yunbin Ye, Valérie Arranz, Claire Letourneux, Guillaume Pezeron, and Françoise Porteu. IEX-1: a new ERK substrate involved in both ERK survival activity and ERK activation. *The EMBO journal*, 21(19):5151–63, oct 2002.

[67] David Garrod and Martyn Chidgey. Desmosome structure, composition and function, 2008.

[68] François Gerbe, Catherine Legraverend, and Philippe Jay. The intestinal epithelium tuft cells: Specification and function, 2012.

[69] Glenn R. Gibson. Fibre and effects on probiotics (the prebiotic concept). *Clinical Nutrition, Supplement*, 2004.

[70] Gary S. Goldberg, Virginijus Valiunas, and Peter R. Brink. Selective permeability of gap junction channels, 2004.

[71] D. A. Goodenough. Connexins, Connexons, and Intercellular Communication. *Annual Review of Biochemistry*, 1996.

[72] Daniel A. Goodenough and David L. Paul. Gap junctions., 2009.

[73] Siamon Gordon, Annette Plüddemann, and Fernando Martinez Estrada. Macrophage heterogeneity in tissues: Phenotypic diversity and functions. *Immunological Reviews*, 262(1):36–55, November 2014.

[74] Siamon Gordon and Philip R. Taylor. Monocyte and macrophage heterogeneity. *Nature Reviews Immunology*, 5(12):953–964, December 2005.

[75] Annina Graeber. Impact of IER3-status on the phenotype of macrophage cell lines, 2019. Master's thesis.

[76] David H. Greegor. Occult blood testing for detection of asymptomatic colon cancer. *Cancer*, 28(1):131–134, jul 1971.

[77] Fiona M. Gribble and Frank Reimann. Enteroendocrine Cells: Chemosensors in the Intestinal Epithelium. *Annual Review of Physiology*, 2016.

[78] P Griess. Bemerkungen zu der Abhandlung der HH. Weselsky und Benedikt "Ueber einige Azoverbindungen". *Chem. Ber.*, 12:426–428, 1879.

[79] Peter Griess. Bemerkungen zu der Abhandlung der HH. Weselsky und Benedikt „Ueber einige Azoverbindungen". *Berichte der deutschen chemischen Gesellschaft*, 12(1):426–428, January 1879.

[80] O Grobe, A Arlt, H Ungefroren, G Krupp, U R Fölsch, W E Schmidt, and H Schäfer. Functional disruption of IEX-1 expression by concatemeric hammerhead ribozymes alters growth properties of 293 cells. *FEBS letters*, 494(3):196–200, apr 2001.

[81] Katherine R. Groschwitz and Simon P. Hogan. Intestinal barrier function: Molecular regulation and disease pathogenesis, 2009.

[82] Francisco Guarner and Juan R. Malagelada. Gut flora in health and disease, 2003.

[83] Martin Guilliams and Lianne van de Laar. A Hitchhiker's Guide to Myeloid Cell Subsets: Practical Implementation of a Novel Mononuclear Phagocyte Classification System. *Frontiers in Immunology*, 6, August 2015.

[84] Barry M. Gumbiner. Regulation of cadherin-mediated adhesion in morphogenesis, 2005.

[85] Jennifer M. Halbleib and W. James Nelson. Cadherins in development: Cell adhesion, sorting, and tissue morphogenesis, 2006.

[86] Gunnar C. Hansson and Malin E V Johansson. The inner of the two Muc2 mucin-dependent mucus layers in colon is devoid of bacteria. *Gut Microbes*, 1(1):51–54, 2010.

[87] Andrea Hartsock and W. James Nelson. Adherens and tight junctions: Structure, function and connections to the actin cytoskeleton, 2008.

[88] Matija Hedl, Jing Li, Judy H. Cho, and Clara Abraham. Chronic stimulation of Nod2 mediates tolerance to bacterial products. *Proceedings of the National Academy of Sciences of the United States of America*, 2007.

[89] Herbert F Helander and Lars Fändriks. Surface area of the digestive tract â revisited. *Scandinavian Journal of Gastroenterology*, 49(6):681–689, jun 2014.

[90] Jean Claude Hervé and Mickaël Derangeon. Gap-junction-mediated cell-to-cell communication, 2013.

[91] I Hirono, K Kuhara, T Yamaji, S Hosaka, and L Golberg. Carcinogenicity of dextran sulfate sodium in relation to its molecular weight. *Cancer letters*, 18(1):29–34, feb 1983.

[92] Yan-Hong Huang, Jim Yujin Wu, Yujin Zhang, and Mei X Wu. Synergistic and opposing regulation of the stress-responsive gene IEX-1 by p53, c-Myc, and multiple NF-kappaB/rel complexes. *Oncogene*, 21(44):6819–28, oct 2002.

[93] T Hudcovic, R Stepankova, J Cebra, and H Tlaskalová-Hogenova. The role of microflora in the development of intestinal inflammation: acute and chronic colitis induced by dextran sulfate in germ-free and conventionally reared immunocompetent and immunodeficient mice. *Folia microbiologica*, 46(6):565–72, jan 2001.

[94] David A. Hume, V. Hugh Perry, and Siamon Gordon. The mononuclear phagocyte system of the mouse defined by immunohistochemical localisation of antigen F4/80: Macrophages associated with epithelia. *The Anatomical Record*, 1984.

[95] Hee-Jeong Im, Mark R Pittelkow, and Rajiv Kumar. Divergent regulation of the growth-promoting gene IEX-1 by the p53 tumor suppressor and Sp1. *The Journal of biological chemistry*, 277(17):14612–21, apr 2002.

[96] John R Ingram, Gareth A O Thomas, John Rhodes, John T Green, Neil D Hawkes, Jill L Swift, Emmanuel D Srivastava, Brian K Evans, Geraint T Williams, Robert G Newcombe, Edward Courtney,

and Suresh Pillai. A randomized trial of nicotine enemas for active ulcerative colitis. *Clinical gastroenterology and hepatology : the official clinical practice journal of the American Gastroenterological Association*, 3(11):1107–14, nov 2005.

[97] Masahiko Itoh, Mikio Furuse, Kazumasa Morita, Koji Kubota, Mitinori Saitou, and Shoichiro Tsukita. Direct binding of three tight junction-associated MAGUKs, ZO-1, ZO-2, and ZO-3, with the COOH termini of claudins. *Journal of Cell Biology*, 1999.

[98] Andrei I Ivanov. Structure and regulation of intestinal epithelial tight junctions: current concepts and unanswered questions. *Advances in experimental medicine and biology*, 763:132–48, 2012.

[99] Andrei I Ivanov, Asma Nusrat, and Charles A Parkos. The epithelium in inflammatory bowel disease: potential role of endocytosis of junctional proteins in barrier disruption. *Novartis Foundation symposium*, 263:115–24; discussion 124–32, 211–8, 2004.

[100] Hanyong Jin, Dae-Shik Suh, Tae-Hyoung Kim, Ji-Hyun Yeom, Kangseok Lee, and Jeehyeon Bae. IER3 is a crucial mediator of TAp73${\$} – *inducedapoptosisincervicalcancerandconfersetoposidesensitivity.Scientificreports*, 5 : 8367, 2015.

[101] Malin E V Johansson, Jessica M Holmén Larsson, and Gunnar C Hansson. The two mucus layers of colon are organized by the MUC2 mucin, whereas the outer layer is a legislator of host-microbial interactions. *Proceedings of the National Academy of Sciences of the United States of America*, 108 Suppl:4659–65, 2011.

[102] Malin E.V. Johansson, Henrik Sjövall, and Gunnar C. Hansson. The gastrointestinal mucus system in health and disease, 2013.

[103] Michael D Kappelman, Sheryl L Rifas-Shiman, Ken Kleinman, Dan Ollendorf, Athos Bousvaros, Richard J Grand, and Jonathan A Finkelstein. The prevalence and geographic distribution of Crohn's disease and ulcerative colitis in the United States. *Clinical gastroenterology and hepatology : the official clinical practice journal of the American Gastroenterological Association*, 5(12):1424–9, dec 2007.

[104] S Kitajima, S Takuma, and M Morimoto. Histological analysis of murine colitis induced by dextran sulfate sodium of different molecular weights. *Experimental animals / Japanese Association for Laboratory Animal Science*, 49(1):9–15, jan 2000.

[105] Olga Klezovitch and Valeri Vasioukhin. Cadherin signaling: Keeping cells in touch. *F1000Research*, 4(F1000 Faculty Rev), August 2015.

[106] A D Kondratyev, K N Chung, and M O Jung. Identification and characterization of a radiation-inducible glycosylated human early-response gene. *Cancer research*, 56(7):1498–502, apr 1996.

[107] Margareth D. Kottke, Emmanuella Delva, and Andrew P. Kowalczyk. The desmosome: Cell science lessons from human diseases. *Journal of Cell Science*, 2006.

[108] Jiří Kratochvíl. Comparison of the Accuracy of Bibliographical References Generated for Medical Citation Styles by EndNote, Mendeley, RefWorks and Zotero. *The Journal of Academic Librarianship*, 43(1):57–66, January 2017.

[109] C. Kraus, T. Liehr, J. Hülsken, J. Behrens, W. Birchmeier, K. H. Grzeschik, and W. G. Ballhausen. Localization of the human beta-catenin gene (CTNNB1) to 3p21: A region implicated in tumor development. *Genomics*, 23(1):272–274, September 1994.

[110] Gerd Krause, Lars Winkler, Sebastian L. Mueller, Reiner F. Haseloff, Jörg Piontek, and Ingolf E. Blasig. Structure and function of claudins, 2008.

[111] Marie-Luise Kruse, Alexander Arlt, Alexander Sieke, Frauke Grohmann, Maike Grossmann, Jörg Minkenberg, Ulrich R Fölsch, and Heiner Schäfer. Immediate early gene X1 (IEX-1) is organized in subnuclear structures and partially co-localizes with promyelocytic leukemia protein in HeLa cells. *The Journal of biological chemistry*, 280(26):24849–56, jul 2005.

[112] R Kühn, F Schwenk, M Aguet, and K Rajewsky. Inducible gene targeting in mice. *Science (New York, N.Y.)*, 269(5229):1427–9, sep 1995.

[113] Paul D. Lampe and Alan F. Lau. The effects of connexin phosphorylation on gap junctional communication, 2004.

[114] Jonathan Landy, Emma Ronde, Nick English, Sue K. Clark, Ailsa L. Hart, Stella C. Knight, Paul J. Ciclitira, and Hafid Omar Al-Hassi. Tight junctions in inflammatory bowel diseases and inflammatory bowel disease associated colorectal cancer. *World Journal of Gastroenterology*, 22(11):3117–3126, 2016.

[115] G L LAQUEUR. CARCINOGENIC EFFECTS OF CYCAD MEAL AND CYCASIN, METHYLAZOXYMETHANOL GLYCOSIDE, IN RATS AND EFFECTS OF CYCASIN IN GERMFREE RATS. *Federation proceedings*, 23:1386–8, jan.

[116] Donata Lissner, Michael Schumann, Arvind Batra, Lea-Isabel Kredel, Anja A. Kühl, Ulrike Erben, Claudia May, Jörg-Dieter Schulzke, and Britta Siegmund. Monocyte and M1 Macrophage-induced Barrier Defect Contributes to Chronic Intestinal Inflammation in IBD. *Inflammatory Bowel Diseases*, 21(6):1297–1305, June 2015.

[117] Yue-Hong Liu, Yue Ding, Chen-Chen Gao, Li-Sheng Li, Yue-Xiu Wang, and Jing-Dong Xu. Functional macrophages and gastrointestinal disorders. *World Journal of Gastroenterology*, 24(11):1181–1195, March 2018.

[118] O H Lowry, N J Rosebrough, A L Farr, and R J Randall. Protein measurement with the Folin phenol reagent. *The Journal of biological chemistry*, 193(1):265–75, November 1951.

[119] N. A. Mabbott, D. S. Donaldson, H. Ohno, I. R. Williams, and A. Mahajan. Microfold (M) cells: Important immunosurveillance posts in the intestinal epithelium, 2013.

[120] Bryan T. MacDonald, Keiko Tamai, and Xi He. Wnt/beta-catenin signaling: Components, mechanisms, and diseases. *Developmental Cell*, 17(1):9–26, July 2009.

[121] M Mähler, I J Bristol, E H Leiter, A E Workman, E H Birkenmeier, C O Elson, and J P Sundberg. Differential susceptibility of inbred mouse strains to dextran sulfate sodium-induced colitis. *The American journal of physiology*, 274(3 Pt 1):G544–51, mar 1998.

[122] Kevin J Maloy and Fiona Powrie. Intestinal homeostasis and its breakdown in inflammatory bowel disease. *Nature*, 474(7351):298–306, 2011.

[123] Igor Malyshev and Yuri Malyshev. Current Concept and Update of the Macrophage Plasticity Concept: Intracellular Mechanisms of Reprogramming and M3 Macrophage "Switch" Phenotype. https://www.hindawi.com/journals/bmri/2015/341308/, 2015. Library Catalog: www.hindawi.com Pages: e341308.

[124] Joachim Mankertz, Jörg Stefan Waller, Bernd Hillenbrand, Shida Tavalali, Peter Florian, Torsten Schöneberg, Michael Fromm, and Jörg Dieter Schulzke. Gene expression of the tight junction protein occludin includes differential splicing and alternative promoter usage. *Biochemical and Biophysical Research Communications*, 2002.

[125] Alberto Mantovani, Antonio Sica, Silvano Sozzani, Paola Allavena, Annunciata Vecchi, and Massimo Locati. The chemokine system in diverse forms of macrophage activation and polarization. *Trends Immunol*, 25(12):677–686, dec 2004.

[126] L. Martinez-Pomares, N. Platt, A. J. McKnight, R. P. da Silva, and S. Gordon. Macrophage membrane molecules: Markers of tissue differentiation and heterogeneity. *Immunobiology*, 195(4-5):407–416, October 1996.

[127] Eva Martini, Susanne M. Krug, Britta Siegmund, Markus F. Neurath, and Christoph Becker. Mend Your Fences: The Epithelial Barrier and its Relationship With Mucosal Immunity in Inflammatory Bowel Disease, 2017.

[128] K. M. McCarthy, S. A. Francis, J. M. McCormack, J. Lai, R. A. Rogers, I. B. Skare, R. D. Lynch, and E. E. Schneeberger. Inducible expression of claudin-1-myc but not occludin-VSV-G results in aberrant tight junction strand formation in MDCK cells. *Journal of Cell Science*, 2000.

[129] R Medzhitov and C A Janeway. An ancient system of host defense. *Current opinion in immunology*, 10(1):12–5, feb 1998.

[130] Shameer Mehta, Anke Nijhuis, Tomoko Kumagai, James Lindsay, and Andrew Silver. Defects in the adherens junction complex (E-cadherin/ ??-catenin) in inflammatory bowel disease, 2015.

[131] Silvia Melgar, Agneta Karlsson, and Erik Michaëlsson. Acute colitis induced by dextran sulfate sodium progresses to chronicity in C57BL/6 but not in BALB/c mice: correlation between symptoms and inflammation. *American journal of physiology. Gastrointestinal and liver physiology*, 288(6):G1328—-38, jun 2005.

[132] Gülistan MeÅe, Gabriele Richard, and Thomas W. White. Gap junctions: Basic structure and function, 2007.

[133] H. B. Mikkelsen and J. J. Rumessen. Characterization of macrophage-like cells in the external layers of human small and large intestine. *Cell & Tissue Research*, 1992.

[134] Charles D. Mills, Kristi Kincaid, Jennifer M. Alt, Michelle J. Heilman, and Annette M. Hill. M-1/M-2 Macrophages and the Th1/Th2 Paradigm. *The Journal of Immunology*, 164(12):6166–6173, June 2000.

[135] Laura L. Mitic, Christina M. Van Itallie, and James M. Anderson. Molecular physiology and pathophysiology of tight junctions I. Tight junction structure and function: Lessons from mutant animals and proteins, 2000.

[136] Matias N. Möller, Ernesto Cuevasanta, Florencia Orrico, Ana C. Lopez, Leonor Thomson, and Ana Denicola. Diffusion and Transport of Reactive Species Across Cell Membranes. *Advances in Experimental Medicine and Biology*, 1127:3–19, 2019.

[137] Steffen Möller, Hajo Nils Krabbenhöft, Andreas Tille, David Paleino, Alan Williams, Katy Wolstencroft, Carole Goble, Richard Holland, Dominique Belhachemi, and Charles Plessy. Community-driven computational biology with Debian Linux. *BMC bioinformatics*, 11 Suppl 12:S5, December 2010.

[138] Natalie A Molodecky, Ing Shian Soon, Doreen M Rabi, William A Ghali, Mollie Ferris, Greg Chernoff, Eric I Benchimol, Remo Panaccione, Subrata Ghosh, Herman W Barkema, and Gilaad G Kaplan. Increasing incidence and prevalence of the inflammatory bowel diseases with time, based on systematic review. *Gastroenterology*, 142(1):46–54.e42; quiz e30, jan 2012.

[139] M. S. Mooseker. Organization, chemistry, and assembly of the cytoskeletal apparatus of the intestinal brush border., 1985.

[140] Kazumasa Morita, Mikio Furuse, Kazushi Fujimoto, and Shoichiro Tsukita. Claudin multigene family encoding four-transmembrane domain protein components of tight junction strands. *Proceedings of the National Academy of Sciences of the United States of America*, 1999.

[141] Richard J Mural, Mark D Adams, Eugene W Myers, Hamilton O Smith, George L Gabor Miklos, Ron Wides, Aaron Halpern, Peter W Li, Granger G Sutton, Joe Nadeau, Steven L Salzberg, Robert A Holt, Chinnappa D Kodira, Fu Lu, Lin Chen, Zuoming Deng, Carlos C Evangelista, Weiniu Gan, Thomas J Heiman, Jiayin Li, Zhenya Li, Gennady V Merkulov, Natalia V Milshina, Ashwinikumar K Naik, Rong Qi, Bixiong Chris Shue, Aihui Wang, Jian Wang, Xin Wang, Xianghe Yan, Jane Ye, Shibu Yooseph, Qi Zhao, Liansheng Zheng, Shiaoping C Zhu, Kendra Biddick, Randall Bolanos, Arthur L Delcher, Ian M Dew, Daniel Fasulo, Michael J Flanigan, Daniel H Huson, Saul A Kravitz, Jason R Miller, Clark M Mobarry, Knut Reinert, Karin A Remington, Qing Zhang, Xiangqun H Zheng, Deborah R Nusskern, Zhongwu Lai, Yiding Lei, Wenyan Zhong, Alison Yao, Ping Guan, Rui-Ru Ji, Zhiping Gu, Zhen-Yuan Wang, Fei Zhong, Chunlin Xiao, Chia-Chien Chiang, Mark Yandell, Jennifer R Wortman, Peter G Amanatides, Suzanne L Hladun, Eric C Pratts, Jeffery E Johnson, Kristina L Dodson, Kerry J Woodford, Cheryl A Evans, Barry Gropman, Douglas B Rusch, Eli Venter, Mei Wang, Thomas J Smith, Jarrett T Houck, Donald E Tompkins, Charles Haynes, Debbie Jacob, Soo H Chin, David R Allen, Carl E Dahlke, Robert Sanders, Kelvin Li, Xiangjun Liu, Alexander A Levitsky, William H Majoros, Quan Chen, Ashley C Xia, John R Lopez, Michael T Donnelly, Matthew H Newman, Anna Glodek, Cheryl L Kraft, Marc Nodell, Feroze Ali, Hui-Jin An, Danita Baldwin-Pitts, Karen Y Beeson, Shuang Cai, Mark Carnes, Amy Carver, Parris M Caulk, Angela Center, Yen-Hui Chen, Ming-Lai Cheng, My D Coyne, Michelle Crowder, Steven Danaher, Lionel B Davenport, Raymond Desilets, Susanne M Dietz, Lisa Doup, Patrick Dullaghan, Steven Ferriera, Carl R Fosler, Harold C Gire, Andres Gluecksmann, Jeannine D Gocayne, Jonathan Gray, Brit Hart, Jason Haynes, Jeffery Hoover, Tim Howland, Chinyere Ibegwam, Mena Jalali, David Johns, Leslie Kline, Daniel S Ma, Steven MacCawley, Anand Magoon, Felecia Mann, David May, Tina C McIntosh, Somil Mehta, Linda Moy, Mee C Moy, Brian J Murphy, Sean D Murphy, Keith A Nelson, Zubeda Nuri, Kimberly A Parker, Alexandre C Prudhomme, Vinita N Puri, Hina Qureshi, John C Raley, Matthew S Reardon, Megan A Regier, Yu-Hui C Rogers, Deanna L Romblad, Jakob Schutz, John L Scott, Richard Scott, Cynthia D Sitter, Michella Smallwood, Arlan C Sprague, Erin Stewart, Renee V Strong, Ellen Suh, Karena Sylvester, Reginald Thomas, Ni Ni Tint, Christopher Tsonis, Gary Wang, George Wang, Monica S Williams, Sherita M Williams, Sandra M Windsor, Keriellen Wolfe, Mitchell M Wu, Jayshree Zaveri, Kabir Chaturvedi, Andrei E Gabrielian, Zhaoxi Ke, Jingtao Sun, Gangadharan Subramanian, J Craig Venter, Cynthia M Pfannkoch,

Mary Barnstead, and Lisa D Stephenson. A comparison of whole-genome shotgun-derived mouse chromosome 16 and the human genome. *Science (New York, N.Y.)*, 296(5573):1661–71, may 2002.

[142] Zoia Muresan, David L. Paul, and Daniel A. Goodenough. Occludin 1B, a variant of the tight junction protein occludin. *Molecular Biology of the Cell*, 2000.

[143] Kenneth Murphy. *Janeway's Immunobiology*. Garland Science, 8th edition edition, 2011.

[144] Peter J. Murray, Judith E. Allen, Subhra K. Biswas, Edward A. Fisher, Derek W. Gilroy, Sergij Goerdt, Siamon Gordon, John A. Hamilton, Lionel B. Ivashkiv, Toby Lawrence, Massimo Locati, Alberto Mantovani, Fernando O. Martinez, Jean-Louis Mege, David M. Mosser, Gioacchino Natoli, Jeroen P. Saeij, Joachim L. Schultze, Kari Ann Shirey, Antonio Sica, Jill Suttles, Irina Udalova, Jo A. van Ginderachter, Stefanie N. Vogel, and Thomas A. Wynn. Macrophage activation and polarization: Nomenclature and experimental guidelines. *Immunity*, 41(1):14–20, July 2014.

[145] Ryuichi Nagashima, Kunihiko Maeda, Yutaka Imai, and Tsuneo Takahashi. Lamina propria macrophages in the human gastrointestinal mucosa: Their distribution, immunohistological phenotype, and function. *Journal of Histochemistry and Cytochemistry*, 1996.

[146] A Nagy. Cre recombinase: the universal reagent for genome tailoring. *Genesis (New York, N.Y. : 2000)*, 26(2):99–109, mar 2000.

[147] Y Nakanishi, T Sato, and T Ohteki. Commensal Gram-positive bacteria initiates colitis by inducing monocyte/macrophage mobilization. *Mucosal Immunology*, 8(1):152–160, jun 2014.

[148] Carl F Nathan. Identification of interferon-gamma as the lymphokine that activates human macrophage oxidative metabolism and antimicrobial activity. *The Journal of Experimental Medicine*, 158(3):670–689, September 1983.

[149] Sandra Nell, Sebastian Suerbaum, and Christine Josenhans. The impact of the microbiota on the pathogenesis of IBD: lessons from mouse infection models. *Nature reviews. Microbiology*, 8(8):564–77, aug 2010.

[150] Friedel Nollet, Patrick Kools, and Frans Van Roy. Phylogenetic analysis of the cadherin superfamily allows identification of six major subfamilies besides several solitary members, 2000.

[151] Ann M. O'Hara and Fergus Shanahan. The gut flora as a forgotten organ, 2006.

[152] I. Okayasu, T. Ohkusa, K. Kajiura, J. Kanno, and S. Sakamoto. Promotion of colorectal neoplasia in experimental murine ulcerative colitis. *Gut*, 39(1):87–92, July 1996.

[153] P C Orban, D Chui, and J D Marth. Tissue- and site-specific DNA recombination in transgenic mice. *Proceedings of the National Academy of Sciences of the United States of America*, 89(15):6861–6865, aug 1992.

[154] Yosuke Osawa, Masahito Nagaki, Yoshiko Banno, David A. Brenner, Yoshinori Nozawa, Hisataka Moriwaki, and Shigeru Nakashima. Expression of the NF-kappa B target gene X-ray-inducible immediate early response factor-1 short enhances TNF-alpha-induced hepatocyte apoptosis by inhibiting Akt activation. *Journal of Immunology (Baltimore, Md.: 1950)*, 170(8):4053–4060, April 2003.

[155] A. Papanikolaou, Q. S. Wang, D. Papanikolaou, H. E. Whiteley, and D. W. Rosenberg. Sequential and morphological analyses of aberrant crypt foci formation in mice of differing susceptibility to azoxymethane-induced colon carcinogenesis. *Carcinogenesis*, 21(8):1567–1572, August 2000.

[156] Luca Pastorelli, Carlo De Salvo, Joseph R. Mercado, Maurizio Vecchi, and Theresa T. Pizarro. Central role of the gut epithelial barrier in the pathogenesis of chronic intestinal inflammation: Lessons learned from animal models and human genetics, 2013.

[157] Mirna Perez-Moreno and Elaine Fuchs. Catenins: Keeping Cells from Getting Their Signals Crossed, 2006.

[158] Martina Perše and Anton Cerar. Dextran sodium sulphate colitis mouse model: traps and tricks. *Journal of biomedicine & biotechnology*, 2012:718617, jan 2012.

[159] Lance W Peterson and David Artis. Intestinal epithelial cells: regulators of barrier function and immune homeostasis. *Nature reviews. Immunology*, 14(3):141–53, 2014.

[160] A Pietzsch, C Büchler, C Aslanidis, and G Schmitz. Identification and characterization of a novel monocyte/macrophage differentiation-dependent gene that is responsive to lipopolysaccharide, ceramide, and lysophosphatidylcholine. *Biochemical and biophysical research communications*, 235(1):4–9, jul 1997.

[161] Daniel K Podolsky. Inflammatory bowel disease. *The New England journal of medicine*, 347(6):417–29, aug 2002.

[162] A. Quaroni, J. Wands, R. L. Trelstad, and K. J. Isselbacher. Epithelioid cell cultures from rat small intestine. Characterization by morphologic and immunologic criteria. *The Journal of Cell Biology*, 80(2):248–265, February 1979.

[163] Eamonn M.M. Quigley. Gut bacteria in health and disease. *Gastroenterology and Hepatology*, 2013.

[164] Eamonn M.M. Quigley and Rodrigo Quera. Small Intestinal Bacterial Overgrowth: Roles of Antibiotics, Prebiotics, and Probiotics. *Gastroenterology*, 130(2):S78–S90, feb 2006.

[165] K Rajewsky, H Gu, R Kühn, U A Betz, W Müller, J Roes, and F Schwenk. Conditional gene targeting. *The Journal of clinical investigation*, 98(3):600–3, aug 1996.

[166] Puneet Kaur Randhawa, Kavinder Singh, Nirmal Singh, and Amteshwar Singh Jaggi. A review on chemical-induced inflammatory bowel disease models in rodents. *The Korean Journal of Physiology & Pharmacology: Official Journal of the Korean Physiological Society and the Korean Society of Pharmacology*, 18(4):279–288, August 2014.

[167] Géraldine Rocher, Claire Letourneux, Philippe Lenormand, and Françoise Porteu. Inhibition of B56-containing protein phosphatase 2As by the early response gene IEX-1 leads to control of Akt activity. *The Journal of biological chemistry*, 282(8):5468–77, feb 2007.

[168] Gerhard Rogler. Chronic ulcerative colitis and colorectal cancer. *Cancer letters*, 345(2):235–41, apr 2014.

[169] Daniel W. Rosenberg, Charles Giardina, and Takuji Tanaka. Mouse models for the study of colon carcinogenesis. *Carcinogenesis*, 30(2):183–196, February 2009.

[170] Tamás Rőszer. Understanding the Mysterious M2 Macrophage through Activation Markers and Effector Mechanisms. https://www.hindawi.com/journals/mi/2015/816460/, 2015.

[171] Carlos A. Rubio and Peter T. Schmidt. Severe Defects in the Macrophage Barrier to Gut Microflora in Inflammatory Bowel Disease and Colon Cancer. *Anticancer Research*, 38(7):3811–3815, July 2018.

[172] Curtis T. Rueden, Johannes Schindelin, Mark C. Hiner, Barry E. DeZonia, Alison E. Walter, Ellen T. Arena, and Kevin W. Eliceiri. ImageJ2: ImageJ for the next generation of scientific image data. *BMC Bioinformatics*, 18(1):529, November 2017.

[173] Juan C. Sáez, Viviana M. Berthoud, Mária C. Brañes, Agustín D. Martínez, and Eric C. Beyer. Plasma membrane channels formed by connexins: Their regulation and functions, 2003.

[174] H Schäfer, A Arlt, A Trauzold, A Hünermann-Jansen, and W E Schmidt. The putative apoptosis inhibitor IEX-1L is a mutant nonspliced variant of p22(PRG1/IEX-1) and is not expressed in vivo. *Biochemical and biophysical research communications*, 262(1):139–45, aug 1999.

[175] H Schäfer, J Diebel, A Arlt, A Trauzold, and W E Schmidt. The promoter of human p22/PACAP response gene 1 (PRG1) contains functional binding sites for the p53 tumor suppressor and for NFkappaB. *FEBS letters*, 436(2):139–43, oct 1998.

[176] H Schäfer, A Trauzold, E G Siegel, U R Fölsch, and W E Schmidt. PRG1: a novel early-response gene transcriptionally induced by pituitary adenylate cyclase activating polypeptide in a pancreatic carcinoma cell line. *Cancer research*, 56(11):2641–8, jun 1996.

[177] D Schilling, M R Pittelkow, and R Kumar. IEX-1, an immediate early gene, increases the rate of apoptosis in keratinocytes. *Oncogene*, 20(55):7992–7, nov 2001.

[178] E. E. Schneeberger and R. D. Lynch. Structure, function, and regulation of cellular tight junctions, 1992.

[179] Cynthia L. Sears. A dynamic partnership: Celebrating our gut flora, 2005.

[180] Mohd Shahid, Ammar A. Javed, David Chandra, Haley E. Ramsey, Dilip Shah, Mohammed F. Khan, Liping Zhao, and Mei X. Wu. IEX-1 deficiency induces browning of white adipose tissue and resists diet-induced obesity. *Scientific Reports*, 6(April):24135, 2016.

[181] L Shen, L Zhi, W Hu, and M X Wu. IEX-1 targets mitochondrial F1Fo-ATPase inhibitor for degradation. *Cell death and differentiation*, 16(4):603–12, apr 2009.

[182] Antonio Sica and Alberto Mantovani. Macrophage plasticity and polarization: In vivo veritas. *The Journal of Clinical Investigation*, 122(3):787–795, March 2012.

[183] Christian Sina, Alexander Arlt, Olga Gavrilova, Emilie Midtling, Marie-Luise Kruse, Susanne Sebens Müerköster, Rajiv Kumar, Ulrich R Fölsch, Stefan Schreiber, Philip Rosenstiel, and Heiner Schäfer. Ablation of gly96/immediate early gene-X1 (gly96/iex-1) aggravates DSS-induced colitis in mice: role for gly96/iex-1 in the regulation of NF-kappaB. *Inflammatory bowel diseases*, 16(2):320–31, feb 2010.

[184] Lesley E. Smythies, Marty Sellers, Ronald H. Clements, Meg Mosteller-Barnum, Gang Meng, William H. Benjamin, Jan M. Orenstein, and Phillip D. Smith. Human intestinal macrophages display profound inflammatory anergy despite avid phagocytic and bacteriocidal activity. *Journal of Clinical Investigation*, 2005.

[185] Goran Söhl and Klaus Willecke. An update on connexin genes and their nomenclature in mouse and man, 2003.

[186] Goran Söhl and Klaus Willecke. Gap junctions and the connexin protein family, 2004.

[187] Robert W. Solomon. Free and open source software for the manipulation of digital images. *AJR. American journal of roentgenology*, 192(6):W330–334, June 2009.

[188] Felix Sommer and Fredrik Bäckhed. The gut microbiota-masters of host development and physiology, 2013.

[189] Stacy L Sommer, Theresa J Berndt, Elena Frank, Jeetendra B Patel, Margaret M Redfield, Xiangyang Dong, Matthew D Griffin, Joseph P Grande, Jan M A van Deursen, Gary C Sieck, Juan C Romero, and Rajiv Kumar. Elevated blood pressure and cardiac hypertrophy after ablation of the gly96/IEX-1 gene. *Journal of applied physiology (Bethesda, Md. : 1985)*, 100(2):707–716, feb 2006.

[190] Imene Soufli, Ryma Toumi, Hayet Rafa, and Chafia Touil-Boukoffa. Overview of cytokines and nitric oxide involvement in immuno-pathogenesis of inflammatory bowel diseases. *World Journal of Gastrointestinal Pharmacology and Therapeutics*, 7(3):353–360, August 2016.

[191] Imke Stachel, Claudia Geismann, Konrad Aden, Florian Deisinger, Philip Rosenstiel, Stefan Schreiber, Susanne Sebens, Alexander Arlt, and Heiner Schäfer. Modulation of Nuclear Factor E2-related Factor-2 (Nrf2) Activation by the Stress Response Gene Immediate Early Response-3 (IER3) in Colonic Epithelial Cells: A novel mechanism of cellular adaption to inflammatory stress. *Journal of Biological Chemistry*, 289(4):1917–1929, January 2014.

[192] Erin C. Steinbach and Scott E. Plevy. The role of macrophages and dendritic cells in the initiation of inflammation in IBD. *Inflammatory bowel diseases*, 20(1):166–175, January 2014.

[193] A. M. Stephen and J. H. Cummings. The microbial contribution to human faecal mass. *Journal of Medical Microbiology*, 1980.

[194] N Sternberg and D Hamilton. Bacteriophage P1 site-specific recombination. I. Recombination between loxP sites. *Journal of molecular biology*, 150(4):467–86, aug 1981.

[195] Tsuyoshi Tajima, Takahisa Murata, Kosuke Aritake, Yoshihiro Urade, Masaki Michishita, Toshiyuki Matsuoka, Shuh Narumiya, Hiroshi Ozaki, and Masatoshi Hori. EP 2 and EP 4 receptors on muscularis resident macrophages mediate LPS-induced intestinal dysmotility via iNOS upregulation through cAMP/ERK signals. *American Journal of Physiology - Gastrointestinal and Liver Physiology*, 2012.

[196] M. Takeichi. The cadherins: Cell-cell adhesion molecules controlling animal morphogenesis. *Development (Cambridge, England)*, 102(4):639–655, April 1988.

[197] M. Takeichi. Cadherin cell adhesion receptors as a morphogenetic regulator. *Science (New York, N.Y.)*, 251(5000):1451–1455, March 1991.

[198] Takuji Tanaka, Hiroyuki Kohno, Rikako Suzuki, Yasuhiro Yamada, Shigeyuki Sugie, and Hideki Mori. A novel inflammation-related mouse colon carcinogenesis model induced by azoxymethane and dextran sodium sulfate. *Cancer Science*, 94(11):965–973, November 2003.

[199] Shoichiro Tsukita, Mikio Furuse, and Masahiko Itoh. Multifunctional strands in tight junctions, 2001.

[200] Jerrold R. Turner. Intestinal mucosal barrier function in health and disease. *Nature Reviews Immunology*, 9(11):799–809, nov 2009.

[201] E R Unanue and P M Allen. The basis for the immunoregulatory role of macrophages and other accessory cells. *Science (New York, N.Y.)*, 236(4801):551–7, may 1987.

[202] Irina V Ustyugova, Liang Zhi, Joel Abramowitz, Lutz Birnbaumer, and Mei X Wu. IEX-1 deficiency protects against colonic cancer. *Molecular cancer research : MCR*, 10(6):760–7, jun 2012.

[203] L. Uys, J. H. S. Hofmeyr, J. L. Snoep, and J. M. Rohwer. Software tools that facilitate kinetic modelling with large data sets: An example using growth modelling in sugarcane. *Systems Biology*, 153(5):385–389, September 2006.

[204] Tomas Valenta, George Hausmann, and Konrad Basler. The many faces and functions of β-catenin. *The EMBO Journal*, 31(12):2714–2736, June 2012.

[205] Laurens G. van der Flier and Hans Clevers. Stem Cells, Self-Renewal, and Differentiation in the Intestinal Epithelium. *Annual Review of Physiology*, 2009.

[206] Gregory D. Van Duyne. A Structural View of Cre- loxP Site-Specific Recombination. *Annual Review of Biophysics and Biomolecular Structure*, 30(1):87–104, jun 2001.

[207] K. Vidal, I. Grosjean, J. P. evillard, C. Gespach, and D. Kaiserlian. Immortalization of mouse intestinal epithelial cells by the SV40-large T gene. Phenotypic and immune characterization of the MODE-K cell line. *Journal of Immunological Methods*, 166(1):63–73, November 1993.

[208] Gernot Walko, Maria J. Castañón, and Gerhard Wiche. Molecular architecture and function of the hemidesmosome, 2015.

[209] Robert H. Whitehead and Pamela S. Robinson. Establishment of conditionally immortalized epithelial cell lines from the intestinal tissue of adult normal and transgenic mice. *American Journal of Physiology - Gastrointestinal and Liver Physiology*, 296(3):G455–G460, March 2009.

[210] Wilks. Morbid appearances in the intestine of Miss Bankes. *Medical Times & Gazette*, 2:264, 1859.

[211] Joanne M Willey, Linda M Sherwood, and Christopher J Woolverton. 36. Clinical Microbiology and Immunology. In *Prescott's Principles of Microbiology*. 2017.

[212] Stefan Wirtz, Clemens Neufert, Benno Weigmann, and Markus F Neurath. Chemically induced mouse models of intestinal inflammation. *Nature protocols*, 2(3):541–6, jan 2007.

[213] Stefan Wirtz and Markus F Neurath. Mouse models of inflammatory bowel disease. *Advanced drug delivery reviews*, 59(11):1073–83, sep 2007.

[214] M X Wu, Z Ao, K V Prasad, R Wu, and S F Schlossman. IEX-1L, an apoptosis inhibitor involved in NF-kappaB-mediated cell survival. *Science (New York, N.Y.)*, 281(5379):998–1001, aug 1998.

[215] R J Xavier and D K Podolsky. Unravelling the pathogenesis of inflammatory bowel disease. *Nature*, 448(7152):427–434, jul 2007.

[216] Min Xu. LyX: Another Scientific Word Processor. *Optics and Photonics News*, 11(11):42–43, November 2000.

[217] Jian Ye, George Coulouris, Irena Zaretskaya, Ioana Cutcutache, Steve Rozen, and Thomas L. Madden. Primer-BLAST: A tool to design target-specific primers for polymerase chain reaction. *BMC bioinformatics*, 13:134, June 2012.

[218] My Young Yoon, Keehoon Lee, and Sang Sun Yoon. Protective role of gut commensal microbes against intestinal infections, 2014.

[219] Teizo Yoshimura, Naoya Yuhki, Stephen K Moore, Ettore Appella, Michael I Lerman, and Edward J Leonard. Human monocyte chemoattractant protein-1 (MCP-1) Full-length cDNA cloning, expression in mitogen-stimulated blood mononuclear leukocytes, and sequence similarity to mouse competence gene JE. *FEBS Letters*, 244(2):487–493, feb 1989.

[220] Y Zhang, S F Schlossman, R A Edwards, Ching-Nan Ou, J Gu, and Mei X Wu. Impaired apoptosis, extended duration of immune responses, and a lupus-like autoimmune disease in IEX-1-transgenic mice. *Proceedings of the National Academy of Sciences of the United States of America*, 99(2):878–83, jan 2002.

[221] Dexi Zhou, Cheng Huang, Zhen Lin, Shuxiang Zhan, Lingna Kong, Chengbo Fang, and Jun Li. Macrophage polarization and function with emphasis on the evolving roles of coordinated regulation of cellular signaling pathways. *Cellular Signalling*, 26(2):192–197, February 2014.

Appendix

A Figure sources

All figures depicted in this thesis, which were not generated by the author himself are listed in the table A.1 together with their respectively source. This also includes figures, which were adapted and modified.

Some of the depicted graphics were generated using the Motifolio™ scientific toolkit library.

Table A.1: List of adapted and modified figures depicted in this thesis.

Figure	Source
1.1	Modified from Blausen [39].
3.2	Adapted from Baumgart et al. [30].
3.3	Created after data from Fearon/Vogelstein et al. [59] and Rogler et al. [168].
4.1	Adapted and modified from Arlt et Schaefer [26].
4.2	Adapted from Costello et al. [46].
8.2	Adapted from Sigma-Aldrich [11].
44.2	Created after data from Stachel et al. [191] and Graeber [75].

B Software

Table B.1 lists the software utilized for acquisition, analysis, processing, validation and visualization of the data incorporated in this thesis. It further lists the software utilized to create this thesis itself. References are given if available. Inquired databases are not listed.

Table B.1: List of software utilized for this thesis. Scientific references are listed if available. Otherwise the developers/distributors URL is listed.

Software	Version	Developer/ distributor	Reference/ URL
Alpha View™	3.0	AlphaInnotec	[3]
Axio Vision™	2.8	Carl Zeiss	[6]
BZ-Viewer™	2.0	Keyence	[8]
CFX Maestro™	4.1	BioRad	[5]
FACSuite™	1.0.5	BD	[4]
Fiji/ImageJ	1.52	The Fiji project**	[172]
GIMP	2.8.22	The GIMP project**	[187]
Gnome Chem Utils	0.14.16	The Gnome project**	[1]
Gnumeric	1.12.35	The Gnumeric project**	[203]
iControl™	1.6	Tecan	[12]
Inkscape	0.92	The Inkscape project**	[49]
LibreOffice suite	6.0.7.3	The LibreOffice project**	[9]
Lyx / LaTex	2.3.3	The Lyx project**	[216]
Motifolio™ toolkit library	n/a	Motifolio	[10]
ND-1000	3.3	Thermo	[13]
Primer-BLAST	rr	NCBI	[217]
Quantity One™	4.5	BioRad	[5]
Revelation™	4.25	Dynex	[7]
Ubuntu GNU/Linux*	16.04 / 18.04	Canonical	[137]
Zen™ software suite	2.0	Carl Zeiss	[6]
Zotero	5.0.82	The Zotero project**	[108]

Legend:

*: Debian based
**: Community based open source project
NCBI: National Center of Biotechnology Information
rr: rolling release
URL: Uniform resource locator

C Animal experiments

All animals were housed and bred under S1 conditions in the central animal housing facility of the Christan Albrechts University Kiel (Building U39, UKSH Campus Kiel) pursuant to the European and German animal welfare regulations.

All experiments were conducted in accordance with the European and German animal welfare regulations and were approved by the admission authorities of the Federal State of Schleswig-Holstein (File no. 155-11/13).

D Declaration of academic honesty (*German*)

Hiermit erkläre ich, dass

1. die Abhandlung - abgesehen von der Beratung durch den Betreuer - nach Inhalt und Form eine eigenständige und nur mit den angegebenen Hilfsmitteln verfasste Arbeit des Doktoranden ist;

2. die Arbeit noch nicht in Gänze oder zum Teil schon einer anderen Stelle im Rahmen eines Prüfungsverfahrens vorgelegen hat, veröffentlicht worden ist oder zur Veröffentlichung eingereicht wurde;

3. die Arbeit unter Einhaltung der Regeln guter wissenschaftlicher Praxis der Deutschen Forschungsgemeinschaft entstanden ist;

4. mir noch kein akademischer Grad entzogen wurde.

Florian Deisinger

E Danksagung

An erster Stelle möchte ich Herrn Prof. Dr. Heiner Schäfer für die Bereitstellung dieses interessanten Themas sowie den guten Arbeitsbedingungen herzlich danken. Insbesondere gilt mein Dank der immer währenden Unterstützung, der sehr gute Betreuung und den vielen förderlichen Ratschlägen sowie für die stets geöffnete Tür.

Herrn Prof. Dr. Thomas Roeder danke ich dafür, sich als Zweitgutachter für diese Arbeit zur Verfügung gestellt zu haben.

Des Weiteren danke ich den Mitgliedern der Prüfungskommision, Herrn Prof. Dr. Hinrich Schulenburg und Herrn Prof. Dr. Thomas Kunze.

Herr Prof. Dr. Alexander Arlt und besonders Frau Dr. Claudia Geismann konnten mir in vielen produktiven Gesprächen immer wieder neue Perspektiven eröffnen.

Nourhane, Leontine, Annina und Magdalena danke ich für ihre moralische Unterstützung und die schöne Zeit im und außerhalb des Labors.

Frau Frauke Grohmann, Frau Iris Kosmol und Frau Maike Witt-Ramdohr danke ich für die gute Zusammenarbeit und die stets nette Arbeitsatmosphäre.

Auch Frau Prof. Dr. Susanne Sebens und das Team von IET standen mir immer mit Rat und Tat zur Seite. Vielen Dank dafür.

Bei Frau Dr. Maren Paulsen und Herrn Dr. Konrad Aden aus der Arbeitsgruppe von Prof. Dr. Rosenstiel, sowie bei Frau Dr. Marie Dowds und Frau Alyn Gerneth möchte ich mich herzlich für ihre Unterstützung bei den Tierversuchen bedanken. Der Arbeitsgruppe Molekulare Kardiologie danke ich für die für die Bereitstellung des LSM sowie des Keyence imaging Systems.

Catharina und Jan waren so nett, diese Arbeit Korrektur zu lesen.

Besonders bedanken möchte ich mich bei meiner Familie und meinen Freunden für ihre vielfältige Unterstützung während der letzten Jahre. Mein Vater und meine Schwester Martina verdienen hier eine besondere Erwähnung.

Der größte Dank gebührt allerdings meiner Mutter. Du hast mich auf so viele Arten unterstützt, aber vor allem hast Du immer an mich geglaubt. Ohne Dich wäre ich nicht der, der ich heute bin. Das werde ich Dir nie vergessen.